Fatigue Damage Evolution in Fibre Composites for Wind Turbine Blades

Jespersen, Kristine Munk

Publication date:
2017

Document Version
Publisher's PDF, also known as Version of record

Fatigue Damage Evolution in Fibre Composites for Wind Turbine Blades.

Department of Wind Energy PhD Report 2017

Kristine Munk Jespersen

DTU Wind Energy PhD-0075(EN)

June 2017

DTU Wind Energy
Department of Wind Energy

Authors: Kristine Munk Jespersen

Title: Fatigue Damage Evolution in Fibre Composites for Wind Turbine Blades.

Department: Wind Energy

2017

Project Period:

April 15th 2014 – April 14th 2017

Education:

PhD

Supervisor:

Associate Professor Lars P. Mikkelsen, DTU Wind Energy

Co-supervisors:

Dr. Jens Zangenberg, LM Wind Power Blades

Senior Scientist Leon Mishnaevsky Jr., DTU Wind Energy

DTU Wind Energy is a department of the Technical University of Denmark with a unique integration of research, education, innovation and public/private sector consulting in the field of wind energy. Our activities develop new opportunities and technology for the global and Danish exploitation of wind energy. Research focuses on key technical-scientific fields, which are central for the development, innovation and use of wind energy and provides the basis for advanced education.

DTU Wind Energy has a staff of approximately 240 and a further 35 PhD-students, spread across 38 different nationalities. The variety of research, education, innovation, testing and consultancy is reflected in the employment profile which includes faculty with research and teaching responsibilities, researchers and technical academic staff, highly skilled technicians and administrative staff.

Our facilities are situated at DTU Risø Campus and at DTU Lyngby Campus. Furthermore the department is running the national test stations in Høvsøre and Østerild.

Technical University of Denmark
Department of Wind Energy
Frederiksborgvej 399
Building 118
4000 Roskilde
Denmark

www.vindenergi.dtu.dk

FATIGUE DAMAGE EVOLUTION IN FIBRE COMPOSITES FOR WIND TURBINE BLADES

PhD thesis

Kristine Munk Jespersen

April, 2017
DTU Wind Energy
Technical University of Denmark

Prepared by:
Kristine Munk Jespersen

Main supervisor:
Lars P. Mikkelsen, Assoc. Professor
Technical University of Denmark
DTU Wind Energy, Section of Composites and Material Mechanics
Mail: lapm@dtu.dk

Co-supervisors:
Jens Zangenberg, Dr.
LM Wind Power Blades
Materials and Process, Composite Mechanics
Mail: jzan@lmwindpower.com

Leon Mishnaevsky Jr, Senior Scientist
Technical University of Denmark
DTU Wind Energy, Section of Composites and Material Mechanics
Mail: lemi@dtu.dk

Technical University of Denmark
DTU Wind Energy, Section of Composites and Material Mechanics
Risø Campus
Frederiksborgvej 399
4000 Roskilde
Denmark
Tel +45 4677 5085
Mail: info@vindenergi.dtu.dk
Web: `http://www.vindenergi.dtu.dk/`

Publication reference data
Kristine Munk Jespersen
Fatigue damage evolution in fibre composites for wind turbine blades
PhD thesis
Technical University of Denmark
DTU Wind Energy, Section of Composites and Material Mechanics
April 2017
DTU Wind Energy PhD-0075 (EN)

Preface

This thesis is submitted to the Technical University of Denmark in candidacy for a degree of Doctor of Philosophy, PhD, in Construction, Production, Civil Engineering and Transport. The work is prepared in accordance with the regulations regarding the PhD programme in Denmark.

The topic treated is tension fatigue damage of unidirectional glass fibre reinforced composite materials with emphasis on the micro-structural damage initiation and progression mechanisms. The application in focus is the composite materials used for the load carrying spars of wind turbine blades. The work was carried out in the Composites and Materials Mechanics section of DTU Wind Energy with co-supervision from LM Wind Power Blades during the period April 2014 to April 2017.

Research funding was provided from "Innovation Fund Denmark" via CINEMA: "the allianCe for ImagiNg and Modelling of Energy Applications", DSF-grant no. 1305-00032B. The project has been supervised by Lars P. Mikkelsen (DTU Wind Energy), Jens Zangenberg (LM Wind Power Blades), and Leon Mishnaevsky (DTU Wind Energy). The research was conducted using mechanical testing equipment from DTU Center for Advanced Structural and Material Testing (CASMAT), Grant No. VKR023193 from Villum Fonden.

Kristine Munk Jespersen

Risø, Denmark
April 2017

Acknowledgements

Starting from a background in mechanical engineering with only limited knowledge on fibre composites and no previous knowledge on X-ray CT, a lot of people have helped me during the PhD project, and this section expresses my gratitude.

Without the kind financial support from the the allianCe for ImagiNg and Modelling of Energy Applications (CINEMA) project, the PhD project could not have been carried out. Furthermore, I am grateful to the CINEMA project and the people involved for providing a great opportunity for cross-field collaboration.

I would like to give a special thanks to my supervisor Lars P. Mikkelsen who, aside from being great company, always supported me and made time to provide the assistance I needed throughout the project. I also give a great thanks to Jens Zangenberg from LM Wind Power Blades for many fruitful discussions, insight, and input to the project. I would like to thank Leon Mishnaevsky from DTU Wind Energy for his input as well.

Many thanks to my co-authors Philip J. Withers, Tristan Lowe, Ying Wang, Jens Zangenberg, Lars P. Mikkelsen, Jens A. Glud, Hiroyki Kawada, and Atsushi Hosoi for providing valuable input to the work. I am also grateful to Hans Lilholt and Povl Brøndsted for useful insight and feedback on my work. I would also like to thank Monica Emerson and her supervisors from DTU Compute for a great collaboration during my project.

I owe personal thanks to my colleagues at DTU Wind Energy for interesting collaboration and discussion along with a great working environment and friendship. I would also like to give my thanks to my office mates during my visits to LM Wind Power for useful input to the project and for always making me feel welcome. I would also like to thank the technicians and engineers in the Composites and Materials Mechanics section at DTU wind energy who assisted me during the project. Here a special thanks goes to Steffen Rasmussen, Antony Fraisse, Erik Vogeley and Vagn Jensen who helped me developing new experimental setups for the project. In addition, I would like to thank the people at Manchester X-ray Imaging Facility at the University of Manchester for allowing me to use their equipment and for providing me with valuable knowledge about X-ray CT.

Part of the work done in the PhD project was conducted abroad during a research stay in Kawada-Hosoi Laboratory at Waseda University in Japan. The stay would not have been possible without the assistance from Yosuke Ueki from Hitachi who provided the contact, thanks. I am also grateful to Hiroyuki Kawada and Atsushi Hosoi who allowed me to stay in their laboratory and for all their help during my stay. Furthermore, I express my gratitude to the students in the laboratory for an excellent personal experience and great friendships. A special thanks goes to Taesung, Sen, Yoshihiro, Motoki, Yui, Daichi, Daiki, Takahiro, and Kohei for many fun times and all their help during my stay.

Finally, heartfelt thanks go to my family and friends who were always there for me when I needed to do something other than work.

Abstract

One of the largest challenges in wind turbine design, is realistically predicting the life-time of the blades. Wind turbine blades experience a high number of fatigue load cycles during their life-time, and the fatigue damage mechanisms of the non-crimp fabric based glass fibre composites used for the load carrying parts of wind turbine blades are not well understood. This PhD project establishes experimental methods making it possible to monitor the damage initiation and progression of fibre composites in 3D using X-ray CT. To overcome the resolution challenges of X-ray CT, a tension clamp solution that applies load to the specimen during X-ray CT examination is presented, and the advantage of combining X-ray CT with other techniques such as transilluminated white light imaging is demonstrated. The established methods are used to monitor the damage initiation and progression of fatigue damage on the micro-scale in the non-crimp fabric based composites used for wind turbine blades.

The results show that fibre fractures in the unidirectional (UD) load carrying fibre bundles initiate from off-axis cracks in the thin supporting backing fibre bundles. With an increasing number of fatigue load cycles, the UD fibre fractures progress gradually into the thickness direction of the UD fibre bundles, which eventually results in final fracture of the fibre composite. It is also found that the UD fibre fracture regions generally grow larger and initiate earlier at cross-over regions of the backing fibre bundles than at single backing fibre bundle regions. Furthermore, UD Fibre fractures are only observed to initiate at locations where the backing fibre bundles are 'in contact' with a UD fibre bundle. By observing the damage progression in 3D, it is also clear that the UD fibre fractures initiated and progressed as local 3D phenomena rather than being homogeneously distributed within the UD fibre bundles. Hence, the results show the importance of considering the problem in 3D.

The knowledge obtained on the fatigue damage mechanisms during the project can not only be used to improve the materials, but also sets the stage for X-ray CT based modelling. This is a step towards more realistic fatigue life-time modelling of fibre composites used for wind turbine blades, which will make it possible to push the design limits of wind turbine blades and thereby decrease the cost of energy for the wind energy production. In addition, the methods established during the PhD project can be applied to other problems, material systems, and load conditions in the future, which opens up for many new opportunities.

Resumé

En af de største udfordringer i vindmølledesign er at realistisk kunne forudse levetiden på vingerne. Vindmøllevinger er udsat for et højt antal belastningscykler gennem deres levetid, og skadesmekanismerne under udmattelse i de ikke-vævet tekstil baserede glasfiber kompositter brugt til de lastbærende dele af vindmøllevinger, er stadig ikke godt forstået. Dette PhD projekt etablerer eksperimentelle metoder, der gør det muligt at følge initieringen og udviklingen af udmattelsesskade i fiber kompositter i 3D ved brug af røntgen tomografi (X-ray CT). For at overkomme udfordringerne i forbindelse med billedopløsning, introduceres en træk-klampeløsning, der kan holde testemnet belastet under X-ray CT undersøgelsen. Endvidere er fordelene ved at kombinere X-ray CT med andre teknikker, så som billeder taget med et højopløsningskamera under gennemlysning af testemnet, demonstreret. De etablerede metoder anvendes til at følge initieringen og udviklingen af udmattelsesskader på mikroskala i de ikke-vævet tekstil baserede kompositter der anvendes i vindmøllevinger.

Resultaterne viser, at fiberbrud i de ensrettede (unidirectional, UD) lastbærende fiberbundter initierer fra tværgående revner i de tynde understøttende fiberbundter. Med stigende antal lastcykler, forekommer fiberbrud gradvist længere og længere inde i tykkelsesretningen af UD fiberbundterne, hvilket til sidst resulterer i endeligt brud af fiberkompositten. Det ses også, at områder med UD fiberbrud i nærheden af krydsregioner af de understøttende fiberbundter, generelt vokser sig større og initierer tidligere end ved områder med enkelte understøttende fiberbundter. Ydermere er initiering af UD fiberbrud kun observeret hvor de understøttende fiberbundter er 'i kontakt' med UD fiberbundterne. Ved at observere skadesudviklingen i 3D, er det også tydeligt at områderne med UD fiberbrud initierer og udvikler sig som lokale 3D fænomener fremfor at være homogent fordelt indeni UD fiberbundterne. Således viser resultaterne også vigtigheden af at betragte problemet i 3D.

Den viden omkring skadesmekanismerne under udmattelse der er opnået i løbet af projektet kan bruges til at forbedre materialerne, men baner også vejen for X-ray CT baseret computer modellering. Dette er et skridt imod mere realistisk modellering af levetiden under udmattelse af fiberkompositter anvendt i vindmøllevinger. Dette vil gøre det muligt at skubbe grænser i designet og derved også sænke prisen på energien produceret af vindmøller. Endvidere kan metoderne etableret under PhD projektet også anvendes på andre problemer, materialesystemer, og belastningsforhold i fremtiden, hvilket åbner op for mange nye muligheder.

Publications

Publications appended to this thesis

[P1] **Jespersen, K. M.**, Zangenberg, J., Lowe, T., Withers, P. J., and Mikkelsen, L. P. (2016). Fatigue damage assessment of uni-directional non-crimp fabric reinforced polyester composite using X-ray computed tomography. *Composites Science and Technology*, 136, pp. 94–103.

[P2] **Jespersen, K. M.**, Wang, Y., Zangenberg, J., Lowe, T., Withers, P. J., and Mikkelsen, L. P. (2016). Ex-Situ Time-Lapse X-Ray Ct Study of 3D Micro-Structural Fatigue Damage Evolution in Uni-Directional Composites. *17th European Conference on Composite Materials*, Munich, Germany, pp. 1-8.

[P3] **Jespersen, K. M.**, and Mikkelsen, L. P. (2016). Fatigue damage observed non-destructively in fibre composite coupon test specimens by X-ray CT. *IOP Conf. Series: Materials Science and Engineering*, 139, 12024.

[P4] **Jespersen, K. M.**, and Mikkelsen, L. P. (2017). Three dimensional fatigue damage evolution in non-crimp glass fibre fabric based composites used for wind turbine blades. *Submitted to Composites Science and Technology*.

[P5] **Jespersen, K. M.**, Glud, J. A., Zangenberg, J., Hosoi, A., Kawada, H., and Mikkelsen, L. P. (2017). Uncovering the fatigue damage initiation and progression in uni-directional non-crimp fabric reinforced polyester composite - Part A: Off-axis cracks and the effect of strain level. *In manuscript*.

[P6] **Jespersen, K. M.**, Zangenberg, J., and Mikkelsen, L. P. (2017). Uncovering the fatigue damage initiation and progression in uni-directional non-crimp fabric reinforced polyester composite - Part B: uni-directional fibre fractures. *In manuscript*.

Other publications and contributions

- Emerson, M. J., **Jespersen, K. M.**, Dahl, A. B., Conradsen, K., and Lars P. Mikkelsen (2017). Individual fibre segmentation from 3D X-ray computed tomography for characterising the fibre orientation in unidirectional composite materials, *Composites Part A*, 97, pp. 83-92, http://doi.org/10.1016/j.compositesa.2016.12.028.
- Mikkelsen, L. P., Emerson, M. J., **Jespersen, K. M.**, Dahl, V. A., Conradsen, K., Dahl, A. B. (2016). X-ray based micromechanical finite element modeling of composite materials. *Presented by first author at: 29th Nordic Seminar on Computational Mechanics*, Gothenburg, Sweden, pp. 1-4.
- **Jespersen, K. M.**, Zangenberg Hansen, J., Lowe, T., Withers, P. J., Mikkelsen, L. P. (2016). 3D X-ray CT of fatigue damage in fibre composites. *Presented by first author at: 24th International Congress of Theoretical and Applied Mechanics*, Montreal, Canada, pp. 1-2.
- Mikkelsen, L. P. and **Jespersen, K. M**, (2016). Residual strains and their relation to the fatigue damage evolution in composite materials. *Presented by first author at: 24th International Congress of Theoretical and Applied Mechanics*, Montreal, Canada, pp. 1-2.
- Mikkelsen, L. P. and **Jespersen, K. M.** (2016). Approach for investigations of progressive fatigue damage in 3D in fibre composites using X-ray tomography. *Presented by first author at: 1st International Symposium on Multi-Scale Experimental Mechanics*, Roskilde, Denmark, pp. 1-2.
- Emerson, M. J., **Jespersen, K. M.**, Dahl, A. B., Conradsen, K., and Mikkelsen, L. P. (2016). Segmentation of individual fibres in a uni-directional composite from 3D X-ray computed tomography data. *Presented by first author at: 3rd International Congress on Materials Science*, St. Charles, United States.
- **Jespersen, K. M.**, Zangenberg, J., Mikkelsen, L. P., Hosoi, A., and Kawada, H. (2015). Fatigue damage assessment of UD composite by 3D X-ray computed tomography. *Presented by first author at: Innovation from JSME (iJSME)*, Hiroshima, Japan, pp. 1-2.
- **Jespersen, K. M.**, Lowe, T., Withers, P. J., Zangenberg, J., and Mikkelsen, L. P. (2015). Micromechanical Time-Lapse X-Ray CT Study of Fatigue Damage in Uni-Directional Fibre Composites. *Presented by first author at: International Conference on Composite Materials*, Copenhagen, Denmark, pp. 1-8.
- **Jespersen, K.M.** (2015), Modelling of Micro-structure from 3D X-ray CT of Fiber Composite, *Presented by first author at: International Symposium on Nanoengineered Composites*, Roskilde, Denmark.
- Emerson, M. J., **Jespersen, K. M.**, Jørgensen, P. S., Larsen, R., and Dahl, A. B. (2015). Dictionary Based Segmentation in Volumes. *In Image Analysis: 19th Scandinavian Conference on Image Analysis*, pp. 504-515.
- **Jespersen, K. M.**, Zangenberg, J., and Mikkelsen, L. P. (2015). Micromechanical Investigation of Fatigue Damage In Uni-Directional Fibre Composites. *Presented by first author at: International Conference on Fatigue of Composites*, Paris, France, pp. 1-8.

Contents

Preface i

Acknowledgements iii

Abstract v

Resumé vii

Publications ix

1 Introduction 1

1.1 Problem statement and motivation 1

1.2 Scientific objectives and achievements 3

1.3 Thesis overview 5

2 Designing against fatigue of wind turbine blades 7

2.1 Fatigue loads on wind turbines 7

2.2 Fibre composites used for wind turbine blades 9

2.3 Current methods to design against fatigue 11

2.4 Fatigue damage mechanisms of fibre composites 13

3 Fatigue damage assessment of fibre composites 19

3.1 Commonly used experimental methods 19

3.2 X-ray CT for materials science purposes 21

3.3 Combining experimental techniques 25

4 Summary of results 27

4.1 Visualising fatigue damage in fibre composites by X-ray CT 27

4.2 Ex-situ X-ray CT and TWLI monitoring of downsized specimens 28

4.3 Ex-situ X-ray CT and tension clamp solution for butterfly specimens . . . 30

4.4 Evaluation of 3D damage progression by Ex-situ fatigue testing 31

4.5 Combining experimental techniques to study fatigue damage initiation and progression 33

4.6 Established ex-situ X-ray CT fatigue testing method 35
4.7 3D damage progression scheme 37

5 Conclusion and outlook **39**

Bibliography **41**

A Appended papers **45**

Chapter 1

Introduction

This PhD thesis considers fatigue of fibre composites used for wind turbine blades, and is written as a compilation of six papers written during the PhD project carried out over 3 years in the Composites and Materials Mechanics section of the DTU Wind Energy department at the Technical University of Denmark (DTU). In addition to the papers, the thesis includes a description of the motivation behind the work, additional background knowledge to understand and put the appended papers into context, and a summary of the results of the PhD project. In the current chapter, the topic covered in the PhD project is introduced and its importance to society is motivated. The scientific objectives and achievements are then outlined, and an overview of the thesis structure is given.

1.1 Problem statement and motivation

With the increased global focus on reducing CO_2 emissions and obtaining a sustainable environment, power generated from sustainable energy sources such as wind turbines has increased significantly over the recent years. Fig. 1.1 illustrates the global cumulative installed wind capacity over the years, and it can be seen that the wind energy sector is rapidly growing and is expected to keep growing in the future.

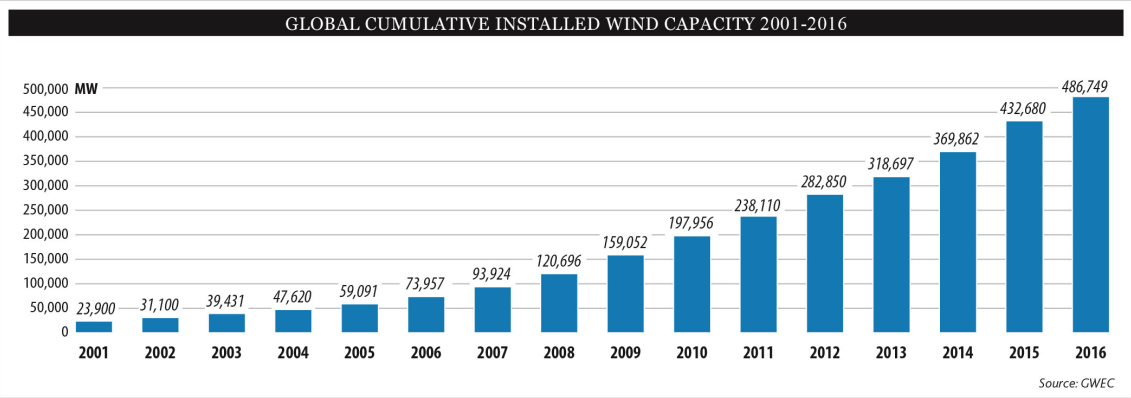

Figure 1.1: Cumulative installed wind capacity from 1997-2016 (source: GWEC [1])

However, to make it possible for wind energy to compete with fossil fuels without government support, it is still necessary to lower the cost of energy (CoE) produced by wind turbines. If defined in a simple manner, the CoE of a wind turbine can be defined as in

Eq. 1.1.

$$CoE = \frac{CoT + CoI + CoM}{PP} \tag{1.1}$$

where CoT is the cost of the turbine, CoI is the installation and transportation cost, CoM is the cost of maintenance, and PP is the power produced. It is seen that the CoE can be decreased by either decreasing the various costs (CoT, CoI, CoM) or by increasing the power produced (PP).

There are several approaches one can take in order to decrease the CoE of a wind turbine. One way is to increase the power produced by increasing the blade length or life time. Even though additional material is necessary to increase the blade length, up til now increasing the blade length has also decreased the CoE, as the power output is proportional to the blade length squared (swept rotor area). In addition, increasing the blade length can make it possible to use the wind turbines in areas with lower wind speeds. Therefore, wind turbines are getting larger and larger, as also shown in Fig. 1.2, and today the longest blades are almost 90 metres in length. The size of wind turbines is expected to increase further the years to come. Hence, it is necessary to design closer to the limit of the materials, which puts additional requirements to their properties.

One way to push the design limit is to obtain a better understanding of the material behaviour, making it possible to decrease the safety factors in the design. In addition, properly understanding the material behaviour could make it possible to improve the material properties. Pushing the design limit would result in less material and thereby reduce both the weight and cost of a wind turbine blade. However, to further push the design limit requires additional knowledge of the material behaviour under the loading conditions present, than currently available.

During a wind turbines 20-30 years of service life, the blades experience a high degree of repeated loading. In fact, the number of load cycles a wind turbine blade experiences is much higher than for other structures such as airplanes and cars. Therefore, material fatigue where the material properties decrease over time under repeated loading, is one of the main design concerns in wind turbine blade design. The main fatigue loads in a wind turbine blade are carried by the 'spar caps' commonly made from non-crimp fabric based fibre composites with the fibres mainly oriented in one direction (unidirectional) namely the loading direction. These unidirectional (UD) composites comprise around 60% of the total blade cost [2], and therefore material savings here would have a significant impact on the CoE.

The challenge, however, is that the damage mechanisms occurring under fatigue loading are not well understood for this type of fibre composite, and therefore several safety factors are necessary on the design. Properly understanding the damage mechanisms would help making realistic prediction methods both for the life-time and the degradation of the mechanical properties during fatigue loading. This is important, since excessive stiffness degradation can cause a wind turbine blade to collide with the tower, and the degradation of other material properties can also lead to catastrophic failures. Furthermore, understanding how fatigue damage initiates and progresses will make it possible to improve fibre composites by modifying e.g. the fabric layup or similar.

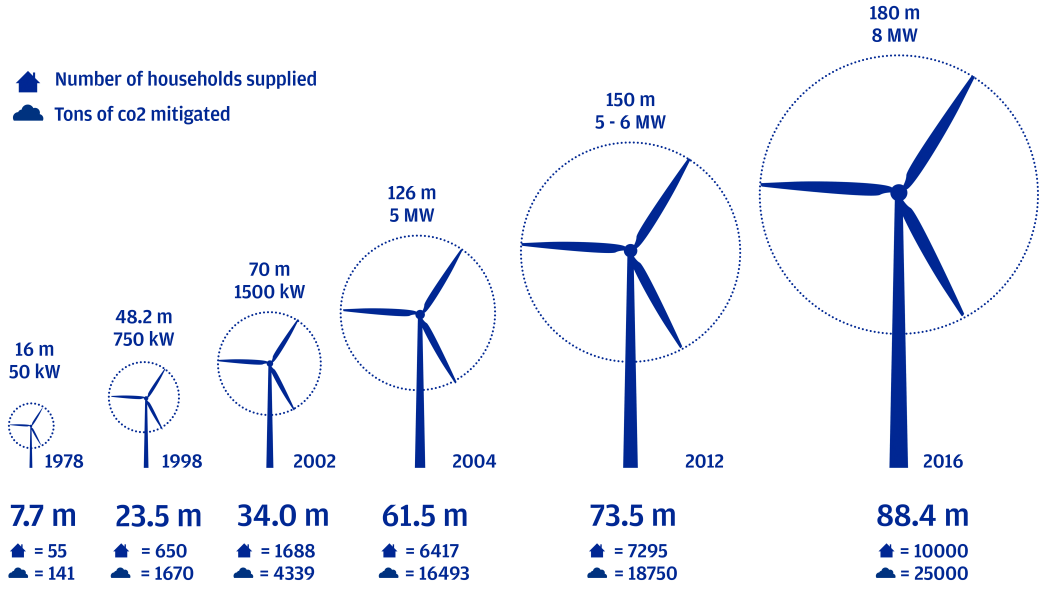

Figure 1.2: Growth in size of LM Wind Power Blades over the years. The blade length is indicated below the wind turbines and the power output in MW above.

To overcome the above mentioned challenges, fatigue damage progression of the UD fibre composites used for the spar caps of wind turbine blades carrying the fatigue loads from the wind and gravity was chosen as the research subject of this PhD project.

1.2 Scientific objectives and achievements

As there are many possible approaches to examine fatigue of fibre composites, it is necessary to choose specific focus areas. This PhD project was carried out with the aim of being able to link the damage mechanics on the micro scale with the macroscopic behaviour. In other words, to obtain a sufficient understanding of the damage mechanisms to be able to establish realistic prediction models. The project was carried out based on the philosophy of being able to perform X-ray CT based modelling of fibre composites under fatigue loading in the future. Fig. 1.3 shows this idea in the framework of the PhD project, that can be split into two main parts pointing towards the same goal. The part about quantification of the micro-structure was carried out in collaboration with DTU Compute, and has resulted in the co-authorship on several proceedings papers and one published journal paper [3]. The main results on this work will be part of a future PhD thesis by Monica Emerson, and focus in the present thesis is on the damage initiation and progression part.

With the base in 3D X-ray CT imaging, fatigue damage was observed at one point in time to obtain initiation knowledge on the damage mechanisms and later over time as

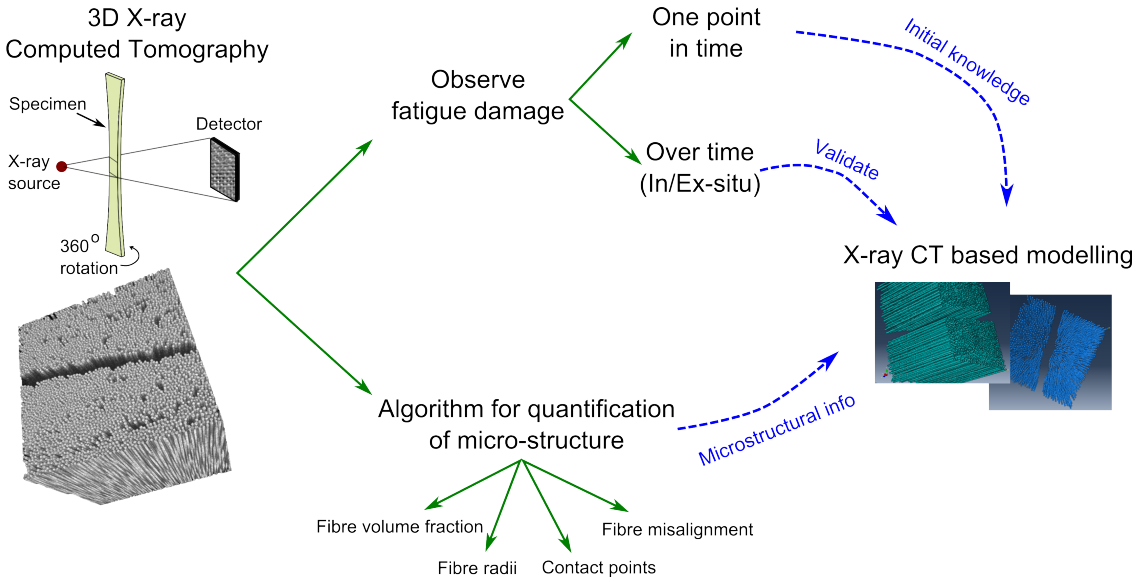

Figure 1.3: Illustration of the PhD project approach.

well. In parallel, studies on quantification techniques on the micro-structure of the fibre composite were carried out. Combining the output of these two parts makes it possible to do X-ray CT based modelling where the fibre architecture observed by X-ray CT is transferred and used for finite element modelling. The observed fatigue damage progression can be used as either input or validation purposes. The PhD project presented in this thesis had main focus on observing the fatigue damage initiation and progression, which resulted in presentation of the results at 7 international conferences with 4 full length proceedings papers [4–7] and 4 journal papers/manuscripts [8–11] (see also list of publications earlier).

The PhD project presented in this thesis was funded by the allianCe for ImagiNg and Modelling of Energy Applications (CINEMA) project, which is a five year project funded by the Innovation Fund Denmark. With the base in 3D imaging techniques primarily being X-ray CT, the CINEMA project focuses on coupling imaging techniques with modelling methods and establishes collaborations across several fields. The two main scientific topics of the CINEMA project is flow and damage, and this PhD thesis was carried out as part of the damage work package. The main collaboration within the CINEMA project was with DTU Compute on automatic segmentation and quantification techniques. Aside from gaining a deeper understanding of the damage mechanisms of fibre composites used for wind turbine blades, the research carried out during this PhD project has set the stage for using the X-ray CT data for finite element modelling by also being part of several collaborations in the CINEMA project.

Aside from the experiments carried out at DTU Wind Energy, X-ray CT experiments were also performed at Manchester X-ray Imaging Facility during two stays of four and ten days. Through these visits, knowledge about X-ray CT and segmentation methods was obtained. The work carried out in collaboration with Manchester X-ray Imaging Facility resulted in a journal paper ([P1]), two proceedings papers, and two posters. In addition, six months of the PhD project was carried out abroad at Waseda University in Japan.

Working in the Kawada-Hosoi laboratory resulted in the establishment of supporting work on using other experimental techniques to monitor damage features that cannot easily be seen with X-ray CT. This initiated the work on combining the advantages of several experimental techniques to lessen their total weaknesses, as will also be discussed later in this thesis. It additionally resulted in a collaborative journal paper currently in manuscript ([P5]) and a possible future PostDoc at this university.

1.3 Thesis overview

This thesis is written as a compilation of six papers made during the PhD project and also provide background information to put them into context. Chapter 2 will give an introduction to fatigue design of wind turbine blades and thereby provide a deeper understanding of why it is important to understand the damage mechanisms better. Here, an introduction to fatigue of fibre composites is also given. Chapter 3 then follows up with an introduction to experimental techniques commonly used for micro-scale damage observations of fibre composites, and a more detailed explanation is given of the X-ray CT technique. Chapter 4 gives a summary of the research results presented in the appended papers [P1-P6] including an explanation of the final established experimental technique and a damage progression scheme. Finally, some conclusions and future aspects are presented in Chapter 5.

Some of the figures in this thesis include a QR code linking to a video related to that figure. A QR code can be scanned by a smart phone using a 'QR code reader' application. The videos behind these QR codes only serve as additional information, and are not meant to be necessary to understand the content of the thesis. Therefore, it is not a requirement that the reader has the available tool to scan these codes.

Chapter 2

Designing against fatigue of wind turbine blades

In this chapter, the main aspects in relation to fatigue of wind turbine blade materials are outlined. First, the relevant blade loads are explained, followed by a description of the different types of materials typically used in the blade cross-section. The general approach used to design against fatigue is then discussed, and finally the fatigue damage mechanisms of fibre composites are introduced.

2.1 Fatigue loads on wind turbines

Fig. 2.1 shows a common wind turbine with a three blade rotor placed in front of the tower relative to the wind direction. The wind direction is measured during operation, and the rotor is automatically turned to face against the wind. When the blades are rotating they mainly experience two types of loading as also illustrated in Fig. 2.1. The wind loads cause the blades to bend backwards towards the tower in a flap-wise bending motion (Fig. 2.1a), and the weight of the blades cause the blades to bend in the direction of the ground in an edge-wise bending motion (Fig. 2.1b). The continuous rotation of the blades along with the variation of the wind speed result in repeated loading and unloading (cyclic loading) of the blades. This type of loading behaviour can give rise to material fatigue. The number of fatigue load cycles wind turbine blades experience during their 20-30 years of service life are in the range of 10^8-10^9 cycles, which is significantly higher than for other structures such as airplanes and cars. Since fatigue damage progression leads to degradation of the material properties such as the strength and stiffness, it is one of the major design concerns when designing a wind turbine blade. As material fatigue can cause premature failure, it usually has catastrophic consequences and should be avoided. Even if the blades themselves do not fail, it is important to maintain the stiffness of the blades so they do not risk colliding with the tower.

To live up to these requirements while still keeping the cost down in order to stay competitive, the materials used for wind turbine blades are chosen carefully to fit the loads present. As a result, the cross-section of a wind turbine blade is a hollow structure made from lightweight sandwich and fibre composite materials. Fig. 2.2 shows a sketch of a typical cross-section of a wind turbine blade with an indication of the load type along with the typical lay-up used [12]. The bending loads caused by the wind and gravity are carried by unidirectional composites, torsion and shear loads are carried by sandwich materials and multidirectional composites. Furthermore, sandwich materials with foams or balsa are commonly used to provide the shape to the aerodynamic shell and give the blade buckling resistance.

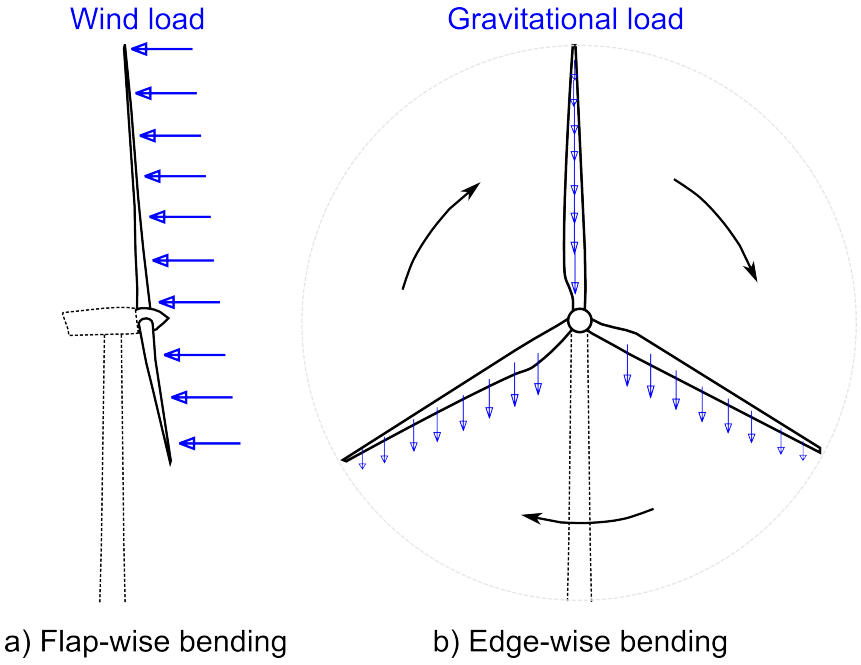

Figure 2.1: Main bending loads on wind turbine blades caused by (a) the wind and (b) the gravity.

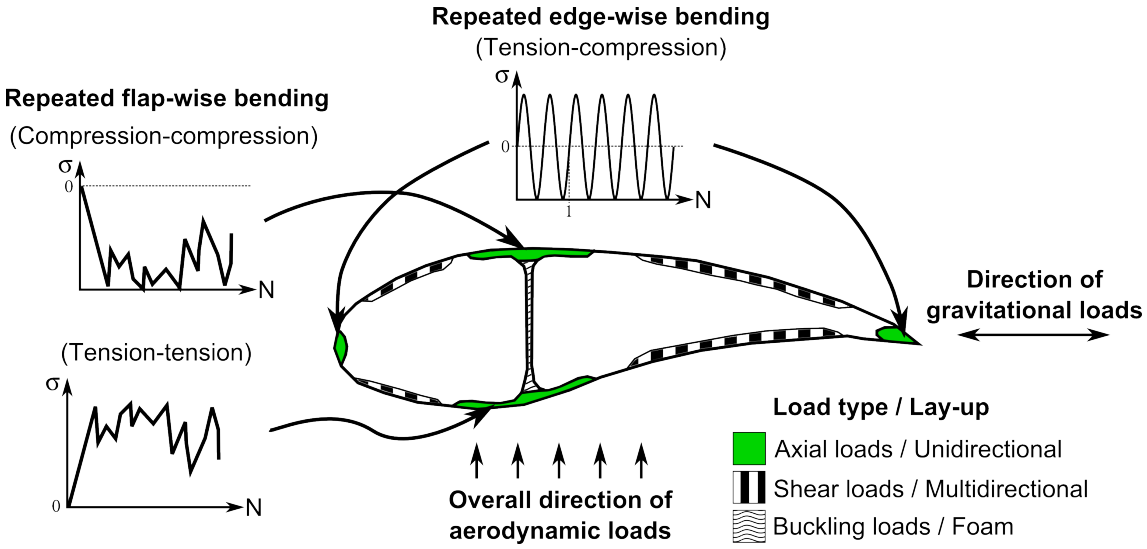

Figure 2.2: Typical cross-section of a wind turbine blade with indications of the loading types and typical composite layups used. Figure adapted from [12].

The parts marked in green in Fig. 2.2 show where the UD composites are used in the blade cross-section. Different parts of the blades experience different types of loading. As illustrated in Fig. 2.2, the UD composites on the suction side of the blade (top) mainly experience repeated compressive loading and on the pressure side (bottom) they experience repeated tensile loading. On the edges that mainly carry the edgewise bending

loads, they experiences a combination of tensile and compressive loading. The damage mechanics occurring in tension and compression are fundamentally different, and therefore they are usually considered separately. Although it is important to understand the fatigue mechanisms of all these loading conditions, the current project considers tension-tension fatigue as an initial step towards a full understanding. The methods can later be expanded to other loading conditions.

2.2 Fibre composites used for wind turbine blades

In this section the basics of composites is explained and a more detailed description of the UD non-crimp fabric (NCF) based composites used for the spar caps is provided.

Fibre composites, or more specifically fibre reinforced plastics, are polymeric materials reinforced by the addition of fibres. By combining the properties of stiff and strong fibres with a ductile polymer matrix, a fibre composite can obtain good strength and stiffness properties while at the same time being light weight and damage tolerant. Furthermore, fibre composites can be tailored to the specific applications by orienting the fibres in the direction of the loads present, decreasing the amount of material necessary. For these reasons, fibre composites are increasingly used in more and more applications, some of which are the wind, aerospace, and automotive industries.

Many types of fibre composites exist and Fig. 2.3 shows some common types. Other types such as pultruded and fillament winded composites also exist, but they will not be discussed in this thesis. The figure shows a comparison between a UD pre-impregnated (prepreg) laminate (Fig. 2.3a), woven fabric based composite (Fig. 2.3b), and non-crimp fabric (Fig. 2.3c), discussed individually in the section below. It should be noted that non-crimp and woven fabrics in principle also can be pre-impregnated, however focus in relation to fabric based composites will be on the vacuum infusing technique. Therefore, in this thesis and the appended papers a 'prepreg based laminate' will refer to the UD type with a reasonably homogeneous distribution of fibres within each layer as shown in Fig. 2.3a.

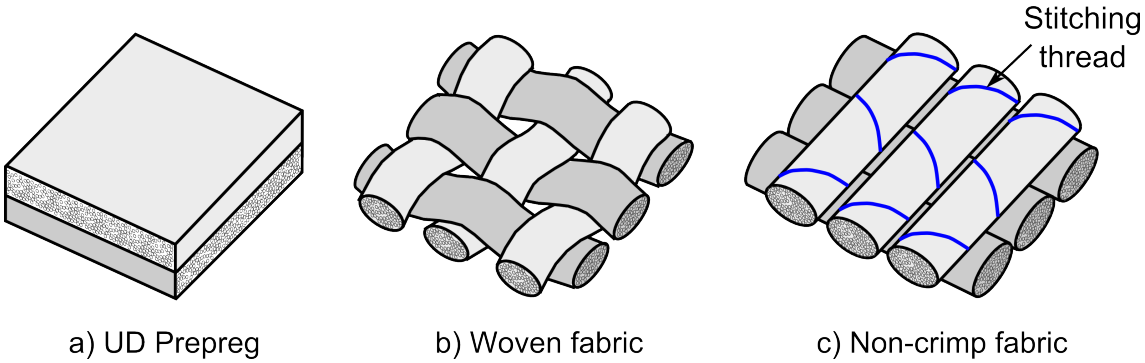

Figure 2.3: Comparison between a (a) UD prepreg laminate, (b) woven fabric, and (c) non-crimp fabric.

2.2.1 UD prepreg laminates

For UD prepreg laminates (Fig. 2.3a) the fibres are impregnated with matrix prior to forming the laminate. Instead of providing the dry fibres as can be done with fabrics, the manufacturer will provide them already impregnated in a matrix that is not completely cured yet. This method makes it possible to provide uni-directional layers of fibres that are only held in place by the semi-cured matrix. Prepregs need to be heated for the final curing to take place, however even at room temperature, or even if frozen, they will cure slowly over time. Therefore, they have limited shelf life and require means of heating such as an autoclave when forming the final component. Due to the production and manufacturing methods prepregs are expensive, but they are generally of high quality with high fibre content and good material properties. This type of composite laminate is commonly used in the aerospace and automotive industries.

2.2.2 Woven fabric based composites

Another type of composite is based on woven fabrics where bundles of fibres are woven into a weave similar to fabrics used for clothing. Fig. 2.3b shows an example of a plain weave, but several types of weaving patterns exist. This type of composite can be useful for impact applications, but also has the advantage of easy layup during manufacturing and the possibility of vacuum infusion to impregnate the fibres with resin, which is cheaper than prepregs. For some applications, 3D woven composites can also be useful as it is possible to obtain special mechanical properties depending on the weaving pattern. Nonetheless, due to the waviness of the fibres caused by the weaving pattern the stiffness and strength are less than for the UD prepreg laminates.

2.2.3 Non-crimp fabric based composites

Non-crimp fabrics utilise many of the advantages from woven fabrics, but with limited waviness of the fibres. Fig. 2.3c shows an example of a non-crimp fabric (NCF) where the fibre bundles are lying on top of one another rather than intertwining as was the case for the woven composite. Instead the fibre bundles are stitched together using stitching thread to obtain the fabric structure necessary for easy handling. Therefore, NCFs can obtain stiffness and strength properties close to those of the UD prepreg based counterparts. However, although at much higher cost, prepregs still can achieve superior material properties.

2.2.4 UD NCF composites used for wind turbine blades

The spar caps of a wind turbine blade that carry the main bending loads from the wind and gravity, are made from UD fibre composites where the fibres primarily is oriented in the loading direction. Since the wind energy industry is highly focused on cost, these UD composites are typically made from non-crimp fabrics infused with a polymer matrix by vacuum infusion. These composites are thick (several centimetres) at the root of the wind turbine blade and become thinner towards the tip. Commonly, layers of fabric are laid up

dry in a mould of the blade and half of a wind turbine blade is infused with the polymer matrix in one go. In some cases even the full blade is infused at the same time. This is a relatively cheap manufacturing method compared to those of the prepreg laminates commonly used in the aerospace and car industries.

The UD NCF based composites used for a wind turbine blades are slightly different from the NCF example shown in Fig. 2.3c. To make it possible to orient the fibre bundles in the same direction while still having a fabric structure, it is necessary to have something holding them together. This is commonly done by stitching the UD fibre bundles to a thin layer of supporting backing fibre bundles (∼10%) oriented in a different direction from the UD fibre bundles. Because of this, these composites are actually not entirely UD and therefore they are sometimes referred to as quasi-UD composites, which also helps not to confuse them with pure UD composites. This name will also be used in this remaining part of this thesis and some of the appended papers. For quasi-UD composites, several types of backing exist and Fig. 2.4 shows schematics of two types. Fig. 2.4a shows a quasi-UD NCF with $\pm 80^\circ$ backing fibre bundles, and Fig. 2.4b another that has backing fibre bundles oriented in the $\pm 45^\circ$ and 90° directions. Due to the bundle structure, this type of composite includes matrix regions where there are no fibres present (in between the fibre bundles). As will be clear later from the results of this PhD project, the backing layer plays an important role in the fatigue damage behaviour of quasi-UD composites.

Since these composites experience a high number of fatigue load cycles during the life of a wind turbine blade, it is necessary to design them in a way that fatigue damage will not be an issue. Therefore, standard methods to design against fatigue of fibre composite materials exist, however due to lack of knowledge on the damage mechanisms they include several uncertainties and safety factors. Current methods commonly used to design against fatigue of composites and their limitations will be covered in the next section.

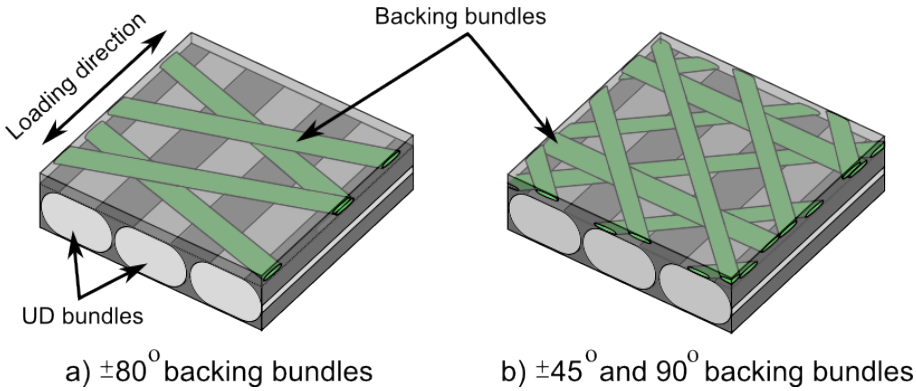

Figure 2.4: Two different types of non-crimp fabric with (a) a $\pm 80^\circ$ and (b) a $\pm 45^\circ$ and 90° backing.

2.3 Current methods to design against fatigue

Although studies considering fatigue of fibre composites [13–15] show that they experience damage mechanisms different from metals, the current methods to design against

fatigue commonly used by industry are still based on prediction methods adopted from steels. A typical approach to estimate the life time of structures under fatigue loading is the S-N curve, also sometimes called a Wöhler curve. Fig. 2.5 shows an example of this principle for constant amplitude loading, which is often the type of fatigue testing method used in the laboratory. Fig. 2.5a shows this type of loading that oscillates with a sinusoidal waveform between a maximum, σ_{max}, and a minimum load, σ_{min}. The ratio between these two is called the load ratio, R, and is defined by Eq. 2.1.

$$R = \frac{\sigma_{min}}{\sigma_{max}} \tag{2.1}$$

A commonly considered load ratio for tension-tension fatigue is R=0.1, and is also that studied in this PhD project. An S-N curve can be used to predict the lifetime as shown in Fig. 2.5b. Each point on an S-N curve is obtained by testing a sample to failure under fatigue loading at different stress (or strain) levels. Therefore, numerous experiments have to be carried out to establish one S-N curve.

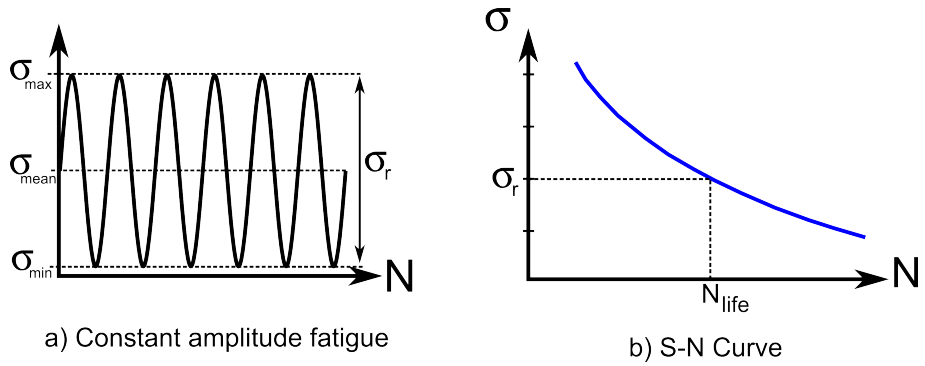

Figure 2.5: Principles of (a) constant amplitude fatigue and an (b) S-N curve.

Wind turbine blade design uses a slightly expanded yet similar approach. Fig. 2.6 shows a simplified example of a typical approach used to estimate the fatigue life of a wind turbine blade based on a given loading history. The wind loads on a wind turbine blade vary over time and therefore the rain flow counting method is commonly used to convert the load history into a stress range histogram stating a number of cycles at different stress ranges. When the stress range histogram is obtained, an S-N curve (or a constant life diagram) can be used to obtain the cycles to failure at each specific stress range. This is then followed by applying Miner's rule [16] to sum up the contribution from each stress range block to a damage parameter for the material [17]. The life is determined to be at its end when the damage parameter is equal to a certain value, which often is 1 [18]. For wind turbine blade design, constant life diagrams also taking the load ratio into account are commonly used rather than one single S-N curve as shown in Fig. 2.6. These constant life diagrams are based on S-N curves obtained from mechanical coupon testing at different stress ratios, and therefore materials testing at the coupon level, as considered in this thesis, plays an important role in the design of the actual wind turbine blades.

Although the approach explained above is well defined and simple to use, it includes

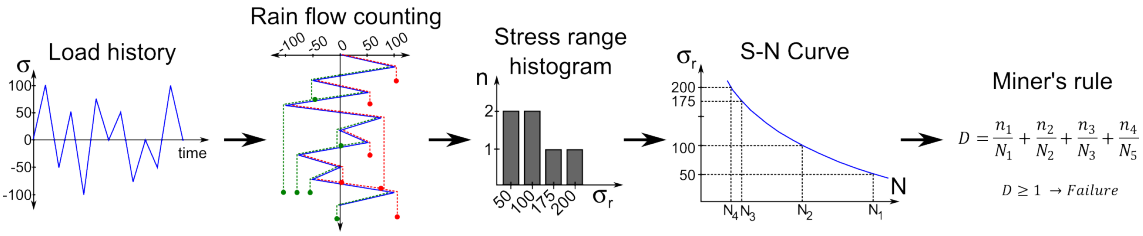

Figure 2.6: Simplified example of estimating the fatigue life based on the load history

a high degree of uncertainty leading to the use of various safety factors in the design. In addition, the approach outlined in Fig. 2.6 does not take into account the order in which the loads of various amplitude occur in the load history. This has been shown to affect the fatigue life of fibre composites [19, 20]. Furthermore, an S-N curve describes the fatigue properties of only one specific material system and stress ratio, and therefore a large number of mechanical tests have to be carried out. Finally, it is difficult to correctly measure the fatigue properties of quasi-UD fibre composites, since failure usually occurs where the test machine is gripping the specimen (tab region) rather than in the central part of the specimen (gauge section). The load is transferred from the test machine into the specimen mainly through shear forces, however these quasi-UD composites are much stronger in the axial direction than when subjected to shear, leading to premature failure in the tabs. Many attempts have been done to improve the test specimen geometry e.g. the butterfly shaped specimen described in [21]. However, although longer life-times were measured premature failure is still being observed.

Hence, the current approach to design against fatigue requires a high degree of experimental input and several safety factors have to be included due to the lack of knowledge on the occurring damage mechanisms. For these reasons, several studies on fatigue of composites have been carried out over the years, however it has still not been possible to realistically predict the lifetime of the quasi-UD composites used for wind turbine blades. The following section will explain the fundamentals of fatigue damage of fibre composites and explain some of what has already been done on this field up til now.

2.4 Fatigue damage mechanisms of fibre composites

Damage occurring in materials subjected to repeated loading at stress levels below the static strength of the material is referred to as fatigue damage. In the case of metals, fatigue damage initiates from defects and gradually grow in size often in a specific direction that depend on the loading conditions. Because of the extensive work carried out on fatigue of metals over the years, the fatigue damage mechanisms are better understood than for fibre composites. As a result, methods exist that can predict the fatigue damage progression in metals often with good results. However, in the case of fibre composites, it is still difficult to model the fatigue damage progression realistically. Although the polymeric material surrounding the fibres itself is a homogeneous material, the presence of the stiff reinforcing fibres makes it difficult to predict how a crack will grow.

Fig. 2.7 shows a sketch of the three basic damage mechanisms occuring in fibre composites: matrix cracking, interfacial debonding, and fibre failure. Cracks can appear in the polymer matrix both in regions of pure matrix and along the interface of the matrix and fibres as shown in Fig. 2.7a. This type of damage is often called matrix cracking. When the matrix and fibre detach from one another it is referred to as interfacial debonding as shown in Fig. 2.7b. Fibre fractures are when fibres break as seen in Fig. 2.7c, and will generally also be associated by interfacial debonding locally close to the fibre fracture.

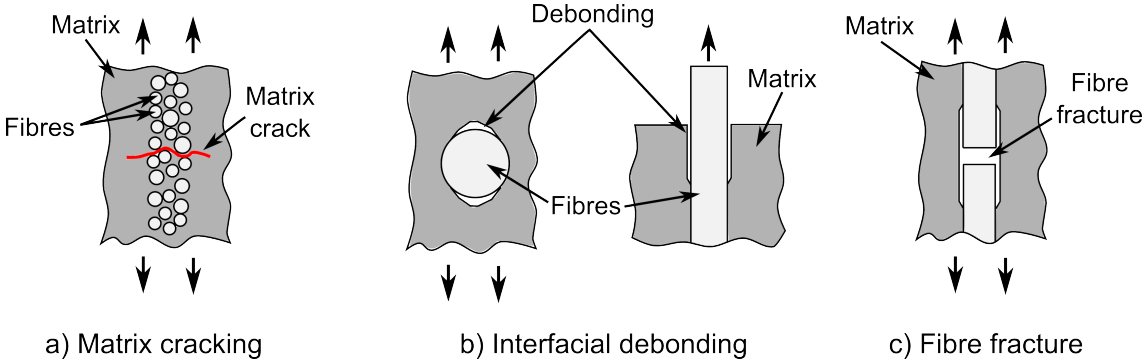

Figure 2.7: Basic types of fracture for fibre composites.

The fatigue damage mechanisms of fibre composites depend on the constituent materials, fibre architecture, lay-up, among other things. Therefore, the damage mechanisms of quasi-UD NCF composites are different from those of the more commonly considered prepreg based laminates. However, a considerable number of studies have been carried out on prepreg based laminates, and it is important to understand the basic mechanisms observed from these studies.

2.4.1 Fatigue damage in prepreg based laminates

In the case of prepreg based laminates commonly considered in the aerospace and automotive industries [13, 14, 22–25], cross-ply and quasi-isotropic lay-ups are commonly studied. For cross-ply composites the fibres are only oriented in the 0° and 90° direction, whereas quasi-isotropic layups try to mimic the isotropic behaviour of metals by placing fibres in the 0°, ±45°, and 90° directions.

Fig. 2.8 shows a schematic of the occurring damage mechanisms during the life-time typically seen for a quasi-isotropic fibre composite established by Reifsnider [26]. Initially (1) matrix cracking occurs in the transverse and off-axis layers causing an initial rapid increase of damage that relaxes with the saturation of these cracks. This is followed by the coupling of cracks through interfacial debonding (2) leading to delamination (3). Finally growth of delaminations occurs (4) and localised fibre fractures are observed, causing an unstable behaviour and eventually final failure (5). During all stages of the fatigue life, some extent of fibre fractures is said to appear. The curve in Fig 2.8 is commonly divided into three stages. Stage I where the damage increases rapidly, stage II where the damage increases almost linearly, and stage III where a rapid damage accumulation is caused by the localisation of damage that leads to final failure. Sometimes these stages are also shown on the normalised stiffness degradation curve during fatigue loading.

Several studies have been done on methods to model the influence of damage on various material properties [13, 14, 27–33], however they usually consider matrix cracking and delamination, which is a big part of the damage for quasi-isotropic and cross-ply composites. Particularly models including the effect of fibre fractures are still lacking. As a result, models where the results are fitted to experimental data to make up for the lack of knowledge on the damage mechanisms still exist.

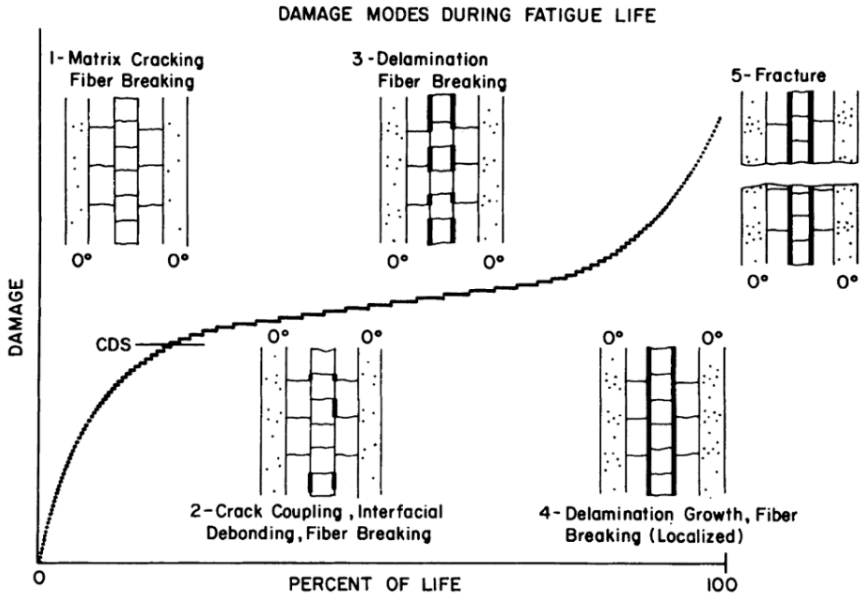

Figure 2.8: Schematic of occurring damage during the fatigue life of a fibre composite laminate proposed by Reifsnider [26]

Fibre fractures play a big role in the degradation of the material properties of quasi-UD composites, and therefore it is especially important to understand their initiation and growth behaviour to be able to do realistic modelling in the future. The next section will present the understanding of damage of quasi-UD composites prior to the current PhD project, but also introduce some terminology to make it easier to understand the results presented in the appended papers.

2.4.2 Fatigue damage in UD NCF composites

The damage mechanisms of the quasi-UD composites used for wind turbine blades are a bit different from prepreg based laminates. Fig. 2.9 shows a sketch of the most commonly observed damage mechanisms for quasi-UD composites subjected to tension fatigue loading. Off-axis cracks in the backing fibre bundles initiate relatively early in the fatigue life, and have been seen to cause fibre fractures in the nearby UD fibre bundles. Interfacial debonding is also observed along the UD fibres near fibre fractures. Sometimes debonding between whole fibre bundles and intralaminar splitting in the UD fibre bundles running along the UD fibre direction, as also indicated in Fig. 2.9, can also be observed.

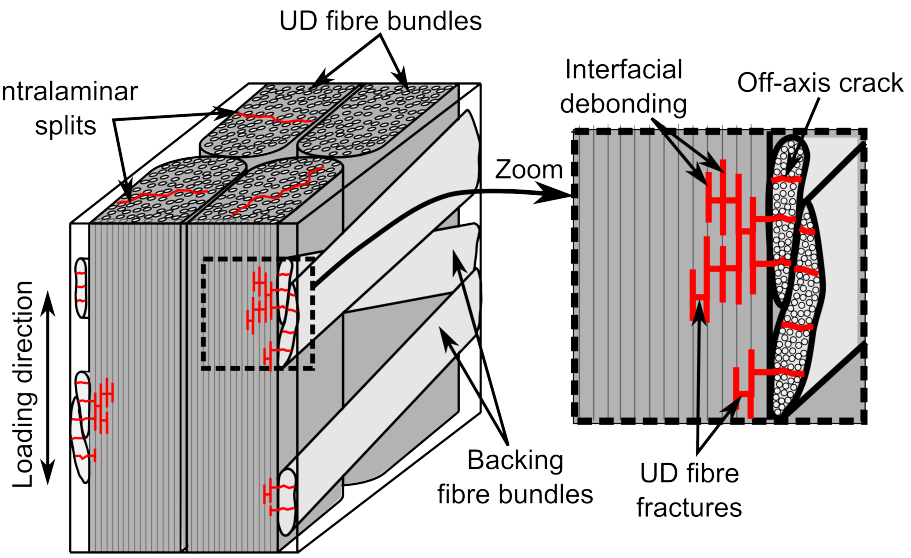

Figure 2.9: Different tension fatigue damage mechanisms commonly seen in quasi-UD composites

Zangenberg et al. [34] established a damage progression scheme for a quasi-UD composite with a backing of the type shown earlier in Fig. 2.4a. A simplified version of the scheme is shown in Fig 2.10 [8]. The figure shows the three main stages of the fatigue life in terms of stiffness degradation, and the accompanied damage mechanisms. The scheme states that the initial stiffness degradation observed in stage I of the fatigue life is caused by off-axis cracks in the backing fibre bundles, which is similar to the scheme by Reifsnider for prepreg based laminates shown earlier in Fig. 2.8. These off-axis cracks in the backing fibre bundles then cause UD fibre fractures in the nearby UD bundles, and the initiation and growth of these fibre fractures are the main cause of the stiffness degradation during stage II. Hence, rather than being delamination controlled as argued in the scheme for prepreg based laminates, the stiffness degradation during stage II was said to be fibre fracture controlled. Stage III is when localisation occurs and the remaining fibres cannot carry the load anymore leading to final failure, which is similar to prepreg laminates. The scheme presented by Zangenberg et al. was established based on scanning electron microscopy (SEM) observations at one specific damage state late in the fatigue life, and therefore this progression process could only be built on speculations.

The work carried out in the current PhD project considered monitoring the actual damage progression in 3D, which has lead to a deeper understanding of the damage initiation and progression of the off-axis crack in the backing fibre bundles and the fibre fractures in the UD fibre bundles. This has resulted in a slightly modified and expanded damage scheme discussed later in Section 4.7. To properly understand the experimental work carried out in this PhD project, it is necessary to outline the most commonly used methods for damage assessment of fibre composites, and this is discussed in the next chapter. A particular focus is put on non-destructive methods that makes it possible to monitor the damage progress during fatigue loading, in particular the 3D imaging technique X-ray CT.

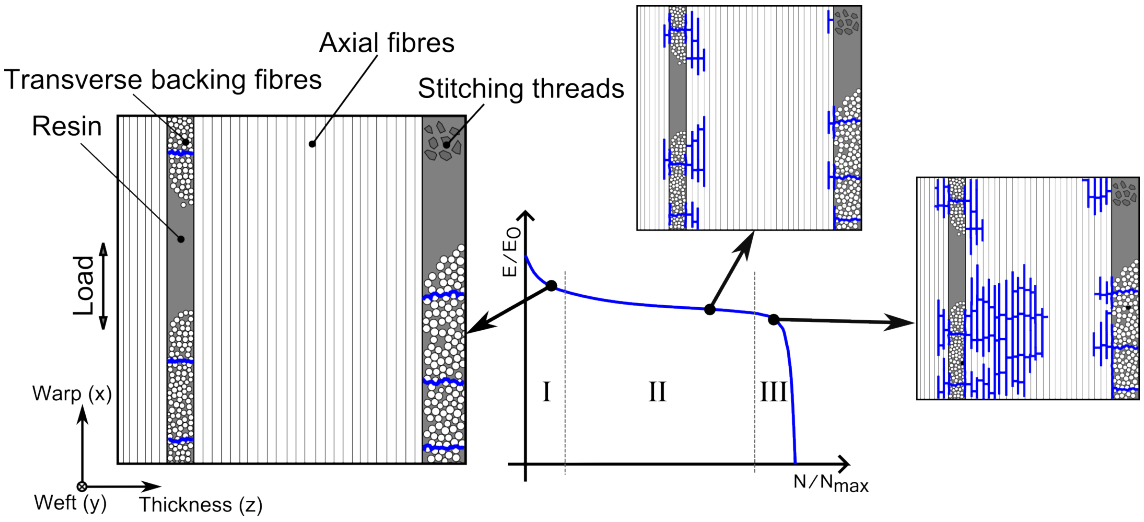

Figure 2.10: Simplified version of damage progression scheme originally proposed by Zangenberg et al. [34] and presented in the simplified form in [8]

Chapter 3

Fatigue damage assessment of fibre composites

In this chapter, the most commonly used experimental methods for damage assessment on the fibre scale of fibre composites will be outlined and some of their advantages and disadvantages discussed. Focus is then put on the non-destructive 3D imaging technique X-ray CT for materials science purposes, and the chapter closes with discussion of ways to combine the advantages of different experimental methods to eliminate or decrease the disadvantages.

3.1 Commonly used experimental methods

A range of different experimental methods that all have their own advantages and disadvantages have been used for observing the damage in fibre composite over the years. For example, some of the commonly used techniques, such as optical microscopy and scanning electron microscopy, have the drawback of being destructive and/or only consider the surface of a specimen. Likewise, non-destructive methods such as acoustic emission, ultrasound, X-ray radiographs, and X-ray computed tomography (CT) each have their individual disadvantages. This section will explain the basics of some of these techniques in relation to damage observations of fibre composites.

3.1.1 Destructive examination

Some of the commonly used experimental techniques to observe damage in fibre composites are optical microscopy and scanning electron microscopy (SEM). Fig. 3.1 shows examples of damage in quasi-UD composites observed by optical microscopy and SEM of an off-axis crack in a backing fibre bundle. It is seen that high resolution can be obtained, making it possible to clearly clearly see the different damage mechanisms mentioned earlier (Fig. 2.9).

However, although examination using these techniques are not in themselves destructive, the sample preparation required usually makes it difficult to continue testing of the considered coupon test specimen, since it is usually necessary to cut out smaller samples for polishing. Furthermore, it is only possible to monitor the surface of the specimen and it is possible that the polishing process induce additional damage to the surface. For these reasons, these techniques are generally referred to as destructive in relation to observing damage in composite materials. Hence, although it is possible to achieve high

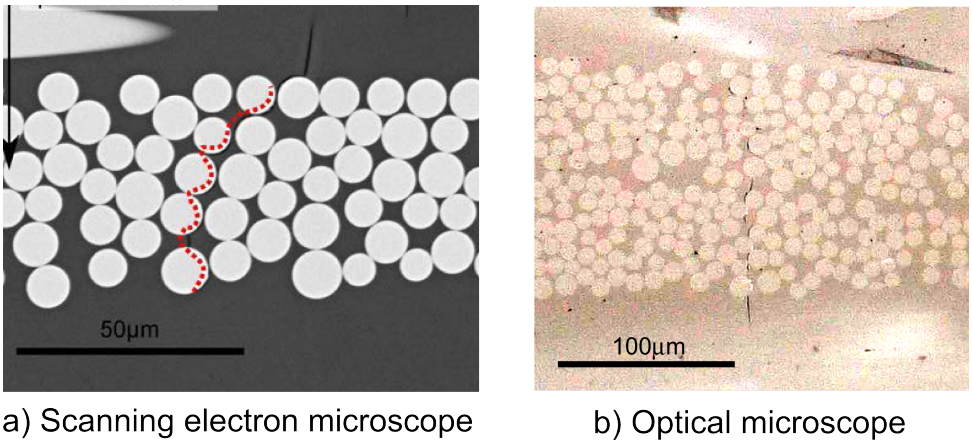

Figure 3.1: Example of matrix cracks observed by (a) scanning electron microscopy (from [34]) and (b) optical microscopy.

resolution providing important knowledge, it is generally not easy to monitor the damage progress using these techniques. Sometimes microscopy has been used to observe the damage progression on specimen edges, however the damage at this location might be highly influenced by edge effects. Other studies have performed loading specimens inside a SEM to monitor the damage progression, however such specimens are very small and the damage monitored is only what is visible on the surface of the specimen.

Approaches where the polymer matrix is burned off and location of fibre fractures are examined under the microscope has also been carried out [34]. This can provide information on what happens inside the specimen, however with the polymer matrix removed the fibres can easily move and it is more difficult to relate the locations of the damage to one another. Furthermore, damage related to the matrix will not be visible and therefore only fibre fractures can be observed by this method.

3.1.2 Non-destructive examination

Non-destructive examination methods are also used for damage assessment of damage in fibre composites, however a general issue of these techniques is that the obtainable resolution is significantly lower than for optical microscopy and SEM imaging. Some of these methods are acoustic emission, thermocamera, camera imaging, X-ray radiography, ultrasound imaging, and X-ray computed tomography (CT), some of which are explained in the following.

Thermocamera imaging

Since initiating and propagating damage generates heat, thermocameras are sometimes used to continuously monitor a specimen during testing (e.g. [35]). This can give an idea of where the damage initiates and grow, however the temperature is measured on the surface of the specimen. Therefore, it is likely that the damage initiates earlier than what is measured by the camera. Similarly, the damage needs to have a certain size before it

will be visible on a thermocamera.

High resolution camera imaging

High resolution cameras can be used to monitor the damage occurring in a test specimen during the test. This is a relatively simple way to obtain knowledge on how a specimen fractures on the macroscopic level. One example could be to monitor the growth of a macroscopic crack propagating along an interface in a double cantilever beam test. Another way high resolution camera imaging can be used is to capture images of a transparent specimen illuminated from the back. The light will reflect on the cracks in the specimen making them visible in the camera images. This technique, also called transilluminated white light imaging (TWLI), has been used to monitor damage in glass fibre composites since they are transparent [25, 36]. However, the technique cannot be used for too thick composites and composites with carbon fibres or other fibres that are not transparent.

X-ray radiography

As an alternative to TWLI that cannot be used for carbon fibre composites, X-ray radiography has sometimes been used to monitor damage as well [13, 24]. X-ray radiography is similar to that used by the doctor to examine bones where the contrast in the image is obtained by the difference in density of the materials subjected to X-rays. To enhance the contrast of the cracks a contrast agent with a high density and low viscosity is usually applied to the specimen before examination. The contrast agent enters cracks from the edges of the specimen and increases their visibility in the radiographs. The main issue with this technique is that the damage has to be connected to the edges to appear in the images, which is not always the case. Furthermore, depending on the image resolution, the cracks needs to have a certain size before they become visible in the radiographs.

3D imaging methods

The techniques mentioned so far only provide 2D images, and in many cases the occurring damage mechanisms are actually 3D features. It is possible to use ultrasound imaging to obtain 3D information of the damage inside a structure, however it is generally used on larger length scales [37]. New advances within X-ray CT has opened up for new opportunities of monitoring damage initiate and progress in 3D. As X-ray CT is the main technique used in the work carried out in this thesis, it will be explained separately in more detail in the next section.

3.2 X-ray CT for materials science purposes

In recent years, X-ray CT has been increasingly used to visualise and study the internal structure of materials in 3D and has provided valuable new knowledge. Especially within

composite materials it has found its use both to characterise the fibre architecture [3, 38–42] and to observe damage [7, 8, 43–53]. Since the contrast in the images depends on a difference in material density, it is especially well suited for glass fibre composites with polymer matrices, as the difference in density is around a factor 2. To give an idea of what can be achieved, Fig. 3.2 shows an example of X-ray CT images at the fibre bundle scale (Fig. 3.2a), fibre scale (Fig. 3.2b), and an example of UD fibre fractures (Fig. 3.2a) obtained during this PhD project. Hence, X-ray CT can be very useful, but there are also several of challenges in relation to using this technique. To properly understand these challenges it is necessary to understand the basic principles of X-ray CT, which is explained in the next section.

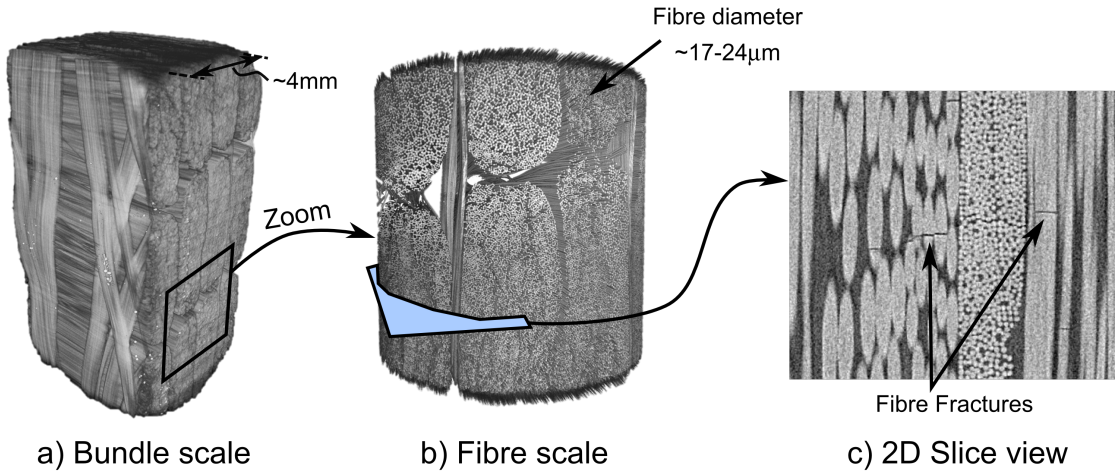

Figure 3.2: 3D visualisation of a quasi-UD composite from X-ray CT experiments carried out in the PhD project. Here (a) shows the bundle structure, (b) fibre architecture, and (c) a slice view showing UD fibre fractures near a cross-over region of the backing fibre bundles.

3.2.1 Basic principles of X-ray CT

An X-ray CT image is in principle a series of X-ray radiographs, or 'projection images', of a sample captured from different angles, which after acquisition are combined into one 3D image. Fig. 3.3 illustrates this principle. The sample is placed on a rotation stage in between an X-ray source and a detector, and then rotated in steps while capturing projection images for each rotation step. Usually this is done over a full rotation (360°) a half rotation (180°). A higher material density makes fewer X-rays pass through to the detector, giving a variation of X-ray counts and thereby also a variation in the intensity of each pixel on the detector. This variation is what gives the contrast in the image, as also illustrated for a simple cylindrical homogeneous sample in Fig. 3.3. On the part of the detector where the sample was in the way of the X-ray's path, the count is lower than for the surrounding parts where they passed through the air. As also mentioned for X-ray radiographs, contrast agent (also sometimes called staining) can be used to enhance the contrast of cracks. However, the contrast agent has to enter from the surface and therefore

only damage connected to the surface will become visible.

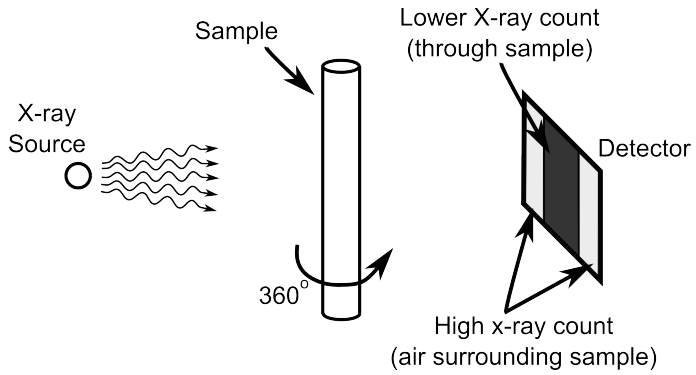

Figure 3.3: Basic principle of X-ray Computed Tomography with a homogeneous cylindrical sample.

The pixel size of the projection images can be modified by adjusting the source-to-sample and sample-to-detector distances (geometrical magnification), and sometimes an additional optical magnification is built into the detector. Since there is a fixed number of pixels on the detector, obtaining a smaller pixel size also results in a smaller considered volume. Although several volumes can be stitched together, this is an important limitation of the technique, as it can take a long time to acquire all the projection images.

After acquiring all the projection images, a reconstruction algorithm is used to create the 3D image. Several reconstruction algorithms exist, but one of the more commonly used is the 'filtered back projection' algorithm. Fig. 3.4 shows the principle of this reconstruction algorithm for the simple case of the cylindrial homogeneous sample shown in Fig. 3.3. Fig. 3.4 shows reconstructed images of the cross-section of the cylindrical sample for 8 (Fig. 3.4a) and 16 (Fig. 3.4b) projection images. For an increasing number of projection images the reconstructed image gets closer to the scanned object, which in this case will give a circle in the top view. The blur caused by this reconstruction method, as also seen by the noise surrounding the circle in Fig. 3.4b, is filtered out subsequently.

The reconstructed image can be stored in different ways depending on the X-ray CT equipment, however it is common to store it as slices of 2D images typically in the tiff format, as it can be opened on any computer. It should be noted however, that some image quality might be lost compared to the original format. The file size depends on the scan settings, but it is not uncommon that a folder with the raw data and the reconstructed image is larger than 10 GB and in some cases it might even been significantly larger. Because of these file sizes, 3D visualisation and other types of data handling puts special requirements to the computer hardware and storage capabilities.

The challenge in relation to handling of X-ray CT data is not only the requirement to the computer, but also that automatic segmentation often is not possible. To segment something in a image means to somehow mark specific features, e.g. fibres or cracks, making it possible to visualise only these features in a 3D image. In some cases, segmentation can be done by applying a threshold of the greyscale values in the image. In other words, only mark pixels with greyscale values in a chosen range. However, it is often the case that simple segmentation methods do not suffice and therefore it is common to do man-

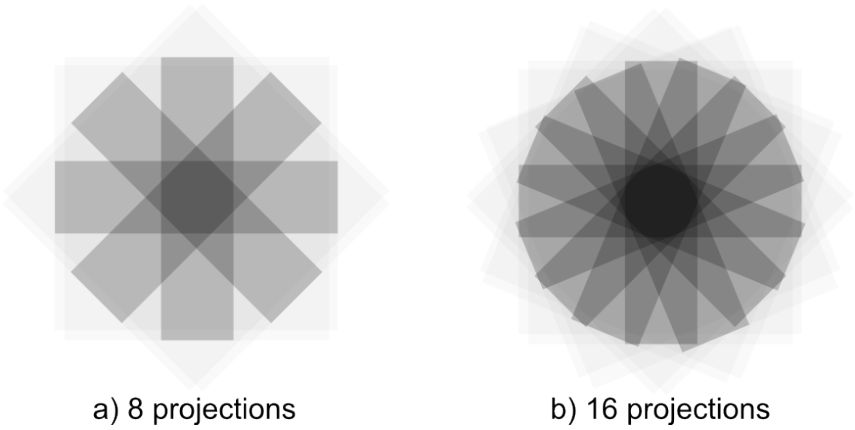

Figure 3.4: Top view of reconstructed image of cylinder by the 'filtered back projection' method for (a) 8 and (b) 16 projection images.

ual segmentation of features in the image. This is very time consuming for 3D images and also based on subjective judgement of the person doing the segmentation. Nevertheless, for the cases where automatic methods cannot be applied this is a necessary part of the data handling of X-ray CT data.

3.2.2 Synchrotron vs. laboratory X-ray CT

X-ray CT can be split into two main types: synchrotron radiation and laboratory (micro-focus) X-ray CT. In synchrotron radiation based X-ray CT, electrons are accelerated in a circular particle accelerator (storage ring), and bending magnets or similar are used to generate X-rays. Since a storage ring needs to have a certain size, synchrotron facilities are very large structures - sometimes even around a kilometre in diameter. Such a facility has several beam lines where X-ray CT can be carried out, however they are generally difficult to access. Laboratory based X-ray CT uses micro-focus based X-ray sources. This type of X-ray CT scanner is a few metres in size and can therefore be placed in a regular laboratory. This makes it much easier to access and gives a larger degree of freedom for the studies that can be carried out. However, the intensity of a micro-focus X-ray source is significantly less than for synchrotron radiation, resulting in much larger scan times for laboratory X-ray CT. A scan taking a few minutes on a synchrotron can easily take several hours on a laboratory X-ray CT scanner. Therefore, synchrotron based X-ray CT is more suited for studies where things change over time. However, for some applications the advantage of being able to perform the X-ray CT experiments in the laboratory outweighs a synchrotrons advantage.

Hence, synchrotron radiation CT is more suited for 'in-situ' experiments where the sample is tested inside the X-ray CT equipment. However, if the material does not experience any significant changes over time, 'ex-situ' experiments can be sufficient. Performing experiments ex-situ can be when the mechanical testing of the sample is performed outside the X-ray CT equipment, and the test is repeatedly interrupted for X-ray CT examination. Particularly for fatigue damage in fibre composites, the damage is not expected to change

while the test is interrupted. In addition, due to the long fatigue life of the quasi-UD composites considered in this PhD project, it is necessary to carry out a high number of fatigue load cycles. Therefore, laboratory X-ray CT and an ex-situ fatigue testing approach was chosen for the work carried out during the current PhD project.

3.3 Combining experimental techniques

Some of the work carried out during this PhD project is done based on the idea of combining X-ray CT with other experimental techniques to overcome some of the weaknesses of X-ray CT. If performing an ex-situ fatigue test where the test is stopped several times for X-ray CT examination, it is possible to use other techniques to monitor the sample during fatigue testing. In principle, it is possible to simultaneously carry out most of the non-destructive examination techniques outlined in Section 3.1.2 during a fatigue test. However, the addition of observation techniques also means more data that has to be handled and linked to one another somehow. Therefore, it makes sense to one by one add techniques that provide additional knowledge and establish appropriate data handling methods gradually. One of the issues of X-ray CT in relation to observing the damage of the quasi-UD composites used for wind turbine blades is that off-axis cracks in the backing bundles are not always visible. Therefore, in this PhD project it was chosen to combine X-ray CT with TWLI imaging where off-axis cracks are easily visible to support the X-ray CT experiments. The work carried out in [P4], [P5], and [P6] appended to this thesis is related to combining these two techniques.

Chapter 4

Summary of results

This chapter summarises the results obtained throughout the PhD project. First, summaries are given of the appended papers [P1-P6], and this is followed by a description of the established ex-situ X-ray CT fatigue testing method including a brief discussion of the future work in this context. Finally damage progression scheme established based on prior knowledge combined with the new the results will be presented and discussed. For clarity, the full paper reference along with the considered material system and specimen type is written in the top of each summary. The summaries provided here are written as short summaries that connect the work together and therefore the reader is referred to the appended papers for more detailed information about each individual study.

4.1 Visualising fatigue damage in fibre composites by X-ray CT

[P1] *Jespersen, K. M., Zangenberg, J., Lowe, T., Withers, P. J., & Mikkelsen, L. P. (2016). Fatigue damage assessment of uni-directional non-crimp fabric reinforced polyester composite using X-ray computed tomography. Composites Science and Technology, 136, 94–103.*

Material system: Glass fibre/polyester, layup $[b/0,b/0]_s$ with b=$\pm 80^\circ$

Specimen type: 410x25x4mm butterfly cut into 110x5x4mm for X-ray CT after testing

The initial work carried out during this PhD project considered establishing a method to observe the micro-structural fatigue damage in a quasi-UD composite with $\pm 80^\circ$ backing fibre bundles (Fig. 2.4a) by laboratory X-ray CT, and was presented in [P1]. The overall experimental approach in [P1] is illustrated in Fig. 4.1. In order to obtain sufficient resolution to observe individual fibre fractures, cut-outs were made from different butterfly specimens tested in fatigue and interrupted at a different number of load cycles. X-ray CT scans were then performed on the cut out samples to observe the internal damage in 3D.

The work presented in [P1] provided knowledge on the typical location of damage regions based on the fibre bundle structure. It was found that fibre fractures in the UD fibre bundles would be located in regions where the supporting backing fibre bundles were crossing over one another. Furthermore, it was found that if there was a layer of matrix material in between the backing and UD fibre bundles, UD fibre fractures were not observed. Hence, damage was found to be local phenomena near the cross-over regions of backing fibre bundles that were 'in contact' with a UD fibre bundle. This was both important to understand how the material could be improved, but also in relation to locating the damage regions in later studies, since obtaining a high resolution X-ray

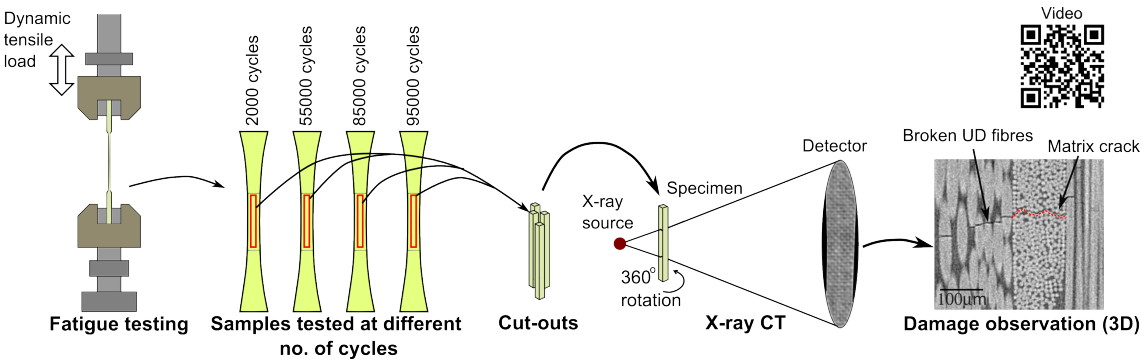

Figure 4.1: Illustration of the experimental approach for the experiments carried out in [P1].

CT image requires a small considered volume. In other words, one needs to know where to look for damage, as it does not appear everywhere in the specimen. Furthermore, the UD fibre fractures appeared as 3D phenomena, highlighting the importance of considering the damage progression in 3D. In addition, the UD fibre fracture regions observed in [P1] seemed to progress into the thickness direction of the UD bundle with an increasing number of cycles as was also stated in the postulate by Zangenberg et al, but the considered damage regions were in different samples and therefore it could not be said for sure at this point.

4.2 Ex-situ X-ray CT and TWLI monitoring of downsized specimens

[P2] *Jespersen, K. M., Wang, Y., Zangenberg, J., Lowe, T., Withers, P. J., & Mikkelsen, L. P. (2016). Ex-Situ Time-Lapse X-Ray Ct Study of 3D Micro-Structural Fatigue Damage Evolution in Uni-Directional Composites. ECCM17 - 17th European Conference on Composite Materials, (June), 26–30.*

Material system: Glass fibre/polyester, layup $[b/0,b/0]_s$ with b=$\pm 80°$

Specimen type: 110x5x4mm rectangular

With the aim of making it possible to monitor the actual damage progression in a specimen during fatigue loading, [P2] presented a method to perform ex-situ X-ray CT fatigue testing on downsized rectangular test specimens. Furthermore, [P2] also presented initial work on using TWLI imaging to monitor the off-axis crack growth in the backing fibre bundles. The overall experimental approach is illustrated in Fig. 4.2. With a length of only 110mm, the downsized specimens could easily be mounted in the X-ray CT scanner, and due to their relatively small cross-sectional area a high image resolution could also be obtained. TWLI imaging was used to continuously monitor the off-axis crack initiation and growth by automatically capturing photos at the maximum load while the fatigue test was running. In addition, the stiffness degradation was measured by extensometers throughout the fatigue test. The fatigue test of one of the downsized specimen was in-

terrupted after a number of fatigue cycles and scanned by X-ray CT in a location chosen based on the damage observed in the TWLI images. This sample was then later tested further in fatigue, and scanned again in the same region. Hence, this was an ex-situ X-ray CT study with two interruption points.

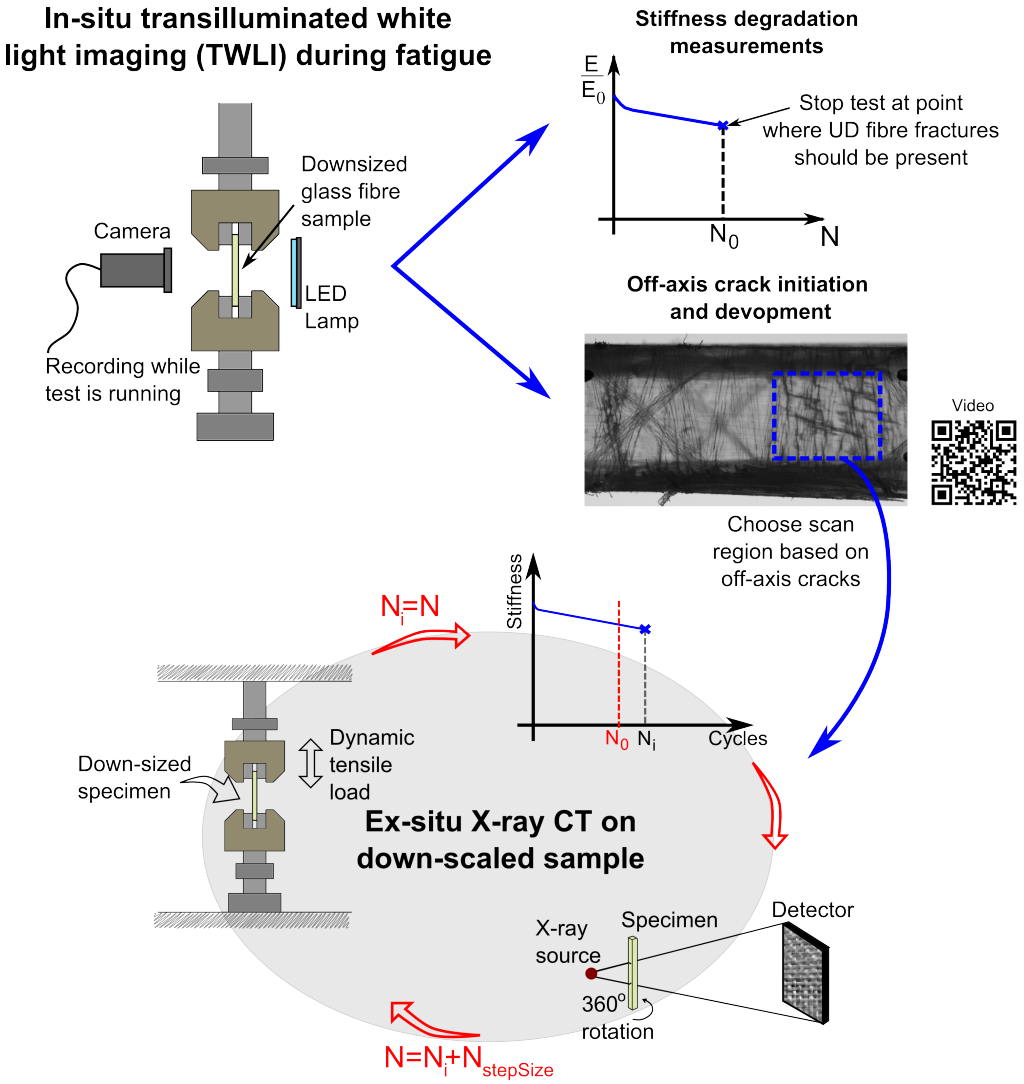

Figure 4.2: Illustration of the experimental approach for the experiments carried out in [P2]. TWLI is used to monitor the off-axis crack development in the backing fibre bundles of a down-sized test specimen and to locate an appropriate region for X-ray CT examination. Ex-situ X-ray CT fatigue testing is then subsequently performed on the specimen in the chosen region.

The region examined by X-ray CT contained UD fibre fractures already at the first interruption point, and no significant change was observed at the next interruption point. However, since the stiffness of the sample had decreased between the two interruption points, it seemed that this particular damage region had stopped growing and that other damage regions progressed instead. However, comparing the measured stiffness degra-

dation to the TWLI images indicated that the stiffness degradation was significantly affected by the edge effect. Therefore, this could also be part of the reason for the stiffness degradation between the two interruption points despite the lack of growth of damage in the considered volume. Hence, the work presented in [P2] showed the importance of considering a sufficiently wide test if the focus is on what is going on away from the edges. Because of this, additional focus was put on making it possible to consider a larger specimen in the later studies carried out during the PhD project.

4.3 Ex-situ X-ray CT and tension clamp solution for butterfly specimens

[P3] *Jespersen, K. M., & Mikkelsen, L. P. (2016). Fatigue damage observed non-destructively in fibre composite coupon test specimens by X-ray CT. IOP Conf. Series: Materials Science and Engineering, 139, 12024. http://doi.org/10.1088/1757-899X/139/1/012024*

Material system: Glass fibre/epoxy, layup $[\pm 45°,b/0,b/0]_s$ with b=$\pm$45°90°

Specimen type: 410x15x4 butterfly

The previous studies only did X-ray CT examination of cut-outs or downsized specimens, and it was clear that downsizing the specimens had a significant effect on the results. One of the challenges in performing X-ray CT of the regular size test specimens is their 410 mm length, since the standard mounting equipment in the X-ray CT scanner cannot easily hold such a specimen. Even if mounted, it was not possible to scan in the gauge region since the rotation stage was too tall. Because of this, part of the work presented in [P3] describes a modification of the mounting method for the sample in order to make this possible. Furthermore, the modified sample mounting method was designed in a way that makes repeated mounting of the sample easier. For the quasi-UD composite considered in [P3] with $\pm 45°$ and $90°$ backing bundles (Fig. 2.4b), the damage was more visible than in the previous studies, making it possible to see the damage even for a 4x15mm large cross-sectional area. Therefore, it was possible to perform an ex-situ test of the 410mm long specimens where the same specimen was repeatedly scanned in the same region at different number cycles of a fatigue test.

To look into the effect of applied tension during X-ray CT scanning on the crack visibility, [P3] also presented a tension clamp solution that could apply a load to the specimen during X-ray CT scanning to open up cracks. Fig. 4.3 shows an illustration of the tension clamp principle. The tension clamp was attached to the specimen while loaded in a static test machine (Fig. 4.3a). Upon unloading of the specimen, the gauge section would remain in tension by the clamp. The experiments carried out with the tension clamp showed that some fibre fractures, which were not visible before, became visible. However, it mainly resulted in increased opening of the cracks that were already visible without the clamp applied. Nevertheless, applying load during scanning showed a clear effect on the crack visibility. The work presented in [P3] mainly focused on presenting the ex-situ fatigue and tension clamp methods, and a more detailed analysis of the observations from the ex-situ study was presented in [P4] described below.

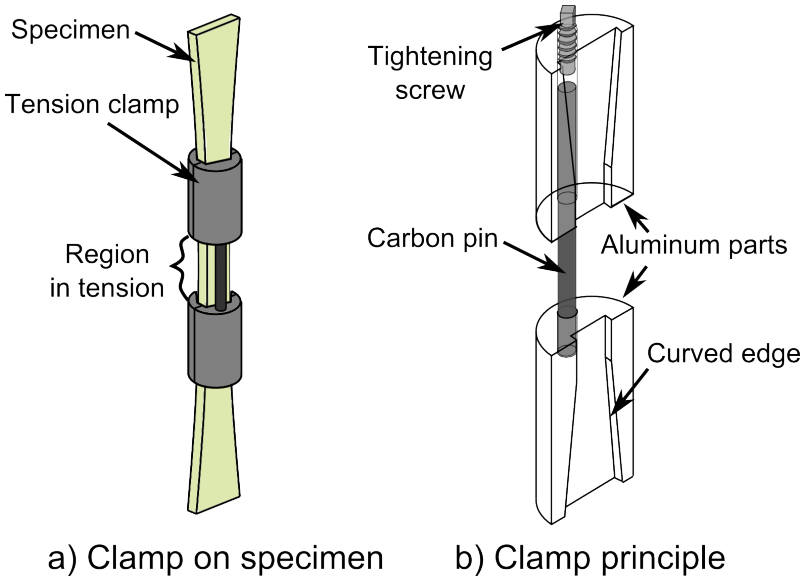

Figure 4.3: Illustration of the tension clamp principle. The clamp is attached to the specimen as shown in (a) while loaded in tension in a test machine. The specimen curvature is used for load transfer to avoid pressure on the specimen surface as shown in (b). For more details see [P3].

4.4 Evaluation of 3D damage progression by Ex-situ fatigue testing

[P4] *Jespersen, K. M., & Mikkelsen, L. P. (2017). Three dimensional fatigue damage evolution in non-crimp glass fibre fabric based composites used for wind turbine blades. Submitted to Composites Science and Technology.*

Material system: Glass fibre/epoxy, layup $[\pm 45°,b/0,b/0]_s$ with b=$\pm$45°90°

Specimen type: 410x15x4 butterfly

The work presented in [P4] considers analysing the fatigue damage progression observed by the ex-situ fatigue X-ray CT method presented in [P3]. The stiffness degradation was measured during the full fatigue test, which was interrupted four times during the fatigue life for X-ray CT examination, as also shown in Fig. 4.4. By locating the same damage regions in the 3D images acquired at each interruption point, it was possible to monitor how the damage, and in particular the UD fibre fractures, had progressed. It was found that the fibre fractures gradually progressed into the UD bundles during cycling. The damage would first initiate and progress from the triple cross-over regions of the backing fibre bundles where the $\pm 45°$ and $90°$ cross over each other. This was then followed by initiation and progression from other cross-over regions. The different damage regions then progressed in parallel and connected to one another, resulting in final failure. Quite late in the fatigue life, intralaminar splitting was observed in the UD bundles as well. In addition, a significant increase in crack face opening of the fibre fractures was

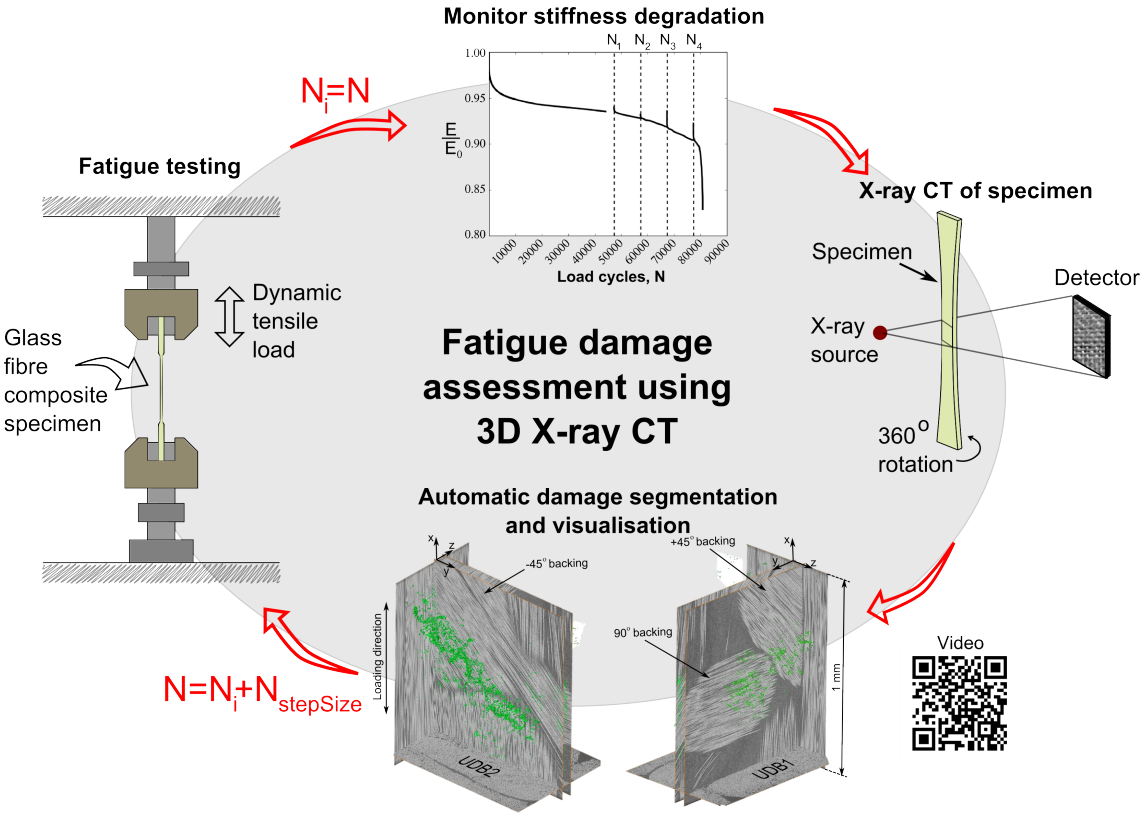

Figure 4.4: Illustration of the ex-situ approach carried out in [P3]. The damage segmentation image shown in the figure was presented in [P4].

observed with an increasing number of cycles. It should be noted that the ex-situ X-ray CT fatigue test was performed without applied load in the X-ray CT scans, meaning that the increase in the crack face opening of the cracks was observed in the unloaded state. The work presented in [P4] gave a detailed understanding of how the damage progressed into the UD bundles in 3D.

In addition to comparing the raw image data sets at each interruption point to one another, an almost automatic method for segmenting the damage in the volume was presented. This was done by using a built-in Matlab function to align the initial dataset with one of the later stages, and then subtract them from each other. This resulted in an image where the changes that occurred between the two damage stages appeared more clearly, and therefore could be segmented by simple thresholding techniques on the grey scale values. In [P4] this method was only used to obtain a rough 3D visualisation of the damage, since the alignment between the two volumes was not perfect. However, it gave a good idea of how the damage inside the UD bundles appeared in 3D, and it was clear that the progression of UD fibre fractures was highly influenced on the nearby local backing fibre bundle arrangement.

4.5 Combining experimental techniques to study fatigue damage initiation and progression

The final study was divided into two parts presented in [P5] and [P6]. In this study, the knowledge obtained through the studies [P1-P4] was combined into a method that could monitor fatigue damage initiation and progression both in stage I and II during the fatigue life (see Fig. 2.10 earlier). [P5] and [P6] consider the same type of quasi-UD composite as studied in [P1] and [P2]. However, in [P5] and [P6] it is a two layer composite with one of the backing layers removed, resulting in one backing layer in the centre of the specimen. This was done to consider the isolated effect of a single backing bundle layer in between two layers of UD bundles, which will usually be the case in the layup used for the real blades. In addition, a modified specimen geometry was used for these studies as a compromise between the small samples considered in [P2], and the regular butterfly test specimens considered in [P3] and [P4]. The slightly smaller width combined with a smaller specimen thickness made it possible to obtain a similar resolution to that of the initial studies presented in [P1] and [P2]. Due to their good fatigue properties, fatigue testing of quasi-UD composites used for wind turbine blades are usually accelerated by applying a higher strain level than what is actually present in the structure and then extrapolating the data using an S-N curve to a higher number of cycles. The work presented in [P5] studies the effect of the strain level on the initiation and progression of damage in the early fatigue life (stage I), and [P6] focuses on fibre fractures that mainly occur during the stable stiffness degradation region of the fatigue life (stage II).

4.5.1 Part A: Studying off-axis crack initiation and growth in backing fibre bundles

[P5] *Jespersen, K. M., Glud, J. A., Zangenberg, J., Hosoi, A., Kawada, H., & Mikkelsen, L. P. (2017). Uncovering the fatigue damage initiation and progression of uni-directional non-crimp fabric reinforced polyester composite - Part A: Off-axis cracks and the effect of strain level. In Manuscript.*

Material system: Glass fibre/polyester, layup [0/b,0] with b=$\pm 80^\circ$

Specimen type: 250x10x2mm butterfly

Part A of the study focused on off-axis crack initiation and growth in the fibre backing bundles monitored by TWLI imaging during the fatigue tests, as was also done in [P2]. To clarify whether the strain level affects the damage mechanisms, the study presented in [P5] considered several specimens tested at different strain levels while continuously monitored by TWLI imaging. Since the off-axis cracks are judged to be the initiators of subsequent serious damage in the UD fibre bundles, a different off-axis crack density in the backing bundles would be expected to influence the damage in later stages of the fatigue life. An automatic method to count the cracks [36] in the TWLI images was applied and slightly modified to quantify the off-axis cracks in the backing bundles. The strain level seemed to affect apparent saturation crack density (where the curves seemed to level out) of off-axis cracks in the backing fibre bundles. From the experiments it was

found that the stiffness degradation was similar for all the tests. If the stiffness degradation during the initial fatigue life (stage I) is caused solely by off-axis cracks in the backing fibre bundles as initially postulated (Fig. 2.10), the stiffness degradation should be related to the measured off-axis crack density. Therefore, this result was a bit unexpected and was in the present work judged to be caused by other damage mechanisms occurring during stage I of the fatigue life as well. Nevertheless, due to the use of a large load cell used, the noise in the stiffness degradation data was large compared to the measured stiffness degradation and therefore it still needs further investigation. Finally, the study presented in [P5] also discussed an S-N curve-like method to simply compare the fatigue properties of different material systems at realistic strain levels without the usual requirement of testing to final failure.

4.5.2 Part B: Studying fibre fractures by ex-situ fatigue testing and tension clamp

[P6] *Jespersen, K. M., Zangenberg, J., & Mikkelsen, L. P. (2017). Uncovering the fatigue damage initiation and progression of uni-directional non-crimp fabric reinforced polyester composite - Part B: uni-directional fibre fractures. In Manuscript.*

Material system: Glass fibre/polyester, layup [0/b,0] with b=$\pm$80°

Specimen type: 250x10x2mm butterfly

In part B of the study, ex-situ fatigue testing was carried out on one of the test specimens from Part A. Because of the knowledge obtained on the damage mechanisms in [P1] and [P2], it was possible to choose a X-ray CT scan region based on the fibre bundle structure where damage would initiate later. Therefore, in contrast to the ex-situ study presented in [P3] and [P4], the ex-situ study presented in [P6] include the stage before damage initiated (zero cycles). UD fibre fractures were seen to initiate first at the cross-over region of the backing fibre backing bundles and later a few UD fibre fractures also initiated where a single backing fibre bundles touched the UD fibre bundle. The UD fibre fractures then progressed into the UD fibre bundle, and more UD fibre fractures could be seen in the region near the cross-over region of the backing fibre bundles than near the single backing fibre bundle. At locations where the backing fibre bundles did not touch the UD fibre bundle, no UD fibre fractures were observed in any of the experiments.

For this quasi-UD composite the damage is generally difficult to see due to small crack openings, and therefore a new tension clamp modified to fit the smaller specimens considered in [P5] was manufactured and applied to see the effect of opening up the cracks. The application of tension to these specimens had a large effect on the visibility of the cracks - more significant than for the case presented in [P3]. As the results presented in Part A ([P5]) of this study indicated that other effects than off-axis cracks might be the cause of initial stiffness degradation in stage I of the fatigue life, the tension clamp was applied to a sample interrupted relatively early in the fatigue life. When scanning without the clamp attached, only a limited amount fibre fractures were observed in the considered regions. However, when load was applied during scanning several fibre frac-

tures became visible. This indicated that off-axis cracks are accompanied by more UD fibre fractures than initially expected, even in the early fatigue life, as was also indicated by the results in Part A. Performing an ex-situ study to monitor the damage progression of this type of composite surely gives useful information on the damage mechanisms, but from the tension clamp experiments it is clear that for this type of quasi-UD composite many fibre fractures are not visible in the unloaded state. Some additional improvement of the tension clamp solution is necessary to use it during an the ex-situ test. However, it is clear that it will be necessary if one wishes to quantify the number of fibre fractures. Nevertheless, it should be possible to combine the tension clamp solution with the ex-situ x-ray CT fatigue experiments, as also discussed in the next section.

4.6 Established ex-situ X-ray CT fatigue testing method

Part of the work carried out throughout the PhD project has resulted in the workflow of an experimental method to monitor the damage initiation and progression of quasi-UD composites under tension fatigue loading during stage I and II of the fatigue life. The overall approach is illustrated in Fig. 4.5 and can be used for ex-situ fatigue testing with or without TWLI depending on the material system, and with or without the tension clamp depending on the specimen geometry.

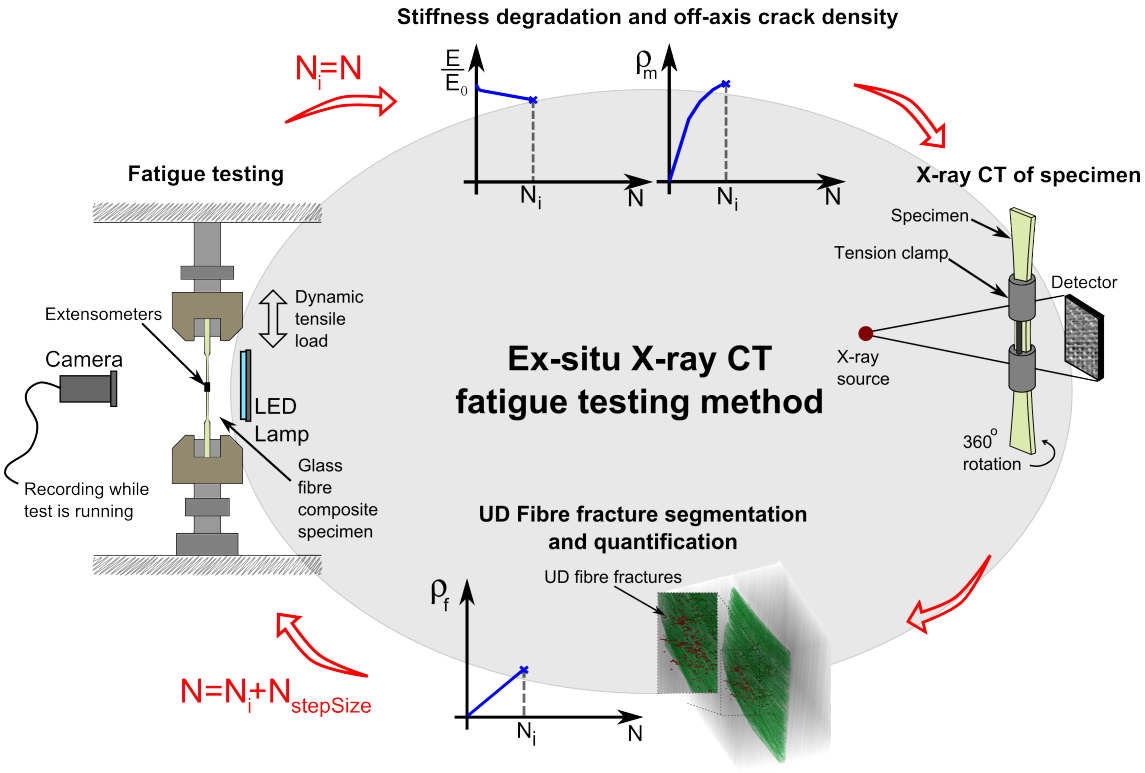

Figure 4.5: Illustration of the final work flow of the established experimental technique combining the individually established methods.

Fig. 4.5 illustrates the ex-situ X-ray CT approach where a test specimen being tested in fatigue while the strain in the gauge section is measured by extensometers mounted on the side of the specimen. At the same time, the specimen is continuously monitored by a high resolution camera (TWLI) to observe the off-axis crack initiation and progression in the off-axis backing fibre bundles, which are also quantified by the automatic crack counting algorithm applied in [P5]. The fatigue test is interrupted after a chosen number of cycles, and the sample is taken out for X-ray CT examination. Although not done in the studies presented in this thesis, the X-ray CT examination could be done with the tension clamp applied to enhance the crack visibility, as also indicated in Fig. 4.5. The X-ray examination can then give a visualisation of the UD fibre fractures in 3D (see [P1] and [P4]), and e.g. also a quantification of individual UD fibre fractures in the future. By testing the sample further and repeating this loop, both the damage initiation and progression of off-axis cracks in the backing fibre bundles and UD fibre fractures can be obtained. The studies [P5] and [P6] presented in this thesis have shown how to carry out this ex-situ fatigue testing approach, and could also be applied for other material systems and load ratios.

In addition, if automatic methods for segmenting individual fibre fractures could be established it would be possible to directly link the off-axis crack growth with the UD fibre fractures in specific damage regions as illustrated in the principle sketch in Fig. 4.6.

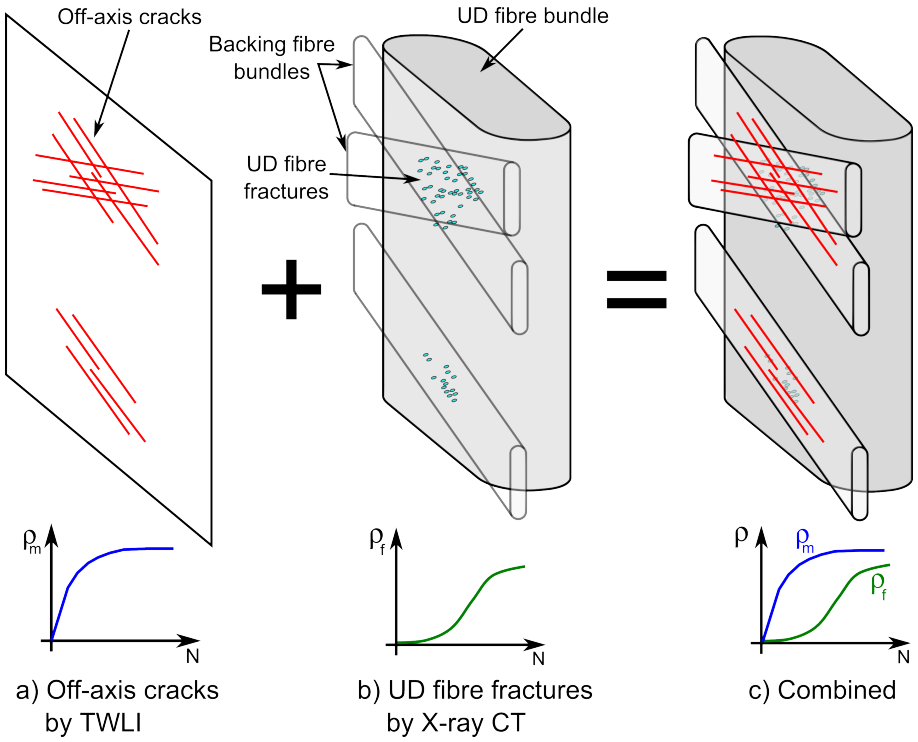

Figure 4.6: Idea of combining the results from different experimental techniques into both a combined visualisation and quantification. In the figure, ρ_m is the off-axis crack density and ρ_f the density of UD fibre fractures.

Fig. 4.6 shows the idea behind this approach, where the goal is to be able to relate off-

axis cracks observed by TWLI with fibre fractures observed by X-ray CT. The idea is to monitor the off-axis cracks by TWLI when the fatigue test is running (Fig. 4.6a) and then use X-ray CT to obtain the development UD fibre fractures as well (Fig. 4.6b). If the damage observed can be quantified and related to one another as sketched in Fig. 4.6c, it will provide a much better understanding of the damage initiation and progression. Furthermore, quantification of the different damage mechanisms is also of great interest both in relation to comparing different material systems, but also for modelling purposes. The work presented in [P5] and [P6] set the stage for doing this, however it is still necessary to establish reliable techniques to map the damage locations from the TWLI images to the X-ray CT data and automatic methods for quantification of individual UD fibre fractures are still lacking.

4.7 3D damage progression scheme

Based on the knowledge obtained throughout this PhD project, a 3D damage progression scheme was established as shown in Fig. 4.7. The damage progression scheme presented here is in general accordance to the postulated damage progression scheme earlier (Fig. 2.10) presented by Zangenberg et al [34], however it has been expanded in relation to the initiation and growth of the off-axis cracks in the backing fibre bundles and includes the 3D aspect of the damage progression, which is important for quasi-UD composites in relation to UD fibre fractures.

Fig. 4.7 shows the established damage progression scheme and the graph in the centre shows the typical shape of a stiffness degradation curve for a fibre composite. At zero cycles the material is assumed to have no damage, as was also seen from the experiments in [P5] and [P6]. After a few cycles, the first off-axis cracks initiate as illustrated in Fig. 4.7a. The off-axis crack initiation depends on the local variation in the bundle structure and is associated by a few UD fibre fractures at locations where the backing fibre bundles (off-axis crack tips) touch a UD bundle, as also shown in Fig. 4.7a. With further cycling, the off-axis cracks in the backing fibre bundles grow and new cracks initiate as illustrated in Fig. 4.7b. Off-axis cracks also initiate in single backing fibre bundles, and again UD fibre fractures initiate together with the off-axis cracks. The initiation and growth behaviour of the off-axis cracks also depends on the local bundle structure in the composite, and therefore can vary from bundle to bundle. In the initial part of stage II of the fatigue life, the off-axis cracks in the backing fibre bundles are close to saturation and UD fibre fractures begin to grow into the thickness direction of the UD bundle as shown in Fig. 4.7c. The backing fibre bundles experience a difference in the crack saturation density depending on the bundle thickness and possibly also the local stress states depending on the local bundle and fibre architecture. At some point, the off-axis cracks saturate and the UD fibre fractures continue to progress into the thickness direction of the UD fibre bundle as illustrated in Fig. 4.7d. Further away from the backing fibre bundles, the UD fibre fractures are generally more spread out, and their progression path seems to depend on the local arrangement of the backing fibre bundles as was seen in [P4]. At some point the damage regions will begin to grow together (Fig. 4.7e), possibility connected by intralaminar splitting as also illustrated earlier in Fig. 2.9. Although the intralaminar splitting was not visible in all the X-ray CT scans, they were observed in some of the experiments in [P3]

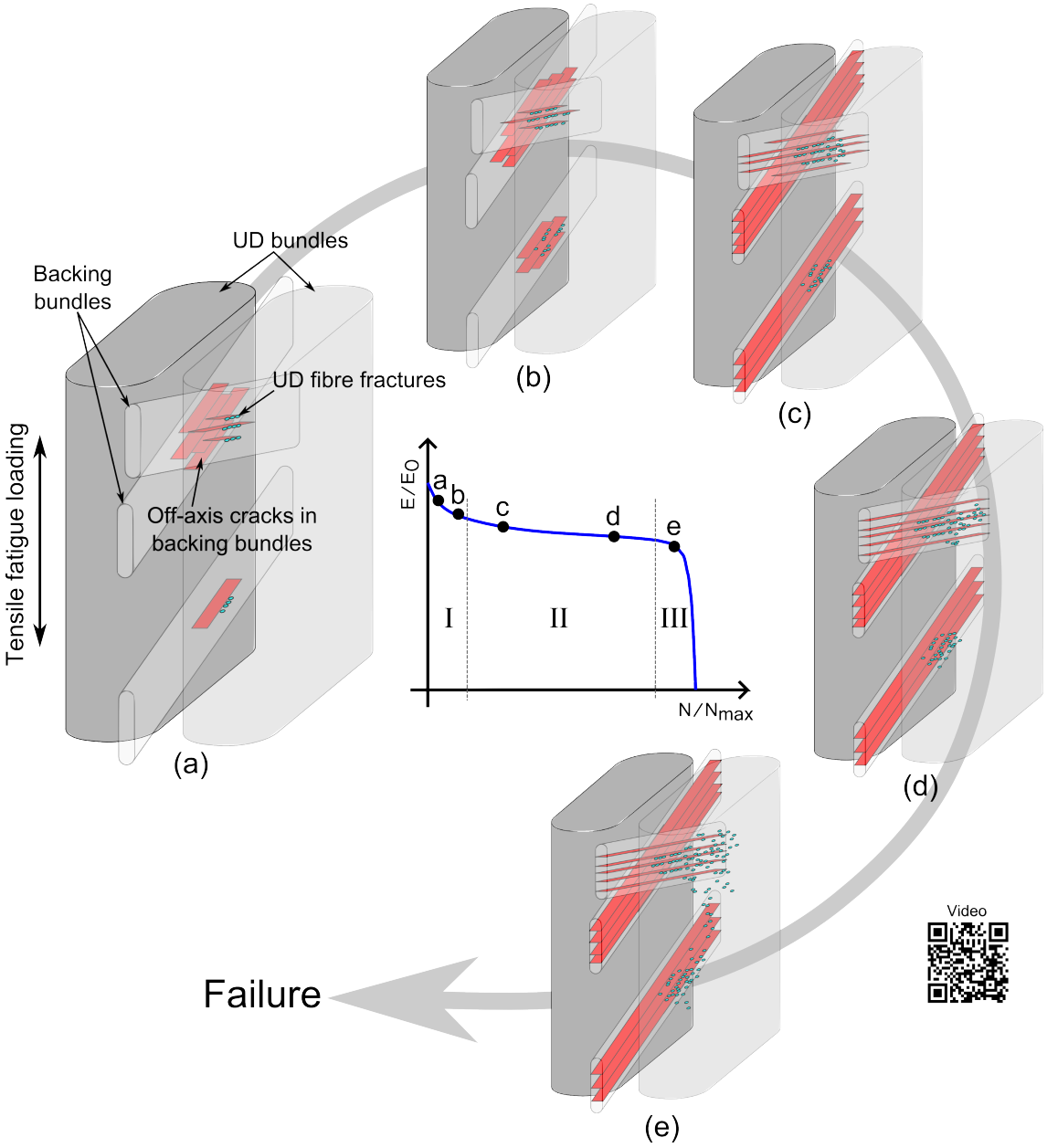

Figure 4.7: Established damage progression scheme related to the stiffness degradation curve.

and [P4]. At some point, the regions of UD fibre fractures will have grown so large that the remaining fibres cannot carry the load anymore and final failure occurs.

The increased understanding here presented as a damage progression scheme can both be used to improve the fatigue properties of quasi-UD composites, but can also serve as a basis for choosing suitable assumptions in future 3D modelling that give more realistic results.

Chapter 5

Conclusion and outlook

This thesis summarised the work carried out during a 3 year PhD project in the Composite and Materials Mechanics section of DTU Wind Energy. Details about the work are presented in the six papers appended to this thesis. The outcome of the project can be split into two main parts; 1) the establishment of experimental methods and 2) understanding fatigue damage mechanisms and setting the stage for X-ray CT based 3D modelling.

During this PhD project, an ex-situ X-ray CT fatigue testing method for monitoring the damage initiation and progression in 3D of quasi-UD composites used for wind turbine blades was established. To overcome the challenges regarding obtaining sufficient image resolution to see damage on the microstructural scale, a tension clamp solution was established to apply tension to the specimen during X-ray CT scanning. In addition, the 2D imaging technique TWLI was used as a supplement to the X-ray CT experiments, providing additional information on the off-axis crack initiation and development, which is difficult to see by X-ray CT. It was demonstrated that different experimental techniques can be combined with great advantage. The presented methods established during the PhD project were demonstrated on two types of quasi-UD NCF based composites, but could also be applied to other material systems, lay-up and loading conditions. Although the current study considered glass fibre composites, the ex-situ X-ray CT approach along with the tension clamp solution could also be applied to e.g. carbon fibre composites. As carbon fibre composites are not transparent TWLI cannot be applied however, the idea of combining the ex-situ X-ray CT fatigue approach with other supplementary methods could also be applied for carbon fibre composites. Depending on the composite lay-up, applying contrast agent to the specimen could also be included in the ex-situ process. In addition, the ex-situ X-ray CT fatigue approach could also be applied to other types of problems such as ply-drops and wrinkles, and for compression-compression and tension-compression fatigue loading.

The experimental results obtained during the PhD project have provided an enhanced knowledge on the damage initiation and progression of quasi-UD composites. Studying the damage progression for two different types of quasi-UD composites, different lay-ups and various specimen geometries, have provided significant knowledge on the controlling damage mechanisms. The knowledge obtained through this PhD project made it possible to establish a 3D damage progression scheme. The observations along with the established damage progression scheme have set the stage for establishing models with suitable assumptions to provide realistic results. It also showed the importance of including the 3D aspect in future models, as the damage was found to initiate as local phenomena and progress as a 3D mechanism. Furthermore, the experiments carried out in the PhD project show the importance of taking the variation of the local fibre architecture and bundle structure into account. With the recent advances within image segmentation

techniques it could be possible to use the X-ray CT data obtained in this PhD project as geometrical input to a finite element modelling software. The monitored damage progression observed experimentally can then be used for validation purposes.

In conclusion, aside from establishing experimental methods, the PhD project presented in this thesis has set the stage for X-ray CT based finite element modelling of the damage progression across length scales. In other words, the work carried out during the PhD project is a step towards realistic fatigue life-time modelling. This is an important part of pushing the design limit of the quasi-UD fibre composites used for wind turbine blades, which would make it possible to make longer or lighter blades resulting in a decreased cost of energy for the wind energy production.

Bibliography

[1] Global Wind Energy Council. Global wind statistics 2016. http://www.gwec.net/wp-content/uploads/vip/GWEC_PRstats2016_EN_WEB.pdf, 2016. [Online; accessed 04-Apr-2017].

[2] R. P. L. Nijssen and P. Brøndsted. Fatigue as a design driver for composite wind turbine blades. In P. Brøndsted and R. P. L. Nijssen, editors, *Advances in Wind Turbine Blade Design and Materials*, chapter 6, pages 175–209. Woodhead Publishing, 2013.

[3] M. J. Emerson, K. M. Jespersen, A. B. Dahl, K. Conradsen, and L. P. Mikkelsen. Individual fibre segmentation from 3D X-ray computed tomography for characterising the fibre orientation in unidirectional composite materials. *Composites: Part A*, 97:83–92, 2017.

[4] K. M. Jespersen, Y. Wang, J. Zangenberg, T. Lowe, P. J. Withers, and L. P. Mikkelsen. Ex-situ time-lapse X-ray CT study of 3D micro-structural fatigue damage evolution in uni-directional composites. In *17th European Conference on Composite Materials*, Munich, June 2016.

[5] K. M. Jespersen, J. Zangenberg, and L. P. Mikkelsen. Micromechanical investigation of fatigue damage in uni-directional fibre composites. In *Proceedings of 6th International Conference on Fatigue of Composites*, 2015. http://orbit.dtu.dk/files/108663074/ICFCPaperDraft_KMUN_Final.pdf.

[6] K. M. Jespersen, T. Lowe, P. J. Withers, J. Zangenberg, and L. P. Mikkelsen. Micromechanical time-lapse X-ray CT study of fatigue damage in uni-directional fibre composites. In *Proceedings of 20th International Conference on Composite Materials*, Copenhagen, 2015. http://iccm20.org/fullpapers/file?f=nDdmYO9mvY.

[7] K. M. Jespersen and L. P. Mikkelsen. Fatigue damage observed non-destructively in fibre composite coupon test specimens by X-ray CT. *IOP Conference Series: Materials Science and Engineering*, 139:012024, 2016.

[8] K. M. Jespersen, J. Zangenberg, T. Lowe, P. J. Withers, and L. P. Mikkelsen. Fatigue damage assessment of uni-directional non-crimp fabric reinforced polyester composite using X-ray computed tomography. *Composites Science and Technology*, 136:94–103, 2016.

[9] K. M. Jespersen and L. P. Mikkelsen. Three dimensional fatigue damage evolution in non-crimp glass fibre fabric based composites used for wind turbine blades. Submitted to Composites Science and Technology, 2017.

[10] K. M. Jespersen, J. A. Glud, J. Zangenberg, A. Hosoi, H. Kawada, and L. P. Mikkelsen. Uncovering the fatigue damage initiation and progression of uni-directional non-crimp fabric reinforced polyester composite - Part A: Off-axis cracks and the effect of strain level. In manuscript, 2017.

[11] K. M. Jespersen, J. Zangenberg, and L. P. Mikkelsen. Uncovering the fatigue damage initiation and progression of uni-directional non-crimp fabric reinforced polyester composite - Part B: uni-directional fibre fractures. In manuscript, 2017.

[12] R. P. L. Nijssen. Fatigue life prediction and strength degradation of wind turbine rotor blade composites. PhD Thesis, Delft University of Technology, the Netherlands, 2006.

[13] K. L. Reifsnider and R. Jamison. Fracture of fatigue-loaded composite laminates. *International Journal of Fatigue*, 4(4):187–197, 1982.

[14] R. D. Jamison, K. Schulte, K. L. Reifsnider, and W. W. Stinchcomb. Characterization and analysis of damage mechanisms in tension-tension fatigue of graphite/epoxy laminates. *Effects of Defects in Composite Materials*, STP30196S:21–55, 1984.

[15] R. Talreja. Fatigue of composite materials: damage mechanisms and fatigue-life diagrams. *Proceedings of the Royal Society A*, 378:461–475, 1981.

[16] M. A. Miner. Cumulative damage in fatigue. *Journal of Applied Mechanics-transactions of the Asme*, 12(3):A159–A164, 1945.

[17] H. Sanchez, T. Escobet, V. Puig, and P. F. Odgaard. Health-aware model predictive control of wind turbines using fatigue prognosis. *IFAC-PapersOnLine*, 48-21:1363–1368, 2015.

[18] K. Vallons, G. Adolphs, P. Lucas, S. V. Lomov, and I. Verpoest. The influence of the stitching pattern on the internal geometry, quasi-static and fatigue mechanical properties of glass fibre non-crimp fabric composites. *Composites: Part A*, 56:272–279, 2014.

[19] M. S. Duragkar, R. K. Paretkar, D. R. Peshwe, and S. A. Paranjpe. Investigation of the load sequence effects in fatigue of damaged composite laminate & characterization of fatigue damage. *Transactions of the Indian Institute of Metals*, 63(2-3):565–569, 2010.

[20] J. N. Yang and D. L. Jones. Load sequence effects on the fatigue of unnotched composite materials. *Fatigue of Fibrous Composite Materials*, 1981(723):213–232, 1981.

[21] J. Zangenberg. The effects of fibre architecture on fatigue life-time of composite materials. PhD Thesis, DTU Wind Energy PhD-0018(EN), 2013.

[22] J. Tong, F. J. Guild, S. L. Orgin, and P. A. Smith. On matrix crack growth in quasi-isotropic laminates—I. experimental investigation. *Composites Science and Technology*, 57(11):1527–1535, 1997.

[23] Jie Tong. Three stages of fatigue crack growth in GFRP composite. *Journal of Engineering Materials and Technology*, 123:139–143, 2001.

[24] A. Hosoi, Y. Arao, H. Karasawa, and H. Kawada. High-cycle fatigue characteristics of quasi-isotropic CFRP laminates. *Advanced Composite Materials*, 16(2):151–166, 2007.

[25] M. Quaresimin, P. A. Carraro, L. P. Mikkelsen, N. Lucato, L. Vivian, P. Brøndsted, B. F. Sørensen, J. Varna, and R. Talreja. Damage evolution under cyclic multiaxial stress state: A comparative analysis between glass/epoxy laminates and tubes. *Composites: Part B*, 61:282–290, 2014.

[26] K. L. Reifsnider. *Fatigue of Composite Materials*. Elsevier, 1991.

[27] Z. Hashin. Analysis of cracked laminates: a variational approach. *Mechanics of Materials*, 4:121–136, 1985.

[28] J. A. Nairn. The strain energy release rate of composite microcracking: a variational approach. *Journal of Composite Materials*, 23(11):1106–1129, 1989.

[29] J. Varna, R. Joffe, N. V. Akshantala, and R. Talreja. Damage in composite laminates with off-axis plies. *Composites Science and Technology*, 59(14):2139–2147, 1999.

[30] J. Varna and L. Berglund. Multiple transverse cracking and stiffness reduction in cross-ply laminates. *Journal of Composites Technology and Research*, 13(2):97–106, 1991.

[31] P. A. Carraro and M. Quaresimin. A stiffness degradation model for cracked multidirectional laminates with cracks in multiple layers. *International Journal of Solids and Structures*, 58:34–51, 2015.

[32] R. Joffe and J. Varna. Analytical modeling of stiffness reduction in symmetric and balanced laminates due to cracks in 90 layers. *Composites Science and Technology*, 59:1641–1652, 1999.

[33] M. Kashtalyan and C. Soutis. Analysis of composite laminates with intra- and interlaminar damage. *Progress in Aerospace Sciences*, 41:152–173, 2005.

[34] J. Zangenberg, P. Brøndsted, and J. W. Gillespie Jr. Fatigue damage propagation in unidirectional glass fibre reinforced composites made of a non-crimp fabric. *Journal of Composite Materials*, 48(22):2711–2727, 2014.

[35] C. Colombo, F. Libonati, F. Pezzani, A. Salerno, and L. Vergani. Fatigue behaviour of a GFRP laminate by thermographic measurements. *Procedia Engineering*, 10:3518–3527, 2011.

[36] J. A. Glud, J. M. Dulieu-barton, O. T. Thomsen, and L. C. T. Overgaard. Automated counting of off-axis tunnelling cracks using digital image processing. *Composites Science and Technology*, 125:80–89, 2016.

[37] R. A. Smith. *Material Science and Engineering - Volume III*, chapter : Composite defects and their detection, pages 103–143. EOLSS, 2002.

[38] H. Altendorf and D. Jeulin. 3D directional mathematical morphology for analysis of fiber orientations. *Image Analysis & Stereology*, 28:143–153, 2011.

[39] M. W. Czabaj, M. L. Riccio, and W. W. Whitacre. Numerical reconstruction of graphite/epoxy composite microstructure based on sub-micron resolution X-ray computed tomography. *Composites Science and Technology*, 105:174–182, 2014.

[40] M. Tausif, B. Duffy, S. Grishanov, H. Carr, and S. J. Russell. Three-dimensional fiber segment orientation distribution using X-ray microtomography. *Microscopy and microanalysis : the official journal of Microscopy Society of America, Microbeam Analysis Society, Microscopical Society of Canada*, pages 1–10, 2014.

[41] M. Axelsson. 3d tracking of cellulose fibres in volume images. *Proceedings - International Conference on*

Image Processing, 4:2005–2008, 2007.

[42] J. Pazmino, V. Carvelli, and S. V. Lomov. Micro-CT analysis of the internal deformed geometry of a non-crimp 3D orthogonal weave E-glass composite reinforcement. *Composites Part B: Engineering*, 65:147–157, 2014.

[43] P. Wright, X. Fu, I. Sinclair, and S. M. Spearing. Ultra high resolution computed tomography of damage in notched carbon fiber-epoxy composites. *Journal of Composite Materials*, 42(19):1993–2002, 2008.

[44] P. Wright, A. Moffat, I. Sinclair, and S. M. Spearing. High resolution tomographic imaging and modelling of notch tip damage in a laminated composite. *Composites Science and Technology*, 70(10):1444–1452, 2010.

[45] A. E. Scott, M. Mavrigirdati, P. Wright, I. Sinclair, and S. M. Spearing. In situ fibre fracture measurement in carbon-epoxy laminates using high resolution computed tomography. *Composites Science and Technology*, 71(12):1471–1477, 2011.

[46] S. C. Garcea, M. Macrigirdato, A. E. Scott, I. Sinclair, and S. M. Spearing. Fatigue micromechanism characterisation in carbon fibre reinforced polymers using synchrotron radiation computed tomography. *Composites Science and Technology*, 99:23–30, 2014.

[47] S. C. Garcea, I. Sinclair, and S. M. Spearing. In situ synchrotron tomographic evaluation of the effect of toughening strategies on fatigue micromechanisms in carbon fibre reinforced polymers. *Composites Science and Technology*, 109:32–39, 2015.

[48] S. C. Garcea, I. Sinclair, and S. M. Spearing. Fibre failure assessment in carbon fibre reinforced polymers under fatigue loading by synchrotron X-ray computed tomography. *Composites Science and Technology*, 133:157–164, 2016.

[49] B. Yu, R. Blanc, C. Soutis, and Withers P. J. Evolution of damage during the fatigue of 3D woven glass-fibre reinforced composites subjected to tension–tension loading observed by time-lapse X-ray tomography. *Composites: Part A*, 82:279–290, 2016.

[50] B. Yu, R. S. Bradley, C. Soutis, P. J. Hogg, and P. J. Withers. 2D and 3D imaging of fatigue failure mechanisms of 3D woven composites. *Composites Science and Technology*, 77:37–49, 2015.

[51] P. J. Schilling, B. P. R. Karedla, A. K. Tatiparthi, M. A. Verges, and P. D. Herrington. X-ray computed microtomography of internal damage in fiber reinforced polymer matrix composites. *Composites Science and Technology*, 65(14):2071–2078, 2005.

[52] F. Sket, R. Seltzer, J. M. Molina-Aldareguía, C. Gonzalez, and J. LLorca. Determination of damage micromechanisms and fracture resistance of glass fiber/epoxy cross-ply laminate by means of X-ray computed microtomography. *Composites Science and Technology*, 72(2):350–359, 2012.

[53] J. Lambert, A. R. Chambers, I. Sinclair, and S. M. Spearing. 3D damage characterisation and the role of voids in the fatigue of wind turbine blade materials. *Composites Science and Technology*, 72(2):337–343, 2012.

Appendix A

Appended papers

Included to the thesis are the following papers.

[P1] **Jespersen, K. M.**, Zangenberg, J., Lowe, T., Withers, P. J., and Mikkelsen, L. P. (2016). Fatigue damage assessment of uni-directional non-crimp fabric reinforced polyester composite using X-ray computed tomography. *Composites Science and Technology*, 136, 94–103.

[P2] **Jespersen, K. M.**, Wang, Y., Zangenberg, J., Lowe, T., Withers, P. J., and Mikkelsen, L. P. (2016). Ex-Situ Time-Lapse X-Ray Ct Study of 3D Micro-Structural Fatigue Damage Evolution in Uni-Directional Composites. *17th European Conference on Composite Materials*, Munich, Germany.

[P3] **Jespersen, K. M.**, and Mikkelsen, L. P. (2016). Fatigue damage observed non-destructively in fibre composite coupon test specimens by X-ray CT. *IOP Conf. Series: Materials Science and Engineering*, 139, 12024.

[P4] **Jespersen, K. M.**, and Mikkelsen, L. P. (2017). Three dimensional fatigue damage evolution in non-crimp glass fibre fabric based composites used for wind turbine blades. *Submitted to Composites Science and Technology*.

[P5] **Jespersen, K. M.**, Glud, J. A., Zangenberg, J., Hosoi, A., Kawada, H., and Mikkelsen, L. P. (2017). Uncovering the fatigue damage initiation and progression of uni-directional non-crimp fabric reinforced polyester composite - Part A: Off-axis cracks and the effect of strain level. *In manuscript*.

[P6] **Jespersen, K. M.**, Zangenberg, J., and Mikkelsen, L. P. (2017). Uncovering the fatigue damage initiation and progression of uni-directional non-crimp fabric reinforced polyester composite - Part B: uni-directional fibre fractures. *In manuscript*.

[P1]

Jespersen, K. M., Zangenberg, J., Lowe, T., Withers, P. J., and Mikkelsen, L. P.

FATIGUE DAMAGE ASSESSMENT OF UNI-DIRECTIONAL NON-CRIMP FABRIC REINFORCED POLYESTER COMPOSITE USING X-RAY COMPUTED TOMOGRAPHY

Composites Science and Technology, 136, 187-193 (2016).

Composites Science and Technology 136 (2016) 94–103

Contents lists available at ScienceDirect

Composites Science and Technology

journal homepage: http://www.elsevier.com/locate/compscitech

Fatigue damage assessment of uni-directional non-crimp fabric reinforced polyester composite using X-ray computed tomography

Kristine M. Jespersen [a, *], Jens Zangenberg [b], Tristan Lowe [c], Philip J. Withers [c], Lars P. Mikkelsen [a]

[a] Department of Wind Energy, Composites and Materials Mechanics, Technical University of Denmark, DTU Risø Campus, 4000, Roskilde, Denmark
[b] LM Wind Power Blades, Composite Mechanics, Jupitervej 6, 6000, Kolding, Denmark
[c] Manchester X-ray Imaging Facility, School of Materials, University of Manchester, Manchester, M13 9PL, United Kingdom

ARTICLE INFO

Article history:
Received 30 March 2016
Received in revised form
27 September 2016
Accepted 6 October 2016
Available online 8 October 2016

Keywords:
Polymer matrix composites (PMCs)
Glass fibres
Fracture
Non-destructive testing
Micro-tomography

ABSTRACT

In this study, the progression of tension-tension fatigue (R = 0.1) damage in a uni-directional (UD) composite made from a non-crimp glass fibre fabric used for wind turbine blades is investigated using multi-scale 3D X-ray computed tomography (CT). Initially, a representative volume is examined at one specific damage level. UD fibre fractures are only observed close to the supporting thin transverse backing layers. Furthermore, UD fibre fractures are only observed at locations where backing fibre bundles intersect one another and are at the same time locally close to a UD bundle. In addition, to study the progression of damage as a function of stiffness degradation at higher resolution four samples are subjected to different numbers of cycles before examination by CT. One sample is examined during the initial stiffness drop, two samples during stable stiffness degradation, and one close to final failure. Damage is observed to occur as chains of individual fibre breaks or clusters of fibre fractures rather than large fracture planes. Our work indicates how fracture of UD fibres initiates from intersecting ±80° backing bundles extending progressively further into the UD layer. The fibre fracture zone becomes more diffuse further from the backing layer. Our work supports a scheme explaining stiffness degradation in terms of UD fibre damage accumulation and demonstrates the importance of 3D and ideally time-lapse imaging studies.

1. Introduction

With increasing global focus on sustainability, the amount of energy produced from wind turbines has been increasing in recent years [1], and this is expected to continue. However, the challenge of making wind energy cost-competitive relative to fossil fuels remains. Since the power output scales with the swept rotor area (i.e. blade length squared), increasing the blade length decreases the cost of energy of the wind turbine. One of the main challenges when designing long blades is material fatigue. During a wind turbine's life-time of around 20–30 years, it experiences a high number of load cycles (in the range of 10^8–10^9 cycles) [2]. The blade is subjected to repeated flap-wise bending from the wind and repeated edge-wise bending from the blade weight combined with the rotation [3]. The main load carrying parts of a wind turbine blade consist of uni-directional (UD) glass fibre composite materials made from non-crimp fabrics (NCF). In addition to the fatigue life-time, the stiffness degradation observed during fatigue loading can become a problem in relation to tower clearance. It is therefore of great interest to understand and describe the fatigue damage mechanisms on a micro-structural level for this material, in order to be able to make more fatigue resistant designs and/or to understand how to reduce cost without compromising the fatigue resistance.

1.1. Fatigue of composites

The progression of fatigue damage in fibre composites, and how to design against fatigue, has received a great amount of focus in the literature. Particularly within the aerospace industry the initiation of off-axis cracks been the focus of many studies [4–10]. Fewer studies (e.g. Refs. [9–12]) have considered damage progression in terms of fibre fractures that occur after the initiation of

* Corresponding author.
E-mail address: kmun@dtu.dk (K.M. Jespersen).

http://dx.doi.org/10.1016/j.compscitech.2016.10.006
0266-3538/

transverse cracking.

Reifsnider and Jamison [9] examined the fatigue mechanisms in both cross-ply and quasi-isotropic carbon fibre/epoxy composites. In both cases the stiffness degradation during fatigue was observed to include three main stages: a steep initial stiffness reduction stage (stage I), a stable degradation stage (stage II), and an unstable stage with final failure (stage III). They found that for both the cross-ply and quasi-isotropic laminates the initial reduction in stiffness seemed to primarily relate to transverse cracking. The stiffness degradation in stage II was said to decrease stably as a consequence of subcritical element damage such as matrix cracking, matrix splitting along fibre directions, fibre/matrix debonding, and delamination causing the stresses in the laminate to redistribute. The damage would then localise and lead to damage in critical elements such as the 0° plies. This would then soon be followed by final failure of the laminate [9,10].

Wind turbine blade materials are subjected to a much higher number of load cycles than aerospace and other composite material applications. In addition, because of the specific loading conditions, UD composites are used to carry the main fatigue loads in a wind turbine blade, whereas quasi-isotropic composites are commonly used in the aerospace industry. Therefore, the material design challenges are rather different, because of the need to tolerate UD fibre damage during operation. The UD NCF composites used for wind turbine blades have a bundle structure and experience slightly different damage mechanisms compared to cross-ply and quasi-isotropic composites. However, the shape of the stiffness degradation curve is similar. A previous study by Zangenberg et al. [11] considered tension-tension fatigue damage in a composite material used for wind turbine blades. The study considered a UD NCF glass fibre/polyester composite with thin supporting off-axis backing layers. In their study a fatigue damage evolution scheme was established as discussed below.

1.2. Tension-tension fatigue damage accumulation scheme

Zangenberg et al. [11] postulated a tension-tension fatigue damage accumulation scheme on the basis of destructive examination techniques (particularly scanning electron microscope (SEM) observations) for the same type of material as considered in the current study (further elaborated later in section 2.1). Fig. 1 shows a simplified version of this scheme (for details see Ref. [11]), which also shows the usual shape of the stiffness degradation during fatigue ($R = 0.1$) for this material type. In the scheme, the damage is taken to initiate as transverse cracks in the thin backing layer of criss-crossed bundles of off-axis fibres. These cracks are believed to initially appear in locations where the backing bundles intersect. However, since the initial stiffness drop was found to fit well with the loss of stiffness contributed by the backing layers [11], the transverse cracks are believed to saturate everywhere in the bundles prior to UD fibre damage occurring. After crack saturation the cracks propagate into the UD fibre bundles, causing debonding and fibre fractures. During a stage where the stiffness degrades stably (II in Fig. 1), a steadily increasing number of UD fibre fractures are believed to cause the stiffness degradation. At some point, the number of fibre fractures will have increased the load on the remaining fibres sufficiently to cause rapid static failure. Zangenberg et al. [11] also burned off the resin and observed interlaminar failure (longitudinal splitting) penetrating 20–40% into the UD bundles in the thickness direction. Nevertheless, the destructive nature of their method meant that it was only possible to look at one moment in time, and only to consider 2D surface views, which is partly why the scheme still remains a postulate.

1.3. X-ray CT of damage in composites

In recent years, the resolution of non-destructive 3D X-ray computed tomography (CT) has improved significantly. This is opening up a range of new opportunities for the use of X-ray CT for material science purposes [13–15]. In X-ray CT, the sample is placed between an X-ray source and a detector. X-rays emitted from the source pass through the sample and on to the detector, leaving a projection image (as for conventional medical 2D radiography). The sample is then rotated in steps, for each of which a projection image is acquired. A reconstruction algorithm is then used to reconstruct a 3D image of the considered volume. The contrast in the images is dependent on the difference in material density. Therefore, in relation to composite materials, X-ray CT is particularly well suited for glass fibre/polymer composites due to the relatively large difference in material density (around a factor of 2).

Several recent studies have considered micro-structural damage of composite materials using synchrotron radiation computed tomography. Wright et al. [16,17] considered static damage in

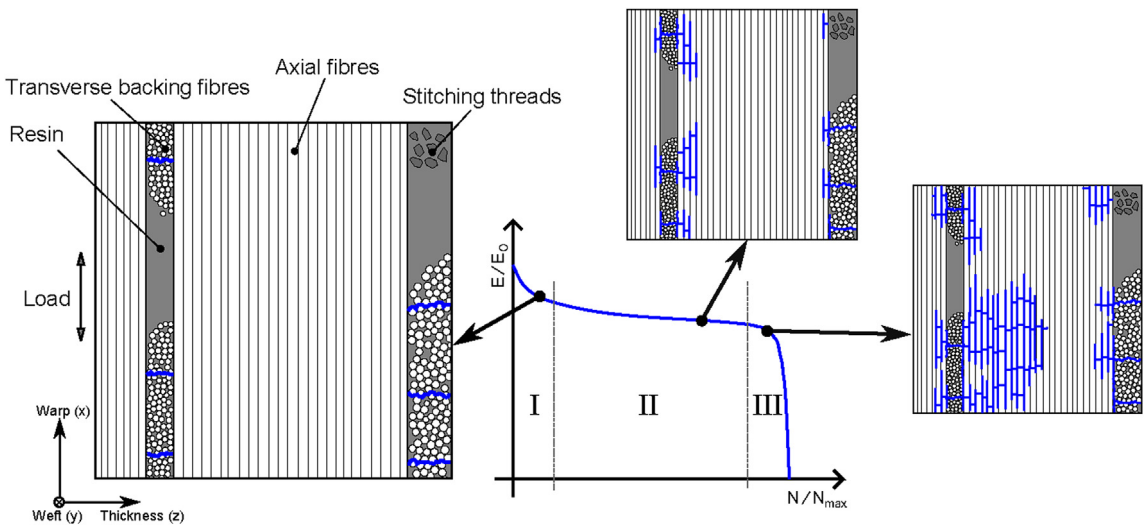

Fig. 1. Simplified version of the tension-tension fatigue damage accumulation scheme postulated by Zangenberg et al. [11] for a UD composite comprising UD fabric with transverse fibre backing layers.

notched carbon fibre reinforced plastic (CFRP) specimens, visualising fibre fractures, intra-laminar delamination and matrix cracking in 3D. Scott et al. [18] performed in-situ static loading of a double notched CFRP specimen, visualising the accumulation of damage for an increasing static load. Synchrotron CT was also used in studies by Garcea et al. [19,20], to evaluate the fatigue damage evolution of a similar specimen during in-situ start-stop fatigue experiments. All these studies considered samples of a few millimetres in size to obtain high resolution. Synchrotron radiation is particularly suited to short in-situ experiments since the fast scan times makes it possible to capture changes over time. On the downside however, synchrotron facilities are often remotely located, beam time is difficult to access and experiments are typically limited to a few days at most, precluding many longer fatigue studies.

The latest laboratory X-ray CT systems can offer micro- and even sub-micron [21] resolution CT comparable to synchrotron systems. These systems make it easier to perform multiple longer timescale studies, albeit using much longer scan times compared to synchrotron CT. Since laboratory X-ray CT systems capable of micro resolution have only recently emerged, only a few studies to date [12,22–25] have used laboratory systems to study material damage at the micro-structural level. The studies have tended not to consider individual fibre fractures because of insufficient resolution (e.g. Ref. [22]). As for synchrotron radiation CT, studies of fibre fractures have examined sample sizes of only a few millimetres (e.g. Ref. [12]). Some studies have used staining techniques to increase the visibility of the damage thereby lessening the resolution requirements. In a recent study by Yu et al. [23], the fatigue damage progression of matrix cracks and delaminations in a larger test specimen (16 × 2mm in cross-section) was studied for a 3D woven carbon fibre composite at 10.7 μm voxel size by staining with contrast agent. For that case the contrast agent was found to properly penetrate into material [24]. However, in order for staining to be effective, all the damage must be interconnected to the outer surfaces. This might not be the case for the UD NCF used for wind turbine blades, since the off axis layers are thin compared to the UD layer thickness and there are resin rich regions, which are large compared to the backing bundles. Furthermore, the damage at the surface is likely to be caused by edge effects and the focus of the current study is on what is happening a distance away from the edges.

The new advances within laboratory X-ray CT make it possible to move from destructive 2D testing to visualising damage in 3D and by extension over time. In this paper, we study the axial tension-tension fatigue damage progression in a UD glass fibre composite in 3D. Based on qualitative observations, the proposed damage accumulation scheme [11] is evaluated with a focus on the three dimensional arrangement of the damage features. Initially, the general locations of fatigue damage regions are investigated using a field of view (FoV) large enough to contain several regions of the backing where the fibre bundles intersect, however with limited resolution. Based on the knowledge obtained on the nature of the damage regions, scans have then been performed at higher resolution on a systematic set of four samples each subjected to a different number of fatigue load cycles.

2. Material and methods

2.1. Composite material system

The composite material is a UD glass fibre/polyester composite made from a non-crimp fabric. The composite consists of layers of UD fabric stacked on top of each other and infused with resin using the vacuum assisted resin transfer moulding (VARTM) infusion technique. For each layer of fabric, parallel UD fibre bundles are stitched to supporting off-axis backing bundles, giving it a fabric-like structure. The stitching thread is made from polyester, hence it has the same density as the matrix material and will not be visible in the performed X-ray CT scans. The dry fabric is shown in Fig. 2, which also illustrates the stitching pattern used to stitch the UD and backing bundles together. The backing bundles are present to keep the UD bundles in place, and do not have a significant effect on the material axial stiffness and strength properties, though they do slightly contribute to the transverse stiffness.

Fig. 3 shows a 3D rendering of the fibre architecture obtained by laboratory X-ray CT. It is seen that the backing bundles are quite unevenly spaced as a result of the stitching pattern, and intersect in some locations. In this paper, the term “backing layer” denotes the space between the layers of parallel UD bundles in the final composite, as also indicated in Fig. 4. These layers contain both backing bundles and resin-rich regions as indicated in Fig. 3.

The composite layup has 4 layers of UD fabric in the stacking sequence $[b/0,b/0]_s$ where “b/0” symbolises a layer of fabric with “b” denoting the (±80°) backing layer and “0” the axial (0°) UD layer of the fabric. Fig. 4 shows a schematic of the stacking sequence and the fabric specification is summarised in Table 1. The matrix is a proprietary unsaturated polyester. It has been cured for more than 24 h at room temperature followed by a post curing sequence at 40° C in an oven for more than 16 h. This is a curing sequence resulting in a fully cured laminate.

Fig. 5 shows a 3D rendering of a higher resolution laboratory CT scan where the matrix material has again been rendered invisible. The approximate dimensions of the UD and backing layers in the final composite are indicated in the figure, which also shows that the backing layers are considerably thinner than the UD layers. In addition, the thickness of the backing layer varies quite a lot as the backing bundles lie on top of one another and cross-over in some locations, whereas in other locations there are no fibres at all.

2.2. Fatigue testing

Two rectangular plates of the composite outlined in section 2.1 were manufactured and cut into butterfly shaped fatigue test specimens as shown in Fig. 6. The butterfly geometry is a special optimized geometry for testing UD composite materials [26], as standard plane specimen geometries tend to fail in the grip area instead of the gauge area. It is reported [26] to give longer fatigue life-times than the standard plane ISO specimens (ISO 527) [27]. The tests were performed at a Servo hydraulic Instron test machine under load control with a sinusoidal waveform. The stress ratio was R = 0.1, the frequency 5 Hz and the strain was monitored by two extensometers ([25mm / ± 2.5 mm]). The maximum fatigue load was 30% of the static strength of the composite. At this stress level the composite is damaged progressively during fatigue testing as

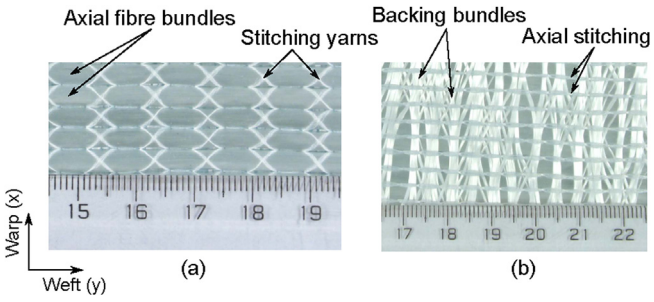

Fig. 2. Photographs of UD1322 UD fabric viewed from (a) the UD bundle side and (b) the backing side.

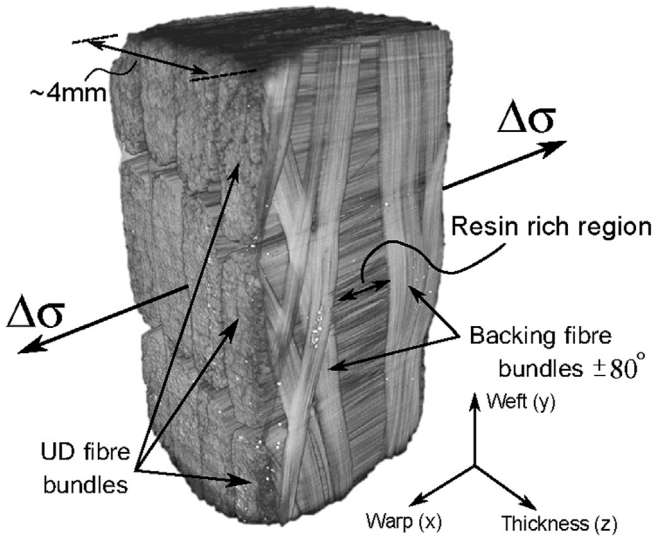

Fig. 3. 3D tomograph of the glass fibre/polyester composite micro-structure obtained by X-ray CT (9.7 μm voxel). The matrix has been rendered transparent by thresholding.

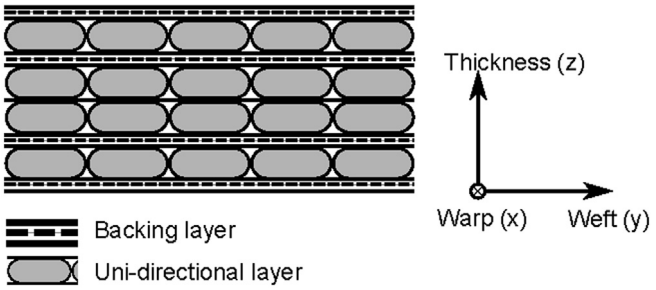

Fig. 4. Schematic showing the composite stacking sequence. The UD fibre direction is out of the plane.

Table 1
Fabric specification (UD1322).

Category	Unit	Axial fibres	Backing fibres	Stitching thread
Material	–	H+ glass	E-glass	Polyester
Area density	[g/m^2]	1322	60	15
Linear density	[tex]	2400	68	7.6
Avg. filament dia.	[μm]	17 or 24	9	N/A

also discussed by Talreja [28].

To examine the damage at different stages during the fatigue life several tests were interrupted prior to failure. A total of 9 tests were carried out and are listed below.

- Two samples were interrupted at 2000 cycles (during the initial stiffness drop region marked by "I" in Fig. 1).
- Two samples were interrupted at 55,000 cycles (during the stable stiffness degradation regime marked by "II" in Fig. 1).
- One sample was interrupted at 85,000 cycles (during the stable stiffness degradation regime marked by "II" in Fig. 1).
- One sample was interrupted at 95,000 cycles (where the stiffness starts to drop drastically marked by "III" in Fig. 1).
- Three samples were tested to failure.

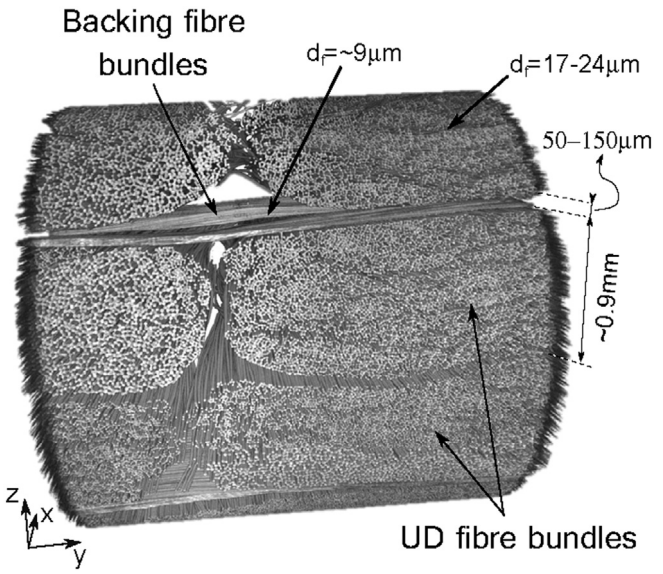

Fig. 5. 3D reconstructed image recorded with the MR settings in Table 2 (3.37 μm voxel size). The matrix and stitching has been rendered invisible to show the fibre architecture.

2.3. X-ray computed tomography

All the samples prepared for X-ray CT in this study were cut using a diamond blade cutter, and two types of cut-out geometries were used (See Fig. 6). The cutout-A geometry was glued to an aluminium pin, which makes it simple to repeatedly mount the sample in the scanner in the same way, even if taken out of the holder. For the cutout-B geometry it is possible to perform further fatigue testing on the down sized sample, which is of interest for future time-lapse studies.

The X-ray CT scans were carried out on a Zeiss Xradia Versa 520 scanner with a 2000 × 2000 pixel detector and a bit depth of 16. Two different sets of scan settings labelled "MR" (medium resolution) and "HR" (high resolution) were used (see Table 2). Data visualisation and segmentation was done using the commercial software "Avizo 9.0" from FEI, and image reconstruction was done using the software "XMReconstructor - Cone Beam 10" from Zeiss.

The MR scan settings considers a larger FoV than HR, and is performed with a binning of 2, which means that the X-ray counts from 2 × 2 pixels on the detector are combined giving a higher image intensity making it possible to decrease the exposure time (see Ref. [29] for more detailed information on X-ray CT). This means that the total scan time is shorter, however, at the compromise of resolution since the detector resolution is binned from e.g. 2000 × 2000 to 1000 × 1000 pixels. Nonetheless, it is much more challenging to process the data from a binning 1 scan, since the file-size is much larger (see Table 2). However, when looking for small features compromising the resolution over scan time and file-size might result in loss of important detail.

An overview of the scans performed in this study can be found in Table 3, and the purpose of these scans is explained in the following sections. The datasets MR3, HR2, HR3, and HR4 along with videos related to Figs. 9 and 11 can be found online [30].[1]

[1] The datasets for MR3 and HR2-4 along with videos of ROI from Figs. 9 and 11 are available at: http://doi.org/10.5281/zenodo.154714 [30]. The data sets can be loaded using the open source software "ImageJ". For use of these data, please make a reference to this paper.

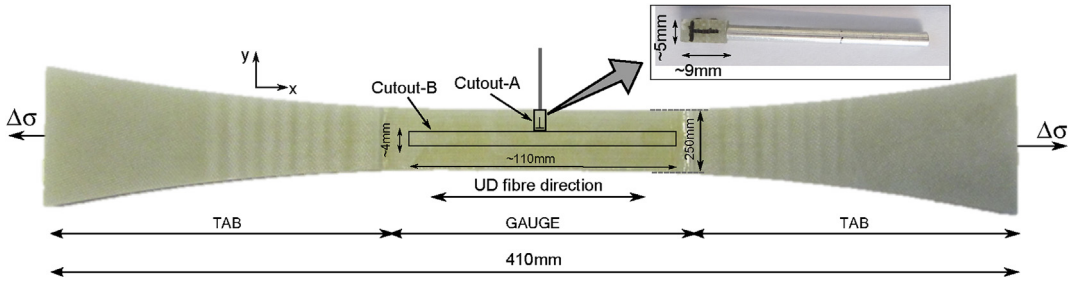

Fig. 6. Butterfly specimen geometry (full length of 410 mm) showing approximate cut-out locations and dimensions. The photo in the top-right corner shows the cut-out A sample glued to an aluminium pin for easy mounting in the scanner.

Table 2
Versa 520 X-ray CT imaging conditions.

Category	MR	HR
Optical magnification	3.98(4X)	3.98(4X)
Source to sample distance	15 mm	11 mm
Detector to sample distance	15 mm	20 mm
Exposure time	3 s	6 s
No. of projections	3201	3201
Accelerating voltage	80 keV	60 keV
Binning of pixels	2	1
Pixel size	3.37 μm	1.2 μm
Field of view on detector	3370 μm	2400 μm
Avg. reconstructed file size	2 GB	16 GB

Table 3
Performed X-ray CT scans. The datasets MR3, HR2, HR3, and HR4 can be found online [30].

Sample	Dataset	Cycles	Geom.	Note
S3	MR3	85,000	Cutout-A	3 overlapping scans along length
S1	HR1	2000	Cutout-B	Initial stiffness drop regime
S2	HR2	55,000	Cutout-B	Stable stiffness degradation regime
S3	HR3	85,000	Cutout-A	Stable stiffness degradation regime
S4	HR4	95,000	Cutout-B	Damage localisation

2.3.1. Medium resolution scans: locating damage regions

In X-ray CT, the resolution decreases with increasing size of the FoV, which means that a small FoV is necessary to obtain high resolution. In previous studies [11,26] the UD fibre fracture regions were found to be local phenomena and therefore locating these regions can be difficult if the FoV is too small. To identify where the damage regions typically occur, a cut-out of ~ 4 × 5 × 10 mm was initially studied with a voxel size of 3.37 μm and cylindrical FoV of ~ 3.4 mm in diameter and ~ 3.4 mm in height ("MR3" in Table 3).

The scanned sample was cut-out from the test specimen subjected to 85,000 cycles where damage is expected to be present. The FoV of the scans encompassed almost the full width of the sample, but excluded the backing layers at the sample surface in the thickness direction. Three overlapping scans were performed along the sample length covering a total length of ~ 6.2 mm. This was done in order to include several regions prone to damage in the scanned volume. The scan settings were chosen with a FoV judged to be as large as possible, while still being able to see fibre fractures. Because of the limited resolution, however, segmentation of individual fibre fractures would include a considerable amount of uncertainty. Therefore higher resolution scans were subsequently performed when studying the damage regions in detail.

2.3.2. High resolution scans: damage regions in several samples

To study the damage at different stages of the fatigue life, the samples subjected to 2,000, 55,000, 85,000 and 95,000 cycles were examined at high resolution. The related scan settings and cut-out geometry used for these scans were previously outlined in Table 3. The scans were performed with a pixel size of 1.2 μm and a cylindrical FoV of ~ 2.4 mm diameter × 2.4 mm height. By utilizing the knowledge of the location of the damage regions obtained from the MR scan, it was possible to locate regions prone to damage despite the small FoV by examining the 2D projection images when setting up the scan.

3. Results and discussion

3.1. Fatigue tests

The S-N curve for the composite is shown in Fig. 7, which also shows the tests that were stopped before failure for X-ray CT inspection. It should be noted that the fitted curve is based on only 5 points and normally a minimum of 10 points is required for a well defined curve. Fig. 8 shows the stiffness degradation curves for all the fatigue tests performed at $\varepsilon/\varepsilon_0 = 0.3$, where ε_0 is the static strain to failure, and highlights the curves for the four test specimens examined using X-ray CT. In Fig. 8 it is seen that the initial stiffness drop is similar for all the tests, but there is some scatter in the gradient in stage II. For the considered strain level, $\varepsilon/\varepsilon_0 = 0.3$, only three tests in total were continued all the way to failure and the number of cycles to failure are seen to vary considerably. It is a known problem that the lifetime from tests of this UD composite can vary as much as by a decade. In part this is due to the fact that some of the samples fail outside the gauge region - even when using the butterfly geometry [26]. Since the slope of the curves is

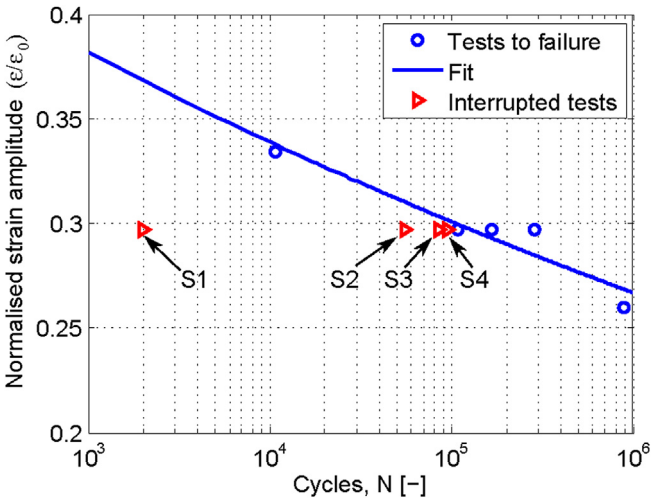

Fig. 7. S-N curve including the interrupted tests S1-4.

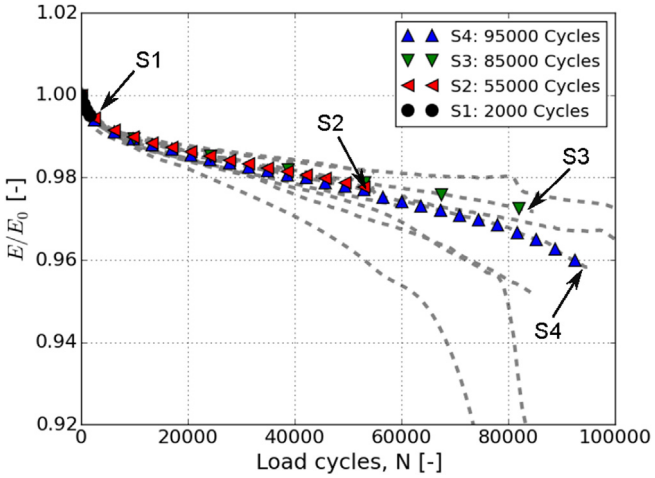

Fig. 8. The degradation in stiffness occurring at an imposed strain amplitude $\varepsilon/\varepsilon_0 = 0.3$ during tension fatigue testing. The symbols denote the stiffness degradation curves for the interrupted test samples imaged by X-ray CT at high resolution. The dashed lines show all the tests. The numbers of cycles at which the tests (S1-S4) were interrupted are marked by arrows.

generally similar (particularly for the four highlighted tests), it makes more sense to focus on the percentage stiffness drop relative to the absolute number of load cycles and not the percentage of total life.

3.2. Location of damage regions

Fig. 9 shows a stitched 2D view of the three medium resolution scans making up the MR3 dataset. Three regions of interest (ROI) contained load carrying UD fibre fractures and were located locally close to the thin off-axis backing layers (also previously discussed in Ref. [31]). For ROI 1 and ROI 3 in Fig. 9, damage was observed on both sides of the backing. For ROI 2, however, damage was only observed on the side to which the backing bundles were stitched. However at this location a layer of matrix was present in between the backing and the UD bundles. Videos slicing through the ROIs in the x-y plane along with the full data sets can be found online [30]. Based on the observations of this volume, damage was found to be present only where both of the following criteria are met (see also Fig. 10):

- There is no visible distance between the backing and the UD bundles.
- The backing bundles intersect.

Similar mechanisms where damage initiate at bundle cross-over regions has also previously been observed for ceramic matrix composites (e.g. Refs. [32,33]).

Fig. 9 also shows an example of the observed broken fibres, and in this location the UD fibres are seen to be misaligned (5–10°) to the loading direction. However, this was not the case for the other damage regions and therefore, as discussed previously [31], it is not believed have much influence. The main damage characteristics are listed below.

- UD fibre fractures are typically observed as a row of fibre breaks likely emanating from transverse cracking in the matrix of the nearby backing fibres.
- The fibre fracture zone spreads out further from the backing layer, and after 85,000 cycles, no damage was observed beyond approximately 300 μm from the backing.

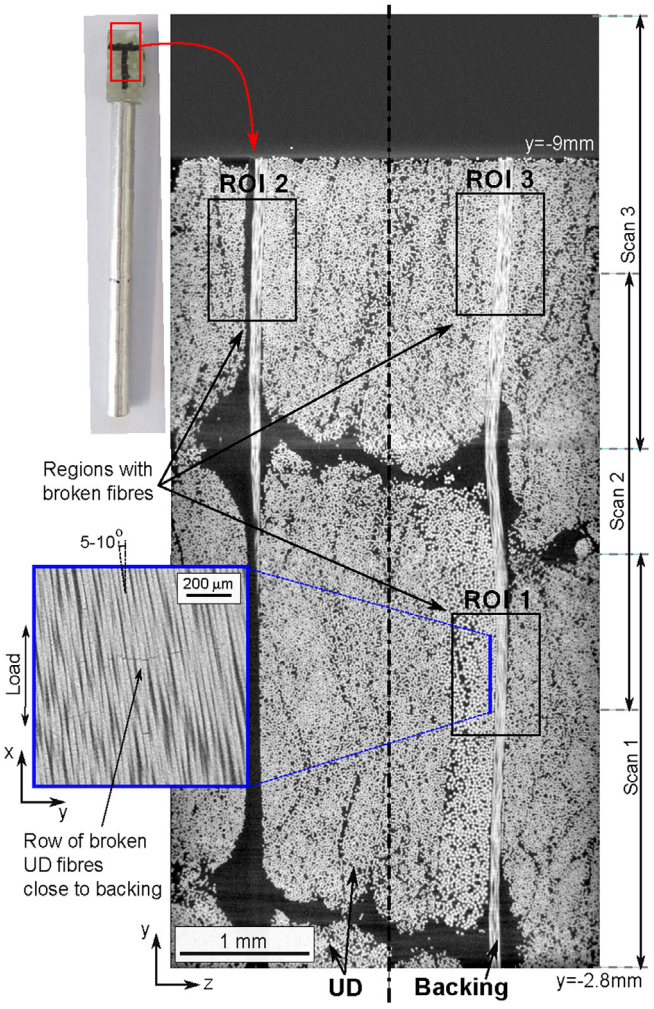

Fig. 9. Stitched virtual interior slice comprising the three CT scans that make up the scan region for the MR3 dataset. The ROI's marked are the only locations where damage was observed. The inset shows broken UD fibres close to the backing layer.

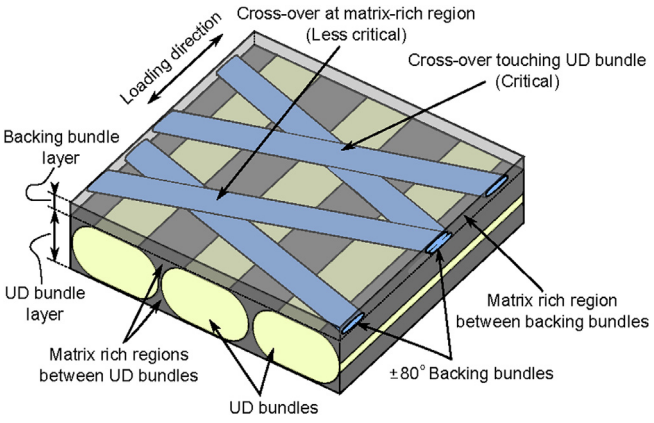

Fig. 10. Simplified sketch of one layer of fabric in the composite showing the difference between critical and less critical cross-over regions. The critical cross-over regions are where both ± 80° and a UD bundle cross over and touch each other.

3.3. Observed damage at different stages of life

For the scans performed at high resolution ("HR" in Table 2), it

was possible to see some additional damage features compared to the medium resolution scan (MR3). These additional damage features were previously outlined in Ref. [34], and include:

1. Matrix/interface cracks parallel to the UD fibres.
2. Matrix cracks extending through the backing bundles into the matrix rich regions between the UD bundle.
3. Matrix cracks in backing bundles (observed rarely).

Of the above mentioned damage features, 1 and 2 are not believed to significantly influence the stiffness degradation, as only a few broken UD fibres were observed near these damage features. Matrix cracks in the backing (point 3) however, are believed to be the cause of the initial stiffness drop observed in the fatigue tests. In addition, they are believed to be the initiator of UD fibre fractures and therefore are of considerable interest. In some locations however, the resolution was not sufficient to detect matrix cracks in the backing bundles as the existing transverse cracks most likely became closed with the load removed.

Fig. 11 shows a virtual slice taken from the high resolution ROI scan performed on the cutout-A sample (HR3). A transverse matrix crack in the backing spans the entire backing layer, and broken UD fibres are observed locally near the matrix crack. The matrix crack is seen to span two layers of backing at this location. A video showing all the slices through the full volume of Fig. 11 can be found online [30].

3.3.1. Damage during initial stiffness drop, stage I

For the initial stiffness drop sample (S1), only subjected to 2000 cycles, it was not possible to identify any damage in the scans performed at 1.2 μm voxel resolution. It is believed however, that matrix cracks are present in the backing layers at this stage, and that they cause the small initial stiffness drop as discussed in section 1.2. It is possible that the crack opening is small due to a small amount of damage in the sample. Further studies are ongoing in order to confirm the presence and locations of matrix cracks at this stage e.g. by applying static tension to the sample during CT scanning to keep open any cracks.

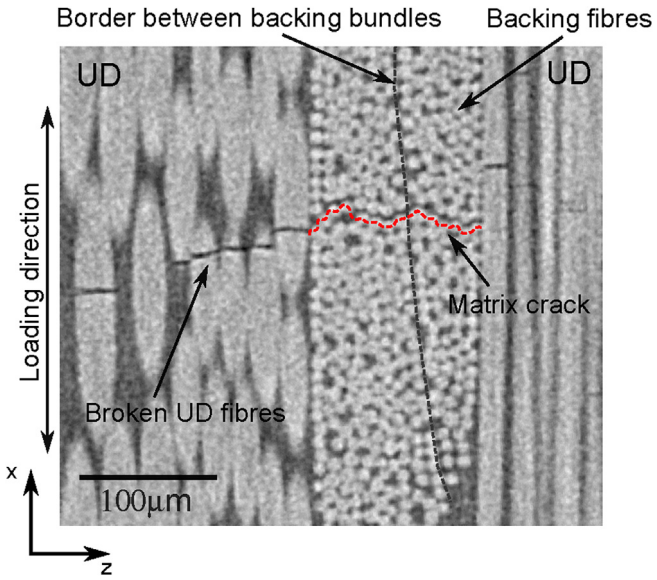

Fig. 11. Virtual slice showing a matrix crack through two intersecting backing bundles and adjacent UD fibre fractures (HR3 scan). A video slicing through the volume can be found online [30].

3.3.2. Damage while stiffness degrades stably, stage II

For the sample subjected to 55,000 cycles (S2) only one small damage region was found in the observed volume (~ 2.4 mm diameter × 2.4 mm height). The broken UD fibres were segmented manually using the Avizo software. The distribution of fibre fractures (represented by red discs) in the UD bundles is shown in Fig. 12. As was also seen in section 3.2, the damage in Fig. 12 occurs where the backing bundles intersect and there is no visible distance between the UD and backing bundles. The damage region is quite small, but it is possible that larger damage regions are present at other locations in the sample because the FoV associated with the scans only cover a small portion of the test sample.

Similarly, Fig. 13 shows the segmentation of individual UD fibre fractures for the high resolution scan (HR3) performed on the test specimen subjected to 85,000 cycles (at ROI 1 in Fig. 9). It is evident that the fibre fractures next to the backing are aligned with the backing fibre direction (for more cases see also [31]), which could be an indication of damage initiation from a matrix crack as suggested by Fig. 11. A bit further from the backing, the UD fibre fractures are more dispersed forming a damaged volume where the fibre damage does not necessarily follow the direction of the backing fibres. Within this volume, both single chains of fibre fractures, small clusters, and small planes of fibre fractures were observed. The chains of single fibre breaks are not necessarily straight nor entirely perpendicular to the load direction. From Fig. 13 it is also clear that the damage mechanism is a local 3D phenomenon, and considering this problem in 2D may give misleading conclusions.

3.3.3. Damage as stiffness starts to fall drastically, stage III

At the onset of drastic damage (S4) a larger damage region is observed (Fig. 14). As observed for S2 and S3, the fibre fractures closest to the backing are seen to line up with the orientation of the backing fibres (see Fig. 15). As also observed for S2 and S3, the UD fibre fractures are spread out into a damaged zone further away from the backing. In this region, the fractures seem to form chains and clusters rather than fracture planes, whereas the damage in Fig. 13 appeared to be arranged in planes to a higher extent. From the top view in Fig. 14, it can be seen that the damage zone extends less than halfway into the UD bundle (~370 μm), while from the 3D view it is seen that it extends quite far (~2 mm) along the UD fibre direction. This was not observed as significantly for the other loading stages.

4. Discussion of the proposed damage progression scheme

In the following, the process of damage progression postulated by Zangenberg et al. [11] outlined earlier in section 1.2 will be discussed in the light of the X-ray CT results. From our results it was seen that fibre fractures were only present where the backing bundles intersect and there is no visible distance between the backing and the UD bundles. In the original damage scheme, UD fibre damage was taken to appear mainly at intersecting backing bundles, and in the current study damage was only observed at these intersecting regions. However, in the study by Zangenberg et al. [11], small damage regions were also present at other locations such as near the stitching thread. At this point, it cannot be ruled out that the fibre fractures also exist at these locations in the samples considered using CT. That is, it is possible that the crack opening is smaller in these regions, as the damage zone is likely to be smaller. If the opening between fibre fractures is smaller (the cracks are closed), it might not be possible to visualise at 1.2 μm voxel size. In addition, the locations of the stitching are difficult to identify, since the stitching thread and matrix have similar densities. This could be investigated by applying tension to the sample

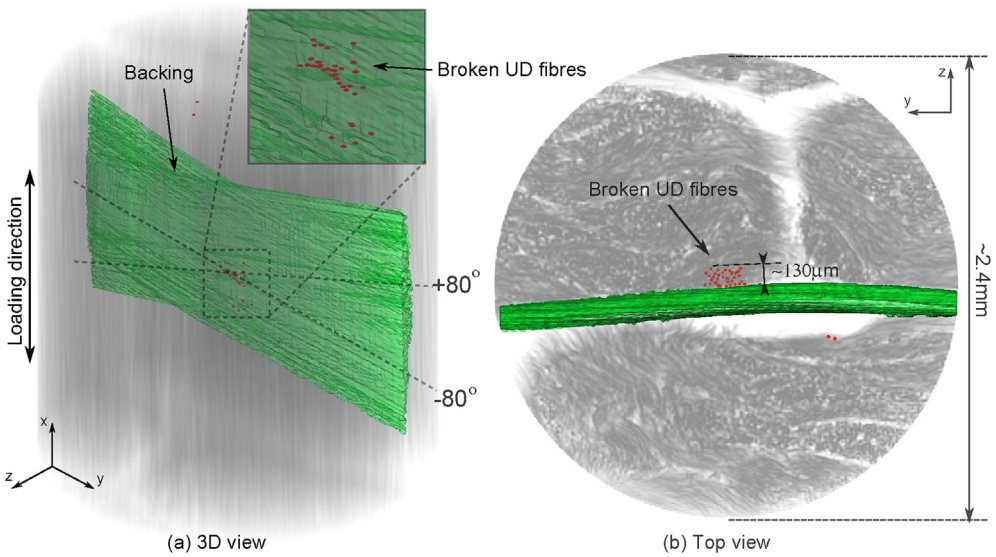

Fig. 12. a) 3D visualisation and b) top view of fibre fractures for the high resolution scan of S2 (dataset HR2). The fibre fractures are marked as red discs, the thin off-axis backing bundles are marked in green, and the UD fibres have been rendered transparent for clarification. (For interpretation of the references to colour in this figure legend, the reader is referred to the web version of this article.)

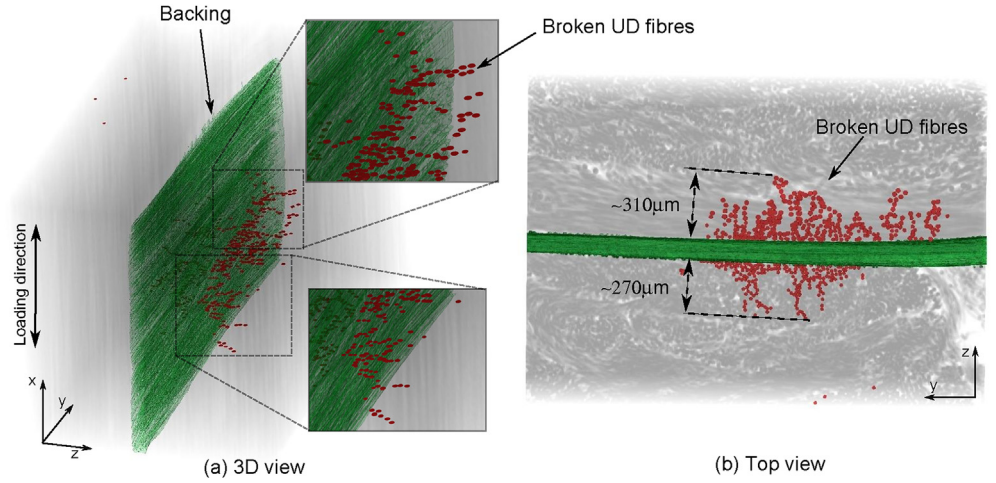

Fig. 13. a) 3D visualisation and b) top view of fibre fractures for the high resolution scan of S3 (dataset HR3). The fibre fractures are marked as red discs, the thin off-axis backing bundles are marked in green, and the UD fibres have been rendered transparent for clarification. (For interpretation of the references to colour in this figure legend, the reader is referred to the web version of this article.)

during scanning, which is currently on-going work.

During the stage (II) where the stiffness degrades steadily, the damage scheme (Fig. 1) suggests that UD fibre fracture damage zones gradually increase in size as a function of the load cycles. When considering the absolute number of cycles, the size of the observed damage regions is seen to increase with the number of load cycles as shown in Table 4. The penetration depth into the UD bundle is estimated by assuming an average bundle thickness of 0.9 mm. The results in Table 4 support the hypothesis that a gradual loss of stiffness is caused by an increasing number of axial fibre fractures in these local regions, extending further and further into the UD bundles as the original damage scheme states. The damage observed in this study shows that many fractures occur in clusters or chains, which may not be captured by a 2D investigation.

Even though the observations by Zangenberg et al. [11] were obtained at one specific damage level and using destructive 2D visualisation techniques, many of the observations in this study corroborate their damage scheme. However it is unlikely that damage sites can be reliably identified from 2D imaging. Further, in this study, it is clearly observed that damage progression is a 3D process, and that looking in 2D might give misleading results depending on the location of the cut surface. The observed damage zones using X-ray CT comprising single chains of fibre fractures extending in various directions, and even clusters of fibre fractures. Therefore, a 3D view is essential and it is preferable to include the damage progression over time in order to fully understand the damage development. In the future, time-lapse experiments tracking a specific ROI in a sample over the three stages will be reported in order to confirm the growth of the fracture zones. This is currently the focus of ongoing work.

5. Conclusion

In this paper, damage evolution under tension fatigue was

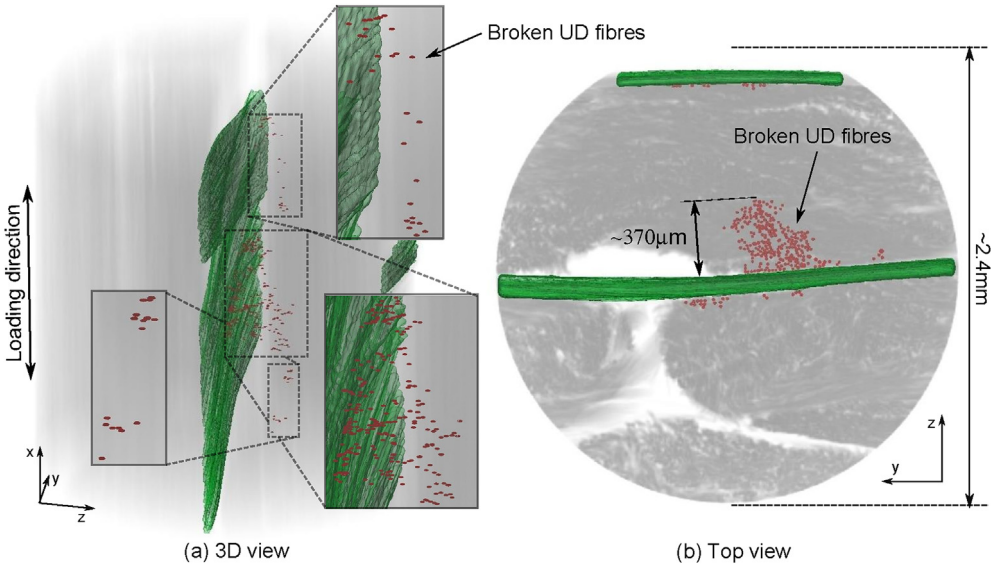

Fig. 14. 3D visualisation and b) top view of fibre fractures for the high resolution scan of S4 (dataset HR4). The fibre fractures are marked as red discs, the thin off-axis backing bundles are marked in green, and the UD fibres have been rendered transparent for clarification. (For interpretation of the references to colour in this figure legend, the reader is referred to the web version of this article.)

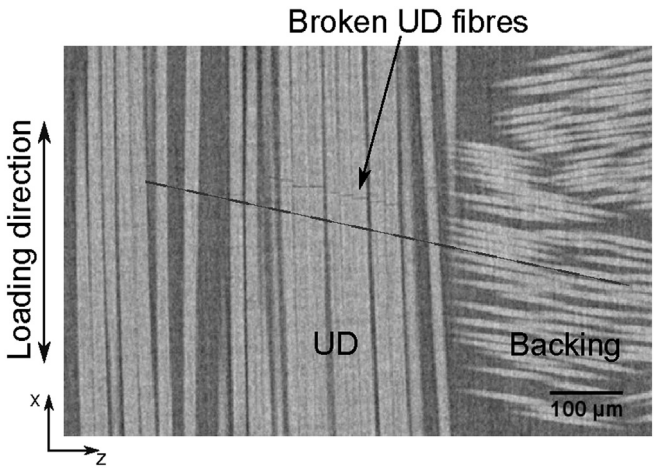

Fig. 15. Broken UD fibres just next to the backing for S4. It is seen that the fibre fractures align with the backing fibre orientation.

Table 4
Max observed damage depth into UD bundle for different load stages both absolute and normalised with an average UD bundle thickness of 0.9 mm.

	S2	S3	S4
Cycles	55,000	85,000	95,000
Penetration depth in UD	130 µm	310 µm	370 µm
Penetration depth in UD (%)	~ 14%	~ 34%	~ 41%

examined using X-ray computed tomography experiments. A hierarchical approach has been taken using both large field of view medium resolution scanning to identify damage zones and small field of view high resolution scanning to analyse the arrangement of fibre fractures. All the damage sites were located around regions where intersecting backing bundles were located next to the UD bundles with no visible distance in between.

Our results have shown that the fibre fractures, for fibres in contact with the backing, were aligned with the direction of the backing. This suggests that the fibre fractures were initiated by matrix cracks in the backing bundles. In addition, except for just next to the transverse backing bundles, the UD fibre fractures were observed to occur as chains and clusters of fibre fractures rather than planes. That is, fibre fractures propagate away from the contacting intersecting backing bundles in chains and planes that could not be determined simply from 2D destructive analyses. In order to properly determine the transition from stage II to stage III, time lapse studies of the fatigue of individual samples are required in the future.

Acknowledgements

The author would like to acknowledge the assistance provided by the Manchester X-ray Imaging Facility, which was funded in part by the EPSRC (grants EP/F007906/1, EP/F001452/1 and EP/I02249X/1). Financial support from CINEMA: “the allianCe for ImagiNg of Energy Materials”, DSF-grant no. 1305-00032B under “The Danish Council for Strategic Research” is gratefully acknowledged. This research was conducted using mechanical testing equipment from DTU Center for Advanced Structural and Material Testing (CASMAT), Grant No. VKR023193 from Villum Fonden. Additionally we would like to thank LM Wind Power for manufacturing of test specimens.

References

[1] Global Wind Statistics (2015), http://www.gwec.net/wp-contentW/uploads/2015/02/GWEC_GlobalWindStats2014_FINAL_10.2.2015.pdf, 2014.
[2] R. P. L. Nijssen, reportFatigue Life Prediction and Strength Degradation of Wind Turbine Rotor Blade Composites, PhD Thesis, Delt University of Technology.
[3] P. Brøndsted, R.P.L. Nijssen, Fatigue as a design driver for composite wind turbine blades, Adv. Wind Turbine Blade Des. Mater. (2013) 175–209, http://dx.doi.org/10.1533/9780857097286.2.175.
[4] A. Gagel, D. Lange, K. Schulte, On the relation between crack densities, stiffness degradation, and surface temperature distribution of tensile fatigue loaded glass-fibre non-crimp-fabric reinforced epoxy, Compos. Part A - Appl. Sci. Manuf. 37 (2) (2006) 222–228, http://dx.doi.org/10.1016/j.compositesa.2005.03.028.
[5] F. Edgren, D. Mattsson, L.E. Asp, J. Varna, Formation of damage and its effects on non-crimp fabric reinforced composites loaded in tension, Compos. Sci. Technol. 64 (5) (2004) 675–692, http://dx.doi.org/10.1016/s0266-3538(03)

00292-6.
[6] J. Tong, F.J. Guild, S.L. Orgin, P.A. Smith, On matrix crack growth in quasi-isotropic laminatesI. experimental investigation, Compos. Sci. Technol. 57 (11) (1997) 1527–1535, http://dx.doi.org/10.1016/S0266-3538(97)00080-8.
[7] J. Varna, R. Joffe, N.V. Akshantala, R. Talreja, Damage in composite laminates with off-axis plies, Compos. Sci. Technol. 59 (1999) 2139–2147, http://dx.doi.org/10.1016/S0266-3538(99)00070-6.
[8] M. Quaresimin, P.A. Carraro, L.P. Mikkelsen, N. Lucato, L. Vivian, P. Brøndsted, B.F. Srensen, J. Varna, R. Talreja, Damage evolution under cyclic multiaxial stress state: a comparative analysis between glass/epoxy laminates and tubes, Compos. Part B 61 (2014) 282–290, http://dx.doi.org/10.1016/j.compositesb.2014.01.056.
[9] K.L. Reifsnider, R. Jamison, Fracture of fatigue-loaded composite laminates, Int. J. Fatigue 4 (4) (1982) 187–197, http://dx.doi.org/10.1016/0142-1123(82)90001-9.
[10] R. Jamison, K. Schulte, K. Reifsnider, W. Stinchcomb, Characterization and analysis of damage mechanisms in tension-tension fatigue of graphite/epoxy laminates, Eff. Defects Compos. Mater. 1984 (836) (1984) 21–55, http://dx.doi.org/10.1520/STP30196S.
[11] J. Zangenberg, P. Brøndsted, J.W. Gillespie Jr., Fatigue damage propagation in unidirectional glass fibre reinforced composites made of a non-crimp fabric, J. Compos. Mater. 48 (22) (2014) 2711–2727, http://dx.doi.org/10.1177/0021998313502062.
[12] F. Sket, R. Seltzer, J.M. Molina-Aldareguía, C. Gonzalez, J. LLorca, Determination of damage micromechanisms and fracture resistance of glass fiber/epoxy cross-ply laminate by means of X-ray computed microtomography, Compos. Sci. Technol. 72 (2) (2012) 350–359, http://dx.doi.org/10.1016/j.compscitech.2011.11.025.
[13] S.R. Stock, X-ray microtomography of materials, Int. Mater. Rev. 44 (4) (1999) 141–164.
[14] E. Maire, P.J. Withers, Quantitative X-ray tomography, Int. Mater. Rev. 59 (1) (2014) 1–43, http://dx.doi.org/10.1179/1743280413y.0000000023.
[15] P.J. Withers, M. Preuss, Fatigue and damage in structural materials studied by X-Ray tomography, Annu. Rev. Mater. Res. 42 (2012) 81–103, http://dx.doi.org/10.1146/annurev-matsci-070511-155111.
[16] P. Wright, X. Fu, I. Sinclair, S.M. Spearing, Ultra high resolution computed tomography of damage in notched carbon fiber-epoxy composites, J. Compos. Mater. 42 (19) (2008) 1993–2002, http://dx.doi.org/10.1177/0021998308092211.
[17] P. Wright, A. Moffat, I. Sinclair, S.M. Spearing, High resolution tomographic imaging and modelling of notch tip damage in a laminated composite, Compos. Sci. Technol. 70 (10) (2010) 1444–1452, http://dx.doi.org/10.1016/j.compscitech.2010.04.012.
[18] A.E. Scott, M. Mavrigirdati, P. Wright, I. Sinclair, S.M. Spearing, In situ fibre fracture measurement in carbon-epoxy laminates using high resolution computed tomography, Compos. Sci. Technol. 71 (12) (2011) 1471–1477, http://dx.doi.org/10.1016/j.compscitech.2011.06.004.
[19] S.C. Garcea, M. Macrigirdato, A.E. Scott, I. Sinclair, S.M. Spearing, Fatigue micromechanism characterisation in carbon fibre reinforced polymers using synchrotron radiation computed tomography, Compos. Sci. Technol. 99 (88) (2014) 23–30, http://dx.doi.org/10.1016/j.compscitech.2014.05.006.
[20] S.C. Garcea, I. Sinclair, S.M. Spearing, In situ synchrotron tomographic evaluation of the effect of toughening strategies on fatigue micromechanisms in carbon fibre reinforced polymers, Compos. Sci. Technol. 109 (2015) 32–39, http://dx.doi.org/10.1016/j.compscitech.2015.01.012.
[21] B.M. Patterson, N.L. Cordes, K. Henderson, J.C.E. Mertens, A.J. Clarke, B. Hornberger, A. Merkle, S. Etchin, A. Tkachuk, M. Leibowitz, D. Trapp, W. Qiu, B. Zhang, H. Bale, X. Lu, R. Hartwell, P.J. Withers, R.S. Bradley, Situ laboratory-based transmission X-ray microscopy and tomography of material deformation at the nanoscale, Exp. Mech. (2016) 1–13, http://dx.doi.org/10.1007/s11340-016-0197-3.
[22] P.J. Schilling, B.P.R. Karedla, A.K. Tatiparthi, M.A. Verges, P.D. Herrington, X-ray computed microtomography of internal damage in fiber reinforced polymer matrix composites, Compos. Sci. Technol. 65 (14) (2005) 2071–2078, http://dx.doi.org/10.1016/j.compscitech.2005.05.014.
[23] B. Yu, R. Blanc, C. Soutis, P.J. Withers, Evolution of damage during the fatigue of 3D woven glass-fibre reinforced composites subjected to tensiontension loading observed by time-lapse X-ray tomography, Compos. Part A 82 (2016) 279–290, http://dx.doi.org/10.1016/j.compositesa.2015.09.001.
[24] B. Yu, R.S. Bradley, C. Soutis, P.J. Hogg, P.J. Withers, 2D and 3D imaging of fatigue failure mechanisms of 3D woven composites, Compos. Sci. Technol. 77 (2015) 37–49, http://dx.doi.org/10.1016/j.compositesa.2015.06.013.
[25] S. Topal, L. Baiocchi, A.D. Crocombe, S.L. Ogin, P. Potluri, P.J. Withers, M. Quaresimin, P.A. Smith, M.C. Poole, A.E. Bogdanovich, Late-stage fatigue damage in a 3D orthogonal non-crimp woven composite: an experimental and numerical study, Compos. Part A Appl. Sci. Manuf. 79 (2015) 155–163, http://dx.doi.org/10.1016/j.compositesa.2015.08.020. URL, http://dx.doi.org/10.1016/j.compositesa.2015.08.020.
[26] J. Zangenberg, reportThe Effects of Fibre Architecture on Fatigue Life-time of Composite Materials, PhD Thesis, DTU Wind Energy PhD-0018(EN).
[27] ISO, Plastics - Determination of Tensile Properties - Part 5: Test Conditions for Unidirectional Fibre-reinforced Plastic Composites, International Organization for Standardization, Geneva, Switzerland, 2009. ISO 527-5:2009(E).
[28] R. Talreja, Fatigue of composite materials: damage mechanisms and fatigue-life diagrams, Proc. R. Soc. Lond. A 378 (1981) 461–475, http://dx.doi.org/10.1098/rspa.1983.0054.
[29] J. Banhart, Advanced Tomographic Methods in Materials Research and Engineering, Oxford Univ. Press, 2008, http://dx.doi.org/10.1093/acprof:oso/9780199213245.001.0001.
[30] K.M. Jespersen, J. Zangenberg, T. Lowe, P. Withers, L. Mikkelsen, X-ray CT Data: Fatigue Damage in Glass Fibre/polyester Composite Used for Wind Turbine Blades, 2016, http://dx.doi.org/10.5281/zenodo.154714 [Data set].
[31] K.M. Jespersen, J. Zangenberg, L.P. Mikkelsen, Micromechanical investigation of fatigue damage in uni-directional fibre composites, in: Proceedings of 6th International Conference on Fatigue of Composites, 2015. http://orbit.dtu.dk/files/108663074/ICFCPaperDraft_KMUN_Final.pdf.
[32] S.F. Shuler, J.W. Holmes, X. Wu, D. Roach, Influence of loading frequency on the room-temperature fatigue of a carbon-fiber/SiC-matrix composite, J. Am. Ceram. Soc. 76 (9) (1993) 2327–2336, http://dx.doi.org/10.1111/j.1151-2916.1993.tb07772.x.
[33] N. Chawla, Y. Tur, J. Holmes, J. Barber, A. Szweda, High-frequency fatigue behavior of woven-fiber-fabric-reinforced polymer-derived ceramic-matrix composites, J. Am. Ceram. Soc. 81 (5) (1998) 1221–1230.
[34] K.M. Jespersen, T. Lowe, P. Withers, J. Zangenberg, L. Mikkelsen, Micromechanical time-lapse X-ray CT study of fatigue damage in uni-directional fibre composites, in: 20th International Conference on Composite Materials, 2015. http://iccm20.org/fullpapers/file?f=nDdmYO9mvY.

[P2]

Jespersen, K. M., Wang, Y., Zangenberg, J., Lowe, T., Withers, P. J., and Mikkelsen, L. P

EX-SITU TIME-LAPSE X-RAY CT STUDY OF 3D MICRO-STRUCTURAL FATIGUE DAMAGE EVOLUTION IN UNI-DIRECTIONAL COMPOSITES

ECCM17, Munich, Germany (2016).

EX-SITU TIME-LAPSE X-RAY CT STUDY OF 3D MICRO-STRUCTURAL FATIGUE DAMAGE EVOLUTION IN UNI-DIRECTIONAL COMPOSITES

Kristine M. Jespersen*[1], Ying Wang[3], Jens Zangenberg[2], Tristan Lowe[3], Philip J. Withers[3], Lars P. Mikkelsen[1]

[1]Department of Wind Energy, Section of Composites and Materials Mechanics, Technical University of Denmark, Risø Campus, 4000 Roskilde, Denmark (Email: kmun@dtu.dk*)
[2]LM Wind Power Blades, Composite Mechanics, Jupitervej 6, 6000 Kolding, Denmark
[3]Manchester X-ray Imaging Facility, School of Materials, University of Manchester, Manchester M13 9PL, United Kingdom

Keywords: Micro-tomography, Glass fibre reinforced polymer, Damage progression, Off-axis cracks, Fibre fractures

Abstract
In this study, the progress of damage under tension-tension fatigue of a uni-directional (UD) glass fibre composite made from a non-crimp fabric is studied using transilluminated white light imaging (TWLI) and X-ray computed tomography (CT). TWLI images are automatically captured throughout the fatigue test, and at two damage levels the test is stopped and the sample is examined by X-ray computed tomography. From the TWLI observations it is apparent that part of the measured initial stiffness drop might be caused by edge effects rather than off-axis cracking. Some of the off-axis cracks are seen to initiate already after the first cycle, whereas some grow gradually and others appear suddenly during cycling. The off-axis cracks are observed to saturate after a few thousand cycles. The UD fibre fracture damage in the region observed by X-ray CT is probably already saturated at the first interruption point, as no significant change is seen between the two X-ray images. However, the study indicates how TWLI can be used as an initial indicator to locate damage regions at an early stage for the future ex-situ X-ray CT experiments.

1. Introduction

Fibre composites are increasingly being used to replace metals in many weight sensitive industries such as the aerospace, automotive and wind energy sector. Compared to airplanes and vehicles, wind turbine blades experience repeated loading to a much higher extent [1]. Variations in the wind causes the blades to repeatedly bend flap-wise in the direction of the tower. In addition, the blade rotation causes the gravitational load of the blades to repeatedly change direction resulting in repeated edge-wise bending of the blades. During the 20-30 years of life of a wind turbine blade the total number of load cycles sum up to the range of $10^8 - 10^9$ cycles [1]. As a result, fatigue is one of the limiting factors when designing a large wind turbine blade [2]. Because of the specific load conditions, uni-directional (UD) fibre composites made from non-crimp fabrics (NCFs) are commonly used to carry the primary bending loads in the blade, and the fatigue damage mechanisms for this material are not well understood. In order to improve the fatigue resistance and/or establish more reliable methods to predict the fatigue life-time, it is necessary to understand the fatigue damage mechanisms on a microstructural level. This is the focus of the current study.

1.1. Fatigue damage progression in fibre composites

Fatigue damage in fibre composites has received much focus in literature, however fatigue damage progression in fibre composites is complex. Several damage mechanisms such as fibre/matrix debonding, matrix cracking, and fibre fractures occur and interact with each other [3]. Furthermore, the damage mechanisms are dependent on many things such as the lay-up, materials, fibre/matrix interface, loading and more. For cross-ply and other angle-ply laminates, tension fatigue damage is known to initiate in the off-axis layers as tunnelling cracks [4, 5]. These cracks then result in more serious damage such as fibre fractures and interlaminar delaminations.

The UD NCF composites used for wind turbine blades generally include thin layers of off-axis fibres, which to some extent makes them similar to "extreme" angle-ply composites with thin off-axis layers compared to the UD. However, in NCFs the fibres are gathered in bundles and the off-axis fibre bundles generally have isolated points where they cross over each other. It has been observed in previous studies [6, 7] that the UD fibre damage during tension fatigue appear locally rather than uniformly distributed across the material. Furthermore, the locations of the UD fibre damage regions are closely related to these cross-over points for the thin off-axis fibre bundles. This leads to quite complex damage mechanisms, which are difficult to monitor and predict.

1.2. Non-destructive damage observation

In-situ (or ex-situ) X-ray CT makes it possible for the progress of internal damage to be observed non-destructively. So far, in-situ X-ray CT experiments of damage progression in fibre composites have generally been performed using synchrotron radiation X-ray CT [8–11] because of the relatively short scan time. However, due to limited access time, fatigue damage progression experiments such as those by Garcea et al. [10, 11] only consider a few thousand load cycles. Recent advances in laboratory X-ray CT has resulted in image quality competitive to synchrotron CT, but at longer scan times. Using laboratory X-ray CT makes it easier to perform longer duration start-stop studies, which would not be possible using synchrotrons due to the limited access. Only a few studies have considered damage in fibre composites using laboratory X-ray CT (e.g. [12–14]) and in particular studies considering individual fibre fractures and the progress of damage over time have been limited to date.

When it comes to damage observation, a limitation of X-ray CT is that it relies on differences in density to get contrast in the image. This means that if cracks are closed, they are likely not to be visible in the image. This is particularly challenging in relation to matrix and interface cracks, although a number of strategies have been applied to improve this [15]. For glass fibre composites transilluminated white light imaging (TWLI) as also used in [4, 5] can be used to monitor cracks in 2D. In the current study, TWLI is used in combination with X-ray CT to observe the damage progression over time in a UD NCF glass fibre composite. The study demonstrates the advantage of combining these observation techniques and highlights promising future aspects.

2. Composite material system and specimen geometry

The considered composite was a UD glass fibre/polyester resin composite made from a non-crimp fabric. The fabric was made from parallel UD fibre bundles, which were stitched to a thin layer of off-axis ($\pm 80^\circ$) supporting backing bundles (the same fabric used in [6, 7]). The composite was made by stacking two layers of fabric with the backing sides facing each other in the centre ($[0/b]_s$), and then impregnating them with resin using vacuum assisted resin transfer moulding (VARTM) infusion. End tabs were glued on to a plate of the composite and small rectangular specimens were cut out for fatigue testing. The specimen length was 117mm with a gauge section of 40mm. The tabs were tapered over a length of

10mm towards the gauge section to decrease stress concentrations in the laminate.

3. Experimental methods

Fig. 1a shows a sketch of the typical shape of the stiffness degradation response for the composite material outlined in Section 2 during tension-tension fatigue. Within the initial few thousand cycles, the stiffness drops by a few percent as indicated by region I in Fig. 1. Thereafter, the stiffness degrades stably for a high number of cycles, which is shown as region II. Finally, as marked by region III, the stiffness starts to decrease drastically followed by final failure. As also indicated in Fig. 1a, the idea is to use TWLI to monitor the initiation and growth of transverse cracks (region I) and then use X-ray CT to monitor the stable stiffness degradation (region II). In previous studies [6, 7], UD fibre fractures have been reported during region II, and X-ray CT is used to observe these failures, as they cannot be seen by the TWLI camera.

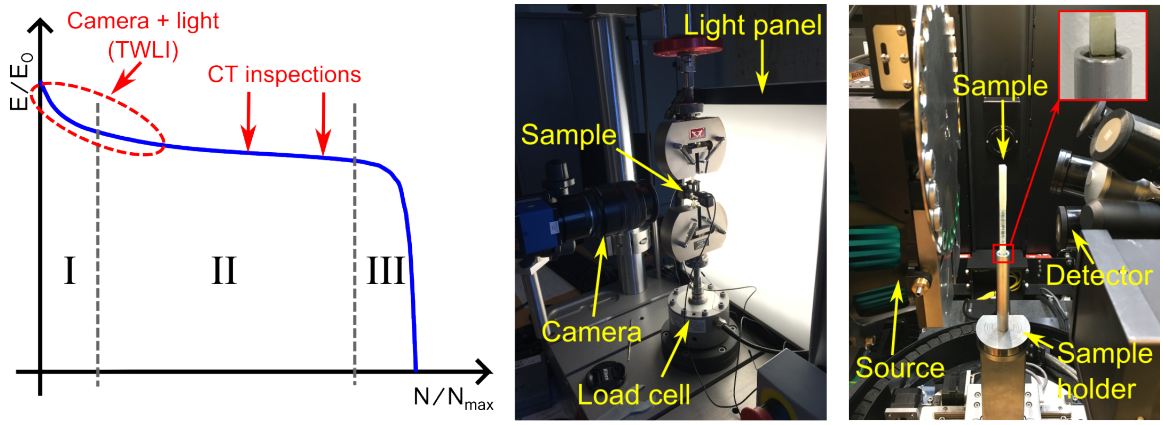

a) Typical stiffness degradation and examination idea

b) Fatigue test

c) X-ray CT

Figure 1. a) shows the typical shape of the stiffness degradation response for the considered material, b) the fatigue test including the TWLI setup, and c) the sample mounted in the X-ray CT scanner.

3.1. Fatigue testing and off-axis crack monitoring

The fatigue tests were carried out on an Instron Electropuls E3000 (max 3 kN) at 0.6% strain in load control with a sinusoidal waveform. The load range based on the desired strain of the test was determined from two initially performed static tensile tests to obtain the initial Young's modulus. The test was carried out with a stress-ratio of R=0.1, a test frequency of 10Hz, and the strain was monitored using one extensometer having a gauge length of 25mm and a maximum deflection of 2.5mm. The test was interrupted at two points in the loading history for X-ray examination.

A camera of type SVS-Vistek SVCam EVO8050 GigE with a Nikon AF Micro Nikkor 60mm 1:2.8D lens was mounted on the fatigue test setup and a light panel was placed behind the test specimen to highlight cracks as shown in Fig. 1b. The camera was connected to a trigger box ensuring automatic image acquisition during the test. As crack initiation and growth appear at a faster pace in the beginning of the test, images were acquired at the peak of every load cycle for the first 100 cycles, after which the number of images acquired was decreased to keep the amount of data down without compromising the results. The aim was to acquire 100 images per fatigue cycle decade.

3.2. X-ray computed tomography

The X-ray CT experiments were carried out on a laboratory type Zeiss Xradia Versa 520 scanner. Two sets of scan settings were used as shown in Table 1. All scans were performed using a detector with 4x optical magnification and a pixel depth of 16 bit. The pixels on the detector were binned down with a factor of 2 (binning 2). The sample was mounted in a specially made cylindrical aluminum holder as shown in Fig. 1c. It was made from a solid cylindrical piece, and a hole corresponding to the longest diagonal on the sample cross section was drilled with a depth of 30 mm. To be able to repeatedly mount the sample in approximately the same way, both the sample and the holder were marked with a pen as also seen in Fig. 1c.

Table 1. Overview of x-ray CT scan settings

Scan name	Source to sample distance (mm)	Detector to sample distance (mm)	Exposure time (s)	No. of projections -	Accelerating voltage (keV)	Pixel size (μm)
MR	24	30	2	3201	70	3.13
HR	24	55	7	4601	70	2.05

Since the UD fibre fractures are local phenomena it can be difficult to locate a region with damage if choosing a location arbitrarily. To locate a damage region in the sample, the photos of the off-axis cracks were evaluated and an initial scan region was located where a medium resolution (MR in Table 1) scan was carried out to confirm the locations of fibre fractures. Based on the observed damage regions in this scan, a re-centered high resolution (HR in Table 1) scan was performed. The re-centering was done to get the damage as central as possible in the field of view (FoV) and was done using the "Scout-and-scan" principle suggested by Zeiss.

4. Results and discussion

Fig. 2 shows the measured stiffness degradation during the fatigue test. The data for the full test are shown in Fig. 2a. Several points of interest have been marked, and point E and F indicates where the fatigue test was interrupted for CT examination. The slight drop in measured stiffness after the interruption is likely to be because two extensometers (instead of one as for the first part) were used to measure the strain for the final 50,000 cycles. However, it is seen that the difference is minimal and that the trend is unaffected. A zoom on the initial stiffness degradation part is shown in Fig. 2b. A steep drop of around 1% in stiffness is observed between 0 cycles and point A, which is more clearly seen in Fig. 2c.

Camera images were acquired during the full test and the corresponding camera images of a few of the points of interest marked in Fig. 2 are shown in Fig. 3. In Fig. 3 it is seen that a few off-axis cracks have appeared after the initial E-modulus test (corresponding to two cycles). A significant increase in the number of off-axis cracks is seen from point 0 to point A (480 cycles), which is probably the origin of the steep initial stiffness drop of around 1% seen in Fig. 2c. The steep linear decrease in stiffness seen between point A and B in Fig. 2b is likely to be caused by a gradual increase in the number of off-axis cracks as seen by the difference between point A and B in Fig. 3. There is only a small difference observed in the number of off-axis cracks between point B and C. However, edge damage is seen to initiate around point B, and it is possible that the stiffness drop between point B and C is more related

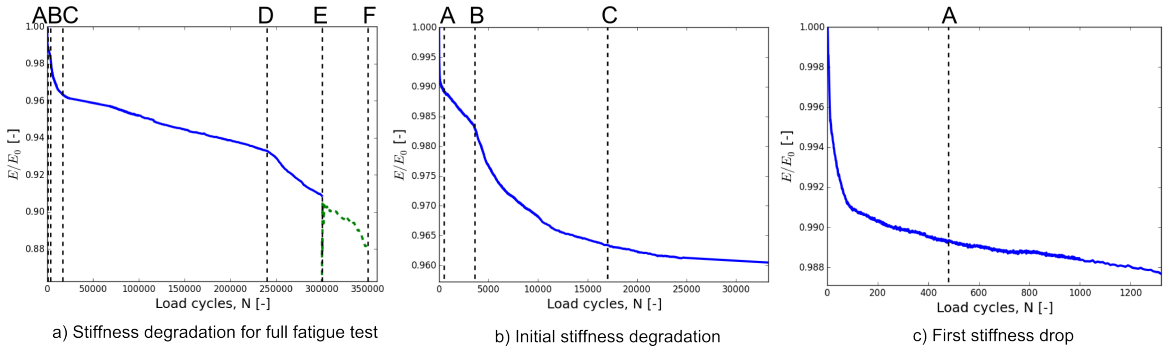

Figure 2. Normalised stiffness degradation for the fatigue test. a) shows the full test, b) a zoom on the initial stiffness degradation region, and c) the first steep stiffness drop. The marked points of interest; A, B, C, D, E, and F correspond to 480, 3600, 17000, 240000, 300000, 350000 cycles, respectively. Point E and F represent the points at which the test was interrupted for X-ray CT.

to edge effects than to actual damage mechanisms of the material. Between point C and D the stiffness degrades stably. At point C, what looks like local delaminations (probably between the backing bundle layers) in the loading direction starts to gradually grow (visible at point D in Fig. 3). After point D the inclination of the stiffness degradation becomes steeper. Perhaps surprisingly, there is almost no difference in the photos taken at point D and E.

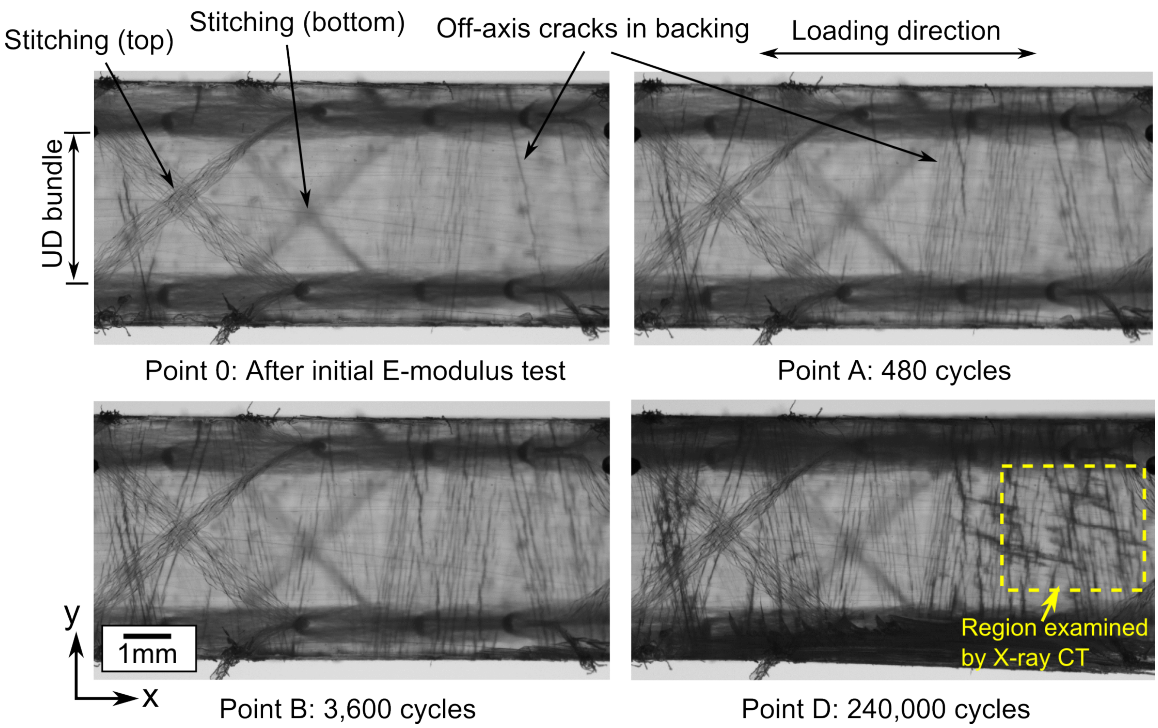

Figure 3. TWLI camera images acquired during fatigue testing. The region imaged by CT in Fig. 4 is shown.

The fatigue test was interrupted at point E, and the sample was examined by X-ray CT in the region where the photos indicated that UD fibre fractures were likely to be present (See point D in Fig. 3). After X-ray CT scanning of the sample, it was fatigued for an additional 50,000 cycles as seen by the dashed green curve between point E and F in Fig. 2a, and scanned once again. Fig. 4 shows a virtual slice of the 3D X-ray CT data in approximately the same location for the two scans. No significant

change in damage is observed although there are a few additional UD fibre fractures (see arrow in Fig. 4). Nevertheless, it may be possible that the two slices are not exactly in the same location or the slice angle is slightly different. Therefore, an automatic quantification method for fibre fractures is necessary for proper comparison, and this is therefore currently a topic of ongoing work. As no or little change in damage was observed, it is likely that the damage region was already saturated at the point of the first scan, and that damage regions in other locations were growing instead. Therefore it is necessary to find and follow damage regions at a point earlier in the fatigue life in order to follow the damage propagation. This can be quite challenging as the FoV is small and the damage regions are isolated local regions. However, the photos of the transverse cracks along with initial overview CT scans can be used as guidance to choose the scan location to follow over time. This is currently ongoing work.

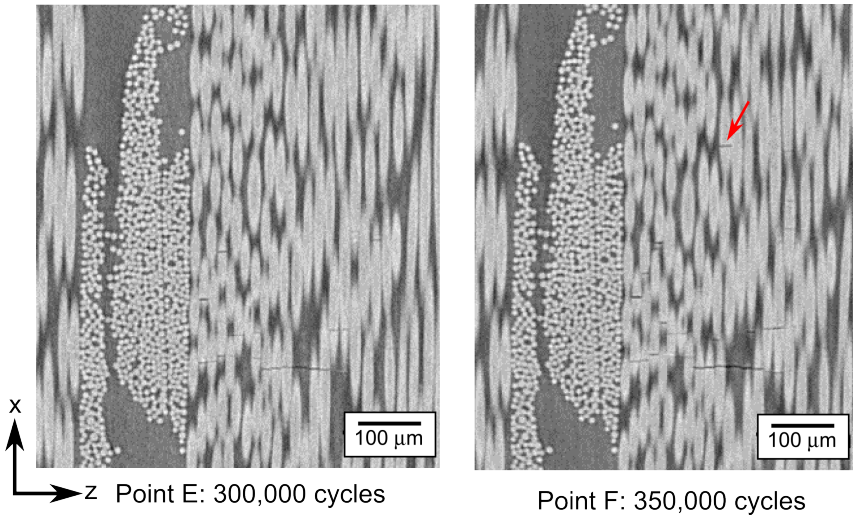

Figure 4. Virtual 2D x-z slice extracted from 3D X-ray CT data for point E and F. No particular change in damage is observed.

Even though the fibre failures are seen quite clearly in Fig. 4, it is not possible to see any matrix cracks in the backing bundles. That is despite knowing from the results in Fig. 3, that they are present. As discussed previously in [7], this is a matter of insufficient resolution (~2-3μm) since the opening of these cracks is small. Here, it is important to remember that the camera photos were taken at the point of maximum load during the fatigue test. Fig. 5 shows the camera images of point D where Fig. 5a is the loaded sample and Fig. 5b is when the load is removed. It is evident that most of the matrix cracks almost close completely when the load is removed, which explains why they are difficult to see using X-ray CT on the unloaded specimen. Therefore it is of interest to also apply tension during scanning, as watching the off-axis cracks in 3D would provide additional useful information about the damage mechanisms as proposed by [15].

5. Conclusion

In this study the tension-tension fatigue damage progression of a uni-directional glass fibre composite made from a non-crimp fabric was studied. The initiation and growth of off-axis cracks were studied by transilluminated white light imaging and the UD fibre fractures were examined by X-ray CT. The measured stiffness degradation was compared to the corresponding camera images and discussed. No change in size of the fibre fracture region was seen by X-ray CT, however it is believed that the observed region was already saturated. The cause of the stiffness degradation between the two interruption points is believed to be the growth of UD fibre fracture regions at other locations in the sample that are not yet saturated. However, this will have to be confirmed. In the future, a damage region will be located at an

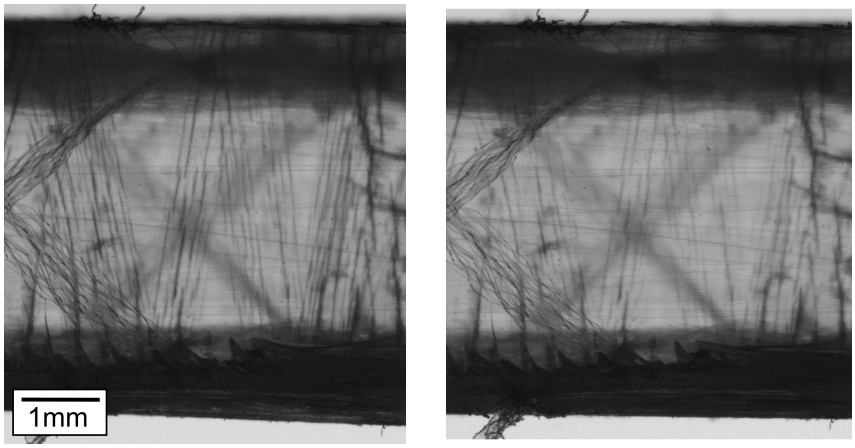

Figure 5. Camera images after 300,000 cycles where a) shows the loaded and b) unloaded sample.

earlier stage with guidance from observed transverse cracks and a quick overview X-ray CT scan, and the growth of the UD fibre fracture region monitored by X-ray CT.

Acknowledgments

The author would like to acknowledge the assistance provided by the Manchester X-ray Imaging Facility, which was funded in part by the EPSRC (grants EP/F007906/1, EP/F001452/1 and EP/I02249X/1). Financial support from CINEMA: "the allianCe for ImagiNg of Energy MAterials", DSF-grant no. 1305-00032B under "The Danish Council for Strategic Research" is gratefully acknowledged. Additionally, we would like to thank LM Wind Power for manufacturing of test specimens.

References

[1] R. P. L. Nijssen. Fatigue life prediction and strength degradation of wind turbine rotor blade composites. *PhD Thesis, Delt University of Technology*, 2006.

[2] R. P. L. Nijssen and P. Brøndsted. Fatigue as a design driver for composite wind turbine blades. *Advances in Wind Turbine Blade Design and Materials*, pages 175–209, 2013.

[3] W. W. Stinchcomb and K. L. Reifsnider. Fatigue damage mechanisms in composites materials: a review. *Fracture Mechanisms, Proceedings of an ASTM-NBS-NSF symposium, ASTM STP 675*, pages 762–787, 1979.

[4] M. Quaresimin, P. A. Carraro, L. P. Mikkelsen, N. Lucato, L. Vivian, P. Brøndsted, B. F. Sørensen, J. Varna, and R. Talreja. Damage evolution under cyclic multiaxial stress state: A comparative analysis between glass/epoxy laminates and tubes. *Composites: Part B*, 61:282–290, 2014.

[5] J. A. Glud, J. M. Dulieu-Barton, O. T. Thomsen, and L. C. T. Overgaard. Automated counting of off-axis tunnelling cracks using digital image processing. *Composites Science and Technology*, 125:80–89, 2016.

[6] J. Zangenberg, P. Brøndsted, and J. W. Gillespie Jr. Fatigue damage propagation in unidirectional glass fibre reinforced composites made of a non-crimp fabric. *Journal of Composite Materials*, 48(22):2711–2727, 2014.

[7] K. M. Jespersen, T. Lowe, P. J. Withers, J. Zangenberg, and L. P. Mikkelsen. Fatigue damage assessment of uni-directional glass/polyester composite using x-ray computed tomography. *Composites Science and Technology*, 2016. (Submitted).

[8] P. Wright, A. Moffat, I. Sinclair, and S. M. Spearing. High resolution tomographic imaging and modelling of notch tip damage in a laminated composite. *Composites Science and Technology*, 70(10):1444–1452, 2010.

[9] A. E. Scott, M. Mavrigirdati, P. Wright, I. Sinclair, and S. M. Spearing. In situ fibre fracture measurement in carbon-epoxy laminates using high resolution computed tomography. *Composites Science and Technology*, 71(12):1471–1477, 2011.

[10] S. C. Garcea, M. Macrigirdato, A. E. Scott, I. Sinclair, and S. M. Spearing. Fatigue micromechanism characterisation in carbon fibre reinforced polymers using synchrotron radiation computed tomography. *Composites Science and Technology*, 99(88):23–30, 2014.

[11] S. C. Garcea, I. Sinclair, and S. M. Spearing. In situ synchrotron tomographic evaluation of the effect of toughening strategies on fatigue micromechanisms in carbon fibre reinforced polymers. *Composites Science and Technology*, 109:32–39, 2015.

[12] P. J. Schilling, B. P. R. Karedla, A. K. Tatiparthi, M. A. Verges, and P. D. Herrington. X-ray computed microtomography of internal damage in fiber reinforced polymer matrix composites. *Composites Science and Technology*, 65(14):2071–2078, 2005.

[13] F. Sket, R. Seltzer, J. M. Molina-Aldareguía, C. Gonzalez, and J. LLorca. Determination of damage micromechanisms and fracture resistance of glass fiber/epoxy cross-ply laminate by means of X-ray computed microtomography. *Composites Science and Technology*, 72(2):350–359, 2012.

[14] B. Yu, R. Blanc, C. Soutis, and Withers P. J. Evolution of damage during the fatigue of 3D woven glass-fibre reinforced composites subjected to tension–tension loading observed by time-lapse X-ray tomography. *Composites: Part A*, 82:279–290, 2016.

[15] B. Yu, R. S. Bradley, C. Soutis, and P. J. Withers. A comparison of different approaches for imaging cracks in composites by x-ray microtomography. *Philosophical Transactions of the Royal Society A*, 2016. http://dx.doi.org/10.1098/rsta.2016.0037, In press.

[P3]

Jespersen, K. M. and Mikkelsen, L. P.

FATIGUE DAMAGE OBSERVED NON-DESTRUCTIVELY IN FIBRE COMPOSITE COUPON TEST SPECIMENS BY X-RAY CT

IOP Conf. Series: Materials Science and Engineering, 139, 12024 (2016).

Fatigue damage observed non-destructively in fibre composite coupon test specimens by X-ray CT

2016 IOP Conf. Ser.: Mater. Sci. Eng. 139 012024

(http://iopscience.iop.org/1757-899X/139/1/012024)

IOP Conf. Series: Materials Science and Engineering **139** (2016) 012024 doi:10.1088/1757-899X/139/1/012024

Fatigue damage observed non-destructively in fibre composite coupon test specimens by X-ray CT

K M Jespersen[1] **and L P Mikkelsen**

Department of Wind Energy, Section of Composites and Materials Science, Technical University of Denmark, Risø Campus, 4000 Roskilde, DK

E-mail: kmun@dtu.dk[1]

Abstract. This study presents a method for monitoring the 3D fatigue damage progression on a micro-structural level in a glass fibre/polymer coupon test specimen by means of laboratory X-ray Computed Tomography (CT). A modified mount and holder made for the standard test samples to fit into the X-ray CT scanner along with a tension clamp solution is presented. Initially, the same location of the test specimen is inspected by ex-situ X-ray CT during the fatigue loading history, which shows the damage progression on a micro-structural level. The openings of individual uni-directional (UD) fibre fractures are seen to generally increase with the number of cycles, and new regions of UD fibre fractures also appear. There are some UD fibre fractures that are difficult to detect since their opening is small. Therefore, the effect of tension on the crack visibility is examined afterwards using a tension clamp solution. With applied tension some additional cracks become visible and the openings of fibre fractures increases, which shows the importance of applied tension during the scan.

1. Introduction

Wind power turbines are increasingly used in many parts of the world to match the increasing demand for sustainable energy. Among sustainable energy sources wind power is one of the most cost efficient technologies, however they are yet to be competitive to fossil fuels. The cost of energy can be decreased by increasing the blade length, as the power output of the wind turbine scales with the blade length squared. One of the main design factors when increasing the length of the blade is material fatigue, since the blades experience a high degree of repeated loading [1]. The wind variation causes the blades to bend in the direction of the tower (flap-wise bending), and the rotation results in the gravitational loads of the blades repeatedly changing direction causing a repeated edge-wise bending motion. With a life-time in the range of 20-30 years the total number of load cycles sums up to 10^8-10^9, which is significantly higher than for e.g. airplanes and cars [2]. Furthermore, it is the degradation of the stiffness rather than the strength which is a concern for wind turbine blades, since the blades might risk hitting the tower. As the blades mainly experience bending loads, uni-directional glass fibre composites made from non-crimp fabrics (NCFs) are commonly used for the load carrying parts of the blades. However, the fatigue mechanism in these NCF composites is not well understood. If the damage mechanism was properly understood on a micro-structural level it would be possible to decrease safety factors and make more fatigue resistant wind turbine blade materials. Therefore, establishing a method capable of monitoring tension-tension fatigue damage progression in a glass fibre/polymer is the focus of this paper.

Fatigue damage progression in composites is a complex process which includes several interacting damage mechanisms. Many of the damage features are small and difficult to monitor non-destructively. The UD NCF composites used for wind turbine blades commonly include cross-crossed thin supporting bundles (backing bundles) to which the UD bundles are stitched to keep them aligned during manufacturing and handling. For these NCF composites the stiffness degradation during fatigue is mainly caused by UD fibre fractures and is also slightly affected by the initial off-axis cracking in the backing bundles. Furthermore, the location of the UD fibre fractures seems to be highly related to the cross-over points of the off-axis backing bundles [3, 4]. Therefore, the damage appears as local fibre fracture regions at various locations rather than purely homogeneously throughout the material. Furthermore, the fibre fractures and off-axis cracks are features of a few micrometers in size and appear as 3D features such as clusters and chains of fibre fractures [4]. All of this makes it difficult to monitor the damage over time experimentally, since a high resolution non-destructive 3D damage monitoring technique is necessary.

Through time, different methods for in-situ damage monitoring have been used in the attempt to monitor damage progression of fibre composites. On a structural level, several methods such as vibraction analysis, acoustic emission, ultrasonic testing [5], and optical sensors [6] techniques have been used to monitor damage in wind turbine blades, however at a millimeter or even centimeter spatial resolution. 2D imaging methods such as SEM and camera imaging have been used to observe the surface damage progression on a micro-structural level [7, 8], and particularly SEM gives invaluable information on small-scale damage mechanisms due to the high resolution. However, using such methods one does not know what happens below the considered surface. In relation to monitoring the damage progression in fibre composites on a micro-structural level in 3D, X-ray Computed Tomography (CT) is probably the most promising technique. Synchrotron radiation CT has due to the short scan times been used for in-situ studies on fibre composites [9, 10, 11, 12]. However, in relation to fatigue damage progression these studies are limited to a few thousand cycles (e.g. [11, 12]) due to the limited access time. Although the scan time is considerably longer, the obtainable resolution for laboratory X-ray CT imaging has recently become competitive to synchrotron CT. Some studies [13, 14, 15] have considered in-situ damage monitoring in composites by laboratory X-ray CT. However, general for most of the studies is that they consider small sample sizes to obtain a high resolution. As considering in-situ loading of down-sized samples might affect the damage mechanisms in the sample, it is of interest to be able to monitor the damage non-destructively in the regular coupon test specimens, which is scope of the current study.

Our work outlines a method capable of monitoring tension fatigue damage in 3D for a glass fibre/polymer coupon test specimen non-destructively by means of laboratory X-ray CT. Modified solutions for mounting the large samples in the X-ray CT scanner and a method to apply tension to the sample during scanning are explained. Furthermore, the study outlines some limitations and some important factors to take into account when evaluating the results.

2. Composite material and test specimens

The considered material is a glass fibre/epoxy composite made from two types of non-crimp fabrics (NCF); a UD and a biax fabric. In the UD fabric thin supporting off-axis backing bundles are stitched to the UD bundles to keep them aligned. The stacking sequence is $[\pm 45,\mathrm{b}/0,\mathrm{b}/0]_s$ where "0" is the UD bundle layer and "b" symbolises the backing layer containing both $\pm 45^\circ$ and 90° fibre bundles. This means that the composite contains 4 layers of UD and has a layer of biax at each surface. The material is similar to that considered in [16].

Plates of the UD laminate were cut into butterfly shaped test specimens (for more information on the specimen geometry, see [17]). The specimen geometry with curved edges is specially designed to test UD composites, as the standard plane geometries tend to fail by shear failure

in the tabs [17]. The specimen length was 410mm, the width of the gauge section was 15mm, and the thickness of the composite was 4.5mm. 140mm long tapered tabs were attached in both ends of the sample.

3. Experimental methods

To investigate the damage progression in the composite, an ex-situ X-ray CT start-stop fatigue test was performed on a full-size butterfly coupon specimen. Every time the test was interrupted the sample was inspected in the same location using X-ray CT, thereby observing the damage progression in terms of individual UD fibre fractures. The influence of applied tension during X-ray CT scanning was examined by a tension clamp solution.

3.1. Fatigue testing

Fatigue tests were performed on a hydraulic Instron test machine (max 250kN) in load control with a sinusodial waveform and a stress ratio of R=0.1. The fatigue test was carried out with a test frequency of 5Hz and the strain was monitored with two extensometers (one on each side of the sample). Two initial static tests were performed on the sample prior to the fatigue test to determine the initial Young's modulus. This was used to determine the load range where a peak strain of 1% was obtained. The sample used for the ex-situ test was stopped four times (after 47300, 57300, 67300, and 77300 cycles) during the fatigue load history for X-ray CT scanning. Another sample was stopped after 67000 cycles, where damage was expected to be present, for investigation of the effect applied tension on the crack visibility.

3.2. X-ray computed tomography

The X-ray CT experiments were carried out on a Zeiss Xradia Versa 520 scanner, using a 2000x2000 pixel detector with a pixel depth of 16 bit. All scans were performed with a binning of 2 of the pixels on the detector. This means that 2x2 pixels are combined into one giving a higher intensity (shorter scan time) but also a larger pixel size (lower resolution). Three different scan settings were used as shown in Table 1. To locate the damage initially in the ex-situ study, a large field of view (LFOV) scan was performed on the sample. After 47300 cycles, it was possible to see an indication of damage despite the coarse resolution (17.4μm voxel size). A high resolution scan was then performed in that region by means of the "Scout-and-Scan" principle provided by Zeiss and using the "ex-situ" scan settings labeled "ES" in Table 1. For the remaining times the test was interrupted only high resolution scans were performed. For the tension clamp experiments elaborated later, the scan settings "TC" were used and include a higher number of projections to make up for presence of two carbon pins necessary to transfer the load.

Table 1. X-ray CT scan settings used for the large field of view (LFOV), ex-situ (ES), and tension clamp (TC) scans.

Scan name	Source to sample (mm)	Detector to sample (mm)	Exp. time (s)	No. of projections -	Accelerating voltage (keV)	Pixel size (μm)	Optical Mag.	Scan time (h)
LFOV	30	88	2	801	60	17.4	0.4x	2
ES	28	35	7	4601	70	3	4x	11
TC	30	50	12	5201	70	2.5	4x	20

Because of the large sample size mounting in the scanner is not possible with the standard mount and sample holders. Therefore, a short mount was manufactured and a grip (Makro Grip 5-Achs-Spanner from Lang) was modified to fit into the scanner. Fig. 1 a shows the sample placed in the scanner using the short mount and special sample holder. Using this setup it is possible to scan a bit more than the bottom half of the 410mm long sample (there is a limitation of how far down the sample can go). Furthermore, the sample can be mounted in the same way every time with a variation of less than 1mm. A fine tuning of the location was done by comparing the 2D projection images to ensure as little variation as possible between the location of the observed region in the ex-situ study.

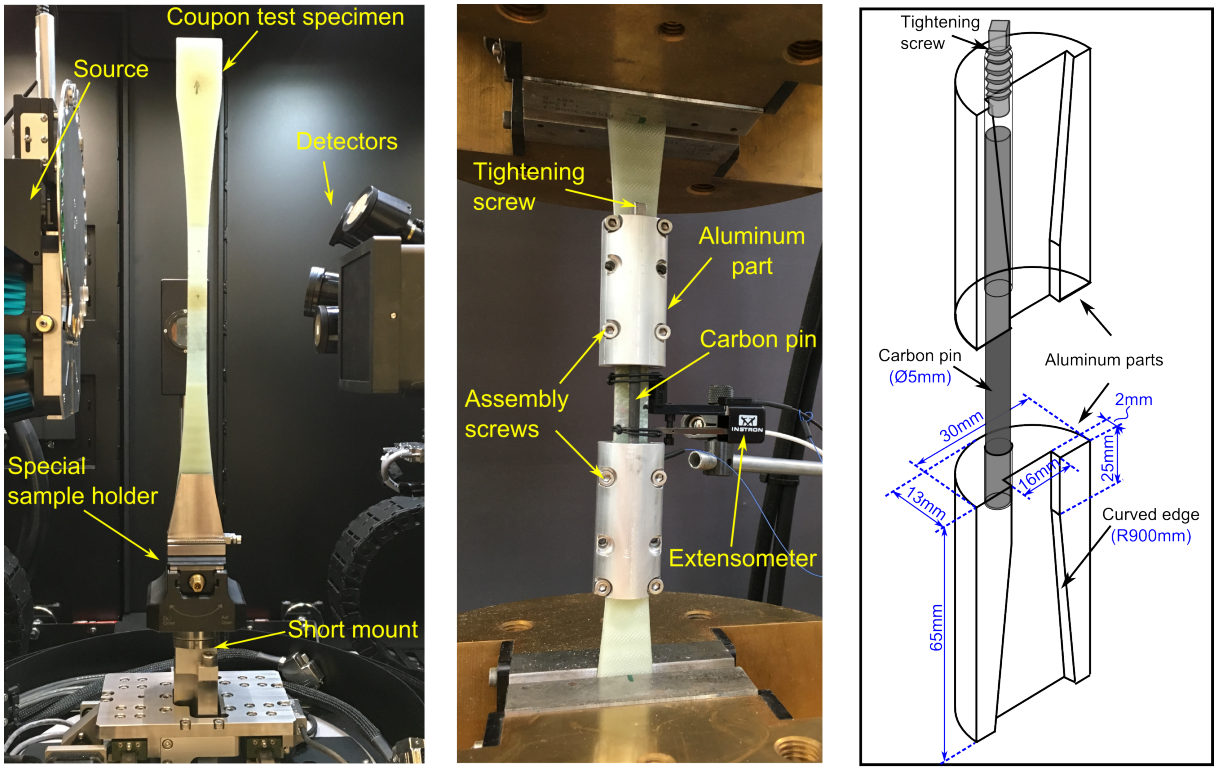

a) Sample mounted in scanner b) Tension clamp on sample c) Principle sketch of clamp tightening mechanism

Figure 1. Specialised experimental setups. a) shows the mounting method for the scanner, b) the tension clamp solution on sample in tension machine, and c) a principle sketch of the tightening mechanism showing half the clamp (scale not exact).

The effect of applied tension on crack visibility was examined using a specially designed tension clamp, which is designed so that the sample can be scanned with the clamp attached. The clamp is shown on the sample in Fig. 1b and Fig. 1c shows a principle sketch of the clamp tightening mechanism along with the approximate dimensions. Fig. 1c only shows half the clamp as it is symmetric, and the holes and assembly screws used to hold the two clamp halves together (seen in Fig. 1b) are excluded for simplicity. While the sample is loaded in a regular tensile test machine, the clamp is mounted on the sample using the assembly screws and the two tightening screws on the top aluminum parts are tightened. By doing so, the carbon pins that transfer the load are also tightened as shown in Fig. 1c. The internal geometry of the aluminium parts of the clamp fits the curvature of the sample, and therefore the aluminum parts are kept in place after the carbon pins are tightened, even after unloading the tensile test machine. That means

that when the load is released on the test machine, the clamp will ensure that the central part of the sample is still in tension. The strain in the sample was measured using an extensometer. The sample was loaded up to 7kN corresponding around 0.2-0.3% strain and then the clamp was mounted on the sample. After removing the load, the clamp stabilised at a strain of 0.17% in the gauge section. Obtaining a higher strain using the clamp was attempted, but even if a higher initial load was used the strain in the gauge section went back to the same value. This could be due to damage in the ends of the carbon pins at high loads, and a slightly modified solution is necessary to obtain higher loads. A possible improvement in the future could be to add reinforcement to the ends of the carbon pins. However, in this study a strain of 0.17% was used, which was the highest obtainable strain for the presented clamp solution.

4. Results and discussion

4.1. Fatigue test result

The measured stiffness degradation of the ex-situ fatigue study is shown by the solid line in Fig. 2a where the four interruption points for CT inspection are marked (N_A-N_D). Slight jumps in the data were observed at each of the interruption points, but since this is due to mounting the extensometers a bit differently every time, the curve sections were off-set to give a continuous curve. Fig. 2a also include two other sets of test data (dashed lines) for a slightly higher strain level (1.1%).

By comparison, it is seen that the shape of the ex-situ fatigue curve is similar to those observed for continuous tests to failure. However, the life-time is less for the ex-situ test performed at 1% strain than for the continuous tests carried out at 1.1% strain, which is opposite of what would be expected. However, Fig. 2b shows the S-N data for samples not affected by X-ray relative to the ex-situ test, and even though the life-time seemed less than for the normal tests, it is not significantly different. Whether this slightly shorter life-time was caused by the effect of X-ray or simply that the sample itself was an outlier cannot be said for certain. However, in addition to the slightly shorter life-time the sample was observed to discolor because of X-ray (Fig. 2c) and it is therefore a subject that requires further investigation.

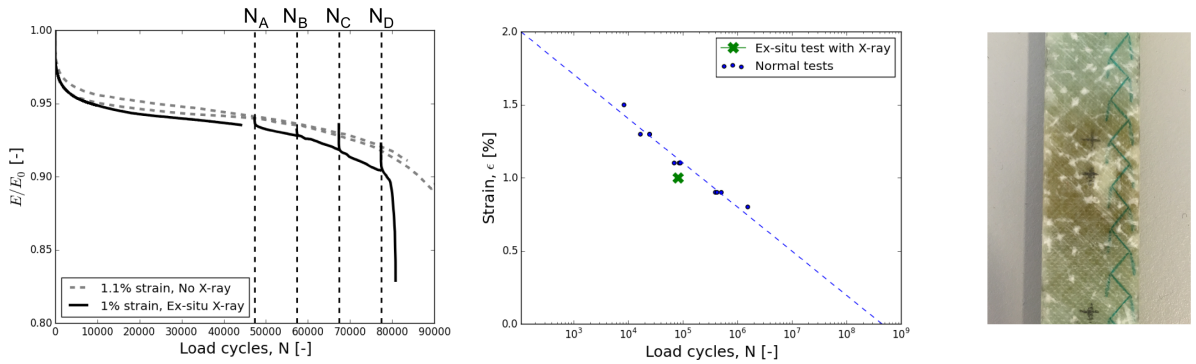

a) Stiffness degradation b) S-N Curve c) Discoloring from X-ray

Figure 2. a) shows the stiffness degradation curve for the ex-situ fatigue test (solid line) and examples of continuous fatigue tests (dashed lines) for samples without X-ray exposure, b) the S-N curve data for samples not affected by X-ray compared to the ex-situ sample, and c) the discoloring observed on the sample after N_D cycles (after all the X-ray experiments).

4.2. Ex-situ X-ray CT monitoring of damage progression

Fig. 3 shows virtual 2D slices of the X-ray CT data (no applied tension) for the four different stages of the fatigue test (N_A-N_D in Fig. 2a). There was a slight variation in the scanned location for each scan because of mounting/dismounting the sample in the holder, however as it is seen from Fig. 3 it is quite a small difference for the scans performed after N_A, N_B, and N_C cycles. The reason for the large variation for the scan performed after N_D cycles was that the bottom of the holder had been disassembled between step N_C and N_D, which is important not to do in future studies. As expected, the UD fibre damage is observed to progress with increasing number of cycles. Both new fibre fractures are observed to appear and the opening

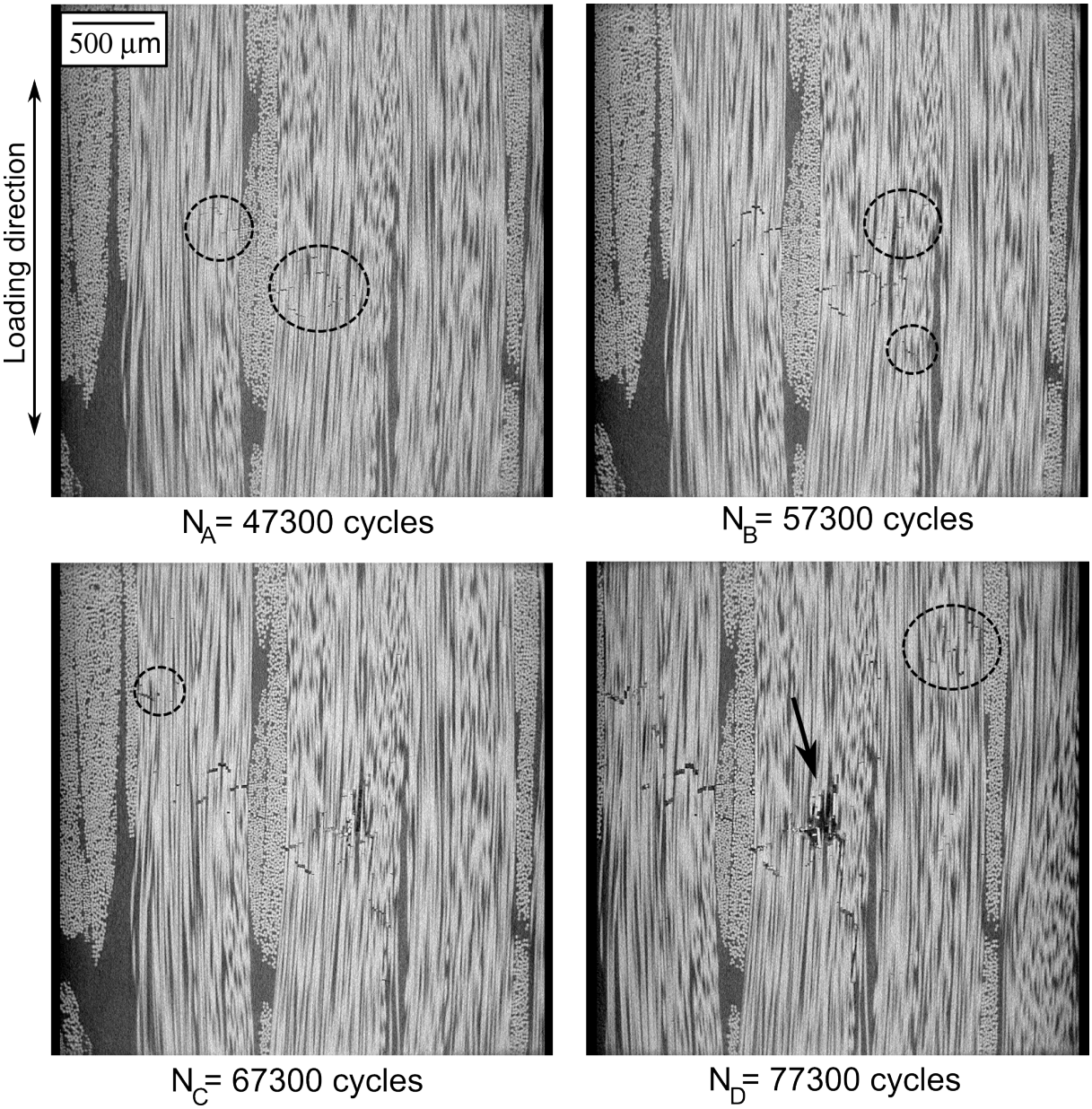

Figure 3. Virtual 2D slice views from 3D X-ray CT scan data showing the damage after each of the four times the fatigue test was interrupted. The ellipses indicate some locations with new damage and the arrow marks a highly damaged region.

of existing fibre fractures is seen to increase for each step. After N_D cycles a damage region with large crack openings compared to other locations was observed (indicated by the arrow in Fig. 3) and the final failure of the sample happened shortly after this (as also seen in Fig. 3). The increasing openings of the UD fibre fractures might be linked of the gradual length increase of the sample during fatigue, however evaluating and comparing the observed damage mechanisms in all the data sets in detail is still ongoing work. In general for all the X-ray data, many fibre fractures were clearly visible, but some had a small opening making them difficult to see. Furthermore, off-axis cracks were not clearly visible because of the small opening. A possible way to increase the visibility of these cracks is to apply tension during scanning in order to open them up, as will be explained in the following section.

4.3. Effect of applied tension during scan

Fig. 4 shows two scans performed in the same damage region of a sample interrupted after 67,000 cycles at 1% strain. Fig. 4a shows a virtual 2D slice from the 3D x-ray data of the unloaded specimen, and Fig. 4b shows the same position with the tension clamp attached keeping the sample at 0.17% strain. It should be noted that 0.17% strain is only around on fifth of the maximum strain during fatigue. Some regions of interest are marked and compared for the loaded sample (region A1-D1) and the unloaded sample (region A2-D2) in Fig. 5.

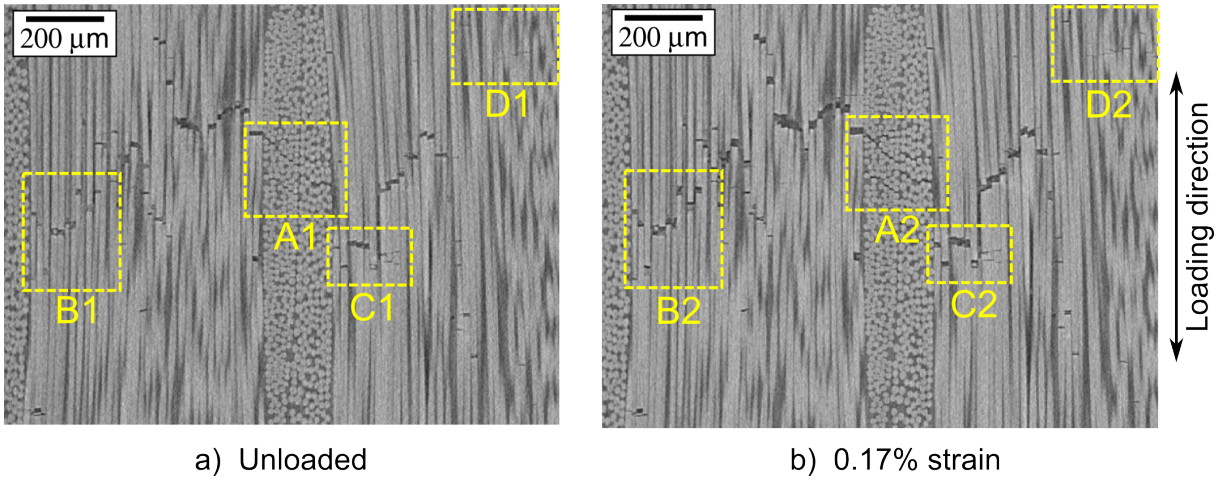

Figure 4. Comparison between observed damage without applied load (a) and with applied load (b). Regions of interest are marked and zoom views can be seen in Fig. 5

By comparing region A1 and A2 in Fig. 5, it is seen that the visibility of the off-axis cracks is only slightly increased at 0.17% strain. The clamp has a larger effect on the visibility of fibre fractures. Some of the fibre fractures are not easy to see without applied tension, whereas they can be seen more clearly with tension (e.g. seen by comparing region B1 and B2). At some locations the opening of the fibre fractures was greatly increased by the tension clamp. In the case of region C1/C2 the opening of some cracks was increased by around a factor two. However, at some locations (e.g. fractures marked by a dashed circle in C2), no change in the opening was observed. There were some locations (e.g. region D1/D2) where the fractures were not visible when the sample was unloaded, whereas they appeared when the sample was strained. The effect of the clamp will be larger if a higher load can be applied, and therefore optimisation of the clamp solution is ongoing work. Furthermore, if an automatic crack counting method was established, it would be possible to quantitatively show the effect of applied tension, and this could also be used to quantify the ex-situ damage. This is currently ongoing work.

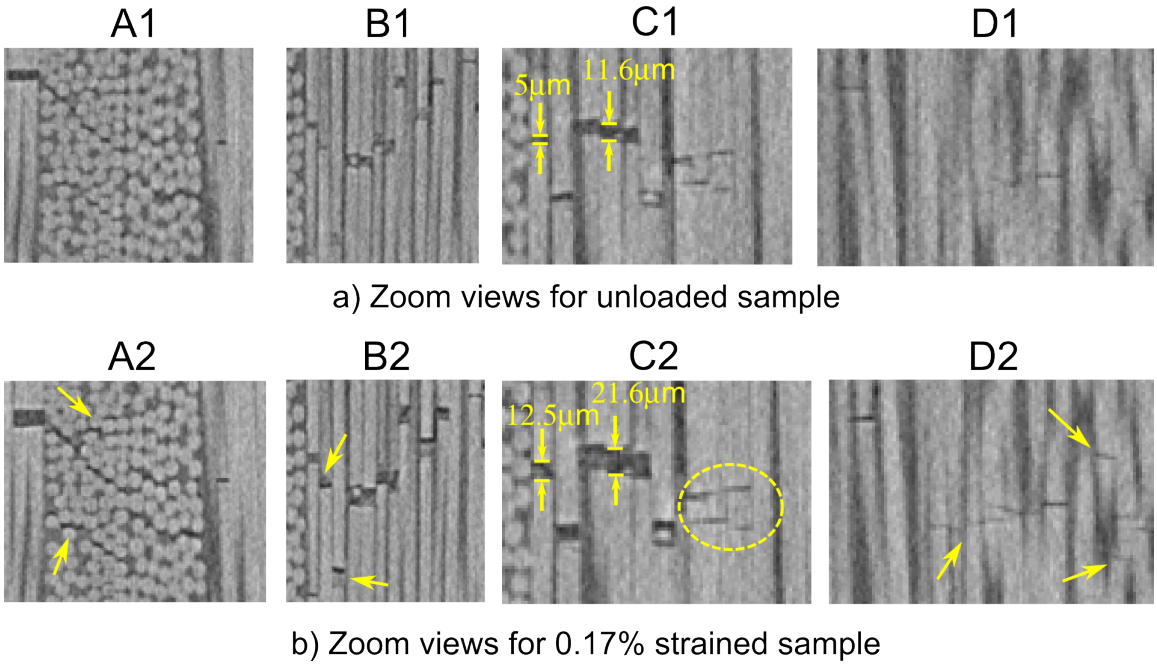

Figure 5. Zoom views in the regions of interest marked in Fig. Fig. 4. a) shows the views for the unloaded sample (A1-D1) and b) the views for loaded sample (A2-D2). The arrows marks some locations with changes when applying load to the sample.

5. Conclusion

In this study, a method for observing fatigue damage progression non-destructively in a glass fibre/polymer coupon test specimens by ex-situ laboratory X-ray CT was explained. Damage was observed in 3D on a micro-structural level including individual fibre fractures and off-axis cracks at four points during the fatigue loading history. The number of fibre fractures along with their opening was seen to increase with increasing number of load cycles. The long time exposure of X-rays on the sample seemed to have a slight negative effect on the tension fatigue life-time, however when scanning four times it did not seem significant. Furthermore, the effect of applying tension during scanning was examined and it was seen that additional fibre fractures and off-axis cracks became visible with load applied. However, it might be necessary to apply a higher strain during scanning to make all the fibre fractures and matrix cracks visible in the X-ray CT images at the considered resolution. Therefore, developing an improved clamp solution is of great interest and is ongoing work.

Acknowledgments

This research was conducted using mechanical testing equipment from DTU Center for Advanced Structural and Material Testing (CASMAT), Grant No. VKR023193 from the Villum Fonden. Financial support from CINEMA: "the allianCe for ImagiNg of Energy MAterials", DSF-grant no. 1305-00032B under "The Danish Council for Strategic Research" is gratefully acknowledged. Additionally, we would like to thank LM Wind Power for manufacturing of test specimens.

References

[1] Nijssen R P L and Brøndsted P 2013 *Advances in Wind Turbine Blade Design and Materials* 175–209
[2] Nijssen R P L 2006 *PhD Thesis, Delt University of Technology*
[3] Zangenberg J, Brøndsted P and Gillespie Jr J W 2014 *Journal of Composite Materials* **48** 2711–2727 ISSN 0021-9983

[4] Jespersen K M, Lowe T, Withers P, Zangenberg J and Mikkelsen L 2016 *Composites Science and Technology* (Submitted)
[5] Pedro F, Márquez G, Mark A, María J, Pérez P and Papaelias M 2012 *Renewable Energy* **46** 169–178
[6] Pereira G F, Mikkelsen L P and McGugan M 2015 *PLOS One* **10** e0141495
[7] Mortell D J, Tanner D A and Mccarthy C T 2014 *Composites Science and Technology* **105** 118–126
[8] Hongwei Z, L M, Brøndsted P, Jinbiao T and Lele G 2010 *Chinese Science Bulletin* **55** 1199–1208
[9] Wright P, Moffat A, Sinclair I and Spearing S M 2010 *Composites Science and Technology* **70** 1444–1452
[10] Scott A E, Mavrigirdati M, Wright P, Sinclair I and Spearing S M 2011 *Composites Science and Technology* **71** 1471–1477
[11] Garcea S C, Macrigirdato M, Scott A E, Sinclair I and Spearing S M 2014 *Composites Science and Technology* **99** 23–30
[12] Garcea S C, Sinclair I and Spearing S M 2015 *Composites Science and Technology* **109** 32–39
[13] Schilling P J, Karedla B P R, Tatiparthi A K, Verges M A and Herrington P D 2005 *Composites Science and Technology* **65** 2071–2078
[14] Sket F, Seltzer R, Molina-Aldareguía J M, Gonzalez C and LLorca J 2012 *Composites Science and Technology* **72** 350–359
[15] Yu B, Blanc R, Soutis C and J W P 2016 *Composites: Part A* **82** 279–290
[16] Pereira G F, Hüther J, Mikkelsen L P and Brøndsted P 2016 *In preparation, DTU Wind Energy*
[17] Zangenberg J 2013 *PhD Thesis, DTU Wind Energy PhD-0018(EN)*

[P4]

Jespersen, K. M. and Mikkelsen, L. P.

THREE DIMENSIONAL FATIGUE DAMAGE EVOLUTION IN NON-CRIMP GLASS FIBRE FABRIC BASED COMPOSITES USED FOR WIND TURBINE BLADES

Submitted (2017).

Three dimensional fatigue damage evolution in non-crimp glass fibre fabric based composites used for wind turbine blades

Kristine M. Jespersen[a,*], Lars P. Mikkelsen[a]

[a] *Department of Wind Energy, Section of Composites and Materials Mechanics, Technical University of Denmark, Risø Campus, 4000 Roskilde, Denmark*

Abstract

This work studies the tension fatigue damage progression of a uni-directional glass fibre composite made from a non-crimp fabric similar to those used for the main load carrying parts of a wind turbine blade. The spatial damage progression in a chosen region of a test specimen is monitored on a micro-structural scale by ex-situ X-ray computed tomography. The centimetre sized specimen remains uncut during the ex-situ experiment. The experimental results indicate that uni-directional fibre fractures initiate from matrix cracks related to the structure of the fabric: first in the thin off-axis backing bundles at triple cross-over regions where the ±45° and 90° backing bundles intersect each other and lie close to a uni-directional bundle, and later followed by damage initiation in the other cross-over regions. Uni-directional fibre fractures were seen to increase in number with increasing number of cycles, and mainly progress in the thickness direction of uni-directional bundles (away from the backing bundles). Furthermore, the crack face separation of individual broken uni-directional fibres was observed to gradually increase with an increasing number of cycles. The progression path of the uni-directional fibre fractures was seen to be very dependent on the local backing bundle arrangement.

Keywords: A. Polymer Matrix Composites (PMCs), A. Glass fibres, B. Fracture, D. Non-destructive testing, Micro-tomography

*Corresponding author.
E-mail address: kmun@dtu.dk (K.M. Jespersen).

1. Introduction

Due to their high specific strength and stiffness along with the possibility to design directionally dependent properties and arbitrary shapes, fibre composite materials are used in more and more applications. The applications span from sports equipment and furniture to airplanes, cars, and wind turbine blades. When making wind turbine blades, advantage is taken of the ability to design the material to fit the loads present in the structure [1]. The main loads in the blade structure are caused by gravitational and aerodynamic loads that lead to almost pure bending loads. Therefore, mainly unidirectional (UD) composites are used for the main load carrying parts of the blades. These composites are commonly made from layers of non-crimp fabrics (NCFs) and the vacuum assisted resin transfer moulding technique. Because of the blade rotation and the variation in the wind, wind turbine blades experience a high degree of cyclic loading giving a risk of fatigue failure. Over a lifetime of 20 to 30 years, a wind turbine blade experiences fatigue loading in the range of 10^8-10^9 cycles which is significantly higher than in most other industries [2]. Therefore, fatigue is a major concern when designing a wind turbine blade, however the fatigue damage mechanisms in these UD NCF composites are not well understood leading to high safety factors.

Particularly in the aerospace and automotive industries many studies have been carried out on fatigue of fibre composites. Although the fatigue resistance of fibre composites generally is good, it is difficult to accurately predict the lifetime due to complex fatigue damage mechanisms. Therefore, at present we cannot take full advantage of their fatigue resistance. During fatigue loading fibre/matrix debonding, matrix cracks, and fibre fractures are the three basic types of damage that occur and interact with one another [3]. The damage accumulating inside the material during fatigue loading leads to a degradation of the mechanical properties such as the stiffness. Fig. 1 shows examples of normalized stiffness degradation curves for three different lay-ups based on experimental data from [4] and [5]. It is seen that the total stiffness degradation during fatigue loading is dependent on the composite lay-up. In other words, the dam-

age mechanisms depend on the composite lay-up and will cause the material to behave differently.

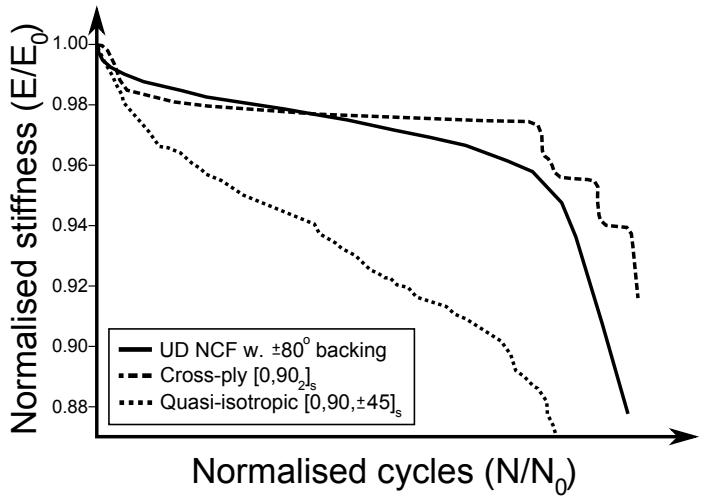

Figure 1: Comparison of normalised stiffness degradation during tension-tension fatigue loading of a cross-ply and a quasi-isotropic prepreg-based laminate [4] along with a unidirectional non-crimp fabric composite with ±80° bundles [5].

The prepreg-based laminates commonly considered in the aerospace and automotive industries usually consist of thin layers, in which the fibres are to some extent homogeneously distributed within each layer. In the remaining part of the current paper, "prepreg-based laminates" will refer to this type of laminate. Particularly in the aerospace industry it is often required that damage will not initiate at all during operation. Therefore, many studies have had focus on transverse crack initiation and progression occurring early in the fatigue life of prepreg-based laminates [4, 6–9]. Reifsnider and Jamison [4] studied the fatigue damage in $[0,90_2]_s$ cross-ply and $[0,90,\pm45]_s$ quasi-isotropic prepreg-based laminates. The dashed and dotted lines in Fig. 1 show the normalised stiffness degradation for the cross-ply and quasi-isotropic layups, respectively.

Reifsnider and Jamison [4] argued that there are three main stages for fibre composites during fatigue. An initial stiffness drop occurring during the early fatigue life (stage I), a stable stiffness degradation stage (stage II), and a final stage where damage

localises and final fracture occur (stage III). For both of the cases considered by Reifsnider and Jamison [4], matrix cracks in the off-axis layers were argued to be the main cause of the initial stiffness drop in stage I. For the quasi-isotropic laminate, gradually growing delaminations were found to be the main reason for the stiffness degradation during stage II. For the cross-ply laminate, cracks were also seen to propagate along the 0° fibres, referred to as longitudinal splitting. In the cross-ply case, 0° fibre fractures were also studied. The locations of the fibre fractures were found to coincide with the position of the transverse matrix cracks in the 90° layer. Furthermore, the density of fibre fractures decreased when moving away from the 90° layer. Therefore, it was suggested that the fibre fractures initiated from stress concentrations at the crack tips of the transverse matrix cracks in the 90° layer.

The UD NCF composites used for wind turbine blades are different from the discussed cross-ply and quasi-isotropic laminates in several ways. For each layer of UD fabric, relatively thick (∼0.5-1mm) UD bundles oriented in the 0° direction are stitched to a thin supporting layer of off-axis backing fibre bundles, which are oriented differently from the 0° direction. The backing bundles have only little effect on the stiffness and strength of the final composite, however they are necessary to keep the UD bundles aligned during manufacturing and handling. Due to the rough bundle structure, the fibres are not homogeneously distributed in the layers as there are matrix rich regions in between the fibre bundles. Because of these differences, UD NCF composites behave differently from prepreg-based laminates with more homogeneously distributed fibres.

Several studies have been carried out on fatigue of NCF composites [5, 10–15]. The shape of the stiffness degradation curve of NCF composites during tension-tension fatigue loading is similar to that of prepreg-based laminates [5, 12–15], as also shown in Fig. 1. However, the controlling damage mechanisms during fatigue loading are different. Zangenberg et al. [15] used scanning electron microscopy to observe the fatigue damage close to final failure of a UD NCF composite with ±80° backing bundles and based on the observations suggested a tension-tension fatigue damage progression scheme. This scheme was later supported by 3D X-ray computed tomography (CT)

experiments by Jespersen et al. [5]. In the above mentioned scheme, the initial stiffness drop observed in stage I was believed to be caused by off-axis matrix cracks in the backing bundles, which is similar to what is seen for most other lay-ups. However, the stiffness degradation during stage II was suggested mainly to be due to an increasing number of fibre fractures in the 0° UD fibre bundles initiating from off-axis cracks in the thin backing bundles. Fibre fractures being the main damage mechanism during stage II is different from the discussed prepreg-based laminates. However, the initiation mechanism for fibre fractures in the 0° bundles is similar to that observed for the 0° layer in the cross-ply laminate discussed earlier. During stage III, the UD fibre fracture regions connect to one another and final failure occurs.

Jespersen et al. [5] used X-ray CT to study the fatigue damage of a UD NCF composite similar to that considered by Zangenberg et al. [15] and the importance of observing the fatigue damage in three dimensions (3D) was emphasised. Although the actual damage progression was not monitored, the damage was observed in several samples at different number of cycles. It was found that the UD fibre fractures primarily initiate at cross-over regions of the backing bundles. Damage initiation at cross-over regions of fibre bundles has also been observed for woven composites [16, 17]. Here, it was argued to be due to a strain mismatch between the transverse and longitudinal bundles, however whether it is a similar mechanism that occurs for the backing bundles and the UD bundles in UD NCF composites is still not clear. To properly understand the underlying mechanisms of the fatigue damage progression, it is necessary to monitor the damage progress in 3D over time. This is experimentally best done in one specific region.

Several studies [5, 18–31] have shown X-ray CT to be a good method for visualising damage in 3D in composite materials. However, those studies considered relatively small specimens (often a few millimetres in cross-section) in order to obtain sufficient image resolution. The damage progression during static tension [20–22] and fatigue loading [23–25] has been examined by in-situ synchrotron radiation CT. However, synchrotron experiments are usually limited to relatively few cycles and can be difficult to access.

In a recent study by the authors [32] a method where it is possible to non-destructively monitor the damage progress in 3D in a standard test specimen using X-ray CT was presented. It is particularly special about this approach that it can be performed in the laboratory on test specimens with a cross-sectional area large enough to be representative and with a high number of fatigue cycles. To the author's knowledge, this was one of the first observations of the fatigue damage progression on a micro-structural scale for a centimetre sized specimen and for a high number of fatigue load cycles. The previous study focused on presenting the ex-situ fatigue the method, and the current study will focus on thoroughly analysing the damage progression in a UD NCF composite for improved understanding of the occurring damage mechanisms during tension-tension fatigue loading.

2. Material and methods

To monitor the fatigue damage progression non-destructively, an ex-situ X-ray fatigue test was carried out. The details about the ex-situ fatigue test method can be found in [32], however it will be briefly explained in the following. The overall idea behind this test method is to test a coupon specimen in a standard fatigue test machine outside the X-ray CT scanner. The fatigue test is then interrupted several times and the specimen taken out and examined by X-ray CT to obtain a 3D image of the internal damage for each step. In the current study, this method is used to monitor the damage progression in the material on a micro-structural level and do 3D segmentation and visualisation of the developing UD fibre fractures. The composite material along with the details of the fatigue and X-ray CT test methods will be explained in the following.

2.1. Composite material

This study considers a glass fibre composite made from four layers of UD and two layers of bi-axial ($\pm 45^\circ$) non-crimp fabric. The UD fabric consist of UD fibre bundles that are stitched to a supporting layer of thin off-axis bundles referred to as 'backing bundles'. The backing bundles are present to keep the UD bundles aligned during

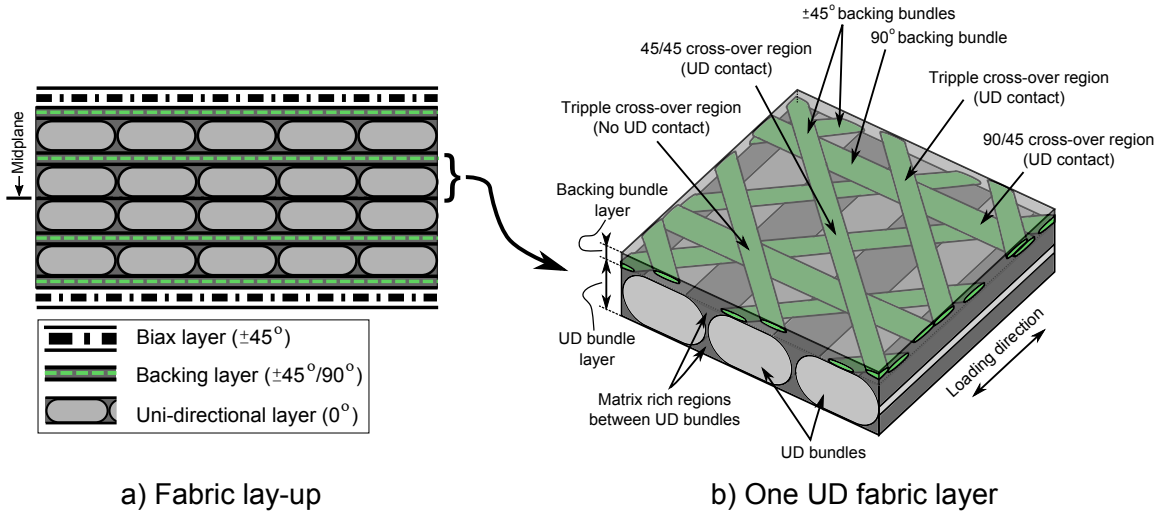

Figure 2: Composite layup and bundle structure. a) Schematic of fabric layup b) Schematic of one UD fabric layer in the composite with definitions of three different types of cross-over regions and examples of "contact" and "no contact". Note the definition of the "backing (bundle) layer" and UD (bundle) layer.

manufacturing and handling, and only has a small effect on the composite stiffness and strength. The lay-up of the composite is $[\text{biaxial,b/0,b/0}]_s$, as shown in Fig. 2a, where 'b/0' represents the UD (0°) fabric layer and 'b' indicates the backing side on the fabric. In the current study, focus is put on damage regions initiating in the UD layers isolated from the biaxial layers. Therefore, the effect of the biaxial layers at the specimen surface will not be discussed in the current study. More specific information about the layup can be found in [33].

The UD fabric is made from 1150 g/m^2 0° direction 2400 tex glass fibre bundles stitched on a backing consisting of 100 g/m^2 ±45° 200 tex glass fibre bundles and 19 g/m^2 90° 200 tex glass fibre bundles (see Fig. 2b for bundle structure). The average total fibre volume fraction of the composite was $V_f = 0.57$. The polymer matrix is an epoxy of type "Huntsman LY1568/3489" cured for 20 hours at 40C° + 5 hours at 75C° resulting in a fully cured matrix.

Fig. 2b shows a sketch of one UD layer including the backing bundles in the composite. The backing fibre bundles cross over each other at some locations. In some

places the ±45° and 90° bundles cross over each other referred to as "triple cross-over regions". In other places two 45° bundles cross over each other referred to as "45/45 cross-over regions", and at locations where a 45° and 90° bundle cross over each other are referred to as "45/90 cross-over regions". Since the UD bundles have an almost oval shape there are matrix rich regions between the bundles as also illustrated in Fig. 2b. In the present study, we distinguish between cross-over regions which are "in contact" and "not in contact" with the UD bundles. Here, the bundles being "in contact" means that the bundles lie so close that there is approximately no difference between the fibre to fibre distance within one bundle and in the two "contacting" bundles.

2.2. Test specimens and fatigue testing

A plate of the composite was cut into 410mm long butterfly shaped specimens as shown in Fig. 3. This is an especially long specimen geometry designed to test UD composites. Rectangular plane specimens tend to fail by shear failure in the tab region (more information on this is given in [34]). For the present study, the end of tab region was made straight, marked by dashed red lines in Fig. 3, both to avoid collision with the X-ray source and to make it easier to repeatedly mount the sample similarly in the sample holder in the CT scanner.

The fatigue tests were carried out on a universal servo-hydraulic Instron test machine in tension-tension mode with a stress ratio of R=0.1 and a test frequency of 5Hz. The strain was monitored using two extensometers and the peak strain was $\epsilon_{max} = 1\%$. To get an indication of when to interrupt the test and where to look for damage by X-ray CT in the sample, the sample was monitored by thermocamera during the test. The first interruption point for the test was after N_1=47300 cycles and was chosen based on the occurrence of a hot-spot on the thermocamera in the gauge section as shown in Fig. 3b. Subsequently, after each X-ray CT scan the fatigue test was continued in steps of 10000 cycles resulting in interrupting the test at 57300, 67300, and 77300 cycles followed by failure of the specimen. It should be noted, that the thermocamera mainly will show damage regions that are near the surface and/or of a sufficient size.

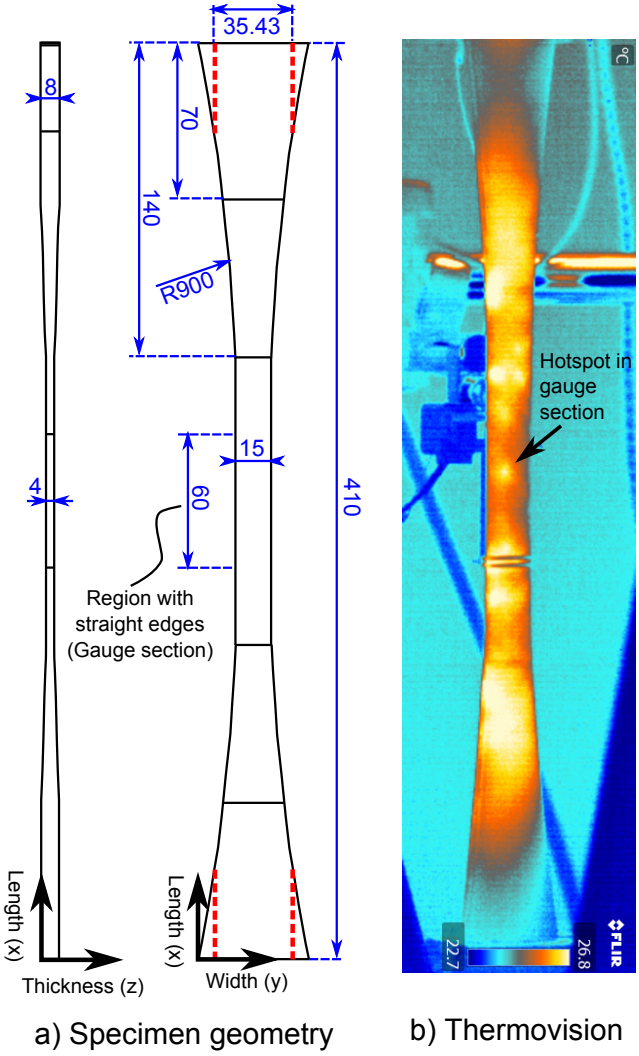

Figure 3: a) shows the butterfly specimen geometry with dimensions given in mm. The dashed red lines show the modification to the original geometry for the ex-situ study. b) shows the thermovision image when the test was interrupted the first time. The X-ray CT scans were performed around the hotspot marked in the figure.

2.3. X-ray CT

The X-ray CT scans were performed on a Zeiss Xradia Versa 520 scanner with a binning of 2 meaning that the intensity of 2x2 pixels is combined, giving shorter scan time but also decrease the resolution. Two types of scans were performed with the settings listed in Table 1. When the fatigue test was interrupted the first time, a large

field of view (LFOV) scan was performed around the region with the hot-spot seen on the thermocamera to locate a damage region (Fig. 3b). A damage region was reasonable visible in the LFOV scan, and a high resolution (HR) scan was then performed in the damage region. This was done using the scout-and-scan principle by Zeiss. A sample holder was specially made for the X-ray CT system to make it possible to mount the 410mm long samples and also to repeatedly mount the sample in the same way during ex-situ fatigue (see [32] for more information about the method). The volume monitored ex-situ was of cylindrical shape of around 3mm in diameter and length and the scan location on the fabric lay-up is illustrated in Fig. 4. Since the sample was repeatedly put in and taken out of the scanner, there is a slight variation in the scan location for each scan volume as marked in Fig. 4 by the solid black, dashed yellow, and blue circles. The variation is so small for interruption point 1-3 that the circles almost lay on top of each other.

Table 1: Versa 520 X-ray CT imaging conditions

Category	LFOV	HR
Optical Magnification	0.4X	4X
Source to sample distance	30 mm	28 mm
Detector to sample distance	88 mm	35 mm
Exposure time	2 s	7 s
No. of projections	801	4601
Accelerating Voltage	60 keV	70 keV
Pixel size	17.4 µm	3 µm

2.4. Automatic UD fibre fracture segmentation

Although the same information in principle lies within a stack of 2D images as in a 3D image, it can be difficult to properly imagine how the damage looks in 3D when

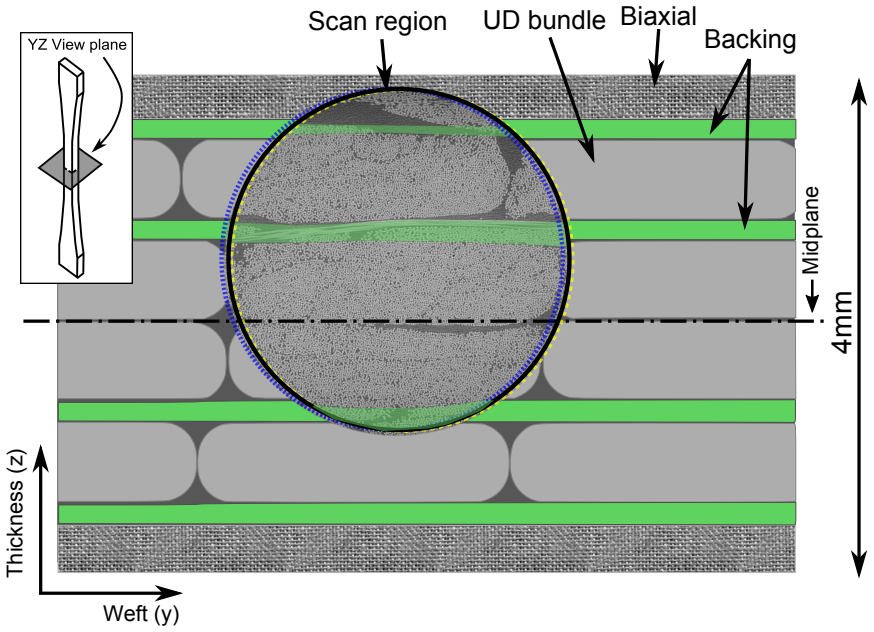

Figure 4: Schematic of the lay-up ([biaxial,/b/0,b/0]$_s$) with definition of the investigated scan region for the ex-situ study. The field of view include three UD fibre bundles that will be labelled UDB1, UDB2, and UDB3 later (see Fig. 7). The nearly coinciding solid black, dashed blue, and yellow circles show the slight variation in position between the scans at interruption point N_1, N_2, and N_3, respectively.

sliding through an image stack. To make 3D visualisation possible, it is necessary to segment out the damage. That is, marking the damage with a coloured mask that can be shown instead of or together with the original greyscale images. For the scans in this study, simple thresholding of the greyscale values cannot be used on the raw images to segment the UD fibre fractures, as they share greyscale values with the polymer matrix. As it is extremely time consuming to manually segment the fractures (and will be based on subjective judgement), an almost entirely automatic method was established for segmentation. This method at its current state is only meant for visualisation purposes and not individual fibre fracture quantification. It consists of three main steps listed below where the two first steps are illustrated in Fig. 5.

1. Align the considered volume with the initial state volume (allowing for translation and rotation)

2. Subtract the initial and the aligned images from each other
3. Filter out noise and segment the fractures by thresholding the image obtained by subtraction

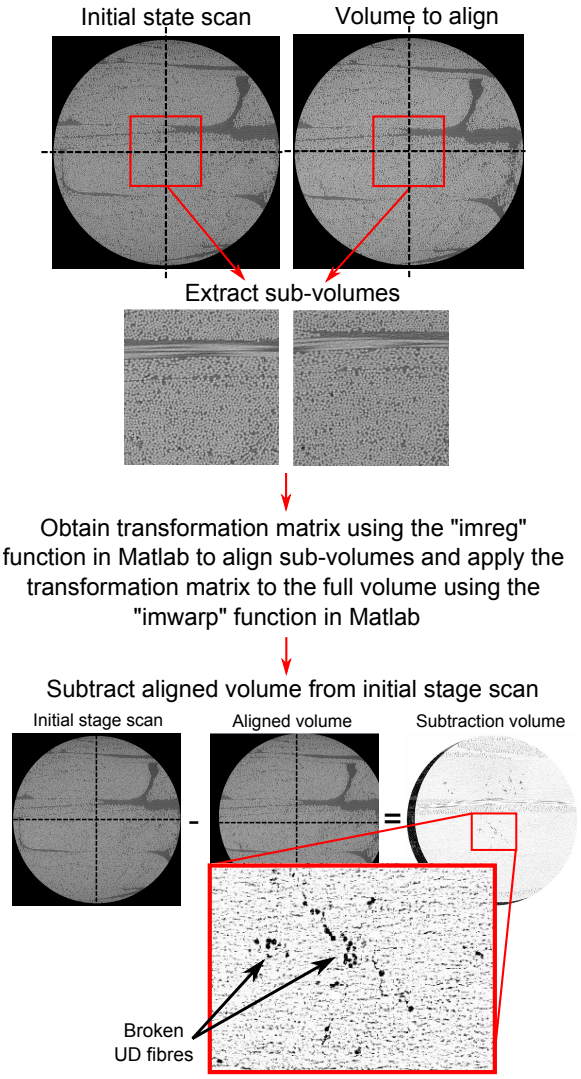

Figure 5: Illustration of the 3D data alignment and subtraction principles. By subtracting the aligned volumes from each other, the difference in the volumes will show up in the subtraction volume. This is seen by the black dots marked as "broken UD fibres" shown on a 2D slice of the subtraction volume. Note that there also is a certain amount of noise in the subtracting image.

As seen in Fig. 5, sub-volumes are used to obtain the transformation matrix used for the alignment using Matlab's Imreg function. This is partly to decrease the calculation

time and help convergence. It should be noted that the step where the transformation matrix is applied to the full images requires a lot of ram (40GB or more for a 1000^3 pixel image). When the aligned full images are subtracted from each other in Matlab, the UD fibre fractures appear more clearly in the subtraction volume than in the original volumes. Therefore, thresholding can be used on the subtraction volume to segment the fractures for visualisation in 3D. The visualisation of the segmented damage was done using the software Avizo 9.0 from FEI and visualised using a "surface" with a smoothing extent of 3. The backing bundles were excluded from the segmentation in the subtraction volume manually. This was done to get a good visualisation UD fibre fractures. It is important to note that this method shows the difference between the images and therefore the increase of damage from the initial state. However, if existing cracks experience a sufficient increase in the crack opening, this will also show up in the subtraction volume. It should also be mentioned that cracks with small openings are likely to be excluded because of the limited resolution and the smoothing. To look into automatic segmentation of detailed mechanisms like fibre clustering (e.g. [25]) it will be necessary to include individual fibre segmentation, such as the segmentation method presented by Emerson et al. [35].

3. Results

In this section the damage mechanisms and progression behaviour observed in the volume considered ex-situ by X-ray CT are shown. Fig. 6 shows the measured stiffness degradation for the ex-situ fatigue X-ray CT test. The interruption points are marked in the figure by N_1 to N_4 and each include a high resolution 3D image dataset (HR settings in Table 1) visualising the damage mechanisms and progression. All the datasets are available online [36][1].

[1]Upon acceptance of the article, the data will instead be published at Zenodo.org for permanent access.

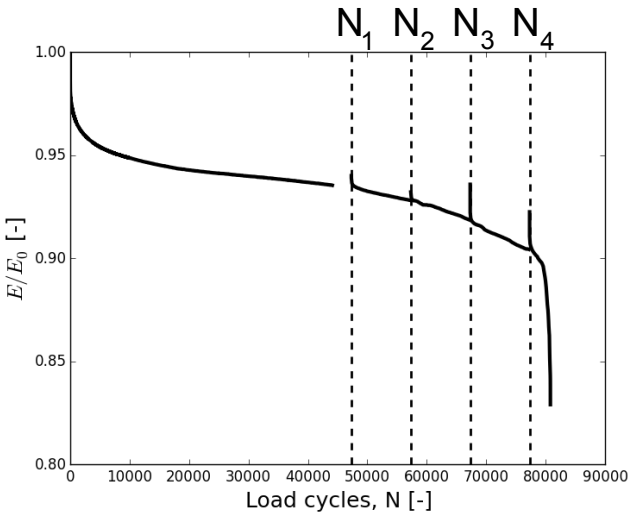

Figure 6: Normalised stiffness plotted against the number of load cycles for the ex-situ fatigue test. The test was interrupted at $N_1 = 47300$, $N_2 = 57300$, $N_3 = 67300$, and $N_4 = 77300$ cycles, as marked in the figure.

3.1. Initial damage state

Before discussing the damage progression observed by the ex-situ fatigue test, the initial damage state will be described. A 3D image dataset contains a lot of information, however it is difficult to visualise on paper. Therefore, only specific 2D views of interest from the raw 3D dataset will be presented. To see all the raw images, please refer to [36]. Fig. 7 shows a YZ-plane slice of the volume with several view planes (XY1-XY4) indicated for later reference. The location of this scan region is the same as earlier indicated on the schematic of the composite layup in Fig. 4. The considered volume includes parts of three UD bundles (numbered UDB1, UDB2, and UDB3 in Fig. 7) along with a contacting triple cross-over region between UDB1 and UDB2 and a contacting 45/45 cross-over region at UDB3 (see Fig. 2b for definitions). The backing layer that includes the triple cross-over region in the considered region is stitched to UDB2.

The approximate distance the UD fibre fractures extended into the UD bundles at the initial damage state is marked by green contour lines on top of the UD bundles. There was a small UD fibre fracture region in UDB1 near the biaxial layer at the

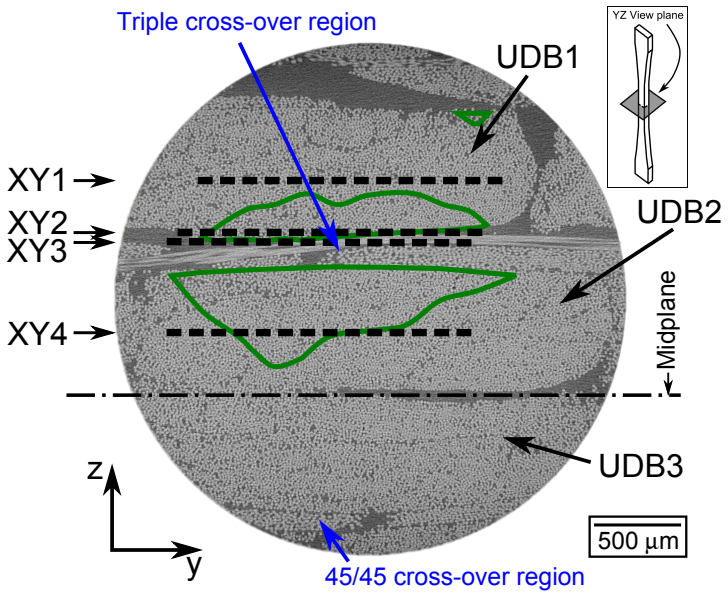

Figure 7: A 2D view of the considered volume (as also shown in Fig. 4) with definitions of the UD bundle numbers (UDB1, UDB2, and UDB3) and XY view planes (XY1-XY4). The green solid contour lines on top of the UD bundles indicate approximately how far the initial UD fibre fractures extend into the thickness (z) direction of the UD bundles. The thick dashed lines on top of the view planes define the location of the views later in Fig. 8.

specimen surface, however most of the UD fibre fractures were observed near the triple cross-over region in UDB1 and UDB2. No UD fibre fractures could be seen in UDB3 at this stage. It is important to note that UD fibre fractures were only observed locally close to backing bundles in contact with the UD bundles. This was also observed [5] for a similar UD NCF composite with $\pm 80°$ backing bundles, where UD fibre fractures were only present at the cross-over regions of the $\pm 80°$ bundles.

Fig. 8 shows four 2D slice views in the XY-plane from the 3D image data at the initial damage state, N_1. The slice locations in the volume are indicated by the bold dashed lines in Fig. 7. View planes XY1 and XY4 are located around the centres of UDB1 and UDB2 in the thickness direction, and correspond to the 2D slice views in Fig. 8a and 8b, respectively. View plane XY2 is located in UDB1 just next to the triple cross-over region, and correspond to the 2D slice view in Fig. 8c. View plane XY3 is located where the $+45°$ and $90°$ backing bundles are in contact with each other within

the backing layer. It corresponds to the 2D slice view in Fig. 8d.

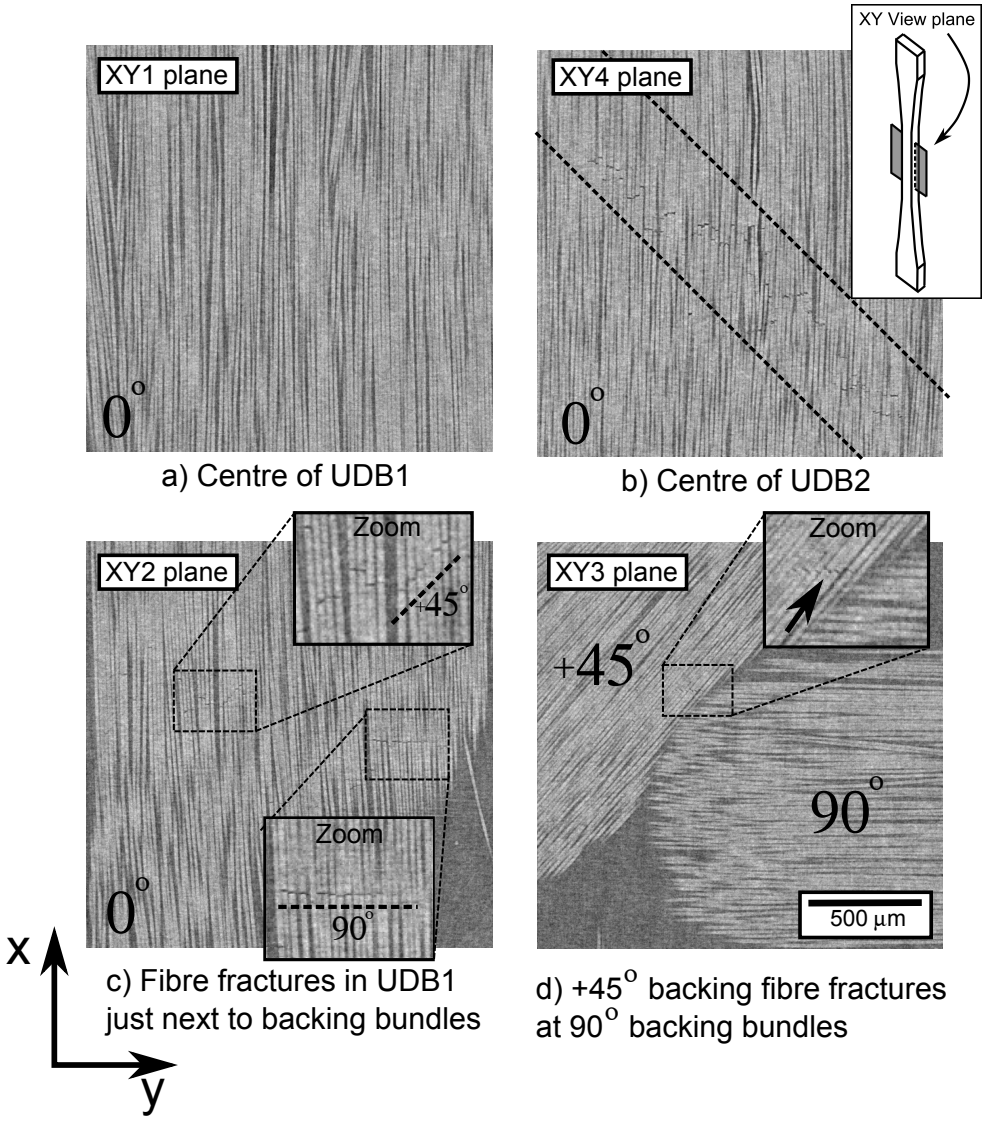

Figure 8: Damage features observed at the initial damage state ($N_1 = 47300$ cycles). The view planes are defined in Fig. 7. a) and b) show the UD fibres around the bundle centres in the thickness direction of UDB1 and UDB2, respectively. c) shows the UD fibres in UDB2 just next to the triple cross-over region where a +45° and 90° backing bundle are in contact with UDB1. d) shows fibre fractures in the +45° backing bundle where it is in contact with the 90° backing bundle.

At the initial damage state, there are no UD fibre fractures observed around the centre of UDB1 as seen in Fig. 8a. This is also indicated in Fig. 7 by the green contour

line. From the green contour line in Fig. 7 it was also seen that the UD fibre fractures extend further into UDB2 than UDB1. Furthermore, the fibre fractures in UDB2 align with the -45° direction, indicated by dashed lines in Fig. 8b. At the interface between UDB2 and the triple cross-over region of the backing layer, UDB2 is in contact with a -45° backing bundle. This is likely related to the UD fibre fractures appearing in this particular pattern in UDB2. Fig. 8c shows the UD fibres of UDB1 that are in contact with a +45 and 90 backing bundle in two different places (see zoom boxes in Fig. 8c). The UD fibre fractures are generally seen to align with the direction of the below backing fibre bundle in contact with the UD bundle. This is even clearer at later damage states (Fig. 9c later), and could indicate initiation from off-axis cracks in the contacting backing bundles. This is similar to that seen [4] for fibre fractures in the 0° layers of prepreg-based cross-ply laminates, and similar observations [5, 15] were also done for a UD NCF composite with a different backing (±80°). Fibre fractures were also observed in the +45 backing fibre bundles as shown in Fig. 8d. As was also seen for the contacting UD and backing bundles, the fibre fractures align with the contacting 90° bundles, which could indicate that they initiated from transverse cracks in the contacting 90° backing bundle.

3.2. The third damage state and 3D visualisation

Before describing the progression over all the interruption points, the third damage state (N_3=67300 cycles) will be discussed and a 3D visualisation of the damage at this state will be presented. This has the purpose of giving an initial understanding of how the slightly more evolved damage looks both in 2D and 3D before discussing the progression in more detail. Fig. 9 shows the same views that were previously presented in Fig. 8, however now after N_3=67300 cycles.

In Fig. 9a, it is seen that the UD fibre fractures have propagated further into UDB1 and are present in the XY1 plane, which was not the case at the initial damage state. By comparing Fig. 9a and 9b it is seen that the fibre fractures are much more scattered in UDB1 than in UDB2. The UD fibre fractures shown in Fig. 9b that align with

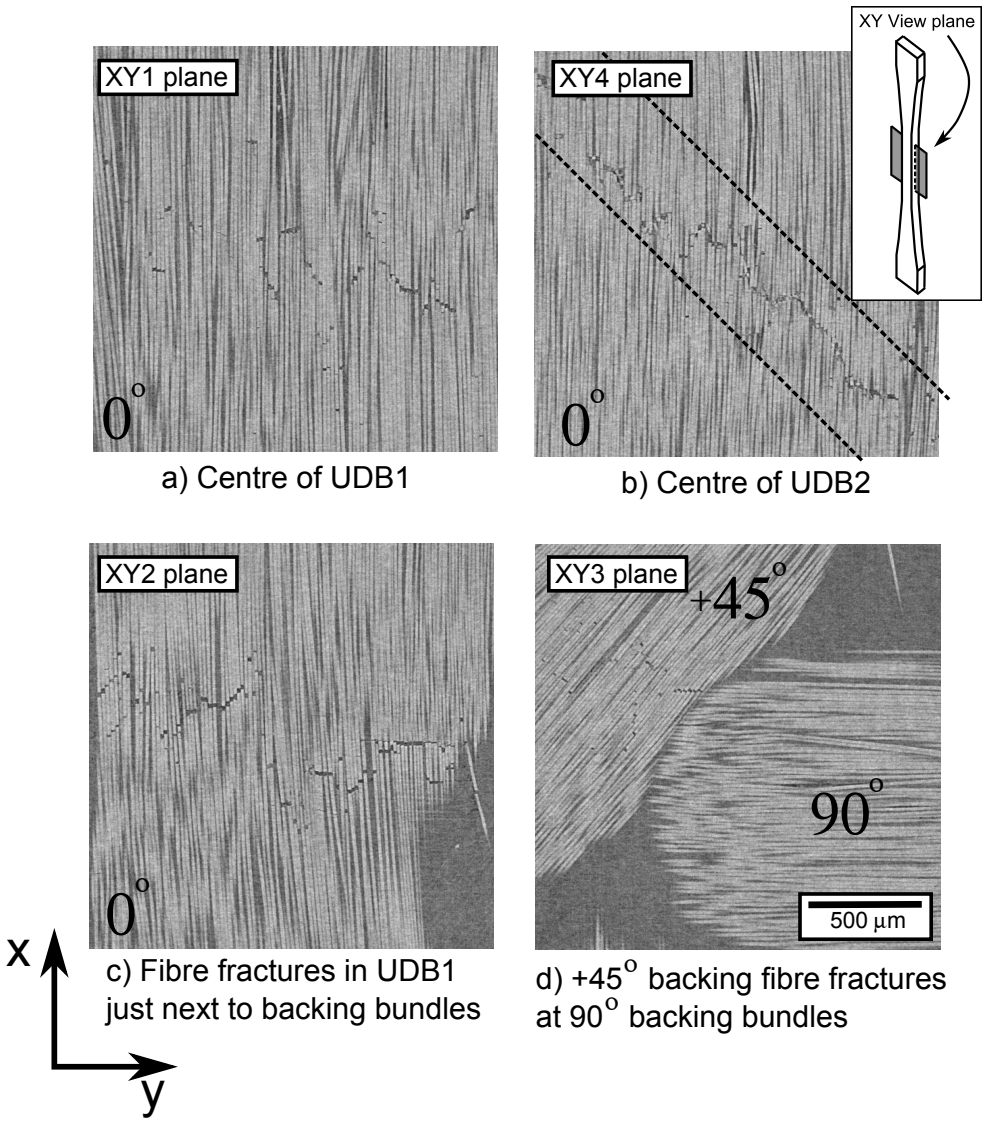

Figure 9: Damage features observed at the damage state $N_3 = 67300$ cycles. The view planes are defined in Fig. 7, and are the same as were shown for the initial damage state in Fig. 8.

the 45° direction have connected to one another, which was less clear in Fig. 8b at the initial damage state. The UD fibre fractures seen in Fig. 9c align with the +45° and 90° direction of the contacting backing bundles. This was also seen at the initial damage state in Fig. 8c, however particularly for the fibre fractures aligning with the +45° direction it is clearer at this damage state. Finally, Fig. 9d shows that additional fibre fractures have appeared in the +45° backing bundles.

Fig 10 shows a 3D visualisation of damage state N_3 obtained by subtracting the initial damage state from state 3 using the method described in Section 2.4. In other words, it shows the difference between the damage states for which chosen views were shown in Fig. 8 and 9. In Fig. 10, the UD fibre fractures are marked in green and are shown together with four 2D view planes from the raw 3D dataset at damage state 3. As mentioned earlier, this will only show the change between the two states, however due to the gradually increasing crack opening (as also seen by comparing Fig. 8 and 9) the segmentation includes most fibre fractures even if they were already present at the initial damage state. Fig 10a shows the UD fibre damage in UDB2 and at this stage the bundle is severed with a roughly -45° fracture plane through most of the bundle, as was also seen in Fig. 9b. The UD fibre damage in UDB1 is shown in 10b and here the fibre breaks are more scattered than in UDB2, which was also seen in Fig. 9a. Fig. 10 illustrate the complexity of the damage mechanism, and it is clear that the arrangement of the backing bundles have an effect on how the UD fibre fractures appear.

3.3. Progression of fatigue damage

In this section, the damage progression observed will be described. At each interruption point the UD fibre fractures extend further and further into the UD bundles in the thickness (z) direction as illustrated in Fig. 11. Fig 11 shows a contour line for each damage state, illustrating approximately how far the UD fibre fractures extend into UD bundles at the different damages states. It should be noted that the fibre fractures not necessarily are present at the same height (x-direction), which can also be seen from the previously shown 3D visualisation in Fig. 10.

The green solid line shows the initial damage state and is the same as was described earlier in Section 3.1. At the damage state N_2 represented by the blue line, all damage regions have expanded, and the damage region in UDB2 has penetrated through the whole thickness of UDB2. At the damage state N_3 represented by the yellow line, the damage region in UDB2 has started growing into UDB3, and a new isolated damage region has initiated in UDB3 at the 45/45 cross-over region. Furthermore, the damage

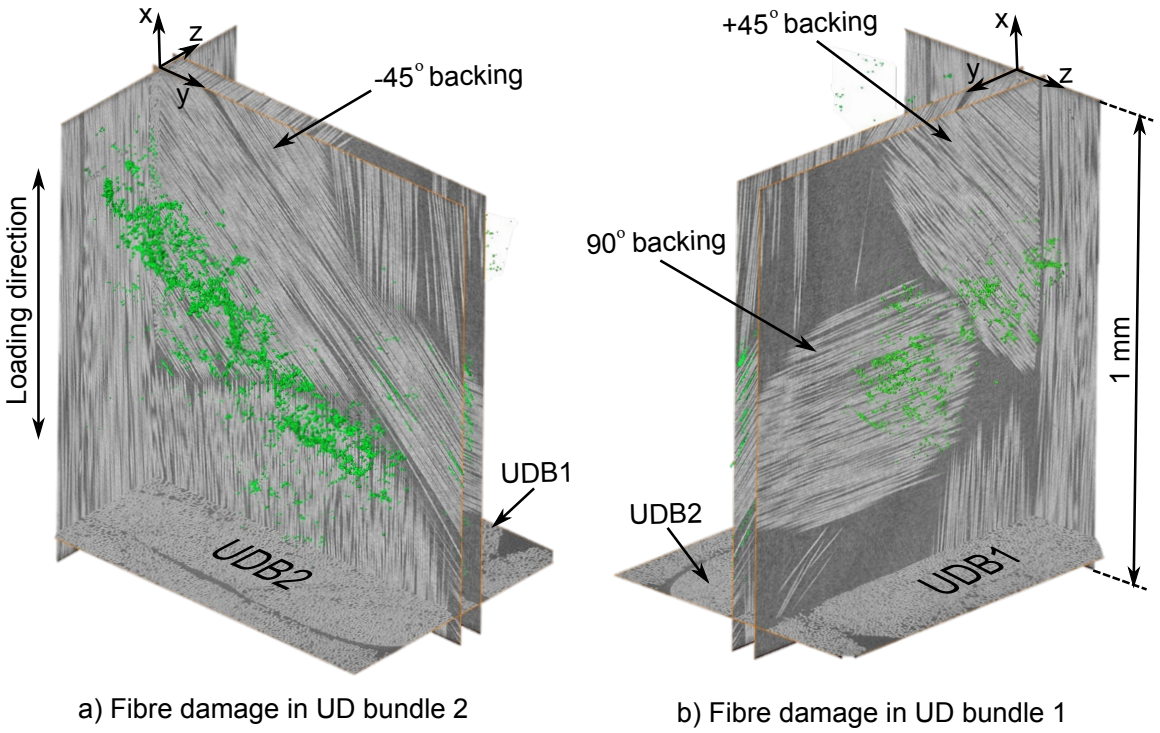

Figure 10: 3D visualisation of UD fibre fractures after $N_3 = 67300$ cycles. The image was obtained using the technique described in Section 2.4 and shows the difference between the initial state scan (N_1) and the third state scan (N_3). Note that (a) and (b) show the same volume, however (a) is rotated 90° clockwise to give (b). A video rotating the segmentation can be found online [36]

regions in UDB1 seem to have connected to one another. At the final damage state N_4 marked by the red line, the damage regions in UDB2 and UDB3 also seem to connect to each other, and shortly after final failure occurred. By comparing the contour lines in Fig. 11, it is seen that the damage regions mainly progresses in the thickness direction (z) rather than in the width direction (y). This suggests that the damage initiates as a line of fractures that appear almost at the same time, rather than expanding from a single point.

The damage progression is illustrated for two different 2D slice views in Fig. 12. The locations of these views in the volume are shown by the thick black dashed lines in Fig. 11. The top four images (Fig. 12a) show the damage progression observed in view plane XZ1 and spans UDB2 and UDB3 including the belonging backing layers.

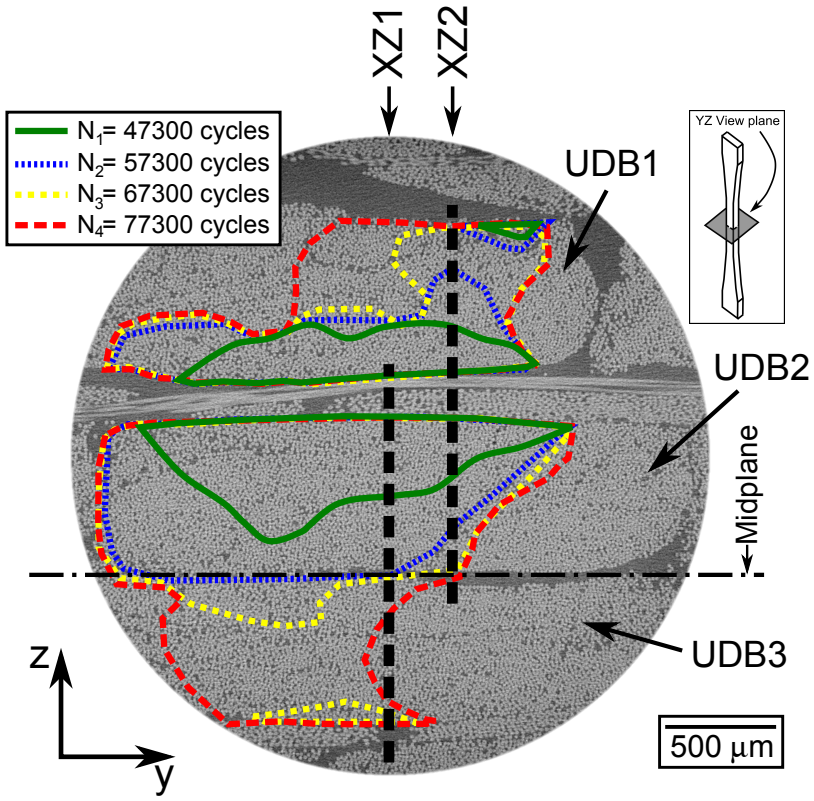

Figure 11: Definition of view planes XZ1-2 and indication of approximately how far the UD fibre fracture extend into the thickness direction of the UD bundles in the considered field of view at the four different damage states.

The bottom four images (Fig. 12b) show the progression observed in view plane XZ2 and spans UDB1 and UDB2 including the backing layers.

Fig. 12a shows how the UD fibre fractures progress from the triple cross-over region of the backing into UDB2. The UD fibre fractures arrest between UDB2 and UDB3 for some time, and then later progresses into UDB3. Around N_3, a new damage region of UD fibre fractures initiate in UDB3 at the 45/45 cross-over region, as marked by the black dashed circle. Generally it is seen that the crack face opening of the UD fibre fractures is gradually increasing with the number of cycles.

Fig. 12b shows how the UD fibre fractures progress into UDB1 and UDB2 from the triple cross-over region of the backing. The fibre fractures in UDB2 initially progresses in a manner where the UD fibre fractures are somewhat connected to each other, but

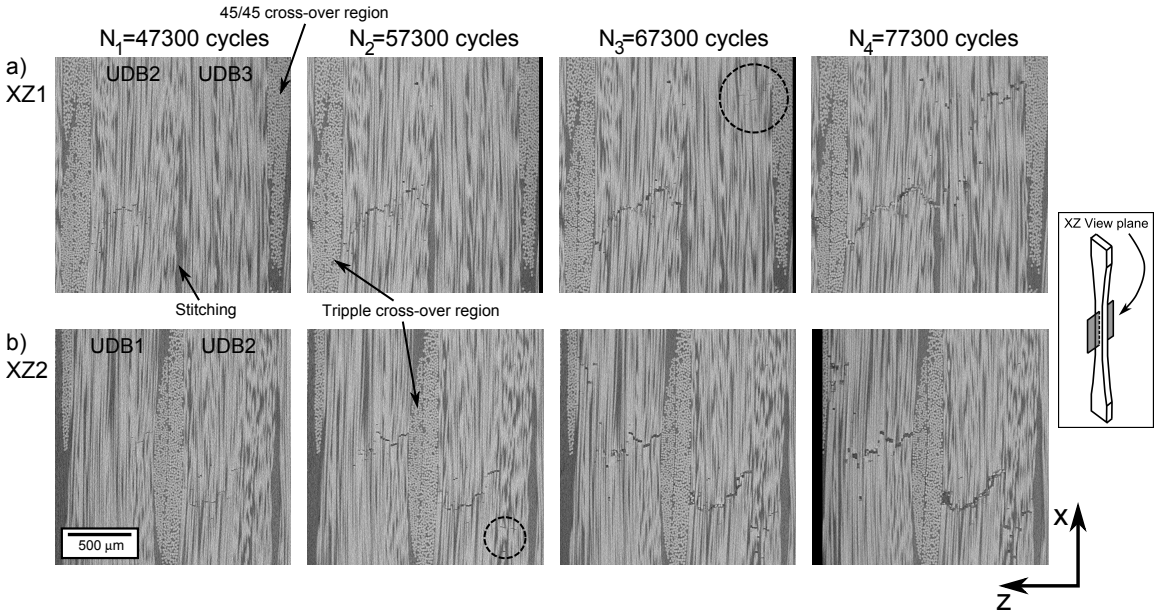

Figure 12: Two chosen examples of how the damage progresses in the considered volume. See Fig. 11 for definitions of the two view planes. For the full volume data, please refer to [36].

around N_2, there is a jump in the fibre fracture path (marked by the dashed black circle). At this location there is a variation in the local UD fibre architecture, and this could have an influence on the fracture path. At N_3 a new damage region at the backing belonging to UDB1 near the biaxial layer appears.

Although the damage regions in UDB1 at N_4 are at different positions in the x-direction, it is likely that they are connected to one another by fibre/matrix debonding and/or matrix cracks. These features are not always visible at the resolution used in the current study, however at the final damage state it was possible to see intralaminar splitting in the UD bundles as shown in Fig. 13a where the most visible intralaminar splitting has been marked by the dashed red lines. This was not visible in the X-ray images at the earlier damage states. Furthermore, fibre fractures in the 90° backing bundles, as marked by the arrow in Fig. 13b, were also observed at the final damage state N_4. Based on these observations, these two additional damage mechanisms seem to appear relatively close to final failure (stage III of the fatigue life).

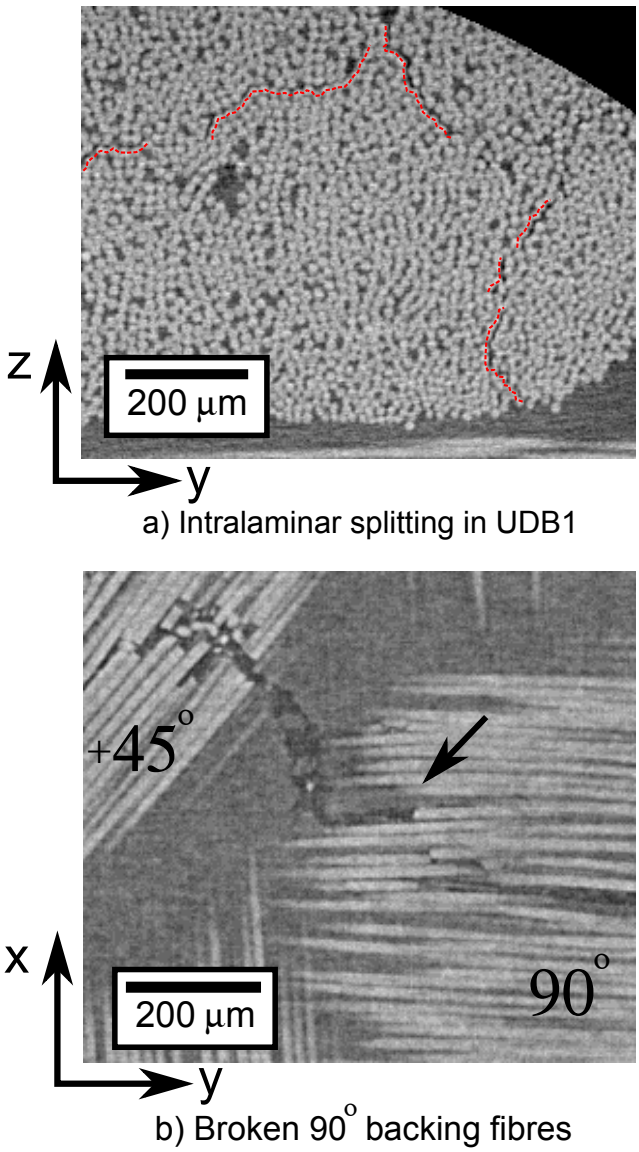

Figure 13: Additional damage features observed at damage state N_4=77300 cycles where (a) shows intralaminar splitting in UDB1 marked by dashed red lines, and (b) show broken fibres in the 90° backing bundle marked by the arrow.

4. Discussion

Six statements based on the observations are listed below and are followed by a discussion of the possible mechanisms and how the knowledge could be applied to improve the fatigue resistance of UD NCF composites.

1. UD fibre fractures are initiated by off-axis matrix cracks in the backing bundles.
2. UD fibre fractures will initiate at cross-over regions of the backing bundles that are in contact with a UD bundle.
3. The triple cross-over regions are more critical than other cross-over regions, and therefore damage will first initiate at the triple cross-over regions and subsequently initiate at other cross-over regions.
4. The UD fibre fractures initiate as lines of fractures from which the damage progress into the thickness direction rather than the width direction of the UD bundles.
5. The initiation and progression of the UD fibre fractures depend on local variations in the fibre architecture within the UD bundles and highly on the local configuration of the backing bundles.
6. Both off-axis matrix crack openings and the crack face separation of individual fibre fractures increase with number of cycles as the sample increases in length during fatigue loading

The damage initiation mechanism described by point 1 is believed to be similar to that observed for cross-ply laminates [4]. Hence, it is believed that cracks in the matrix and/or debonding of the fibre and matrix in the off-axis backing bundles result in stress concentrations on the UD bundles that cause UD fibre failures. The stress concentrations are believed to be most critical at cross-over regions where the UD and backing bundles are in contact with each other (point 2), as UD fibre fractures are rarely seen to appear if there is a layer of polymer matrix in between the bundles [5, 15]. Hence, it is likely that, if sufficiently thick, a layer of matrix will arrest the off-axis crack from progressing into the UD bundles. According to point 3, the fibre fracture regions are believed to initiate at the triple-cross over regions first. The stress state in these regions is complex, and therefore the exact mechanism needs further investigation using micro-mechanical modelling. However, during manufacturing three bundles crossing over each other could give a locally higher compression of the nearby

UD bundles, which can give a local higher fibre volume fraction leading to an increased number of fibre/fibre contact points. This has also been seen by Zangenberg [34]. Zangenberg argued that the locally increased number of fibre/fibre contact points could cause damage to initiate in these regions due to stress concentrations between the fibres. This also links to point 5, however further studies are still needed to properly understand how the fibre architecture affects the damage propagation. It is believed that the UD fibre fractures initiating as a row of fractures as stated in point 4 is related to the width of the contacting part of the cross-over regions of the backing bundles. Along the contacting part, the off-axis cracks in the backing bundles will result in stress a concentration along a line which could be the cause of this behaviour.

From the statements, it is clear that there are several possible modifications that are likely to improve the fatigue performance. For example, the number of cross-over regions could be decreased by modifying the orientation of the off-axis backing bundles. Another option could be to make sure the cross-over regions of the backing lie on top of the matrix rich regions in between the UD bundles. However, this might require increased control during manufacturing. It might also be possible to completely remove the backing and only keep the UD bundles in place with stitching thread, however then the material will have a low transverse stiffness and strength, which might give problems for some applications. Furthermore, it might be a challenge to keep the UD bundles properly aligned during manufacturing and handling.

To understand exactly what mechanisms control the damage initiation and progression observed in the experiments, it will be necessary to model the problems. If one could realistically model the stress state around the cross-over regions, it would for example be possible to model different types of backing lay-up that could help to discover materials with improved fatigue performance. The results presented in this paper has given knowledge for establishing more realistic models and can also serve as a validation base for models established in the future.

5. Conclusion

In the presented study, the tension-tension fatigue damage progression of a unidirectional glass fibre composite made from a non-crimp fabric was studied in 3D by ex-situ X-ray computed tomography. The damage was visualised in 3D by an automatic segmentation method. The damage mechanisms and damage progression was studied from both the 3D visualisation and the original 3D images. The damage was found to have initiated near triple cross-over regions of the backing bundles followed by damage initiation at other cross-over regions. It was found that UD fibre fractures gradually increase in numbers along with the number of cycles, and the observations suggest that the UD fibre breaks initiate from off-axis cracks in the thin supporting backing bundles. In addition, the opening of the fibre breaks was also seen to increase with increasing number of cycles. The UD fibre fracture regions seemed to mainly progress into the thickness direction of the UD bundle, whereas the width of the damage region was rather constant. Finally, aside from being highly affected by the local backing bundle arrangement, the observations indicated that the UD fibre fracture progression might be influenced by local variations in the fibre architecture. However, further work including modelling will have to be carried out to confirm what specific parameters controls the fracture pattern.

Acknowledgements

Financial support from CINEMA: "the allianCe for ImagiNg of Energy MAterials", DSF-grant no. 1305-00032B under "The Danish Council for Strategic Research" is gratefully acknowledged. This research was conducted using mechanical testing equipment from DTU Center for Advanced Structural and Material Testing (CASMAT), Grant No. VKR023193 from Villum Fonden. Finally, we would like to thank Hans Lilholt and Povl Brøndsted from DTU Wind Energy for their assistance in the writing process and fruitful discussions, and Anthony Fraisse from DTU Wind Energy for his assistance with mechanical tests.

References

[1] R. P. L. Nijssen, P. Brøndsted, Fatigue as a design driver for composite wind turbine blades, Advances in Wind Turbine Blade Design and Materials (2013). doi:10.1533/9780857097286.2.175.

[2] R. P. L. Nijssen, Fatigue life prediction and strength degradation of wind turbine rotor blade composites, PhD Thesis, Delt University of Technology (2006).

[3] W. W. Stinchcomb, K. L. Reifsnider, Fatigue damage mechanisms in composites materials: a review, In: Fatigue Mechanisms 675 (1979) 762–787.

[4] K. L. Reifsnider, R. Jamison, Fracture of fatigue-loaded composite laminates, International Journal of Fatigue 4 (4) (1982) 187–197. doi:10.1016/0142-1123(82)90001-9.

[5] K. M. Jespersen, J. Zangenberg, T. Lowe, P. J. Withers, L. P. Mikkelsen, Fatigue damage assessment of uni-directional non-crimp fabric reinforced polyester composite using x-ray computed tomography, Composites Science and Technology 136 (2016) 94–103. doi:10.1016/j.compscitech.2016.10.006.

[6] J. Tong, F. J. Guild, S. L. Orgin, P. A. Smith, On matrix crack growth in quasi-isotropic laminates—I. experimental investigation, Composites Science and Technology 57 (11) (1997) 1527–1535. doi:10.1016/S0266-3538(97)00080-8.

[7] J. Varna, R. Joffe, N. V. Akshantala, R. Talreja, Damage in composite laminates with off-axis plies, Composites Science and Technology 59 (14) (1999) 2139–2147. doi:10.1016/S0266-3538(99)00070-6.

[8] M. Quaresimin, P. A. Carraro, L. P. Mikkelsen, N. Lucato, L. Vivian, P. Brøndsted, B. F. Sørensen, J. Varna, R. Talreja, Damage evolution under cyclic multiaxial stress state: A comparative analysis between glass/epoxy laminates and tubes, Composites: Part B 61 (2014) 282–290. doi:10.1016/j.compositesb.2014.01.056.

[9] R. D. Jamison, K. Schulte, K. L. Reifsnider, W. W. Stinchcomb, Characterization and Analysis of Damage Mechanisms in Tension-Tension Fatigue of Graphite/Epoxy Laminates, Effects of Defects in Composite Materials STP30196S (1984) 21–55. doi:10.1520/STP30196S.

[10] A. Gagel, D. Lange, K. Schulte, On the relation between crack densities, stiffness degradation, and surface temperature distribution of tensile fatigue loaded glass-fibre non-crimp-fabric reinforced epoxy, Composites: Part A 37 (2) (2006) 222–228. doi:10.1016/j.compositesa.2005.03.028.

[11] F. Edgren, D. Mattsson, L. E. Asp, J. Varna, Formation of damage and its effects on non-crimp fabric reinforced composites loaded in tension, Composites Science and Technology 64 (5) (2004) 675–692. doi:10.1016/s0266-3538(03)00292-6.

[12] K. Vallons, G. Adolphs, P. Lucas, S. V. Lomov, I. Verpoest, The influence of the stitching pattern on the internal geometry , quasi-static and fatigue mechanical properties of glass fibre non-crimp fabric composites, Composites: Part A 56 (2014) 272–279. doi:10.1016/j.compositesa.2013.10.015.

[13] S. Adden, P. Horst, Stiffness degradation under fatigue in multiaxially loaded non-crimped-fabrics, International Journal of Fatigue 32 (1) (2010) 108–122. doi:10.1016/j.ijfatigue.2009.02.002.

[14] P. Horst, S. Adden, Fatigue behavior of non-crimp fabrics, Key Engineering Materials 385-387 (2008) 545–548. doi:10.4028/www.scientific.net/KEM.385-387.545.

[15] J. Zangenberg, P. Brøndsted, J. W. Gillespie Jr., Fatigue damage propagation in unidirectional glass fibre reinforced composites made of a non-crimp fabric, Journal of Composite Materials 48 (22) (2014) 2711–2727. doi:10.1177/0021998313502062.

[16] N. Chawla, Y. K. Tur, J. W. Holmes, J. R. Barber, A. Szweda, High-frequency fatigue behavior of woven-fiber-fabric-reinforced polymer-derived ceramic-matrix composites, Journal of the American Ceramic Society 81 (5) (1998) 1221–1230. doi:10.1111/j.1151-2916.1998.tb02472.x.

[17] S. F. Shuler, J. W. Holmes, X. Wu, D. Roach, Influence of Loading Frequency on the Room-Temperature Fatigue of a Carbon-Fiber/SiC-Matrix Composite, Journal of the American Ceramic Society 76 (9) (1993) 2327–2336. doi:10.1111/j.1151-2916.1993.tb07772.x.

[18] E. Maire, P. J. Withers, Quantitative X-ray tomography, International Materials Reviews 59 (1) (2014) 1–43. doi:10.1179/1743280413y.0000000023.

[19] P. J. Withers, M. Preuss, Fatigue and damage in structural materials studied by X-Ray tomography, Annual Review of Materials Research 42 (2012) 81–103. doi:10.1146/annurev-matsci-070511-155111.

[20] P. Wright, X. Fu, I. Sinclair, S. M. Spearing, Ultra high resolution computed tomography of damage in notched carbon fiber-epoxy composites, Journal of Composite Materials 42 (19) (2008) 1993–2002. doi:10.1177/0021998308092211.

[21] P. Wright, A. Moffat, I. Sinclair, S. M. Spearing, High resolution tomographic imaging and modelling of notch tip damage in a laminated composite, Composites Science and Technology 70 (10) (2010) 1444–1452. doi:10.1016/j.compscitech.2010.04.012.

[22] A. E. Scott, M. Mavrigirdati, P. Wright, I. Sinclair, S. M. Spearing, In situ fibre fracture measurement in carbon-epoxy laminates using high resolution computed tomography, Composites Science and Technology 71 (12) (2011) 1471–1477. doi:10.1016/j.compscitech.2011.06.004.

[23] S. C. Garcea, M. Macrigirdato, A. E. Scott, I. Sinclair, S. M. Spearing, Fatigue micromechanism characterisation in carbon fibre reinforced polymers using syn-

chrotron radiation computed tomography, Composites Science and Technology 99 (2014) 23–30. doi:10.1016/j.compscitech.2014.05.006.

[24] S. C. Garcea, I. Sinclair, S. M. Spearing, In situ synchrotron tomographic evaluation of the effect of toughening strategies on fatigue micromechanisms in carbon fibre reinforced polymers, Composites Science and Technology 109 (2015) 32–39. doi:10.1016/j.compscitech.2015.01.012.

[25] S. C. Garcea, I. Sinclair, S. M. Spearing, Fibre failure assessment in carbon fibre reinforced polymers under fatigue loading by synchrotron X-ray computed tomography, Composites Science and Technology 133 (2016) 157–164. doi:10.1016/j.compscitech.2016.07.030.

[26] F. Sket, R. Seltzer, J. M. Molina-Aldareguía, C. Gonzalez, J. LLorca, Determination of damage micromechanisms and fracture resistance of glass fiber/epoxy cross-ply laminate by means of X-ray computed microtomography, Composites Science and Technology 72 (2) (2012) 350–359. doi:10.1016/j.compscitech.2011.11.025.

[27] P. J. Schilling, B. P. R. Karedla, A. K. Tatiparthi, M. A. Verges, P. D. Herrington, X-ray computed microtomography of internal damage in fiber reinforced polymer matrix composites, Composites Science and Technology 65 (14) (2005) 2071–2078. doi:10.1016/j.compscitech.2005.05.014.

[28] B. Yu, R. Blanc, C. Soutis, W. P. J., Evolution of damage during the fatigue of 3D woven glass-fibre reinforced composites subjected to tension–tension loading observed by time-lapse X-ray tomography, Composites: Part A 82 (2016) 279–290. doi:10.1016/j.compositesa.2015.09.001.

[29] B. Yu, R. S. Bradley, C. Soutis, P. J. Hogg, P. J. Withers, 2D and 3D imaging of fatigue failure mechanisms of 3D woven composites, Composites Science and Technology 77 (2015) 37–49. doi:10.1016/j.compositesa.2015.06.013.

[30] S. Topal, L. Baiocchi, A. D. Crocombe, S. L. Ogin, P. Potluri, P. J. Withers, M. Quaresimin, P. A. Smith, M. C. Poole, A. E. Bogdanovich, Late-stage fatigue damage in a 3D orthogonal non-crimp woven composite: An experimental and numerical study, Composites: Part A 79 (2015) 155–163. doi:10.1016/j.compositesa.2015.08.020.

[31] J. Lambert, A. R. Chambers, I. Sinclair, S. M. Spearing, 3D damage characterisation and the role of voids in the fatigue of wind turbine blade materials, Composites Science and Technology 72 (2) (2012) 337–343. doi:10.1016/j.compscitech.2011.11.023.

[32] K. M. Jespersen, L. P. Mikkelsen, Fatigue damage observed non-destructively in fibre composite coupon test specimens by x-ray ct, IOP Conference Series: Materials Science and Engineering 139 (2016) 012024. doi:10.1088/1757-899X/139/1/012024.

[33] G. Pereira, J. Hütler, L. P. Mikkelsen, P. Brøndsted, Cure-induced strain and fatigue performance of a non-crimp glass fibre reinforced epoxy, (Submitted 2017).

[34] J. Zangenberg, The effects of fibre architecture on fatigue life-time of composite materials, PhD Thesis, DTU Wind Energy PhD-0018(EN) (2013).

[35] M. J. Emerson, K. M. Jespersen, A. B. Dahl, K. Conradsen, L. P. Mikkelsen, Individual fibre segmentation from 3D X-ray computed tomography for characterising the fibre orientation in unidirectional composite materials, Composites: Part A (2017). doi:10.1016/j.compositesa.2016.12.028.

[36] K. M. Jespersen, L. P. Mikkelsen, Three dimensional fatigue damage evolution in non-crimp glass fiber fabric based composites used for wind turbine blades [Data set], https://dk-sid.migrid.org/cgi-sid/ls.py?share_id=Cd4jZFMRNl (2017).

[P5]

Jespersen, K. M., Glud, J. A., Zangenberg, J., Hosoi, A., Kawada, H., and Mikkelsen, L. P.

UNCOVERING THE FATIGUE DAMAGE INITIATION AND PROGRESSION IN UNI-DIRECTIONAL NON-CRIMP FABRIC REINFORCED POLYESTER COMPOSITE PART A: OFF-AXIS CRACKS AND THE EFFECT OF STRAIN LEVEL

In manuscript (2017).

Uncovering the fatigue damage initiation and progression in uni-directional non-crimp fabric reinforced polyester composite Part A: Off-axis cracks and the effect of strain level

Kristine M. Jespersen[a,*], Jens A. Glud[b], Jens Zangenberg[c], Atsushi Hosoi[d], Hiroyuki Kawada[d], Lars P. Mikkelsen[a]

[a] *Department of Wind Energy, Section of Composites and Materials Mechanics, Technical University of Denmark, Risø Campus, 4000 Roskilde, Denmark*
[b] *Department of Mechanical and Manufacturing Engineering, Aalborg University, Denmark*
[c] *LM Wind Power Blades, Composite Mechanics, Jupitervej 6, 6000 Kolding, Denmark*
[d] *Waseda University, Japan*

Abstract

In this study, a method using transilluminated white light imaging to monitor the off-axis cracks in the thin supporting backing fibre bundles present in quasi-UD composites used for wind turbine blades is presented. A crack counting algorithm is applied to automatically count the cracks in images obtained in-situ during fatigue testing. Fatigue tests are performed at different strain levels and both qualitative and quantitative observations are carried out. It is found that off-axis cracks not only initiate at the specimen edges but also at isolated locations inside the specimen, which could be related to the microstructural features. There is observed a clear effect of strain level on the measured crack density, however surprisingly the measured stiffness degradation is found to be independent of the strain level. Hence, the off-axis cracks in the backing fibre bundles might not be the main cause of the stiffness degradation in stage I of the fatigue life as initially expected.

Keywords: A. Polymer Matrix Composites (PMCs), A. Glass fibres, B. Fracture, D. Non-destructive testing, Fatigue of Composites

[*] Corresponding author. Tel.: +45 28250993.
E-mail address: kmun@dtu.dk (K.M. Jespersen).

1. Introduction

Due to their high specific stiffness, strength, and fatigue resistance, fibre composites are increasingly used for structural purposes in structures like airplanes, cars and wind turbine blades. Especially for wind turbine blades materials, fatigue is a big concern due to the very high number of load cycles caused by the variation in the wind and the oscillating gravitational loads coming from the blade rotation. More specifically, a wind turbine blade is usually designed to last 20-30 years which corresponds to more than 10^8 load cycles [1, 2]. Composite and sandwich materials are used to obtain as light and long blades as possible and the cross-section of a blade is carefully designed in a way that fits the loads present. As a result, the spars that carry the main fatigue loads almost only experience axial loads and are therefore made from fibre composites where most of the fibres are oriented in the direction of the load. For this purpose, uni-directional (UD) non-crimp fabric (NCF) based composites are commonly used [1, 3, 4]. For such fabrics, the UD fibres (aligned in the axial blade direction) are arranged in fibre bundles that are stitched to a thin layer of supporting backing fibre bundles oriented in an off-axis direction. Due to the presence of a small fraction of off-axis fibres, this type of composite have also been referred to as quasi-UD NCF composites and will be named so in the rest of this paper.

1.1. Designing against fatigue

The currently used methods to design against fatigue, such as constant life diagrams based on coupon testing, have been adopted from steels although the damage mechanisms are fundamentally different [1–3]. Due to the lack of understanding of the fatigue damage mechanisms of composites, a lot of uncertainties are present in this design method [2] resulting in numerous safety factors in the design. This is likely to result in conservative designs. For example, fatigue tests are usually accelerated to save time by testing at a higher strain level and frequency than what is present in the actual structure. However, studies have shown an influence of the strain level during fatigue on the saturation crack density [5–7] and even on the damage mechanisms such

as delamination behaviour [7]. Uncertainties in the test methods is also related to that it is difficult to test the quasi-UD composites used for wind turbine blades since they are much stronger in the axial direction than in shear. Therefore, they tend to fail in the tab rather than in the gauge section even for the butterfly shaped test geometry optimised for testing quasi-UD composites [8]. Hence, the obtained fatigue life from coupon testing most likely give conservative values. To be able to establish new design methods that are more suited for fibre composites, it is necessary to first understand the underlying fatigue damage mechanisms of the materials.

1.2. Fatigue damage mechanisms of fibre composites

The initiation and progression of damage during fatigue loading of fibre composites is a complex matter. During fatigue loading matrix cracking, fibre/matrix debonding, and fibre fractures occur and interact with one another. A schematic of a typical stiffness degradation curve for a fibre composite subjected to fatigue loading is shown in Fig. 1.

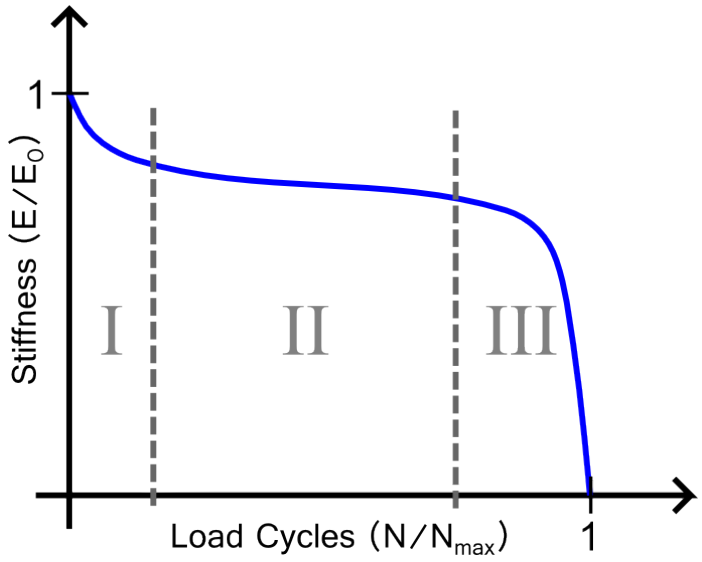

Figure 1: Schematic of a typical stiffness degradation curve for a fibre composite subjected to fatigue loading.

As also marked in Fig. 1, Reifsnider and Jamison [9, 10] suggested to split the stiff-

ness degradation into three main stages: the initial rapid stiffness degradation (stage I), the stable stiffness degradation (stage II), and the final stage where localisation and final failure occurs (stage III). The mechanisms that occur during these stages depend highly on the composite lay-up. Several studies [5–7, 9–11] have considered the fatigue damage mechanisms of prepreg based laminated composites with a somewhat homogeneous distribution of fibres within each layer, which are commonly used in the aerospace industry. In contrast to one layer of the discussed prepreg based composites, the quasi-UD NCF composites used for wind turbine blades have a fibre bundle structure, a small portion ($\sim$10%) of off-axis backing fibre bundles within each layer, and uses stitching thread to tie the bundles together. As a consequence, the damage mechanisms for quasi-UD composites are different from the prepreg based composites. Studies have also been carried out on damage progression in NCF composites [12–20], however due to the complex behaviour the damage mechanisms are still not well understood.

A review by Vallons et al [2] focusing on quasi-UD composites highlighted the need to understand the effects of defects and the variations in the fibre architecture caused by the stitching and the supporting off-axis fibre bundles to which the UD bundles are stitched. Although the stitching has been discussed to be sites for in-plane matrix cracks initiation [2], the stitching pattern seems to have a relatively limited effect on the fatigue life [14, 21]. In relation to fatigue damage progression, other works [17–19] have highlighted the importance of the effect of the supporting off-axis backing fibre bundles.

Based on scanning electron microscopy experiments, Zangenberg et al [17] established a postulated damage progression scheme for a quasi-UD composite with backing fibre bundles oriented in the $\pm 80^\circ$ direction. The postulate state that the initial stiffness degradation in stage I of the fatigue life (see Fig. 1) is caused by off-axis cracking in the $\pm 80^\circ$ backing fibre bundles. During the stable stiffness degradation (stage II), the stiffness degradation was said to be caused mainly by fibre fractures progressing into the UD fibre bundles initiating from off-axis cracks in the backing fibre bundles. At some point, the UD fibre fracture accumulation would be sufficient to cause final

failure of the composite. The damage scheme proposed by Zangenberg et al [17] was later supported by 3D X-ray computed tomography (CT) experiments by Jespersen et al [18, 19], and there is significant evidence pointing towards off-axis cracks in the backing bundles being the starting point for more critical damage such as UD fibre failures. However, it is necessary to monitor the actual damage progression throughout both stage I and stage II, both in terms of off-axis cracks and UD fibre fractures, to properly understand the damage mechanisms during fatigue. Establishing a method to do so is the focus of the current study.

The work is split into two parts related to stage I and II of the fatigue life (Fig. 1), since the initiation and progression of damage during these two stages is considered by different experimental techniques. The current paper serves as Part A, which considers the damage initiation and progression of off-axis cracks related to stage I of the fatigue life, and Part B [22] considers the initiation and progression of UD fibre fractures occurring during stage II of the fatigue life. To study the fatigue damage during the initial fatigue life (stage I), the current study continuously monitors the initiation and progression of off-axis matrix cracks in the backing fibre bundles during fatigue testing by transilluminated white light imaging (TWLI). An automatic crack counting algorithm [23] is used to obtain the crack density as a function of the number of fatigue load cycles. This not only has the advantage of saving time, but also reduces the 'human factor' by comparing the crack densities counted using the same input parameters for all the tests. The crack density is defined relative to the backing fibre bundle structure, which is obtained by large field of view X-ray CT experiments. Fatigue tests are performed at initial strain levels between 0.2% and 0.8% strain.

2. Composite material and specimen geometry

The current study considers a glass fibre composite made from two layers of quasi-UD non-crimp fabric infused with a polyester matrix by vacuum assisted resin transfer moulding. The fabric consists of parallel bundles of UD fibres stitched to a layer of thin supporting $\pm 80^{\circ}$ backing fibre bundles. The backing fibre bundles were removed

from one of the layers in the gauge section of the composite resulting in the layup [0/b,0/b]→[0/b,0] in the considered region. Here "0" indicate the UD bundle side and "b" the backing bundle side of the fabric. This was done in order to examine the damage mechanisms around one layer of backing fibre bundles located in between two layers of UD fibre bundles, which will generally be the case in the layup used for a wind turbine blade. The thickness of the final composite was 2mm.

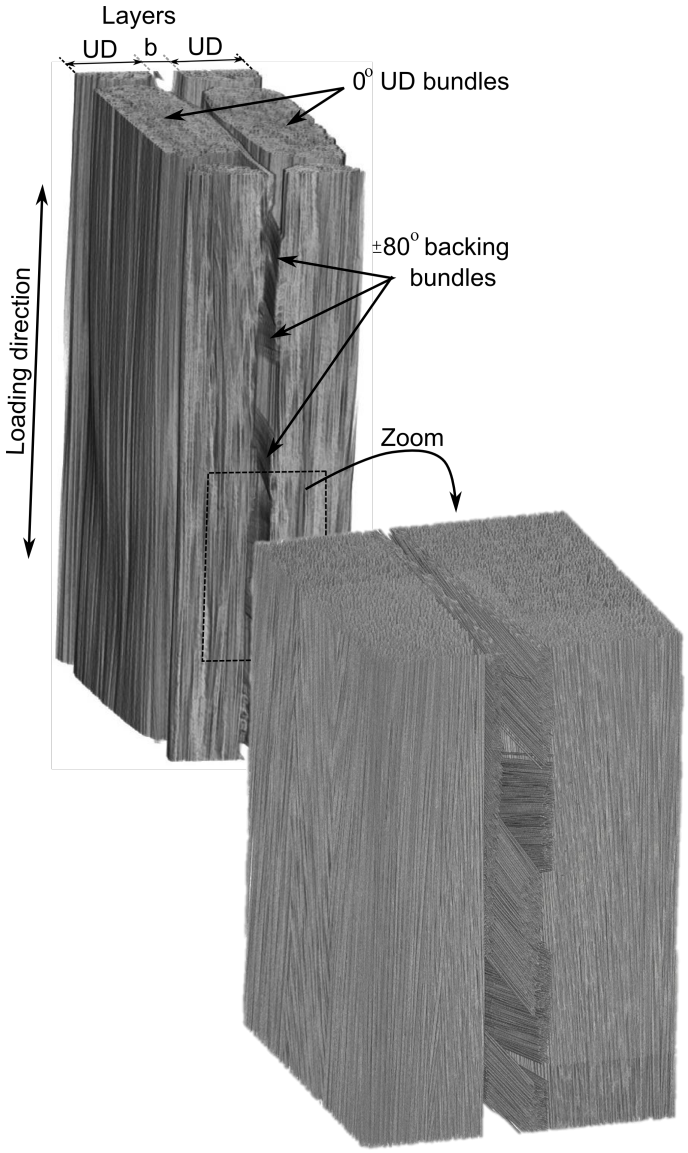

Figure 2: Example of bundle structure obtained by X-ray CT

Fig. 2 shows a 3D rendering of the composite obtained by X-ray CT where the matrix has been rendered invisible to illustrate the bundle architecture. It is seen that due to the fibre bundle structure there are regions of high fibre volume fraction and other regions where there are no fibres at all. Fig. 3a shows a illustration of the layup and Fig. 3b shows a sketch of one quasi-UD layer with backing. It is seen that the backing bundles (marked in green) are crossing over one another at some locations and in other locations there are large matrix rich regions between the bundles.

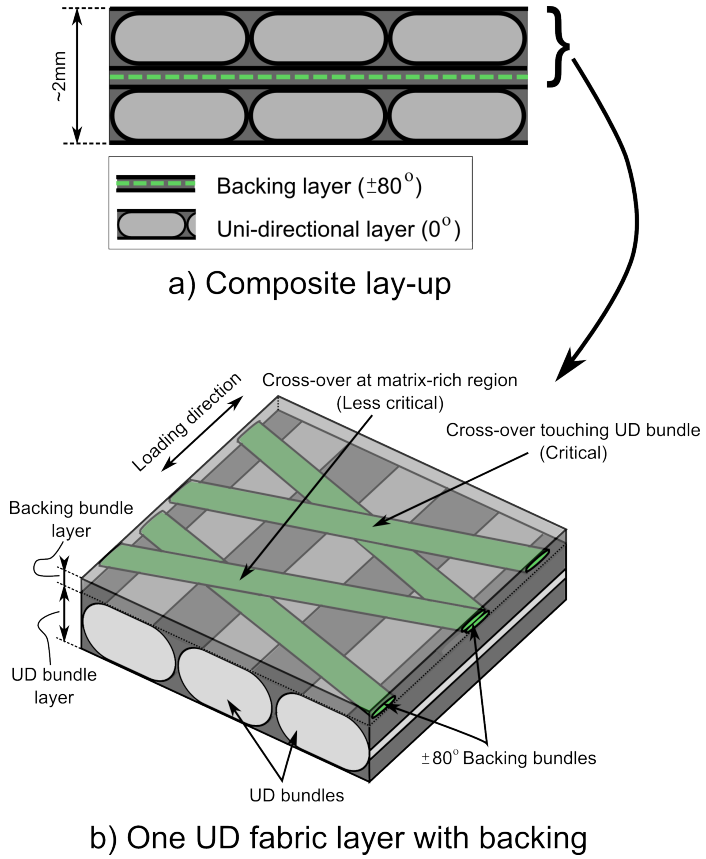

Figure 3: Schematic of (a) the composite layup and (b) one layer of fabric.

A plate of the quasi-UD composite was manufactured, tabs glued on, and cut into 250 mm long specimens with the geometry shown in Fig. 4. The test specimens were cut out so that the region where one backing layer had been removed was located in the centre of the test specimens (gauge section). The used specimen geometry was a

slightly downscaled version of the butterfly geometry [8] commonly used to test UD composites in fatigue. The new specimen geometry was designed with the purpose of combining the advantages of the TWLI [6, 23] and X-ray CT [18, 19] techniques to study both the fatigue damage initiation and progression throughout the fatigue life. The best resolution in X-ray CT is obtained when the cross-section of the specimen is as small as possible. However, a previous study [20] showed that the edge effect had a large influence on the results for a sample width of 5 mm. Therefore, the specimen geometry used in this study (Fig. 4) was designed as a compromise between the full size butterfly specimen geometry [8, 18] and the small samples earlier considered in [20], resulting in a width of 10 mm in the gauge section.

3. Experimental methods

3.1. Fatigue testing and off-axis crack monitoring

Tension-tension (R=0.1) fatigue tests were carried out in load control with a sinusodial waveform at initial strain levels in the range $\varepsilon_{max} = 0.25 - 0.8\%$. Before the fatigue test, two initial static tensile tests are carried out to determine the initial material stiffness and thereby the load necessary to obtain a given initial strain level. The initial stiffness measured from the static tests is determined in the interval 0.05-0.25% strain. Table 1 shows a summary of the tests carried out. The strain was monitored using two extensometers as seen in Fig. 5. The extensometers were mounted on the edge of the specimen to be able to measure the strain in the considered region also shown in Fig. 5 and at the same time monitor the sample with a camera. To make it possible to use the automatic crack counting algorithm explained later in Section 4.1, pen markers were drawn around the centre of the sample with a 20mm distance in between as also marked in the photo of the "considered region" shown in Fig. 4.

During all the performed fatigue tests, TWLI was used to monitor the sample continously. The sample was lit up by an LED lamp on the back and a Nikon D7000 camera with a Tokina Macro 100 F2.8D lens was used to capture images during the test as shown in Fig. 5. This gave a pixel size of around 5μm in the photos. The camera was

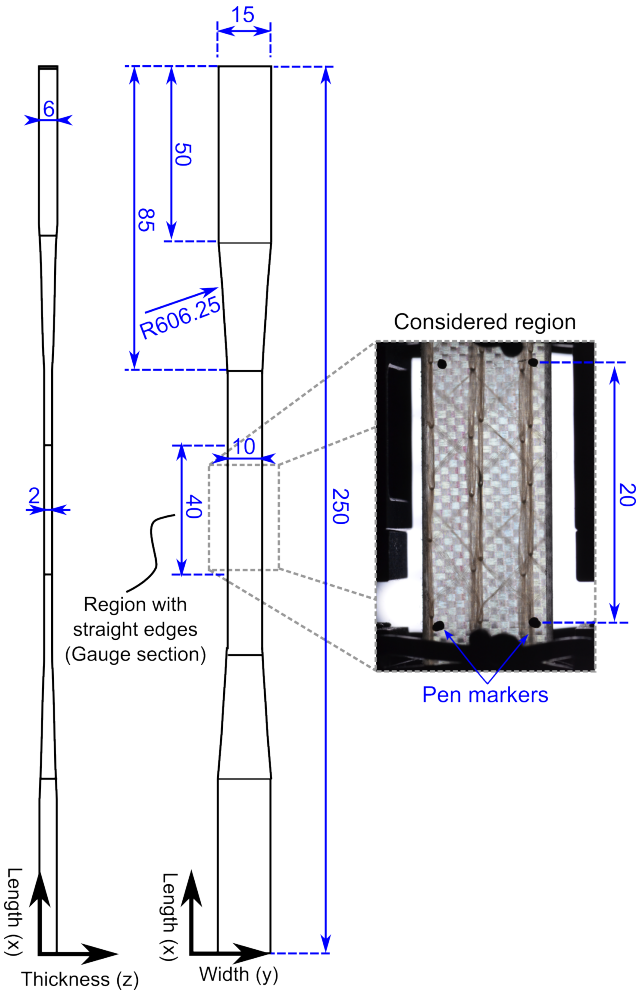

Figure 4: Specimen geometry used for fatigue test. A photo of the considered region is shown with indications of the pen markers used for the automatic crack counting algorithm.

connected to a trigger box programmed to take photos at the point of max load for specific cycle numbers during the fatigue test. One photo was taken before the sample had been introduced to any load and another photo was taken after the two initial static tests. For some of the tests, off-axis cracks were seen to have initiated already after the initial static tests. During the fatigue test 100 photos were taken during each cycle decade. Hence, the trigger box was programmed to take 100 photos during the first 100 cycles, every 10th cycle up to 1000 cycles, every 100th cycle up to 10000 cycles, and so on. However, if the stiffness experienced a sudden drop (more than 1%), the camera

Table 1: Overview of performed fatigue tests

Sample ID	Strain	Tested cycles	Test frequency
EPS08-1	0.80%	100,000	5 Hz
EPS06-1	0.60%	100,000	5 Hz
EPS06-2	0.60%	100,000	5 Hz
EPS06-3	0.60%	100,000	5 Hz
EPS06-4	0.60%	1,000,000	5 Hz
EPS05-1	0.50%	500,000	5 Hz
EPS05-2	0.50%	500,000	5 Hz
EPS05-3	0.50%	500,000	5 Hz
EPS04-1	0.40%	2,000,000	5 Hz
EPS04-2	0.40%	2,000,000	5 Hz
EPS04-3	0.40%	2,000,000	5 Hz
EPS025-1	0.25%	10,000,000	10 Hz
EPS020-1	0.20%	10,400,000	10 Hz

was automatically triggered to take photos with a larger frequency. This approach was chosen in order to capture the damage intiation and progression without getting an overload of data.

3.2. X-ray Computed Tomography

X-ray CT experiments were carried out on a Zeiss Xradia Versa 520 scanner to obtain the fibre bundle structure. During a full 360° rotation of the sample, 1601 projection images were captured. The scans were performed with an accelerating voltage of 80 keV and a power of 7 mA. A 2000x2000 pixel detector with 0.4x optical magnification was used. The scans were performed with a binning of 2 resulting in 1000x1000 pixels in the projection images. To obtain a field of view of around 20x20mm (covering the region considered by the TWLI experiments) the scans were performed with a source-to-sample distance of 40mm and a detector-to-sample distance of 100mm resulting in

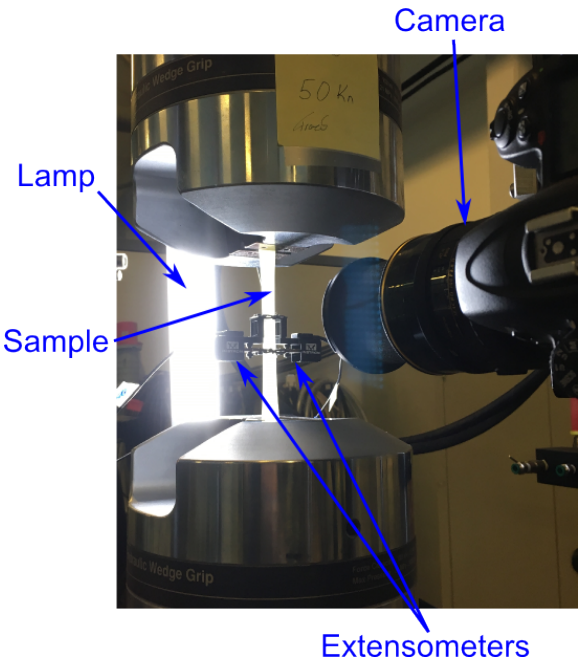

Figure 5: Fatigue testing setup with camera in front of the sample and illuminating LED panel on the back.

a voxel size of 19.5 µm. The scan time for each scan was a bit less than 2 hours.

4. Crack quantification method

4.1. Automated crack counting method

The crack detection algorithm used for automatically quantifying the damage is explained in detail in [23] and includes three overall steps; image compensation, image filtering, and crack counting. In the image compensation step, all the images are compensated for the deformation when loading the sample and other movements to be able to normalise them relative to the initial image of the unloaded and undamaged specimen. The image filtering step has the purpose of separating the cracks observed in different layers with different fibre orientations. This is done using Gabor-filtering which can be used to highlight the cracks oriented in a specific direction and thereby provide separate images for each crack orientation. The normalised and filtered images for each crack orientation are then thresholded to obtain binary images and the cracks

are thinned down to one pixel thick lines. To count the cracks, the images are rotated to be vertically aligned. The cracks are counted by going through the image pixels row by row, and the presence of a black pixel defines the start of a crack. For each crack start, the column belonging to that pixel is searched for additional black pixels connected to the crack. Since the cracks are likely not to be perfectly aligned, neighboring columns are also searched if a white pixel is found. The end of a crack is obtained when a white pixel is reached and no black pixels are present in the nearby pixels. The start and end points of the crack are stored, and the counted crack is deleted from the image. This is then repeated until there are no more cracks in the image.

Since the algorithm initially was used for laminates with a relatively homogeneous distribution of fibres within each layer, it did not work well with too much variation in the orientation of the cracks within each layer. The reason is that the algorithm looks for cracks in a specific angle which is given as input. Since there can be quite some variation of the local orientation angle of the backing fibre bundles in the considered material, it was necessary to modify the algorithm slightly to obtain good results. This was done by automatically determining the average orientation angle of the cracks in each individual backing fibre bundle, and look for cracks in each backing fibre bundle one by one. This modification requires one initial manual step where the approximate regions of the backing fibre bundles have to be marked, however this only has to be done once per sample and only roughly. Fig. 6 shows an example of the results from the automatically counted cracks for EPS06-1.

One challenge when counting cracks both automatically and manually is to validate the results. In the current study, the crack counting for all the tests were performed with the same input parameters for the counting algorithm. This means that the degree of missed cracks should be similar for all the tests, and therefore comparable to one another.

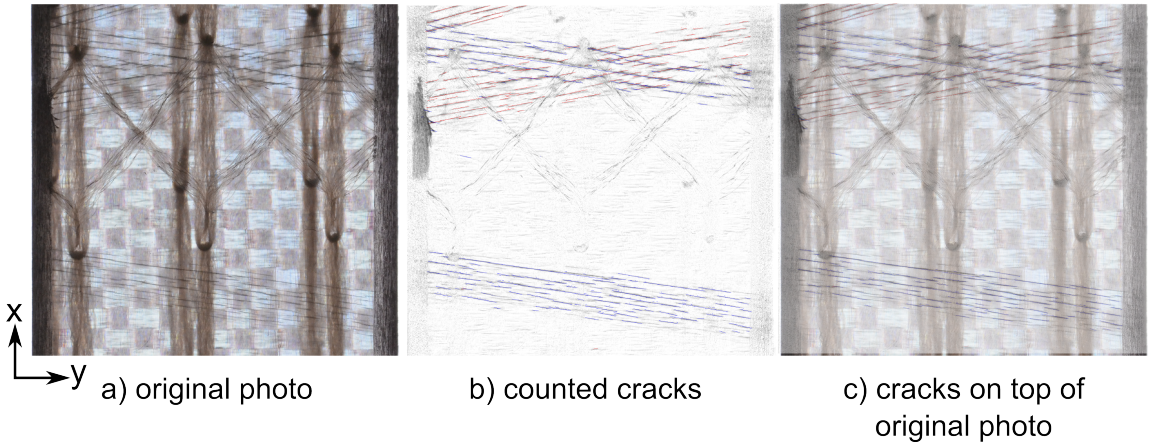

Figure 6: Example of counted cracks compared to the original photo for EPS06-1

4.2. Crack density relative to bundle structure

For composites with a reasonably homogeneous distribution of fibres within each layer, the crack density is usually defined proportional to the total crack surface area as done in [6, 23]. However, the considered composite has a rough fibre bundle structure with large regions of pure matrix. Therefore, it is necessary to define the off-axis crack density relative to the backing fibre bundle area. In the present work, the crack density, ρ, is defined as:

$$\rho = \frac{\sum_{i=1}^{N_c} L_i}{A_{bb}} \tag{1}$$

where $\sum_{i=1}^{N_c} L_i$ is the sum of the measured length of all observed cracks, and A_{bb} is the 'projected backing bundle area', which corresponds to the surface area of all the backing bundles in the x-y plane defined in Fig. 6a (see also Fig. A.18 in Appendix A). Based on the crack density, an average crack spacing can be defined as $S = 1/\rho$ [24, 25].

In order to obtain the backing bundle structure of the considered region, a large field of view X-ray CT scan was performed on all the tested samples prior to fatigue testing, as explained earlier in Section 3.2. In principle, it would be possible to extract the bundle structure in 3D from the X-ray CT images. However, at present there is no

automated way to do so and therefore it would require complete manual segmentation of the bundles. This is both time consuming, and with the relatively large voxel size of 19.5 microns it is difficult to distinguish the backing fibre bundles from the UD fibre bundles at locations where they lie close to each other.

Therefore, a simpler and less time consuming method was established to obtain the projected backing bundle area in 2D as illustrated in Fig. 7. Initially, the 3D dataset was sliced into a stack of 2D images in the plane parallel to the backing bundles. The 2D images containing the backing fibre bundles were then extracted, made opague (30%), and combined into an overlay image. In the overlay image, the edges of all the backing bundles then had become visible. The projected backing bundle area was then segmented by manually marking the area in the open source software ImageJ [26]. After applying a threshold to the image, the projected backing bundle area was calculated using the 'Analyze particles' function in ImageJ.

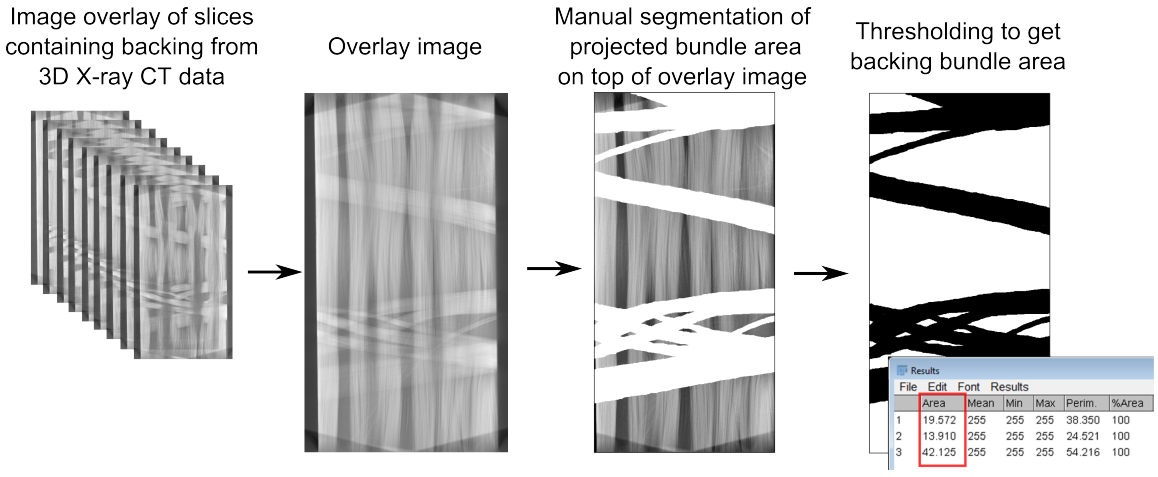

Figure 7: Sketch of principle for segmentation of projected backing bundle area

5. Results and discussion

The off-axis crack initiation and progression is a complex process and will therefore be discussed first based on qualitative observations. This is then followed by discussions based on quantitative measures of the crack density. Here the effect of the applied initial

peak strain during the fatigue tests is also discussed. Finally, the measured stiffness degradation is compared to a simple model and discussed.

5.1. Crack initiation and growth behaviour of off-axis cracks

Fig. 8 shows an example of the cracks in the EPS08-1 (see Table 1) sample after 100,000 cycles (Fig. 8a) along with the same photo with the projected backing bundle area shown on top (Fig. 8b). The projected backing bundle area and the cracks have been manually aligned to obtain Fig. 8b. Although the backing fibre bundles cannot be seen in the camera images, Fig. 8 shows that the pattern in which the cracks appear match the projected backing bundle area obtained by X-ray CT. Hence, the visible off-axis cracks are not evenly distributed in the sample, but appear nearly exclusively in the backing fibre bundles. This is the case for all the tests. It should be noted that the cracks monitored using TWLI are cracks in the backing located in the centre of the composite, hence not surface cracks.

Although the lay-up definition of the fabrics refers to the backing as $\pm 80°$, fig. 9 shows that there is a significant variation in the backing fibre bundle structure from sample to sample. Even within each individual sample, there is a significant variation in the backing fibre bundle architecture. This variation seems to be a result of the stitching procedure that locally influences the backing fibre bundle orientation during manufacturing of the fabric. The local variation in the backing fibre bundle structure also shows the importance of defining the crack density relative to the projected backing bundle area as mentioned in Section 4, since it is clear that in relation to the backing fibre bundle structure, the considered region is not large enough to be representative.

Fig. 10 shows an example of the off-axis crack progression for a region in one of the samples tested at 0.6% strain (EPS06-2). Videos showing the off-axis crack progression for all the performed tests can be found online [27]. Fig. 10a shows the sample before any load was applied, and no off-axis cracks were present at this stage. For this strain level, $\epsilon_{max} = 0.6\%$, some off-axis cracks already initiated after the first cycle as shown in Fig. 10b. This was the case for all the tests performed at strain levels of 0.6% and

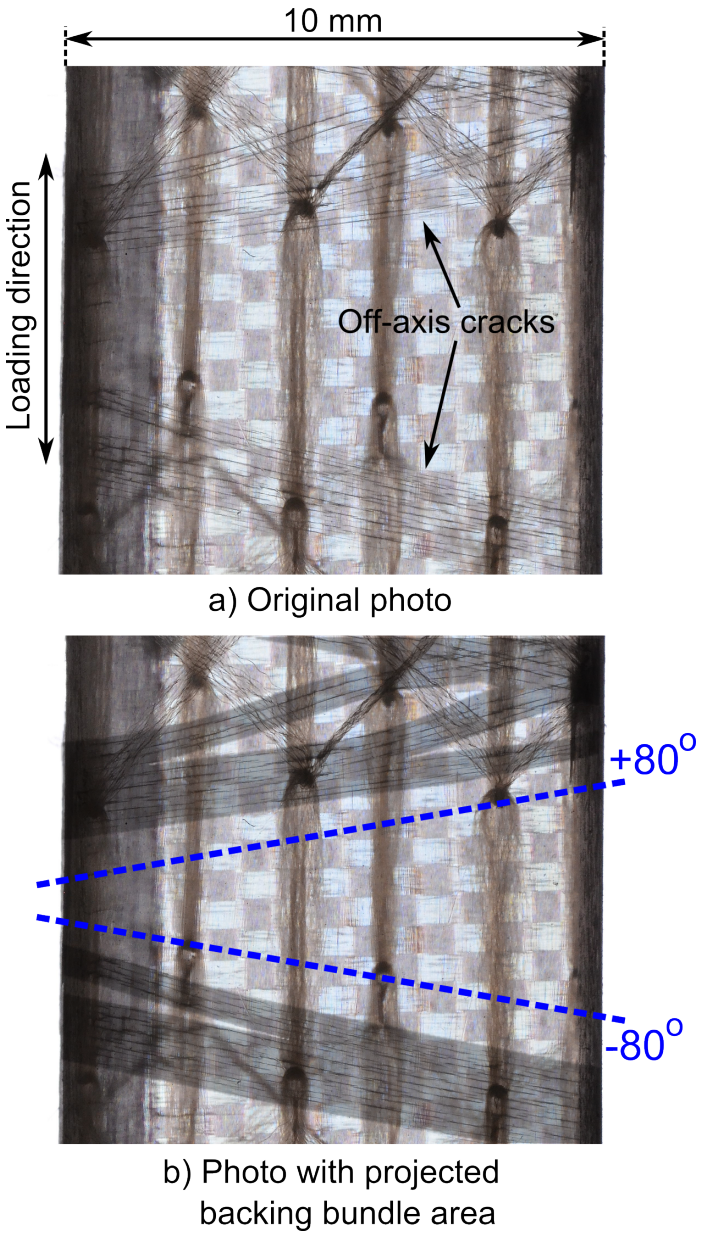

Figure 8: Example of (a) cracks in the backing bundles for sample tested at 0.8% strain for 100,000 cycles and (b) the same photo with the backing bundles obtained by X-ray CT marked in grey on top.

0.8%. With further cycling the number of off-axis cracks then continuously increased, as seen by comparing Fig. 10b, c, and d. In general, off-axis cracks initiate at different times and grow in parallel with one another.

Fig. 11 shows zoom views of the regions A and B marked in Fig. 10. From Fig. 11a

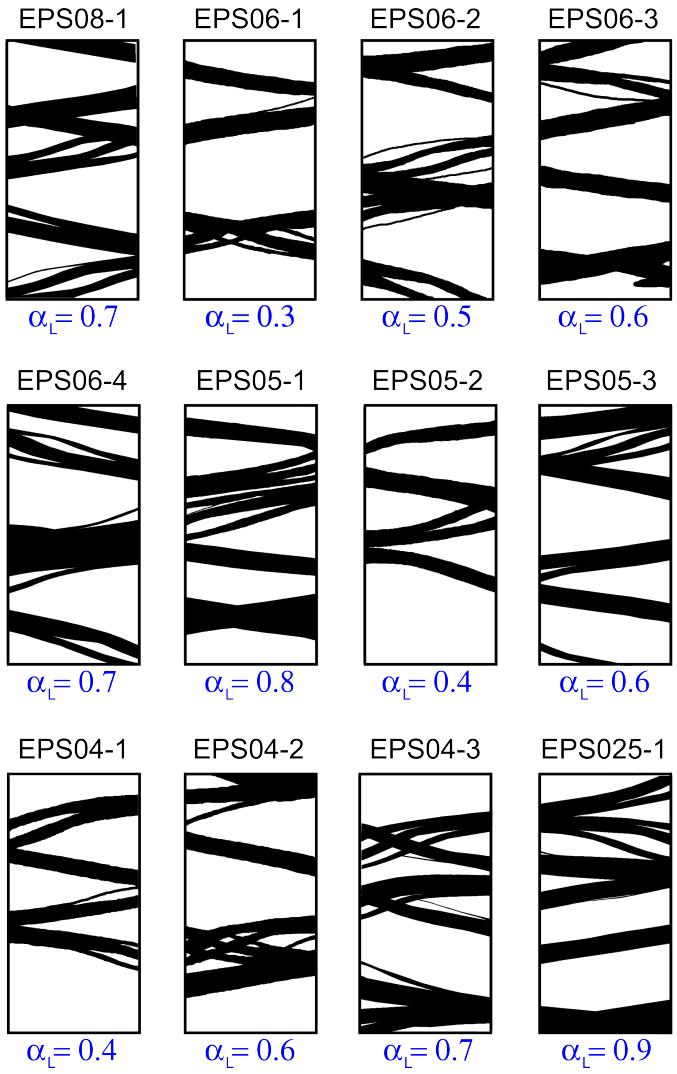

Figure 9: Projected backing bundle areas for all the tested specimens in the considered area (10x20mm) obtained by X-ray CT. The parts marked in black show the backing bundles. α_L is defined by equation 2.

it is seen that some cracks initiate from the edges as would be expected for laminates with reasonably homogeneously distributed fibres within each layer, but other cracks initiate away from the edges. Fig. 11a also shows small $-80°$ cracks initiating as small "branches" from a $+80°$ crack at the cross-over region of the backing fibre bundles. Looking at Fig. 11b it can also be seen that some cracks appear to have a larger opening than others. Similar effects were observed for all the tests (e.g. see videos

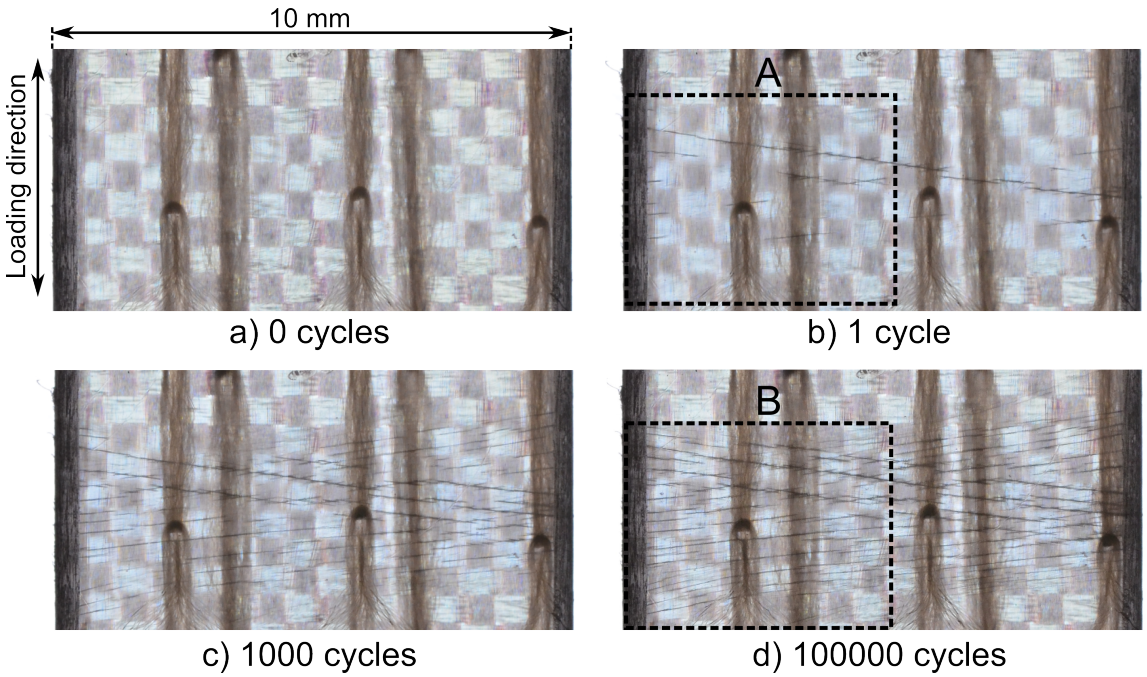

Figure 10: Example of off-axis crack growth at 0.6% strain (Eps06-4). Zoom views of the two marked regions A and B are shown in Fig. 11

online [27]).

5.2. Effect of strain level on the off-axis crack development

Figure 12 shows the crack density measured using the method described in Section 4 as a function of the fatigue load cycles for all the samples. For all the tests performed at 0.8% and 0.6% strain, one of the tests at 0.5% and one of the tests at 0.4% strain, it is seen that cracks already have formed after the first cycle. There seems to be a high degree of scatter on the static strain threshold limit for the initiation of off-axis cracks, which is likely to be related to the variation in the fibre bundle architecture. The development of the crack density seems to reach a state where a close to linear behaviour in the semi-log plot is obtained.

5.2.1. Crack interaction and saturation

Although no clear saturation crack density was reached in the semi-log plot, the applied maximum strain seems to affect the level where the curves start to level out

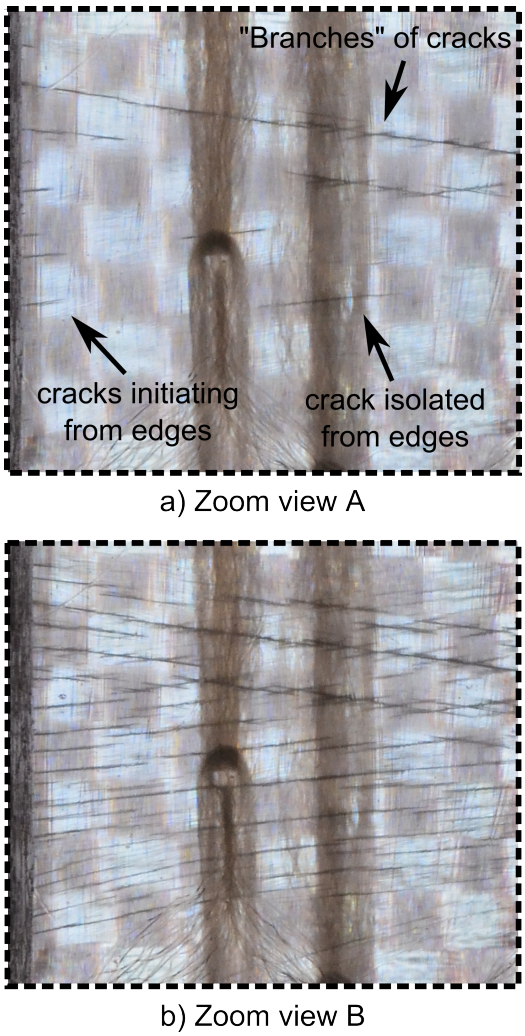

Figure 11: Selected zoom views from Fig. 10 (the same region at two different damage states)

resulting in a low average crack growth speed (see Fig. 14 later), and these levels will be referred to as the apparent saturation values. Similar observations have also been reported for other lay-ups e.g. [6, 24]. However, the case of 0.8% strain is very similar to the 0.6% strain tests. It could be that above a certain strain level the growth behaviour of the off-axis cracks is less affected by the strain level, however this would need further investigation.

Fig. 13 shows the development of the average crack spacing, S, inside the backing bundles as a function of cycles for the tests. The average crack spacing obtained when

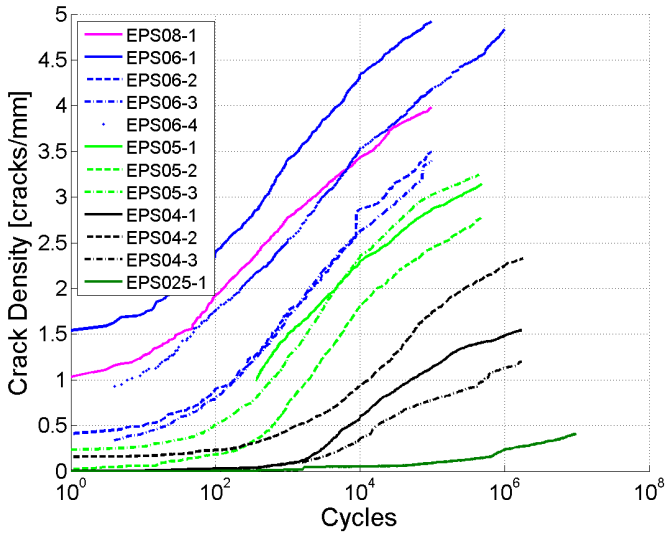

Figure 12: Off-axis crack density as a function of the fatigue load cycles for all the performed tests.

each of the tests were stopped was 0.25 mm for 0.8% strain, in the range 0.20-0.29 mm for 0.6% strain, 0.31-0.36 mm for 0.5% strain and 0.43-0.83 mm for 0.4% strain. For 0.25% strain the crack density was still so low that the average crack spacing was unrealistically high and was therefore left out. The backing fibre bundle thickness was measured approximately in the X-ray CT images, and was found to go down to 0.10 mm for single bundles and up to 0.25 mm for cross-over regions. Crack interaction typically occur when the crack spacing is comparable to the layer thickness (S smaller than five times the layer thickness [24]), and for a quasi-isotropic laminate subjected to fatigue loading Tong [24] observed crack saturation when the crack spacing was around the same as the layer thickness. From Fig. 13 it is seen that particularly for 0.6% strain the final crack spacing is similar to approximate the backing fibre bundle thickness. However, for the lower strain levels the apparent saturation seems to be obtained at a significantly larger value of the crack spacing.

5.2.2. Average crack growth speed

Fig. 12 shows that the slope of the curves at each individual strain level is similar, and that the off-axis crack growth is delayed at lower strain levels. This is also seen

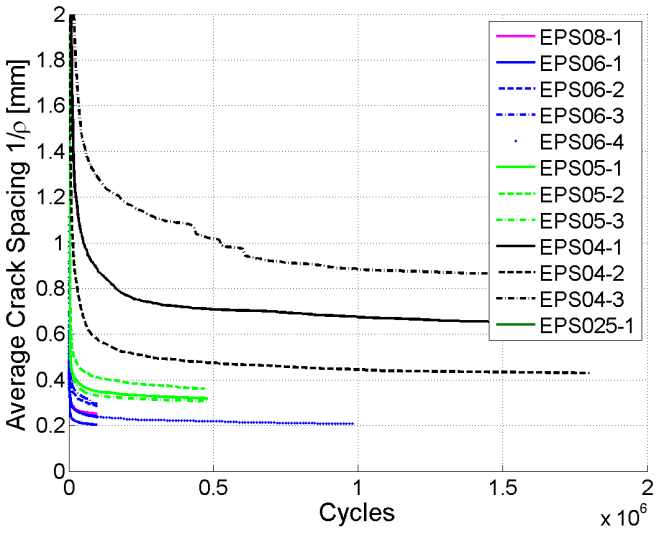

Figure 13: The average crack spacing ($S = 1/\rho$) as a function of the number of fatigue load cycles.

more clearly in Fig. 14, which shows the 'average crack growth speed' defined by the slope of the curves in Fig. 12. The slope of the curves was calculated for each data point by performing a linear interpolation of the nearby data points over a given window length. In other words, the slope was obtained by fitting a line to a number of nearby points depending on the chosen window length. This means that for a larger window length, a higher degree of smoothing is obtained. A window length of one decade in length was chosen, which resulted in the plot in Fig. 14. It is seen that the average crack growth speed for the higher strain levels is higher than for the lower strain levels in the beginning, but that all the tests have reached a slow speed (go towards zero) before the tests were interrupted. Furthermore, for the strain levels 0.8% and 0.6% the average crack growth speed seems to decrease almost linearly with the number of cycles in the log-log scale, whereas this is not the case for 0.5% and 0.4% strain. The slope of a curve appearing linear in the crack density plot shown in Fig. 12 will appear linear in the log-log plot shown in Fig. 14.

Based on the observations, it would seem there are some differences in the occurring damage mechanisms at different strain levels. Hosoi et al [7] also observed that the strain

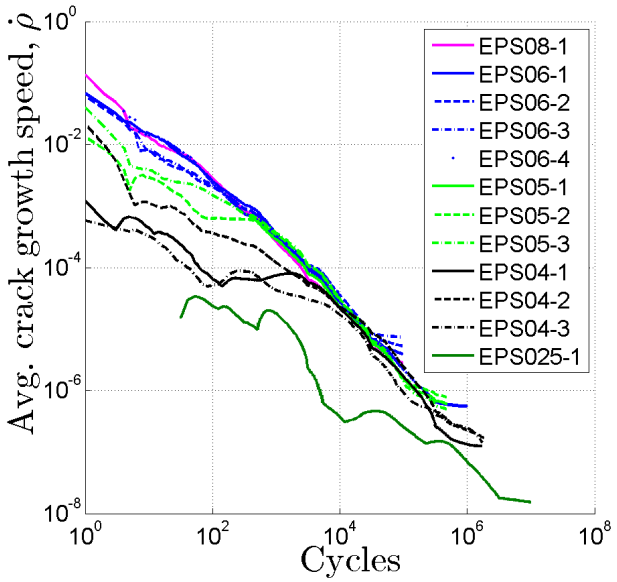

Figure 14: The average crack growth speed defined estimated as the slope of the crack density curve in Fig. 12.

level during fatigue testing can even affect the behaviour of delamination growth, and therefore it is not unlikely that the strain level also has an affect here. However, as mentioned it seems that other effects than strain level affects the off-axis crack growth. In other words, it is possible that the crack initiation and progression behaviour is affected not only by the strain level, but also by these local variations in the fibre bundle structure.

5.3. Stiffness degradation

In Fig. 15, the measured stiffness during the test was normalised and plotted against the number of load cycles. The noise in the data is because the used load cell was large (250kN) compared to the applied load (<10kN). The stiffness degradation is similar for all the tests except the one carried out at 0.8% strain. This is a bit unexpected, as there is a significant difference in off-axis crack density for the samples. Assuming that the stiffness degradation during fatigue stage I is solely caused by off-axis cracking, there should be a difference in the measured stiffness as well since the stiffness is measured

in the same region as the cracks are counted.

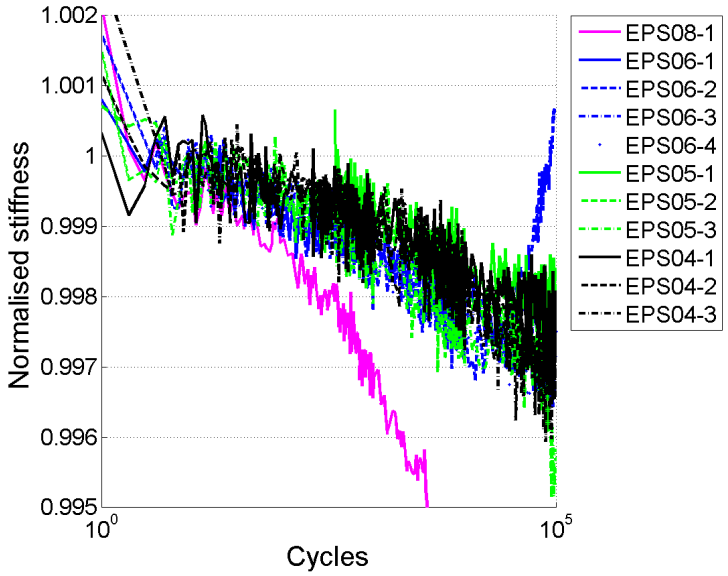

Figure 15: Stiffness degradation as a function of fatigue load cycles for all the tests. The noise is caused by testing at low loads compared to the size of the used load cell.

Fig. 16 shows the relationship between the measured crack density and the stiffness degradation for the different strain levels. Since the stiffness was normalised with the average of the first 10 cycles, the off-axis cracks that had initiated during these first cycles would not contribute to the measured stiffness degradation. Therefore, the initial crack density averaged over the first 10 cycles was subtracted from the crack density results. If the stiffness degradation was only caused by off-axis cracks, the curves in Fig. 16 would be expected to overlap for all the performed tests. However, that is not the case, which could indicate that other damage mechanisms aside from off-axis cracking occur.

The ply-discount method can be used to find a lower bound for the stiffness degradation due to off-axis cracks in the backing fibre bundles by estimating the contribution of the backing fibre bundle layer to the axial stiffness as shown in Appendix A. The fraction of backing fibre bundles relative to the matrix area, α_L , is defined by Eq. 2 where A_{bb} is the projected backing bundle area and A_{tot} is the full considered region

approximated to 10x20mm^2.

$$\alpha_L = \frac{A_{bb}}{A_{tot} - A_{bb}} \tag{2}$$

The contribution of the backing fibre bundles to the composite stiffness depends on the projected backing bundle area as shown in Fig. A.19. The lower limit of the stiffness is in the range of 0.5-2% depending on the chosen layer thicknesses (ranging from 0.10mm for single bundles to 0.25mm for cross-over regions) and projected backing bundle area. It is seen that the tests generally have not reached this level.

Since the ply-discount method only gives a lower bound, the more sophisticated GLOB-LOC [28] model is also used. The solid and dashed red lines in Fig. 16 show predictions of the stiffness degradation using the GLOB-LOC model [28] modified to take in to account the locally higher off-axis crack density due to the bundle structure. This was done by using the crack density defined relative to the backing bundle area to determine the crack opening displacement (COD) and crack sliding displacement (CSD), and then using the crack density determined relative to the full area for the remaining calculations. The COD and CSD were determined from empirical relationships including crack interaction established in [29] and [30], respectively.

The stiffness degradation predicted by this model is highly dependent on the layer thickness, and therefore it is shown for a small and large yet realistic value of the backing fibre bundle thickness. These values were obtained by measuring the backing bundle thicknesses in the high resolution X-ray CT experiments presented in Part B of the current study [31]. For the large backing bundle thickness ($t_b = 0.12$mm) the predicted stiffness degradation due to the off-axis cracks initially follows a similar trend of the experimental data. However, many of the tests the predicted stiffness degradation due to off-axis cracks is less than for the experimental data. Furthermore, it seems that the stiffness degradation measured experimentally does not level out as proposed by the model. This could indicate that other damage mechanisms occur aside from off-axis cracks such as fibre fractures, which is investigated further in Part B of the current

paper [31].

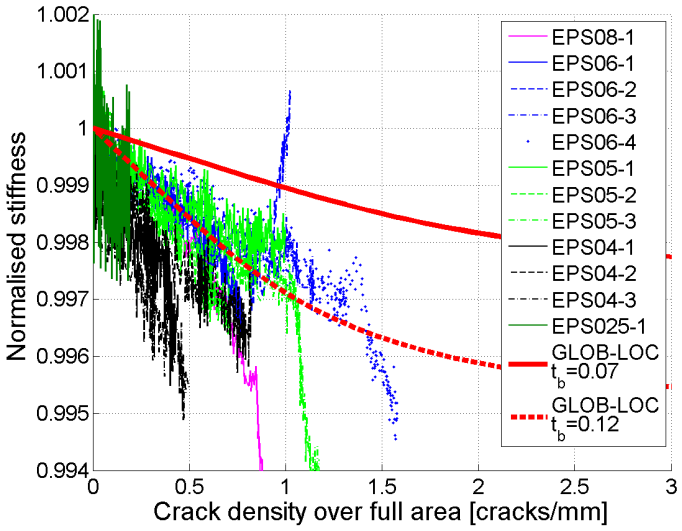

Figure 16: Stiffness degradation as a function of the measured crack density for all the tests. The crack density after the first cycle has been subtracted from the results. The solid and dashed red lines shows the stiffness degradation estimated by the GLOB-LOC model for two different backing fibre bundle thicknesses.

6. Applying the method to compare material systems

Due to the long fatigue life-time (10^8-10^9 cycles) the tests performed for the UD NCF composites used for wind turbine blades are usually accelerated by testing at a higher strain. However, the results of the current study indicate that accelerating the test influences the damage mechanisms in the material. The method presented in the current study makes it possible to compare the fatigue properties of material systems at realistic strain levels. This can be done by establishing an S-N curve for different crack densities as shown in Fig. 17 for the material considered in the current study. The curve shows how many cycles it took to reach a certain crack density, in this case $\rho = 1, 2, 3$. The test performed at 0.25% strain only reached a crack density of 0.19 after 10^7 cycles and therefore is not part of Fig. 17. The lines shown in Fig. 17 are manually drawn trendlines. This provides a way to describe the damage state of the composite aside

from measuring the stiffness degradation, which does not solely describe one damage mechanism.

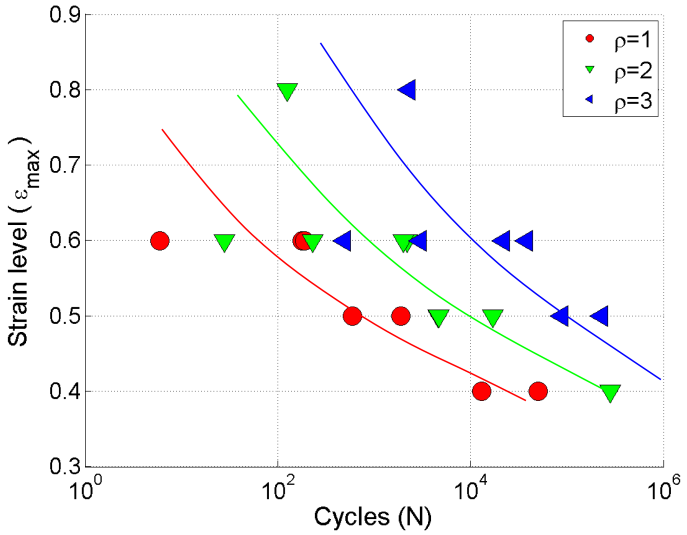

Figure 17: S-N curve for different crack densities with emprical trendlines.

As the fatigue damage progression is highly related to the off-axis cracks in the backing fibre bundles, the type of curve shown in Fig. 17 gives a simple method to compare the fatigue properties of quasi-UD NCF composites. For example it can be used to compare the effect of various manufacturing conditions such as the curing temperature and curing cycles, different constituent materials, fibre diameters or similar. In addition, linking the off-axis crack density with the subsequently occurring critical damage mechanisms such as UD fibre fractures could make it possible to predict the lifetime based on the initial damage states in the future. Monitoring the progression of UD fibre fractures to get closer to such an understanding is the main subject of part B of this work [22].

7. Conclusion

In the current study, a method for monitoring and automatically quantifying the off-axis crack density in the backing fibre bundles of a quasi-UD NCF composite tested

in fatigue was presented. Fatigue tests were carried out at different strain levels, and the crack density seemed to level out at different values off-axis crack densities. In addition, the off-axis crack initiation was delayed at lower strain levels. Hence, it was clear that the strain level had an influence on the fatigue damage mechanisms. In addition, the measured stiffness as a function of the off-axis crack density was compared to the GLOB-LOC model and it was seen that the measured stiffnesses were larger than that predicted by the model. Therefore, it was argued that the stiffness degradation during the initial fatigue life is not only caused by off-axis cracks in the backing fibre bundles, but accompanied by other damage mechanisms such as UD fibre fractures.

Acknowledgements

Financial support from CINEMA: "the allianCe for ImagiNg of Energy MAterials", DSF-grant no. 1305-00032B under "The Danish Council for Strategic Research" is gratefully acknowledged. This research was conducted using mechanical testing equipment from DTU Center for Advanced Structural and Material Testing (CASMAT), Grant No. VKR023193 from Villum Fonden. Additionally we would like to thank LM Wind Power for manufacturing of test specimens. Finally, we would like to thank Steffen Rasmussen and Anthony Fraisse from DTU Wind Energy for their assistance with mechanical tests.

Appendix A. Estimation of axial stiffness contribution from backing layer

The estimation of the stiffness contribution of the backing layer to the axial stiffness described here is similar to the unit cell approach done by Zangenberg et al. [17]. However, the approach explained here include the actual ratio between the backing bundles and pure matrix regions by means of the projected backing bundle area obtained from X-ray CT experiments.

The bundle structure was homogenised as shown in Fig. A.18. Hence, the projected surface area of the backing bundles shown in Fig. A.18a correspond to the area $A_{bb} =$

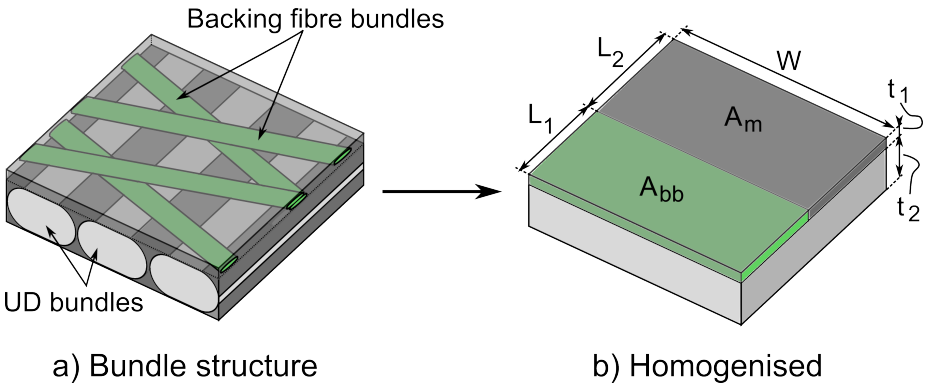

Figure A.18: Definition sketch and homogenisation principle of the fibre bundle structure.

$L_1 \cdot W$ in Fig. A.18b, and similarly the surface area of the matrix regions correspond to the area $A_m = L_2 \cdot W$. If assuming that the backing bundles have a rectangular cross-section, the backing layer can be described by the dimensionless parameter given by Eq. A.1. Furthermore, the thickness ratio between the backing layer and the UD layer is given by Eq. A.2.

$$\alpha_L = \frac{L_1}{L_2} = \frac{L_1}{L - L_1} = \frac{A_{bb}/W}{L - A_{bb}/W} = \frac{A_{bb}}{A_{tot} - A_{bb}} \tag{A.1}$$

$$\alpha_t = \frac{t_1}{t_2} \tag{A.2}$$

Here, $L \cdot W$ is the considered area on the specimen, and the projected backing bundle area, A_{bb}, can be obtained e.g. by X-ray CT as explained in Section 4.2 of the current paper.

Using the Halpin-Tsai equation (semi-empirical), the stiffness of the backing bundles in the direction transverse to the fibres can be estimated by:

$$E_t^b = E_m \frac{1 + \xi \eta V_f}{1 - \eta V_f} \quad with \quad \eta = \frac{E_f^b/E_m - 1}{E_f^b/E_m + \eta} \tag{A.3}$$

where E_t^b is the Young's modulus of the backing fibres. The parameter ξ is a fitting parameter depending on geometry, and for this case it has been suggested to use a value of $\xi = 2$ [32].

Since the backing fibre bundles are oriented in the ±80° the stiffness contribution to the axial direction of the composite can be modified by:

$$\frac{1}{E_x^b} = \frac{1}{E_L^b}\cos^4\theta + \left(-\frac{2\nu_{LT}}{E_L^b} + \frac{1}{G_{LT}}\right)\sin^2\theta\cos^2\theta + \frac{1}{E_t^b}\sin^4\theta \tag{A.4}$$

where θ is the orientation angle of the backing fibres, E_L^b is the stiffness of the backing layer in the fibre direction, E_T^b the stiffness of the backing layer in the direction transverse to the fibres, G_{LT} the shear modulus of the backing layer, and ν_{LT} the Poissons ratio of the backing layer. However, for the current lay-up ($\theta = 80°$) this step can be excluded as there is no significant difference ($E_x^b \approx E_t^b$).

The stiffness of the backing layer can then be calculated as the backing fibre bundles and the matrix regions coupled in series by Eq. A.5.

$$E_x^{bl} = \frac{E_x^b E_m}{E_x^b \alpha_L + E_m}(1 + \alpha_L) \tag{A.5}$$

The total axial stiffness of the composite with the layup [0,b,0] can then be found from:

$$E_x^c = \frac{\alpha_t E_x^{bl} + 2E_a}{1 + \alpha_t} \tag{A.6}$$

The lower limit for the stiffness degradation at saturation of off-axis cracks in the backing layer can be found by setting $E_x^b = 0$. For the calculations done in this study the following material properties are used: $E_f^b = 70$GPa, $E_f^a = 87.5$GPa, $E_m = 3.3$GPa, $\nu_f = 0.3$, $\nu_m = 0.35$, and an average fibre volume fraction of $V_f = 0.55$ (same as in [8]). Aside from material properties, this lower limit is depending on both the ratio between the layer thicknesses α_t and the ratio describing the amount of backing fibre bundles relative to matrix, α_L. Fig. A.19 shows the stiffness contribution from the backing bundles for different values of α_L and for two different values of α_t. The first value of α_t is based on the ratio between the area density of the backing fibre bundles relative to the UD fibre bundles and the second value is based on the approximate layer thicknesses measured in the high resolution X-ray CT images presented in Part B of

the current study [22]. For the specimens considered in the current study, α_L varied in the range of ∼0.3-0.8, and it is seen that depending on the values of α_L and α_t, the stiffness contribution from the backing fibre bundles is in the range of 0.5-2%.

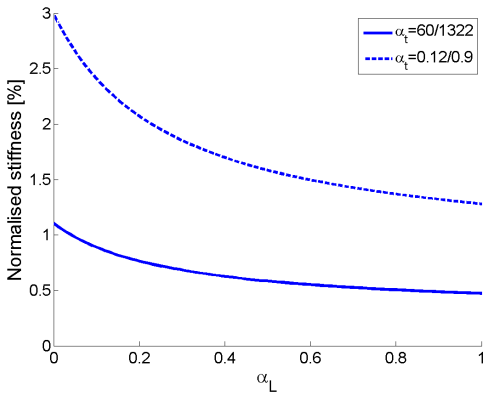

Figure A.19: Contribution of backing fibre bundles to the composite stiffness as a function of α_L for two different values of α_t

References

[1] R. P. L. Nijssen, P. Brøndsted, Fatigue as a design driver for composite wind turbine blades, Advances in Wind Turbine Blade Design and Materials (2013). doi:10.1533/9780857097286.2.175.

[2] K. Vallons, G. Adolphs, P. Lucas, S. V. Lomov, I. Verpoest, Quasi-UD glass fibre NCF composites for wind energy applications: a review of requirements and existing fatigue data for blade materials, Mechanics & Industry 14 (3) (2013) 175–189. doi:10.1051/meca/2013045.

[3] P. Brøndsted, H. Lilholt, H. A. Lystrup, Composite materials for wind power turbine blades, Annual Review of Materials Research 35 (2006) 505–538. doi:10.1146/annurev.matsci.35.100303.110641.

[4] R. P. L. Nijssen, Fatigue life prediction and strength degradation of wind turbine rotor blade composites, PhD Thesis, Delt University of Technology (2006).

[5] J. Tong, F. J. Guild, S. L. Orgin, P. A. Smith, On matrix crack growth in quasi-isotropic laminates—I. experimental investigation, Composites Science and Technology 57 (11) (1997) 1527–1535. doi:10.1016/S0266-3538(97)00080-8.

[6] M. Quaresimin, P. A. Carraro, L. P. Mikkelsen, N. Lucato, L. Vivian, P. Brøndsted, B. F. Sørensen, J. Varna, R. Talreja, Damage evolution under cyclic multiaxial stress state: A comparative analysis between glass/epoxy laminates and tubes, Composites: Part B 61 (2014) 282–290. doi:10.1016/j.compositesb.2014.01.056.

[7] A. Hosoi, Y. Arao, H. Karasawa, H. Kawada, High-cycle fatigue characteristics of quasi-isotropic CFRP laminates, Advanced Composite Materials 16 (2) (2007) 151–166. doi:10.1163/156855107780918964.

[8] J. Zangenberg, The effects of fibre architecture on fatigue life-time of composite materials, PhD Thesis, DTU Wind Energy PhD-0018(EN) (2013).

[9] K. L. Reifsnider, R. Jamison, Fracture of fatigue-loaded composite laminates, International Journal of Fatigue 4 (4) (1982) 187–197. doi:10.1016/0142-1123(82)90001-9.

[10] R. D. Jamison, K. Schulte, K. L. Reifsnider, W. W. Stinchcomb, Characterization and Analysis of Damage Mechanisms in Tension-Tension Fatigue of Graphite/Epoxy Laminates, Effects of Defects in Composite Materials STP30196S (1984) 21–55. doi:10.1520/STP30196S.

[11] J. Varna, R. Joffe, N. V. Akshantala, R. Talreja, Damage in composite laminates with off-axis plies, Composites Science and Technology 59 (14) (1999) 2139–2147. doi:10.1016/S0266-3538(99)00070-6.

[12] A. Gagel, D. Lange, K. Schulte, On the relation between crack densities, stiffness degradation, and surface temperature distribution of tensile fatigue loaded glass-

fibre non-crimp-fabric reinforced epoxy, Composites: Part A 37 (2) (2006) 222–228. doi:10.1016/j.compositesa.2005.03.028.

[13] F. Edgren, D. Mattsson, L. E. Asp, J. Varna, Formation of damage and its effects on non-crimp fabric reinforced composites loaded in tension, Composites Science and Technology 64 (5) (2004) 675–692. doi:10.1016/s0266-3538(03)00292-6.

[14] K. Vallons, G. Adolphs, P. Lucas, S. V. Lomov, I. Verpoest, The influence of the stitching pattern on the internal geometry , quasi-static and fatigue mechanical properties of glass fibre non-crimp fabric composites, Composites: Part A 56 (2014) 272–279. doi:10.1016/j.compositesa.2013.10.015.

[15] S. Adden, P. Horst, Stiffness degradation under fatigue in multiaxially loaded non-crimped-fabrics, International Journal of Fatigue 32 (1) (2010) 108–122. doi:10.1016/j.ijfatigue.2009.02.002.

[16] P. Horst, S. Adden, Fatigue behavior of non-crimp fabrics, Key Engineering Materials 385-387 (2008) 545–548. doi:10.4028/www.scientific.net/KEM.385-387.545.

[17] J. Zangenberg, P. Brøndsted, J. W. Gillespie Jr., Fatigue damage propagation in unidirectional glass fibre reinforced composites made of a non-crimp fabric, Journal of Composite Materials 48 (22) (2014) 2711–2727. doi:10.1177/0021998313502062.

[18] K. M. Jespersen, J. Zangenberg, T. Lowe, P. J. Withers, L. P. Mikkelsen, Fatigue damage assessment of uni-directional non-crimp fabric reinforced polyester composite using x-ray computed tomography, Composites Science and Technology 136 (2016) 94–103. doi:10.1016/j.compscitech.2016.10.006.

[19] K. M. Jespersen, L. P. Mikkelsen, Fatigue damage observed non-destructively in fibre composite coupon test specimens by x-ray ct, IOP Conference Series: Mate-

rials Science and Engineering 139 (2016) 012024. doi:10.1088/1757-899X/139/1/012024.

[20] K. M. Jespersen, Y. Wang, T. Zangenberg, J. Lowe, P. J. Withers, L. P. Mikkelsen, Ex-situ time-lapse X-ray CT study of 3D micro-structural fatigue damage evolution in uni-directional composites, in: 17th European Conference on Composite Materials, Munich, 2016, pp. 1–8.

[21] L. E. Asp, F. Edgren, A. Sjögren, Effects of stitch pattern on the mechanical properties of non-crimp fabric composites, in: 11th European Conference on Composite Materials, Rhodos, 2004, pp. 1–6.

[22] K. M. Jespersen, J. Zangenberg, L. P. Mikkelsen, Uncovering the fatigue damage initiation and progression of uni-directional non-crimp fabric reinforced polyester composite - Part B: uni-directional fibre fractures, Submitted (2017).

[23] J. A. Glud, J. M. Dulieu-barton, O. T. Thomsen, L. C. T. Overgaard, Automated counting of off-axis tunnelling cracks using digital image processing, Composites Science and Technology 125 (2016) 80–89. doi:10.1016/j.compscitech.2016.01.019.

[24] J. Tong, Three Stages of Fatigue Crack Growth in GFRP Composite, Journal of Engineering Materials and Technology 123 (2001) 139–143. doi:10.1115/1.1286234.

[25] Z. Hashin, Analysis of cracked laminates: a variational approach, Mechanics of Materials 4 (1985) 121–136.

[26] J. Schindelin, I. Arganda-Carreras, E. Frise, V. Kaynig, M. Longair, T. Pietzsch, S. Preibisch, C. Rueden, S. Saalfeld, B. Schmid, J.-Y. Tinevez, D. J. White, V. Hartenstein, K. Eliceiri, P. Tomancak, A. Cardona, Fiji: an open-source platform for biological-image analysis, Nature Methods 9 (7) (2012) 676–682.

[27] K. M. Jespersen, J. A. Glud, Z. J., A. Hosoi, H. Kawada, L. P. Mikkelsen, Uncovering the fatigue damage initiation and progression in uni-directional non-crimp fabric reinforced polyester composite - Part A [Data set], https://dk-sid.migrid.org/cgi-sid/ls.py?share_id=bh6dZnjOiJ (2017).

[28] P. Lundmark, J. Varna, Constitutive Relationships for Laminates with Ply Cracks in In-plane Loading, International journal of damage mechanics 14 (3) (2005) 235 – 259. doi:10.1177/1056789505050355.

[29] J. Varna, Modelling mechanical performance of damaged laminates, Journal of Composite Materials 47 (20-21) (2013) 2443–2474. doi:10.1177/0021998312469241.

[30] J. A. Glud, J. M. Dulieu-Barton, O. T. Thomsen, L. C. T. Overgaard, A stochastic multiaxial fatigue model for off-axis cracking in FRP laminates, Submitted to International Journal of Fatigue (2017).

[31] K. M. Jespersen, Z. J., L. P. Mikkelsen, Uncovering the fatigue damage initiation and progression in uni-directional non-crimp fabric reinforced polyester composite - Part B [Data set], https://dk-sid.migrid.org/cgi-sid/ls.py?share_id=fPiQiSINRx (2017).

[32] R. Jones, Mechanics of composite materials, Taylor & Francis,, 1999.

[P6]

Jespersen, K. M., Zangenberg, J., and Mikkelsen, L. P.

UNCOVERING THE FATIGUE DAMAGE INITIATION AND PROGRESSION IN UNI-DIRECTIONAL NON-CRIMP FABRIC REINFORCED POLYESTER COMPOSITE PART B: UNI-DIRECTIONAL FIBRE FRACTURES

In manuscript (2017).

Uncovering the fatigue damage initiation and progression in uni-directional non-crimp fabric reinforced polyester composite Part B: uni-directional fibre fractures

Kristine M. Jespersen[a,*], Jens Zangenberg[b], Lars P. Mikkelsen[a]

[a] *Department of Wind Energy, Section of Composites and Materials Mechanics, Technical University of Denmark, Risø Campus, 4000 Roskilde, Denmark*
[b] *LM Wind Power Blades, Composite Mechanics, Jupitervej 6, 6000 Kolding, Denmark*

Abstract

The current work is part B of a study examining the damage initiation and progression in unidirectional (UD) non-crimp fabric based glass fibre composites used for wind turbine blades. Part A considered off-axis crack initiation and growth during the initial stiffness drop stage (stage I) of the fatigue life, and this part considers the UD fibre fractures that mainly occur during the stable stiffness degradation stage (stage II) of the fatigue life. In this work, an ex-situ X-ray CT fatigue testing method is used to monitor the initiation and progression of unidirectional fibre fractures, and a tension clamp solution is applied during X-ray CT scanning to study the influence of applied load on the crack visibility. It is found that the UD fibre fractures initiate and progress from regions where the off-axis backing fibre bundles are 'in contact' with a UD fibre bundle. Damage is seen to first initiate at a cross-over region of the backing fibre bundles, and later at a region with only one backing fibre bundle. In addition, applying tension to the specimen during X-ray CT scanning is found to reveal a significant amount of UD fibre fractures that are not visible in scans performed the unloaded state. With load applied, a significant number of UD fibre fractures were observed already at the end of stage I of the fatigue life. This supports the conclusion also drawn from part A of the study, that UD fibre fractures initiate together with the off-axis in the backing fibre

* Corresponding author.
E-mail address: kmun@dtu.dk (K.M. Jespersen).

bundles during stage I of the fatigue life.

Keywords: A. Polymer Matrix Composites (PMCs), A. Glass fibres, B. Fracture, D. Non-destructive testing, Micro-tomography

---

1. Introduction

This paper serves as part B of a study examining the damage initiation and progression in quasi-unidirectional (quasi-UD) non-crimp fabric (NCF) based composites subjected to tension-tension fatigue loading. The considered material is used for the load carrying parts of wind turbine blades, and a motivation behind the work was presented in the part A of the study [1]. Fig. 1 shows an illustration of the typical stiffness degradation for a fibre composite subjected to fatigue loading, where the fatigue life is divided into three main stages. Part A [1] considered the initiation and progression of off-axis cracks in the thin supporting backing fibre bundles during the initial fatigue life (stage I) by transilluminated white light imaging (TWLI). The current study will mainly consider the damage occurring during stage II of the fatigue life. As UD fibre fractures are believed to be the main cause of the stiffness degradation observed during stage II of the fatigue life [2, 3], part B of the study presented here will consider the initiation and progression of fibre fractures in the UD fibre bundles. As also illustrated in Fig. 1, X-ray computed tomography (CT) is used to monitor the fatigue damage initiation and progression using an ex-situ approach, and tension clamp experiments will be used to apply load during X-ray CT scanning in two different stages of the fatigue life.

Previous studies [3, 4] on quasi-UD composites subjected to fatigue loading argued that UD fibre fractures is the controlling damage mechanism occuring during stage II of the fatigue life. In addition, it has been found that the UD fibre fractures appear as local 3D phenomena rather than being homogeneously distributed in the composite. Hence, to properly understand how the damage initiate and progress during stage II of the fatigue life for quasi-UD composites, it is necessary to use a 3D imaging technique with sufficient resolution to observe damage on the micro-scale. Furthermore, to be

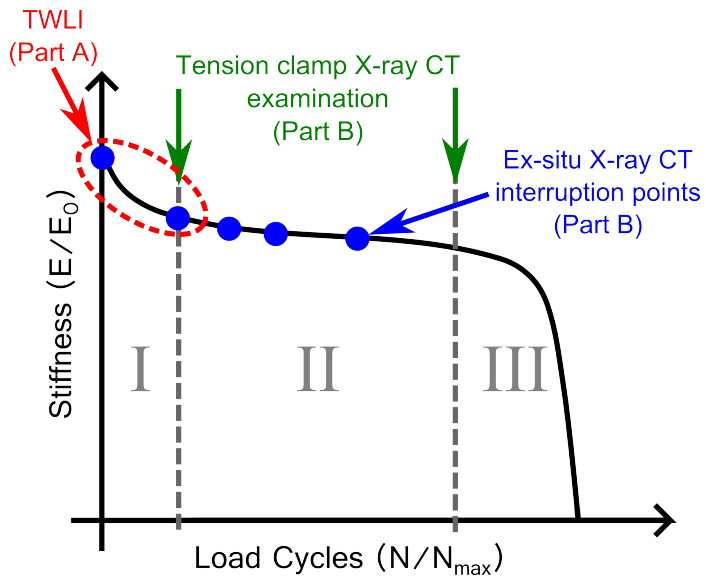

Figure 1: Illustration of the connection between the experiments carried out in Part A and Part B of the current work.

able to observe the damage actually progress, it has be non-destructive. At present, X-ray CT is one of the best techniques available for this purpose.

Because of the new possibilities X-ray CT has brought to the materials science world, an increasing number of studies are using the technique to observe damage of composite materials [3–18]. Synchrotron radiation X-ray CT has been used to study damage progression under static tension [7–9] and later also the progression of fatigue damage [10–12] in notched carbon fibre composites. However, although synchrotron radiation X-ray CT is well suited for in-situ experiments because of the short scan times, the experimental sites are generally difficult to access and the studies usually have to be carried out over no more than a few days. Although at significantly longer scan times, recent improvements of laboratory based X-ray CT have made it possible to obtain an image resolution similar to that of synchrotron radiation X-ray CT. As a result, an increasing number of studies are using laboratory based X-ray CT for micro-structural damage assessment of composites [3, 4, 13–16], since there is more flexibility to the studies. However, generally studies performed by X-ray CT consider small specimens to obtain sufficient image resolution. Downsizing a fatigue test specimen too much

has been found to influence the stiffness degradation due to the edge effect [19] and furthermore for quasi-UD composites the considered volume might not be representative due to the fibre bundle structure. Therefore, a big challenge when using X-ray CT for this purpose, is the compromise between considering a representative volume unaffected by the edge effect and obtaining sufficient image resolution.

To overcome these challenges, the test specimen geometry used in the current study was as a compromise between the regular butterfly specimen geometry [20] commonly used for testing of UD composites, and the downscaled test specimens considered in an earlier study [19]. Using this specimen geometry, it was possible to obtain high image resolution in the X-ray CT images. In addition, a tension clamp solution was used during X-ray CT scanning to enchance the crack visibility.

2. Material and methods

This section explains the methods used for the ex-situ X-ray CT fatigue test and the tension clamp experiments. Brief descriptions of the considered composite material and specimen geometry is given, however more detailed descriptions can be found in part A of the study [1].

2.1. Composite material and test specimens

The composite material considered in this study is a UD non-crimp glass fibre fabric based composite with a polyester matrix and the layup [0/b,0] where 'b' indicates the backing fibre bundle layer consisting of $\pm 80^\circ$ fibre bundles. The specimens were 250mm long with a cross-sectional area of 10x2mm^2 in the gauge section. For more information about the material and specimen geometry, the reader is referred to Part A [1] of the current work.

2.2. Fatigue testing

The specimens examined by X-ray CT in this paper are three of the specimens (EPS06-1, EPS06-3, and EPS06-4) also considered in part A [1], which all were tested

at 0.6% strain. The full list of fatigue tests performed and more details can be found in part A of this study [1]. The specimen EPS06-1 was used for the ex-situ experiments. The ex-situ X-ray CT fatigue test was interrupted after 100,000, 150,000, 200,000, and 500,000 cycles for X-ray CT examination, as also shown in table 1. The specimen was also initially scanned before any load was applied. The fatigue tests of the specimens EPS06-3 and EPS06-4 used for the tension clamp experiments were interrupted after 100,000 and 1,000,000 cycles, respectively. This can also be seen from table 1.

Table 1: Overview interruption points for the three considered specimens

	Interruption 1	Interruption 2	Interruption 3	Interruption 4
EPS06-1	100,000	150,000	200,000	500,000
EPS06-3	100,000			
EPS06-4	1,000,000			

2.3. Tension clamp experiments

A tension clamp solution was used to apply load to the specimen during X-ray CT examination of the specimens EPS06-3 and EPS06-4 interrupted after 100,000 and 1,000,000 cycles, respectively. Hence, the tension clamp experiments both considered fatigue damage of specimens relatively early and late in the fatigue life as also illustrated earlier in Fig. 1. The tension clamp was a modified version of the clamp described in [4] that could fit the smaller specimen geometry used in the current study. The tension clamp is made from two aluminium parts connected by two carbon pins loaded in compression when the clamp was straining the specimen. To attach the tension clamp, the test specimen was first loaded in tension in a regular tensile testing machine. The clamp was then mounted by screws on the strained specimen. When the load was removed from the test machine, the tension clamp kept the gauge section of the specimen loaded. For more detailed information and an illustration of the principle of the clamp, the reader is referred to [4].

The tension clamp utilises the curvature of the specimen edges to keep the aluminium parts in place and thereby transfer the load with no pressure on the specimen surface. Therefore, if damage is induced to the specimen it will be at the curved part of the specimens outside the gauge section. Visually the specimen did not seem to have suffered significant damage. In the current study, the specimen was initially loaded up just below 0.6% strain, and the strain applied by the clamp was measured to be around 0.5% after leaving it for around one hour after it was attached. At this point the load seemed to have stabilised, but as will be clear from the results presented later, some relaxation occurred during the subsequent scanning.

2.4. X-ray CT experiments

All the X-ray CT experiments were carried out on a Zeiss Xradia Versa 520 scanner with a 2000x2000 pixel detector and 4x optical magnification. A binning of 2 was used resulting in 1000x1000 pixels in the final projection images.

For the ex-situ experiments the source-to-sample distance was 20 mm and a sample-to-detector distance was 40mm giving a pixel size of 2.32 μm in the projection images. The projection images were captured with an accelerating voltage of 80keV, a power of 7mA and an exposure time of 2.5 seconds. The tension clamp experiments were carried out with similar settings, but because of the presence of the clamp it was necessary to increase the source-to-sample distance to 25 mm and the sample-to-detector distance to 50 mm to obtain a similar pixel size (2.25 μm). This resulted in an exposure time of 5 seconds for these scans. To obtain good image quality the performed scans were performed with 5201 projections, but the number of projections could possibly be reduced a bit to lower the scan time without a significant loss of image quality.

Image reconstruction was performed using the "XMReconstructor - Cone Beam 10" from Zeiss, and data visualisation was done using the open source software "ImageJ" [21]. All the reconstructed X-ray CT data sets can be downloaded online [22]. Each reconstructed dataset is 2GB in size. For the ex-situ experiments there are 8 data sets and for the tension clamp experiments there are 4 data sets.

3. Results and discussion

In this section, the results obtained from the ex-situ fatigue study and the tension clamp experiments will be presented and discussed. Fig. 2 shows the stiffness degradation measured during the fatigue tests of the three considered specimens EPS06-1, EPS06-3, and EPS06-4. For EPS06-1 subsequently tested further during the ex-situ test, the data is only included until the first interruption point. Dismounting and re-mounting the extensometers seemed to have affected the measured stiffness degradation significantly for the test, and therefore this data is not included. Nevertheless, the measured stiffness degradation for the tests is seen to have a shape similar to that shown earlier in Fig. 1. Furthermore, assuming they will follow a similar trend to EPS06-4, the interruption points for EPS06-1 and EPS06-3 are seen to be around where the curve begins to show a linear degradation behaviour, hence in the end of stage I. EPS06-4 is seen to have been interrupted significantly later in stage II the fatigue life.

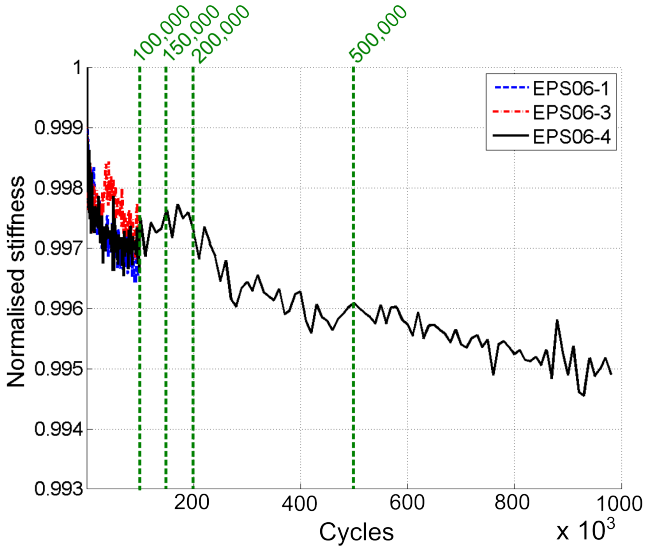

Figure 2: Stiffness degradation of the considered tests

3.1. Initiation and progression of UD fibre fractures

In a previous study considering a rather similar material system [3], UD fibre fractures were found to initiate primarily at locations where the backing fibre bundles were

crossing over one another and at the same time were in 'contact' with a UD fibre bundle. Here being in 'contact' means that the bundles lie so close to each other that the distance between their fibres become similar to that inside the individual bundles. In the current study this information was used to determine the locations to scan, where damage was expected to initiate. By performing a large field of view scan before fatigue testing, the scan region could be chosen based on the bundle structure using the Scount-and-Scan principle provided by Zeiss.

Fig. 3a shows the locations of the two regions considered in the ex-situ fatigue study relative to the projected backing bundle area indicated in black (see also part A [1] for more information). Fig. 3b and 3c show 3D visualisations of the considered volumes obtained by X-ray CT. As can be seen, region I is a volume containing a cross-over region of the backing fibre bundles in contact with the UD bundles on both sides (Fig. 3b), and region II a single backing fibre bundle only in contact with one of the UD bundles (Fig. 3c).

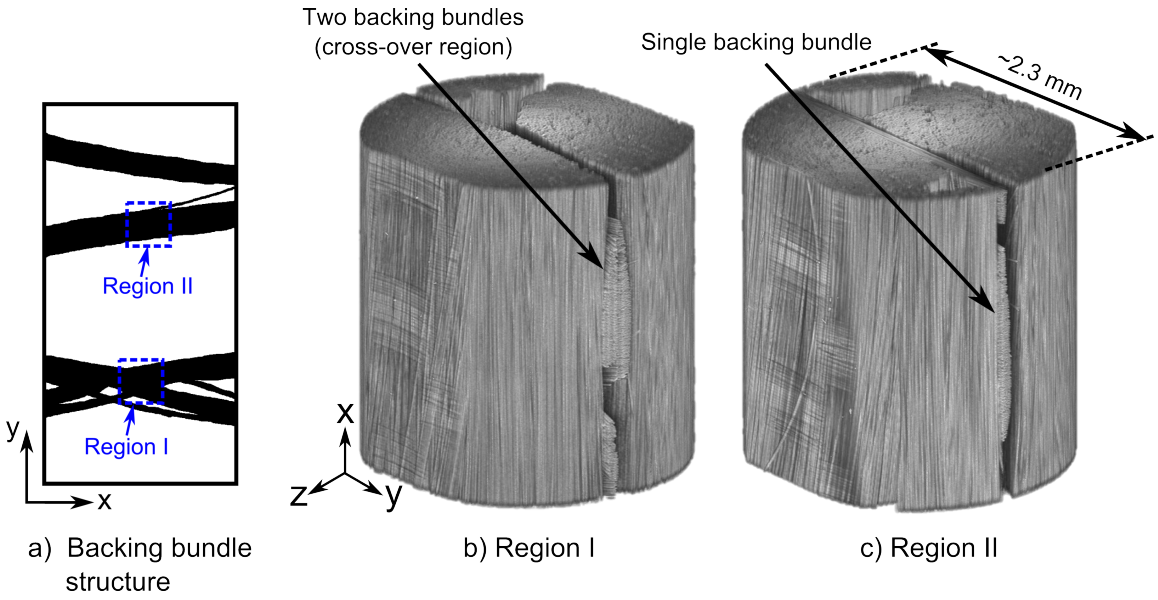

Figure 3: The approximate locations of the two regions considered by X-ray CT in specimen EPS06-1 are shown on top of the bundle structure in (a) and the 3D volumes obtained by X-ray CT are shown in (b) and (c) for region I and II, respectively.

Fig. 4 shows a 2D slice view of the damage progression observed in region I by ex-situ X-ray CT. The full 3D image data can be found online [22]. Before any load was applied, no damage could be observed in the X-ray CT images. At the first interruption point after 100,000 cycles, a few UD fibre fractures was seen to have initiated at the cross-over region as also marked by the red dashed circle in Fig. 4b. UD fibre fractures were seen to gradually progress from the cross-over region of the backing fibre bundles in contact with the UD fibre bundle and into the thickness direction of the UD bundle. This is seen by the difference between Fig. 4b and 4c. After 500,000 cycles the UD fibre fractures had progressed even further and already existing fibre fractures had become more visible. This indicates an increased crack face opening of the fibre fractures, even though it was scanned by X-ray CT in the unloaded state. This kind of permanent increase of the crack face opening of fibre fractures in the unloaded state have also been observed in a previous study for a similar material system [3].

Another thing that can be noticed from Fig. 4, is that off-axis cracks in the backing fibre bundles are not visible. However, Fig. 5 shows photos of the off-axis cracks near scan region I captured by TWLI, and it is seen that several off-axis cracks are present already at the first interruption point of the ex-situ study. Hence, since the off-axis cracks are practically closed, the resolution in the X-ray CT images is not sufficient to see this type of cracks. Previous studies [3, 4] have also shown the difficulty of seeing this type of cracks by X-ray CT, which is also the reason why the current study included TWLI in the ex-situ fatigue testing approach. Fig. 5 also shows that there is no significant change in the off-axis crack density after the first interruption point of the ex-situ test, which indicate that they have reached saturation.

Although to a smaller extent than for cross-over regions of the backing fibre bundles, Zangenberg et al. [2] also observed UD fibre fractures at single backing bundles in contact with UD bundles late in the fatigue life for a similar quasi-UD composite. However, for X-ray CT experiments carried out on quasi-UD composites, this has not been observed so far [3, 19]. To study this further, it was chosen to carry out ex-situ X-ray CT of a single backing bundle region as well (Fig. 3c) for the final three

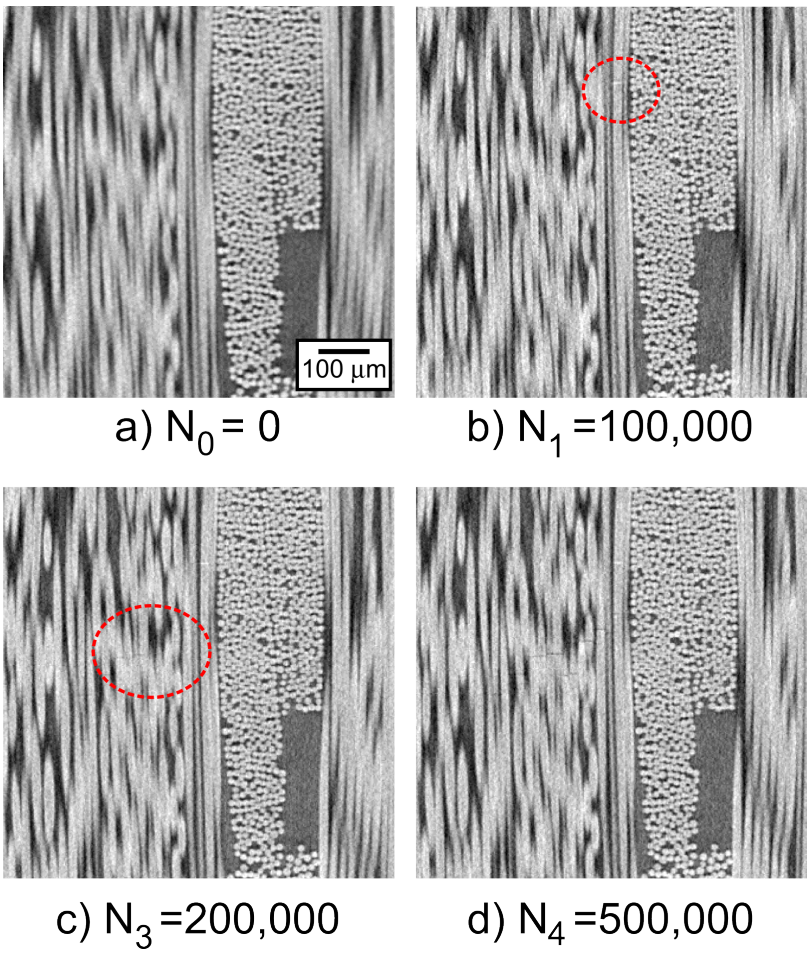

Figure 4: A 2D slice view in Region I in specimen EPS06-1 during the ex-situ test. The red circles mark regions with UD fibre fractures that have become visible.

interruption points of the ex-situ test. Fig. 6 shows a 2D slice view of the damage progression observed at the single backing fibre bundle. No or limited damage was observed in this region after 150,000 cycles (Fig. 6a), but at later stages small regions of UD fibre fractures were observed to initiate in the UD bundle in contact with the backing fibre bundle. One of these regions are marked by a red dashed circle in Fig. 6b and seen slightly more clearly at the later damage state shown in Fig. 6c. UD fibre fractures were observed to appear near the cross-over region (region I) earlier in the fatigue life than near the single backing fibre bundle (region II). In addition, the damage region near the cross-over region appeared larger than at the single backing

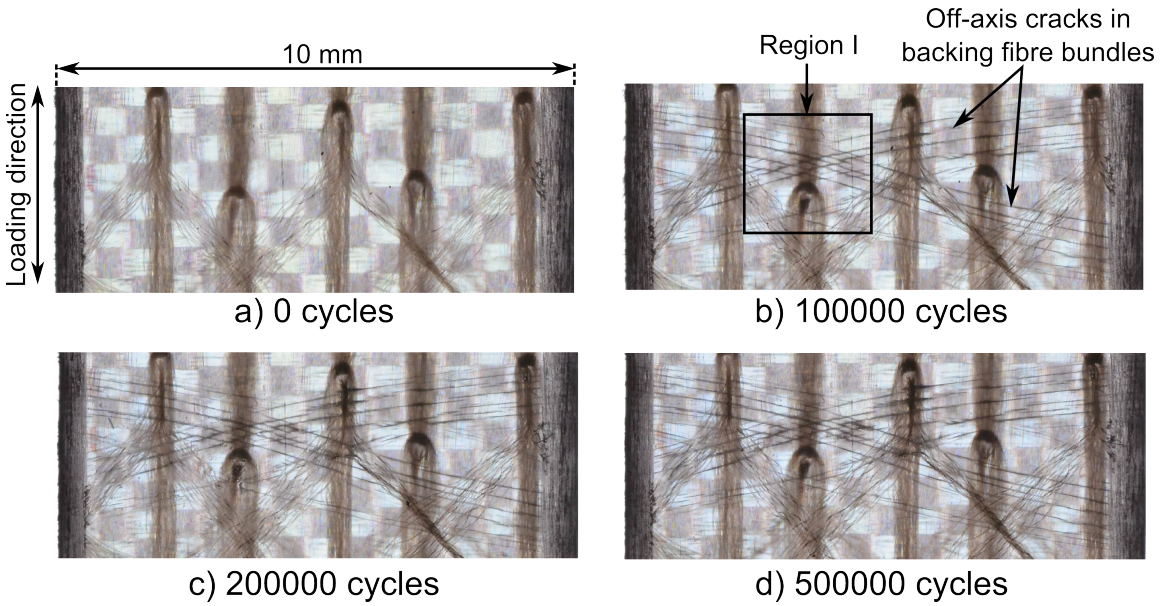

Figure 5: TWLI images showing off-axis cracks in the backing fibre bundles near region I of specimen EPS06-1 at each of the stopping poitns for the ex-situ test shown in Fig. 4.

fibre bundle region.

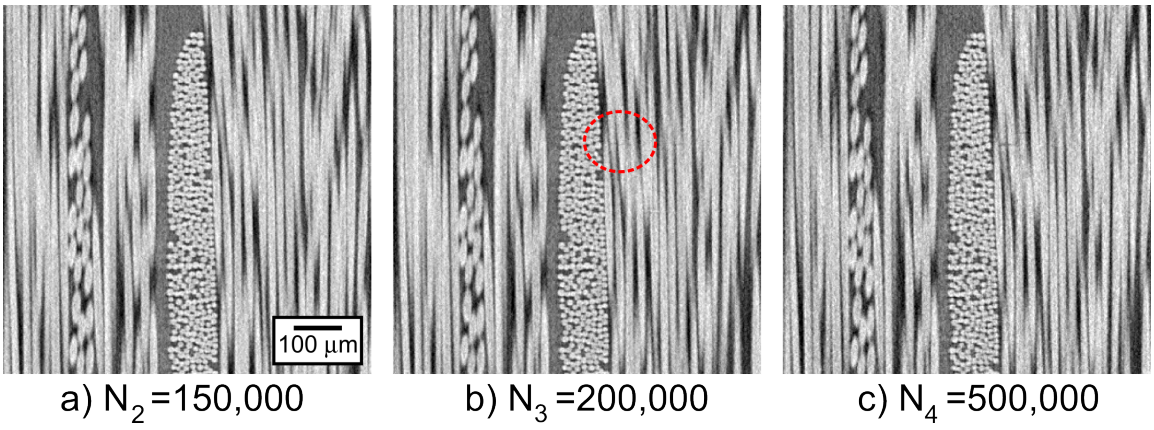

Figure 6: A 2D slice view in Region II of specimen EPS06-1 during the ex-situ test. The red circle mark a region with UD fibre fractures that have become visible.

3.2. Effect of applied tension on the crack visibility

One thing that is clear from the damage progression presented in the previous section, is that the crack face opening of the fibre fractures observed in the images

is relatively small. It is likely that additional fibre fractures with no or very small openings exist but cannot be seen in these images. Therefore, load was applied during X-ray CT scanning to open up cracks and study the effect of applied load on the crack visibility in the X-ray CT scans. Two samples (EPS06-3 and EPS06-4) were scanned in two different regions each, with and without tension clamp applied. Fig. 7 shows the locations of the scan regions on top of the projected backing bundle area (region A-D). The off-axis cracks observed by TWLI are shown for each region in the figure. From the TWLI images it is seen that several off-axis cracks were present in all the considered regions when the X-ray CT scans were performed.

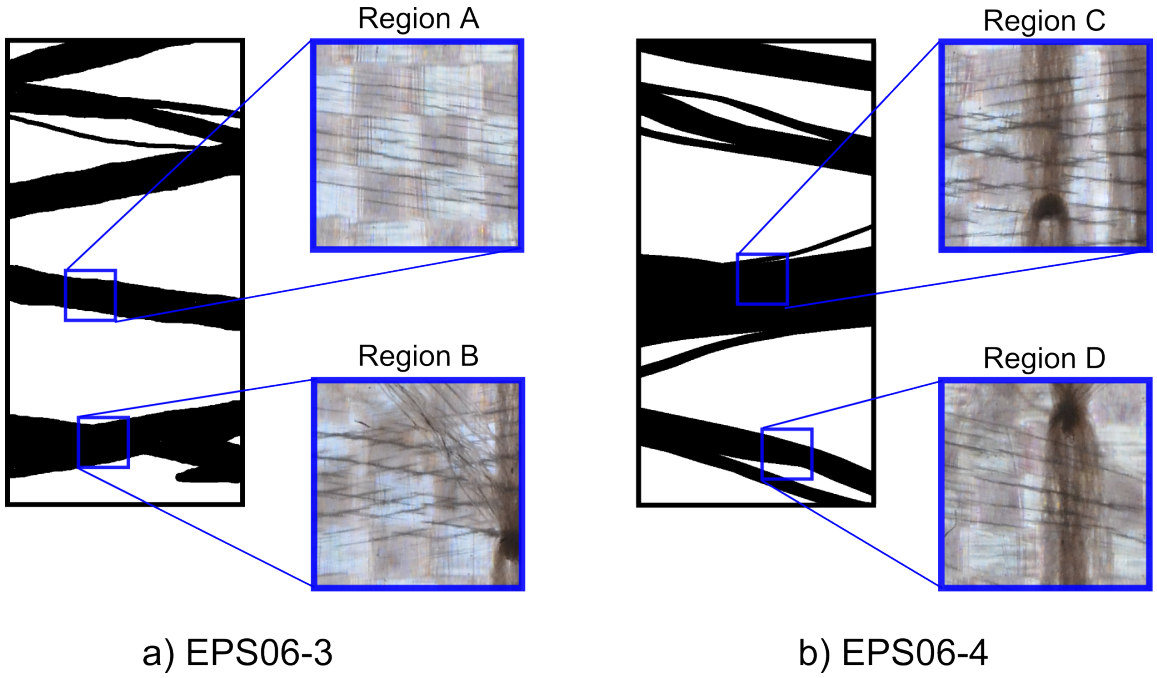

Figure 7: Locations of the scan regions on top of the backing fibre bundle structure for the tension clamp experiments for (a) the specimen EPS06-3, and (b) the specimen EPS06-4. The TWLI images of the off-axis cracks are shown for the four considered regions (A-D).

Fig. 8 shows 2D slice views from the 3D images of the two regions examined by X-ray CT with and without applied tension during scanning in the specimen EPS06-3 (region A and B). The full 3D image datasets can be found online [22]. The specimen was scanned with load applied first and then subsequently scanned in the unloaded

state. Therefore, even if not visible, any damage present in the loaded state also exists in the unloaded state. The fatigue test of specimen EPS06-3 was interrupted after 100,000 cycles, which is relatively early in the fatigue life (around the end of stage I). Fig. 8a shows a region with a single backing fibre bundle (region A), and Fig. 8b a cross-over region of the backing fibre bundles (region B). A significant improvement of the visibility of cracks can be observed when tension is applied during X-ray CT scanning. As seen in Fig. 8a, no off-axis cracks nor fibre fractures were visible in region A in the unloaded state. However, when load was applied, several UD fibre fractures became visible and some off-axis cracks could also be seen in the backing fibre bundles near the UD fibre fractures.

For region B shown in Fig. 8b, it is seen that the tension clamp had caused the X-ray CT image to be out of focus. The images look similar to a reconstruction with incorrect centering of the image, but it was caused by movement during scanning. Region B was scanned prior to region A and the load applied by the clamp must have relaxed a bit during the first scan. However, since this problem was not observed for the subsequent scan of region A, it must mean that the relaxation leveled out after several hours (each X-ray CT scan took around 10 hours). Hence, it is necessary to wait longer than one hour before X-ray CT scanning of a sample with the tension clamp applied to avoid the relaxation to affect the image quality. Nevertheless, despite the blurry image it is clear that there is a significant number of UD fibre fractures that were not visible in the unloaded state.

Fig. 9 shows 2D slice views from the 3D images of the two regions examined by X-ray CT with and without applied tension during scanning in the specimen EPS06-4. The full 3D image datasets can be found online [22]. This test was interrupted after 1,000,000 cycles, which is relatively late in the fatigue life (see also Fig. 2 earlier). Fig. 9b shows a backing bundle, which is in contact with only one UD bundle. As was also seen for the case shown in Fig. 8, the load has affected both the visibility of the UD fibre fractures and the off-axis cracks significantly. Furthermore, the tension clamp experiments showed that UD fibre fractures also exist at single fibre bundles, which

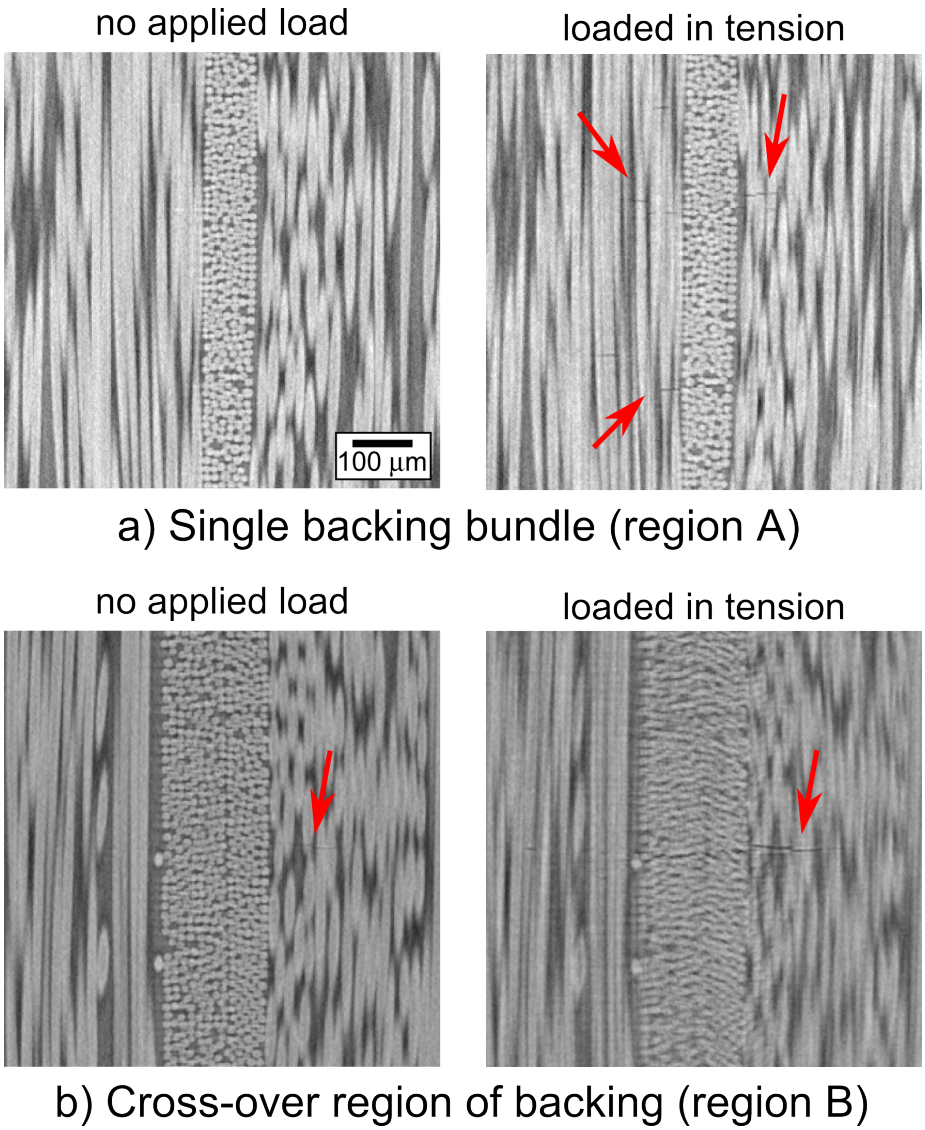

Figure 8: 2D slice views of region A and B (see Fig. 7) for EPS06-3 (100,000 cycles) with and without applied load during X-ray CT scanning.

was not observed in previous X-ray CT studies on this particular quasi-UD composite [3, 19].

3.3. Off-axis cracks as damage initiators

In addition to making it easier to see the UD fibre fractures, applying tension during the X-ray CT scan also increased the visibility of the off-axis cracks in the backing fibre

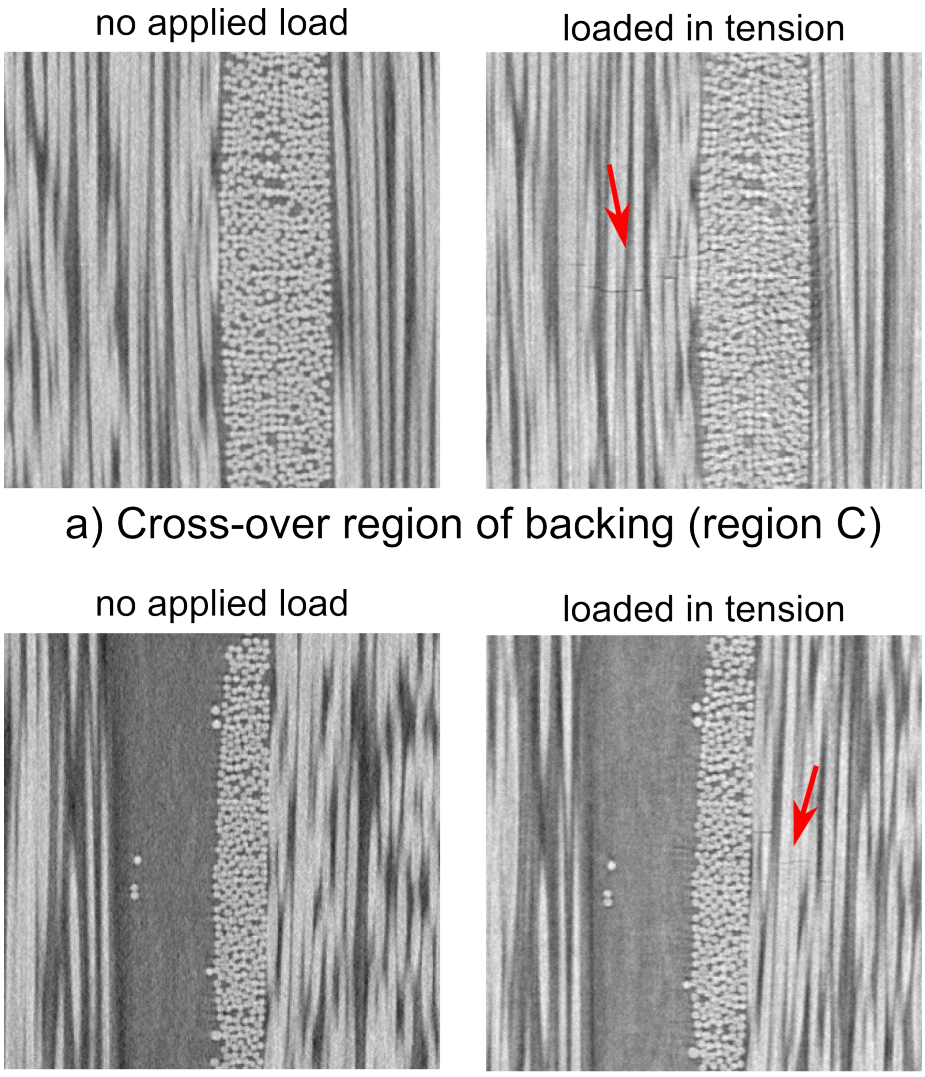

Figure 9: 2D slice views of region C and D (see Fig. 7) for EPS06-4 (1,000,000 cycles) with and without applied load during X-ray CT scanning.

bundles as seen from the examples in Fig. 10. The transilluminated white light imaging experiments performed in part A of the current study [1], showed that off-axis cracks are present even if not visible in the X-ray CT scans. When the tension clamp was applied, it was possible to see indications of these off-axis cracks at the regions with UD fibre fractures as also seen from Fig. 10. These observations strongly indicate that the UD fibre fractures indeed have initiated from off-axis cracks in the backing

fibre bundles, as also argued in previous studies [2, 4]. Furthermore, even with load applied during X-ray CT scanning, UD fibre fractures were not observed when there was a layer of matrix of a certain thickness in between the backing fibre bundle and the UD fibre bundle. This is believed to be because UD fibre fractures initiate from stress concentrations at the tips of the off-axis cracks in the backing, and that a sufficiently thick layer of matrix causes the crack to arrest.

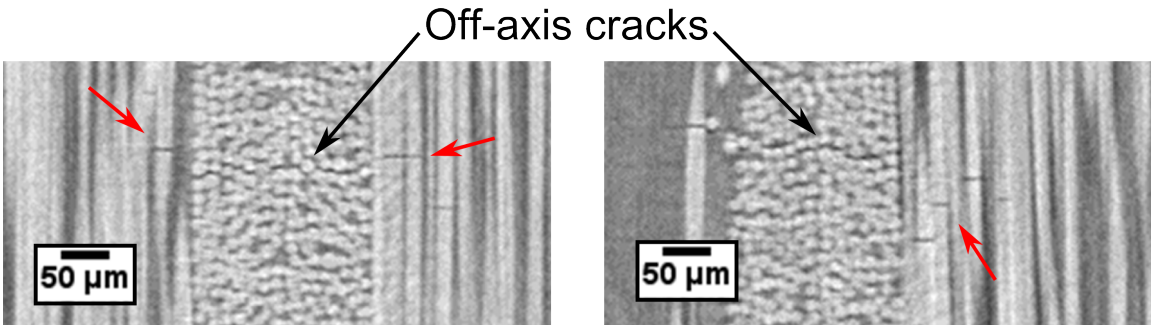

Figure 10: Examples of off-axis cracks visible for EPS06-04 with the tension applied during CT scanning using the tension clamp.

3.4. UD fibre fractures during the early fatigue life

In part A of the current study [1] it was argued that other damage mechanisms than off-axis cracking in the backing fibre bundles were present even during stage I of the fatigue life. From the tension clamp experiments shown in Fig. 8 it was seen that a significant number of UD fibre fractures were present even after 100,000 cycles, which is around the end of stage I of the fatigue life. These observations support the argument from part A. In addition, studies on prepreg based laminates often considered in the aerospace and automotive industries also state that fibre fractures occur over all stages of the fatigue life [23], and in this regard it is likely that similar mechanisms come into play for the considered quasi-UD composites.

Although present, fibre fractures are generally disregarded in prediction models, since they are not the controlling damage mechanism of stage I and II of the fatigue life for common layups such as quasi-isotropic and cross-ply laminates. In the case of

composites with thicker off-axis layers, the fibre fractures appearing early in the fatigue life might have a smaller contribution to the normalised stiffness degradation of the composite, since the off-axis layers contribute to a significantly larger percentage of the total composite stiffness than for the considered quasi-UD composites. In the case of quasi-UD composites, the initiation of even a few fibre fractures might overshadow the stiffness degradation from off-axis cracks in the backing fibre bundles, since the backing fibre bundles contribute only a few percent to the axial stiffness of the composite. Therefore, UD fibre fractures initiating together with off-axis cracks in the backing fibre bundles could be part of the explanation for the variation in the curves of the off-axis crack density as a function of the measured stiffness degradation for the tests presented in Part A of the current study.

4. Modified fatigue damage progression scheme

In a previous study by Zangenberg et al. [2] a damage progression scheme for a quasi-UD composite similar to the one considered in the current study was presented. The damage progression scheme was established based on scanning electron microscopy images at one damage state late in the fatigue life. Therefore, the order in which the damage mechanisms appeared could only be based on speculations. Using the additional information obtained through part A and B of the current study, the damage progression scheme by Zangenberg et al. [2] has been slightly modified and expanded. Fig. 11 shows the modified version of the damage progression scheme, where the initial state with no damage has been left out. The graph in the center of Fig. 11 shows the typical stiffness degradation of a fibre composite with five points marked (a-e). The figure include a principle sketch of the damage present at each of the damage states associated to these points.

The main modification done to the damage progression scheme is in the early fatigue life. The original scheme stated that off-axis cracks in the backing fibre bundles would initiate first in all the backing fibre bundles, and that this was the cause of the rapid stiffness degradation observed during stage I of the fatigue life. Although part A of

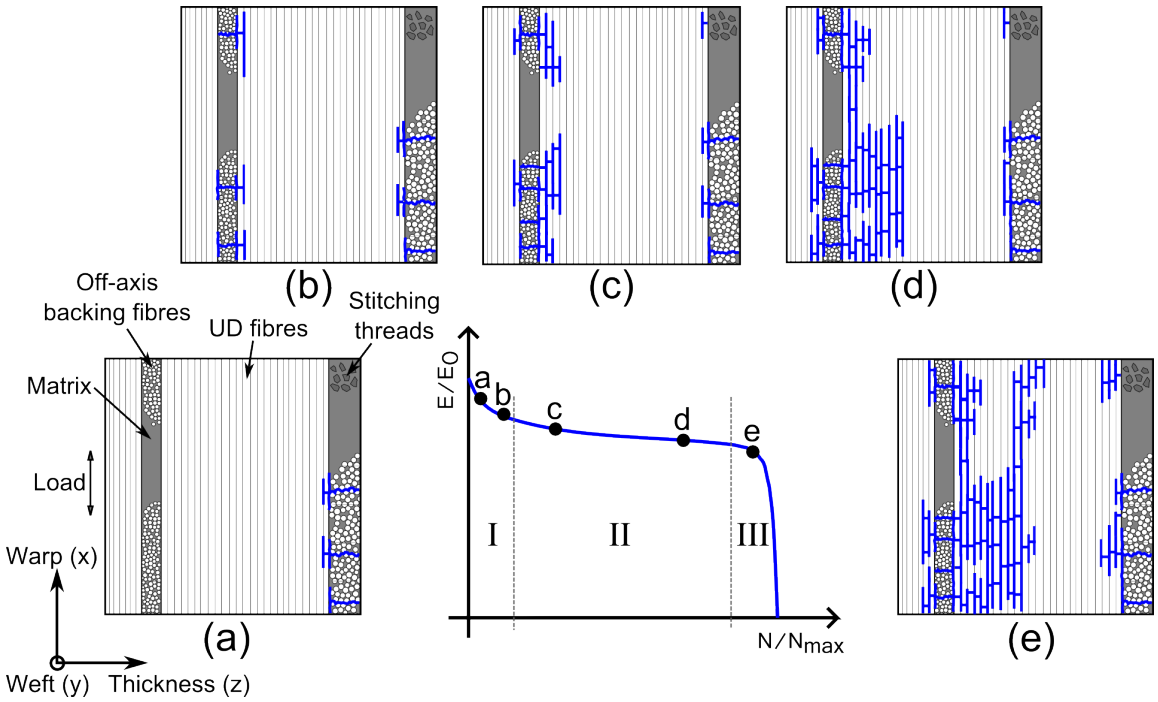

Figure 11: Slightly modified and expanded version of the damage progression scheme proposed by Zangenberg et al. [2]

the current study showed that the off-axis cracks indeed initiate early in the fatigue life, the results also indicated that other damage mechanisms took place during stage I. In addition, the tension clamp experiments carried out on the specimen interrupted around the end of stage I of the fatigue life, showed that several UD fibre fractures were present already at this stage. Therefore, it is believed that some UD fibre fractures initiate together with the off-axis cracks in the backing fibre bundles as illustrated in Fig. 11a.

The TWLI experiments presented in part A of the study showed that the off-axis cracks might not initiate simultaneously in the different backing fibre bundles. This is shown in the scheme by the difference between Fig. 11a and 11b. In addition, new off-axis cracks might initiate between existing cracks in the backing bundles as shown in the bottom-left backing fibre bundle shown in Fig. 11c. Because of the difference in the backing fibre bundle thickness the crack density per backing bundle varies, as

was also seen from the experiments carried out in part A of the study [1]. Some fibre fractures might initiate near regions of the stitching thread as well, however as this has not been seen in the X-ray CT images it seems that that the effect of the backing fibre bundles is more significant. Nevertheless, the stitching thread is made from polyester same as the matrix, and therefore they are not visible in the images. During stage II of the fatigue life, the UD fibre fractures gradually grow into the thickness direction of the UD fibre bundles (Fig. 11c to 11d), which is in accordance to the original progression scheme by Zangenberg et al. [2]. Damage regions will start growing together (Fig. 11e) and when the remaining UD fibres cannot carry the load anymore final failure occurs.

The scheme presented in Fig. 11 show only 2D views of the damage progression, however as seen from the observations in the current study the UD fibre fractures appear as local 3D phenomena rather than being homogeneously distributed in the UD fibre bundles. This is illustrated in Fig. 12 which shows a sketch of how the UD fibre fractures near a cross-over region of the backing fibre bundles might be distributed at a relatively late stage stage of the fatigue life. Several of this type of local damage regions are present in the material depending on the local bundle structure. Furthermore, it is clear that the UD fibre fractures do not severe the UD fibre bundles in 2D fracture planes, and that considering quasi-UD composites in 3D is important.

As seen from Fig. 11 and 12, the damage mechanisms are quite complicated for this type of fibre composite. The damage initiates and grow with different speed in different local regions of the material that also might initiate at different number of cycles. Furthermore, the initiation and growth of damage is highly related to the local fibre and bundle structures. Therefore, to be able to do realistic predictions of the damage initiation and progression in the future, it is necessary to do 3D modelling and also include the effect of the real fibre bundle structure. The presented results and the damage scheme illustrate the importance of establishing methods for modelling the damage progression, that includes the effect of fibre fractures as well. Recent advances within image analysis techniques (e.g. [24]) have made it possible to extract individual fibres from X-ray CT data, and it could be possible to extract the fibre bundle structure

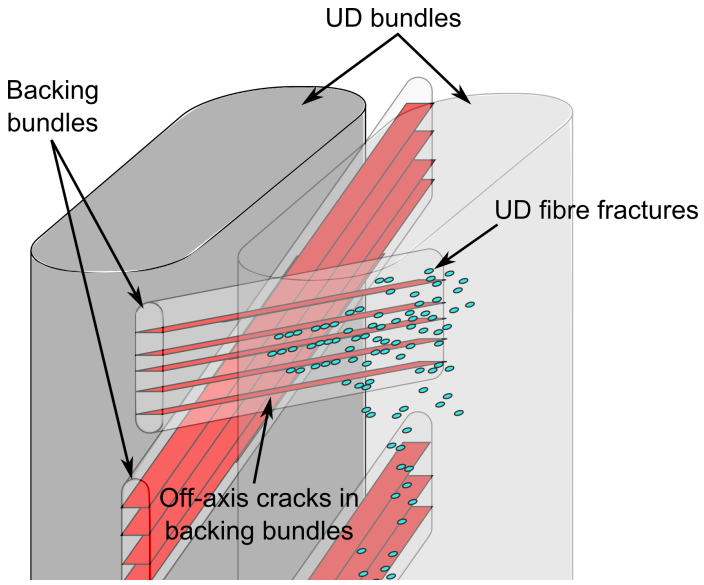

Figure 12: A 3D illustration of how a UD fibre fracture region could look like inside a UD fibre bundle.

by similar means. This allows one to use the actual material structure on different length scales in a finite element model. Therefore, the work carried out through the two parts of the current study that lead to the damage progression scheme shown in Fig. 11 serves as a good base for establishing a multi-scale X-ray based finite element model. Such an approach makes it possible to both include the real fibre and bundle structure obtained by X-ray CT and the effect of fibre fractures in a future finite element model. The 3D data sets along with the monitored damage progression provided by the current study can be used for this purpose.

5. Conclusion

In this study the initiation and progression of UD fibre fractures was monitored in two different regions of a quasi-UD composite using an ex-situ X-ray CT fatigue testing approach. By monitoring two different regions, it was observed that UD fibre fractures initiated first at thr cross-over region of the backing fibre bundles and later at the single backing fibre bundle region. UD fibre fractures were only observed at locations where the UD fibre bundles were in contact with the UD fibre bundle, which

indicated that the UD fibre fractures initiate from off-axis cracks in the backing fibre bundles. Although generally not visible in the X-ray CT scans, the off-axis cracks were shown to be present by TWLI carried out in Part A of the study. A tension clamp solution was applied to two specimens interrupted early and late in the fatigue life to investigate the crack visibility in the X-ray CT scans. These experiments showed that applying load during X-ray CT scanning had a large influence on the crack visibly for the considered material. By applying load, some off-axis cracks also became visible and they were seen to be accompanied by UD fibre fractures highly indicating that these fibre fractures initiated from the off-axis cracks. In the future, including the clamp as part of the ex-situ study could provide additional knowledge on the damage initiation and progression, although it will need a few improvements for it to be possible.

Acknowledgements

Financial support from CINEMA: "the allianCe for ImagiNg of Energy MAterials", DSF-grant no. 1305-00032B under "The Danish Council for Strategic Research" is gratefully acknowledged. This research was conducted using mechanical testing equipment from DTU Center for Advanced Structural and Material Testing (CASMAT), Grant No. VKR023193 from Villum Fonden. Additionally we would like to thank LM Wind Power for manufacturing of test specimens.

References

[1] K. M. Jespersen, J. A. Glud, J. Zangenberg, A. Hosoi, H. Kawada, L. P. Mikkelsen, Uncovering the fatigue damage initiation and progression of uni-directional non-crimp fabric reinforced polyester composite - Part A: Off-axis cracks and the effect of strain level, In manuscript (2017).

[2] J. Zangenberg, P. Brøndsted, J. W. Gillespie Jr., Fatigue damage propagation in unidirectional glass fibre reinforced composites made of a non-crimp fab-

ric, Journal of Composite Materials 48 (22) (2014) 2711–2727. doi:10.1177/0021998313502062.

[3] K. M. Jespersen, J. Zangenberg, T. Lowe, P. J. Withers, L. P. Mikkelsen, Fatigue damage assessment of uni-directional non-crimp fabric reinforced polyester composite using x-ray computed tomography, Composites Science and Technology 136 (2016) 94–103. doi:10.1016/j.compscitech.2016.10.006.

[4] K. M. Jespersen, L. P. Mikkelsen, Fatigue damage observed non-destructively in fibre composite coupon test specimens by x-ray ct, IOP Conference Series: Materials Science and Engineering 139 (2016) 012024. doi:10.1088/1757-899X/139/1/012024.

[5] E. Maire, P. J. Withers, Quantitative X-ray tomography, International Materials Reviews 59 (1) (2014) 1–43. doi:10.1179/1743280413y.0000000023.

[6] P. J. Withers, M. Preuss, Fatigue and damage in structural materials studied by X-Ray tomography, Annual Review of Materials Research 42 (2012) 81–103. doi:10.1146/annurev-matsci-070511-155111.

[7] P. Wright, X. Fu, I. Sinclair, S. M. Spearing, Ultra high resolution computed tomography of damage in notched carbon fiber-epoxy composites, Journal of Composite Materials 42 (19) (2008) 1993–2002. doi:10.1177/0021998308092211.

[8] P. Wright, A. Moffat, I. Sinclair, S. M. Spearing, High resolution tomographic imaging and modelling of notch tip damage in a laminated composite, Composites Science and Technology 70 (10) (2010) 1444–1452. doi:10.1016/j.compscitech.2010.04.012.

[9] A. E. Scott, M. Mavrigirdati, P. Wright, I. Sinclair, S. M. Spearing, In situ fibre fracture measurement in carbon-epoxy laminates using high resolution computed tomography, Composites Science and Technology 71 (12) (2011) 1471–1477. doi:10.1016/j.compscitech.2011.06.004.

[10] S. C. Garcea, M. Macrigirdato, A. E. Scott, I. Sinclair, S. M. Spearing, Fatigue micromechanism characterisation in carbon fibre reinforced polymers using synchrotron radiation computed tomography, Composites Science and Technology 99 (2014) 23–30. doi:10.1016/j.compscitech.2014.05.006.

[11] S. C. Garcea, I. Sinclair, S. M. Spearing, In situ synchrotron tomographic evaluation of the effect of toughening strategies on fatigue micromechanisms in carbon fibre reinforced polymers, Composites Science and Technology 109 (2015) 32–39. doi:10.1016/j.compscitech.2015.01.012.

[12] S. C. Garcea, I. Sinclair, S. M. Spearing, Fibre failure assessment in carbon fibre reinforced polymers under fatigue loading by synchrotron X-ray computed tomography, Composites Science and Technology 133 (2016) 157–164. doi:10.1016/j.compscitech.2016.07.030.

[13] F. Sket, R. Seltzer, J. M. Molina-Aldareguía, C. Gonzalez, J. LLorca, Determination of damage micromechanisms and fracture resistance of glass fiber/epoxy cross-ply laminate by means of X-ray computed microtomography, Composites Science and Technology 72 (2) (2012) 350–359. doi:10.1016/j.compscitech.2011.11.025.

[14] P. J. Schilling, B. P. R. Karedla, A. K. Tatiparthi, M. A. Verges, P. D. Herrington, X-ray computed microtomography of internal damage in fiber reinforced polymer matrix composites, Composites Science and Technology 65 (14) (2005) 2071–2078. doi:10.1016/j.compscitech.2005.05.014.

[15] B. Yu, R. Blanc, C. Soutis, W. P. J., Evolution of damage during the fatigue of 3D woven glass-fibre reinforced composites subjected to tension–tension loading observed by time-lapse X-ray tomography, Composites: Part A 82 (2016) 279–290. doi:10.1016/j.compositesa.2015.09.001.

[16] B. Yu, R. S. Bradley, C. Soutis, P. J. Hogg, P. J. Withers, 2D and 3D imaging

of fatigue failure mechanisms of 3D woven composites, Composites Science and Technology 77 (2015) 37–49. doi:10.1016/j.compositesa.2015.06.013.

[17] S. Topal, L. Baiocchi, A. D. Crocombe, S. L. Ogin, P. Potluri, P. J. Withers, M. Quaresimin, P. A. Smith, M. C. Poole, A. E. Bogdanovich, Late-stage fatigue damage in a 3D orthogonal non-crimp woven composite: An experimental and numerical study, Composites: Part A 79 (2015) 155–163. doi:10.1016/j.compositesa.2015.08.020.

[18] J. Pazmino, V. Carvelli, S. V. Lomov, Micro-CT analysis of the internal deformed geometry of a non-crimp 3D orthogonal weave E-glass composite reinforcement, Composites Part B: Engineering 65 (2014) 147–157. doi:10.1016/j.compositesb.2013.11.024.

[19] K. M. Jespersen, Y. Wang, J. Zangenberg, T. Lowe, P. J. Withers, L. P. Mikkelsen, Ex-situ time-lapse X-ray CT study of 3D micro-structural fatigue damage evolution in uni-directional composites, in: 17th European Conference on Composite Materials, Munich, 2016, pp. 1–8.

[20] J. Zangenberg, The effects of fibre architecture on fatigue life-time of composite materials, PhD Thesis, DTU Wind Energy PhD-0018(EN) (2013).

[21] J. Schindelin, I. Arganda-Carreras, E. Frise, V. Kaynig, M. Longair, T. Pietzsch, S. Preibisch, C. Rueden, S. Saalfeld, B. Schmid, J.-Y. Tinevez, D. J. White, V. Hartenstein, K. Eliceiri, P. Tomancak, A. Cardona, Fiji: an open-source platform for biological-image analysis, Nature Methods 9 (7) (2012) 676–682.

[22] K. M. Jespersen, Z. J., L. P. Mikkelsen, Uncovering the fatigue damage initiation and progression in uni-directional non-crimp fabric reinforced polyester composite - Part B [Data set], https://dk-sid.migrid.org/cgi-sid/ls.py?share_id=fPiQiSINRx (2017).

[23] K. L. Reifsnider, R. Jamison, Fracture of fatigue-loaded composite laminates, International Journal of Fatigue 4 (4) (1982) 187–197. doi:10.1016/0142-1123(82)90001-9.

[24] M. J. Emerson, K. M. Jespersen, A. B. Dahl, K. Conradsen, L. P. Mikkelsen, Individual fibre segmentation from 3D X-ray computed tomography for characterising the fibre orientation in unidirectional composite materials, Composites: Part A (2017). doi:10.1016/j.compositesa.2016.12.028.

Technical University of Denmark
Department of Wind Energy
Frederiksborgvej 399
Building 118
4000 Roskilde
Denmark
Telephone 46 77 50 85

info@vindenergi.dtu.dk
www.vindenergi.dtu.dk